



**HAL**  
open science

# Thermal diodes based on phase-change materials

Suraju Olawale Kasali

► **To cite this version:**

Suraju Olawale Kasali. Thermal diodes based on phase-change materials. Thermics [physics.class-ph]. Université de Poitiers, 2021. English. NNT : 2021POIT2254 . tel-03721032

**HAL Id: tel-03721032**

**<https://theses.hal.science/tel-03721032v1>**

Submitted on 12 Jul 2022

**HAL** is a multi-disciplinary open access archive for the deposit and dissemination of scientific research documents, whether they are published or not. The documents may come from teaching and research institutions in France or abroad, or from public or private research centers.

L'archive ouverte pluridisciplinaire **HAL**, est destinée au dépôt et à la diffusion de documents scientifiques de niveau recherche, publiés ou non, émanant des établissements d'enseignement et de recherche français ou étrangers, des laboratoires publics ou privés.

# THESIS

For obtaining the grade of

**DOCTOR OF THE UNIVERSITY OF POITIERS**

*École nationale supérieure d'ingénieurs de Poitiers*

National Diploma - Decree of May 25, 2016

Speciality : Energetic, Thermal and Combustion

Presented by

**Suraju Olawale KASALI**

---

## **Thermal diodes based on phase-change materials**

---

Director of the thesis

M. Karl JOULAIN

Co-supervisor of the thesis

M. Jose ORDONEZ-MIRANDA

Defended on January 29, 2021

In front of the commission of examination

---

### **Jury**

M. Sebastian VOLZ	CNRS Director of Research, LIMMS, Tokyo	Reporter
M. Konstantinos TERMENTZIDIS	CNRS Researcher (HDR), Insa Lyon	Reporter
M. Xavier ALVAREZ	Professor, Autonomous University of Barcelona	Examiner
M. Franck ENGUEHARD	Professor, University of Poitiers, Institute PPRIME	Examiner
M. Karl JOULAIN	Professor, University of Poitiers, Institute PPRIME	Examiner
M. Jose ORDONEZ-MIRANDA	CNRS Researcher (HDR), Institute PPRIME	Examiner



# Acknowledgements

Le succès de cette thèse de doctorat n'est pas seulement parce que j'ai travaillé dur, mais aussi les contributions d'autres personnes qui ont contribué à cela. Certains ont joué des rôles visibles tandis que d'autres ont travaillé en arrière-plan. Je n'en mentionnerai que quelques-uns, et j'apprécie sincèrement la contribution de chacun.

Tout d'abord, je voudrais exprimer ma sincère gratitude à mes directeurs de thèse, le professeur Karl JOULAIN et le Dr Jose ORDONEZ-MIRANDA pour leurs soutiens continus à la recherche, leurs motivations, leurs enthousiasmes et la richesse de leurs connaissances. Ils ont vraiment formé une bonne équipe de recherche pour moi et je n'aurais pas pu imaginer avoir de meilleurs conseillers et mentors pour mon doctorat. Je tiens également à remercier tous les membres du jury de ma thèse, plus particulièrement le président, le professeur Franck ENGUEHARD et les deux journalistes, le professeur Sebastian VOLZ et le Dr Konstantinos TERMENTZIDIS, pour leurs encouragements, leurs commentaires réfléchis et leurs questions très difficiles pendant la défense. Je dirais que tout cela m'a rendu fort et j'en ai appris davantage sur la physique.

Mes sincères remerciements vont au chef d'équipe Professeur associé Younès EZZAHRI et aux autres membres de l'équipe qui d'une manière ou d'une autre ont contribué au succès de cette thèse. Je tiens également à remercier les personnels administratifs et technique de l'institut, Bouba EL HARCHI, Hélène GRASSIN, Jean-Christophe VERGEZ, et Janick LAUMONIER pour leurs soutiens pendant la thèse. Mes remerciements particuliers vont également à mes collègues et amis,

Refet Ali YALCIN, Kamal ALAILI, Julien DJEUMEGNI, Olabode BANKOLE, Abdallah ALLOUCHE, Ahmed ABD ELMOLA, Kenneth OMABE, Adio SALOU, Hugo PROD'HOMME, Younes MAMMADI et Kenza MAHMOUDI pour leurs idées partagées et pour les bons moments que nous avons passés ensemble.

Pour terminer, ma profonde gratitude va à ma famille et en particulier à ma mère, Nusirat KASALI, pour son soutien moral et spirituel tout au long de ma vie. Je tiens à remercier sincèrement ma charmante épouse ALEGE-KASALI Bashirat Olajumoke et notre adorable fils Anas KASALI pour leurs soutiens, leurs compréhensions et leurs patiences pendant la durée de cette thèse de doctorat.

Je tiens à remercier le Tertiary Education Trust Fund (TETFUND) Nigeria pour son soutien financier à cette thèse de doctorat. Surtout, il y en a un derrière toutes les connexions humaines ci-dessus. Il est le Dieu tout-puissant et Il a organisé chaque plan et a permis de rassembler les personnes nécessaires, garantissant ainsi que cette thèse de doctorat soit brillamment couronnée. Je crois personnellement que Dieu guide ceux qui croient en lui, il m'a donc guidé à travers ce périple !

A tous et aux oubliés de cette liste, Merci!

# Abstract

The thermal rectification of conductive and radiative thermal diodes based on phase-change materials, whose thermal conductivities and effective emissivities significant change within a narrow range of temperatures, is theoretically studied and optimized in different geometries. This thesis is divided into three parts. In the first part, we comparatively model the performance of a spherical and cylindrical conductive thermal diodes operating with vanadium dioxide ( $\text{VO}_2$ ) and non-phase-change materials, and derive analytical expressions for the heat flows, temperature profiles and optimal rectification factors for both diodes. Our results show that different diode geometries have a significant impact on the temperature profiles and heat flows, but less one on the rectification factors. We obtain maximum rectification factors of up to 20.8% and 20.7%, which are higher than the one predicted for a plane diode based on  $\text{VO}_2$ . In addition, it is shown that higher rectification factors could be generated by using materials whose thermal conductivity contrast is higher than that of  $\text{VO}_2$ . In the second part, on the other hand, we theoretically study the thermal rectification of a conductive thermal diode based on the combined effect of two phase-change materials. Herein, the idea is to generate rectification factors higher than that of a conductive thermal diode operating with a single phase-change material. This is achieved by deriving explicit expressions for the temperature profiles, heat fluxes and rectification factor. We obtain an optimal rectification factor of 60% with a temperature variation of 250 K spanning the metal-insulator transitions of  $\text{VO}_2$  and polyethylene. This enhancement of the rectification factor leads us to the third part of our work, where we model and optimize the thermal rectification of a plane, cylindrical and spherical radiative thermal diodes based on the utilization of two phase-change materials. We analyze the rectification factors of these three diodes and obtain the following optimal rectification factors of 82%, 86% and 90.5%, respectively. The spherical geometry is thus the best shape to optimize the rectification of radiative heat currents. In addition, potential rectification factors greater than the one predicted here can be realized by utilizing two phase-change materials with higher emissivities contrasts than the one proposed here. Our analytical and graphical results provide a useful guide for optimizing the rectification factors of conductive and radiative thermal diodes based on phase-change materials with different geometries.

**Keywords :** Phase-change materials, Rectification factors, Heat flows, Interface thermal resistance, Heat flux, Emissivities, Thermal conductivities, Conductive thermal diode, Radiative thermal diodes.





# Résumé

Nous étudions dans cette thèse la rectification thermique de diodes thermiques radiatives ou conductive constituées de matériaux à changement de phase. Cette thèse est divisée en trois parties. Dans les premières parties, nous modélisons comparativement les performances d'une diode thermique conductive sphérique et cylindrique constitués de  $\text{VO}_2$  présentant un transition de phase et des matériaux n'en présentant pas. Des expressions analytiques aux bornes des diodes sont établies. Les expressions des flux thermiques, des facteurs de rectifications ainsi que les profils de température à l'intérieur de la diode sont obtenus. Nos résultats montrent que les différentes géométries de diodes ont un impact significatif sur les profils de température et les flux thermiques, mais moins un sur les facteurs de rectification. Dans ce travail, nous avons obtenu des facteurs de rectification maximaux allant jusqu'à 20.8% et 20.7%, qui sont supérieurs à ceux prédit pour une diode plane constituée de  $\text{VO}_2$ . Nous montrons également que des facteurs de rectification similaires à ceux obtenus avec le  $\text{VO}_2$  dans les géométries sphériques et cylindriques peuvent être atteints avec des matériaux à changement de phase dont le contraste de conductivité est plus important que dans le cas du  $\text{VO}_2$ . Dans la deuxième partie, nous étudions la rectification de diodes thermiques constituées de deux matériaux à changement de phase avec l'idée de générer un facteur de redressement plus élevé que dans le cas d'une diode thermique conductive ne comprenant qu'un matériau à changement de phase unique. La encore, le travail a conduit à l'établissement d'expressions explicites pour les profils de température, les flux thermiques et le facteur de rectification. Nous avons obtenu un facteur de rectification optimal de 60% avec une variation de température de 250 K couvrant les transitions métal-isolant des deux matériaux. Dans la troisième partie de notre travail, nous avons modélisé et optimisé la rectification thermique de diodes thermiques planes, cylindriques et sphérique radiatives à base de deux matériaux à changement de phase. Nous avons calculé et analysé les facteurs de rectification de ces trois diodes et obtenu les facteurs de rectification optimaux respectifs pour les trois géométries 82%, 86% et 90.5%. Nos résultats montrent que la géométrie sphérique est la meilleure pour optimiser la rectification des courants thermiques radiatifs. De plus, des facteurs de rectification potentiellement supérieurs à ceux prédits ici peuvent être réalisés en utilisant deux matériaux à changement de phase avec des contrastes d'émissivités plus élevés que ceux proposés ici. Ces résultats analytiques et graphiques fournissent un guide utile pour optimiser les facteurs de rectification des diodes thermiques conductives et radiatifs basées sur des matériaux à changement de phase de géométries différentes.

**Mots-clés :** Matériaux à changement de phase, facteurs de rectification, flux de chaleur, résistance thermique d'interface, flux de chaleur, émissivités, conductivités thermiques, diode thermique conductives, diodes thermiques radiatifs.

# Contents

<b>Acknowledgements</b>	<b>iii</b>
<b>General Introduction</b>	<b>1</b>
<b>1 The theory of heat transfer in solid materials</b>	<b>11</b>
1.1 Introduction	13
1.1.1 Heat equation	14
1.1.2 Conductive heat transfer	14
1.1.3 Radiative heat transfer	16
1.1.4 Radiative heat transfer in Blackbody	17
1.1.5 Far and Near-field radiative heat transfer	19
1.2 Thermal components	22
1.2.1 Thermal diode and rectification factor	22
1.2.2 Thermal conductivity	23
1.2.3 Effective emissivity	24
1.2.4 Interface thermal resistance	25
1.3 Thermochromic materials: so-called "smart" materials	26
1.3.1 Phase-change materials	27
1.4 A review of VO <sub>2</sub>	29
1.4.1 Properties of vanadium oxides	30
1.4.2 The MIT of VO <sub>2</sub>	30
1.5 The elementary mechanism of MIT	33
Mott Transition mechanism	33
Peierls Transition mechanism	34
1.5.1 Percolation process during the MIT of VO <sub>2</sub>	37
1.6 Crystallography Structure of VO <sub>2</sub>	37
1.6.1 Energy Band Structure of VO <sub>2</sub>	40
1.6.2 Optical properties of VO <sub>2</sub>	41
1.6.3 Mechanical properties of VO <sub>2</sub>	44
1.6.4 The excitation of the MIT of VO <sub>2</sub>	46
1.7 Applications of VO <sub>2</sub>	47
1.7.1 Thermal sensor MIT in VO <sub>2</sub> thin film	48
1.7.2 Memristor devices using the MIT of VO <sub>2</sub>	51
1.7.3 Three-terminal field effect transistor switches utilizing the MIT of VO <sub>2</sub>	53
1.8 The deposition techniques of VO <sub>2</sub> thin film	55
1.8.1 Chemical vapor deposition	55
1.8.2 Sol-gel Technique	57
1.8.3 Pulsed laser deposition	58

1.9	Conclusions . . . . .	60
1.10	Résumé du chapitre 1 . . . . .	62
<b>2</b>	<b>Geometrical effects on conductive thermal diodes based on VO<sub>2</sub></b>	<b>67</b>
2.1	Introduction . . . . .	69
2.2	Analytical solution of spherical and cylindrical thermal diodes . . .	70
2.2.1	Spherical conductive thermal diode . . . . .	71
	Forward configuration . . . . .	71
	Backward configuration . . . . .	76
2.2.2	Cylindrical conductive thermal diode . . . . .	76
	Forward configuration . . . . .	76
	Backward configuration . . . . .	79
2.3	Rectification factor . . . . .	80
2.3.1	Spherical diode . . . . .	80
2.3.2	Cylindrical diode . . . . .	81
2.4	Results and discussion . . . . .	83
2.5	Conclusions . . . . .	88
2.6	Résumé du chapitre 2 . . . . .	89
<b>3</b>	<b>Dual phase-change materials conductive thermal diode</b>	<b>93</b>
3.1	Introduction . . . . .	95
3.2	Analytical solution of heat conduction model . . . . .	97
3.3	Heat fluxes and temperature profiles . . . . .	97
3.3.1	Forward configuration . . . . .	97
3.3.2	Backward configuration . . . . .	102
3.4	Rectification factor . . . . .	103
3.4.1	Forward and backward configuration . . . . .	103
3.5	Temperature evolution of heat fluxes and rectification factor . . . .	106
3.6	Heat fluxes and interface temperatures . . . . .	109
3.7	Temperature dependence rectification factor . . . . .	112
3.8	Conclusions . . . . .	115
3.9	Résumé du chapitre 3 . . . . .	116
<b>4</b>	<b>Radiative thermal diodes based on two phase-change materials</b>	<b>121</b>
4.1	Introduction . . . . .	123
4.2	Modeling of plane, cylindrical and spherical radiative thermal diodes	125
4.2.1	Plane radiative thermal diode . . . . .	128
4.2.2	Cylindrical radiative thermal diode . . . . .	130
4.2.3	Spherical radiative thermal diode . . . . .	131
4.3	Temperature dependence and rectification factor of a plane geom- etry . . . . .	133
4.4	Temperature dependence and rectification factors of cylindrical geometry . . . . .	135
4.5	Temperature dependence and rectification factor of a spherical ge- ometry . . . . .	137
4.6	Rectification factors of plane, cylindrical and spherical geometries .	139
4.7	Conclusions . . . . .	142
4.8	Résumé du chapitre 4 . . . . .	144

<b>General conclusions and Perspectives</b>	<b>149</b>
<b>Bibliography</b>	<b>157</b>
<b>List of publications and conferences</b>	<b>181</b>
I Publications . . . . .	181
Articles in peer-reviewed journals . . . . .	181
II Conférences . . . . .	182
Oral presentation . . . . .	182
Présentations par affiche . . . . .	182



# List of Figures

1.1	Scheme of a one-dimensional heat conduction situation. . . . .	15
1.2	Spectral emissive power of a blackbody [Inc96]. . . . .	18
1.3	Scheme of (a) far-field and (b) near-field radiative heat transfer [Bie20]. . . . .	20
1.4	Scheme of a thermal diode operating in the (a) forward and (b) backward configurations. $T_h$ and $T_c$ denotes hot and cold temperatures respectively. . . . .	22
1.5	Scheme of a contact thermal resistance. . . . .	25
1.6	The MIT temperature of VO <sub>2</sub> and some selected oxides [Yan11]. . .	28
1.7	Phase diagram of the VO <sub>x</sub> system [Yan11]. . . . .	31
1.8	Temperature dependence of the infrared transmittance of (a) Undoped and (b) W-doped VO <sub>2</sub> [Liv97]. . . . .	32
1.9	Scheme of a Peierls transition. . . . .	35
1.10	Images of a scanning near-field infrared microscopy of VO <sub>2</sub> film at different temperatures during its MIT process [Qaz07]. . . . .	36
1.11	(a) Tetragonal $P4_2/mnm$ high-temperature and (b) monoclinic ( $P2_1/c$ ) low-temperature structures of VO <sub>2</sub> and its relation to the rutile structure [Goo71]. . . . .	38
1.12	Tetragonal lattice structure of VO <sub>2</sub> above the phase transition temperature. Large red spheres represent V ions while the small blue ones stand for O ions [Eye02]. . . . .	38
1.13	Low temperature monoclinic $M_1$ lattice of VO <sub>2</sub> [Eye02]. . . . .	39
1.14	Band structure of VO <sub>2</sub> in its insulator and metal phases [Goo71]. . .	41
1.15	Electrical resistance as functions of Temperature of VO <sub>2</sub> film deposited on Al <sub>2</sub> O <sub>3</sub> [Ruz08]. . . . .	42
1.16	(a) Infrared reflectance as functions of incident photon energy for different temperatures and (b) Reflectance as a function of temperature at different photon energies [Ruz08]. . . . .	43
1.17	Young's modulus, as functions of the temperature of VO <sub>2</sub> thin films deposited on single crystal silicon for three different lengths [Sep08]. . . . .	45
1.18	Different MIT-triggering in strongly-correlated oxides [Yan11]. . . .	47
1.19	(a) The I-V characteristics of a VO <sub>2</sub> based device for different temperatures and (b) Infrared image collected using a special infrared system marked by FLIR [Yan11]. . . . .	49

1.20	(a) A VO <sub>2</sub> thermal sensor device based on the temperature and voltage dependency of the conductivity and the coplanar VO <sub>2</sub> device and (b) Scheme of a nanowire gas sensor device, where $P_G$ and $P_L$ indicate the heat fluxes dissipating into the gas and metal contacts, respectively [Yan11]. . . . .	50
1.21	I-V characteristics of the VO <sub>2</sub> nanowire gas sensor device at different $A_r$ pressure [Yan11]. . . . .	51
1.22	(a) Scheme of a VO <sub>2</sub> memristor device, (b) Three I-V curves displaying the hysteretic nonlinear memristor behavior of a VO <sub>2</sub> [Yan11] and (c) Memory capacitance of a hybrid VO <sub>2</sub> device during its heating and cooling process [Dri09]. . . . .	52
1.23	(a) Scheme of a three-terminal gated switch devices using MIT of VO <sub>2</sub> and (b) Current density as functions of applied electric field on the VO <sub>2</sub> channel with the gate open at room temperature. The inset shows the three-terminal VO <sub>2</sub> device structure [Yan11]. . . . .	54
1.24	Scheme of a typical APCVD setup rig [War14]. . . . .	56
1.25	Scheme of a PLD process [McG17]. . . . .	59
2.1	Scheme of a spherical (or cylindrical) conductive thermal diode consisting of a VO <sub>2</sub> and Non-PCM, and operating in the (a) forward and (b) backward configurations. The surfaces $r = a$ and $r = c$ are set at the temperatures $T_h$ and $T_c$ , for the forward configuration, while they are reversed in the backward one. . . . .	72
2.2	Thermal conductivity of VO <sub>2</sub> , as functions of temperature within its corresponding MIT. Dots represent experimental data reported in the literature [Oh10]. . . . .	73
2.3	Temperature evolution of the forward and backward heat flows of a (a) spherical and (b) cylindrical thermal diodes operating with a terminal of VO <sub>2</sub> . Calculations were done for three representative interface thermal resistances and $T_c = 300$ K [Kas19]. . . . .	84
2.4	Rectification factor of a (a) spherical and (b) cylindrical thermal diodes, as a function of the hotter temperature $T_h$ . Calculations were done for three representative values of the effective thermal resistances, $T_c = 300$ K, $a = 1$ $\mu\text{m}$ and $b = 10$ $\mu\text{m}$ [Kas19]. . . . .	85
2.5	Rectification factor of a (a) spherical and (b) cylindrical thermal diodes, as a function of the hotter temperature $T_h$ and effective thermal resistance $\delta$ and $\mu$ , respectively. Calculations were done for three representative values of the effective thermal resistances, $T_c = 300$ K, $a = 1$ $\mu\text{m}$ and $b = 10$ $\mu\text{m}$ [Kas19]. . . . .	87
2.6	Schéma d'une diode thermique conductive sphérique (ou cylindrique) constituée une VO <sub>2</sub> et d'un Non-PCM, et fonctionnant dans les configurations avant et arrière. Les surfaces $r = a$ et $r = c$ sont fixées aux températures $T_h$ et $T_c$ , pour la configuration avant, alors qu'elles sont inversées dans la configuration arrière. . . . .	90

3.1	Scheme of a dual PCMs conductive thermal diode operating in the (a) forward and (b) backward configurations. Hot and cool thermal shells are set at the temperatures $T_h$ and $T_c$ , respectively [Kas20a]. . . . .	98
3.2	Thermal conductivities of VO <sub>2</sub> and PE, as functions of the temperature within their corresponding MIT. Dots and triangles stand for experimental data reported in the literature [Oh10; Zha15], while lines represent the theoretical predictions of equations (3.2a) and (3.2b), respectively [Kas20a]. . . . .	99
3.3	Rectification factor, forward and backward heat fluxes of the conductive thermal diode of VO <sub>2</sub> and PE, as functions of the temperature $T_h$ . Calculations were done for $T_c = 300$ K and $\rho = 0$ mm <sup>2</sup> KW <sup>-1</sup> [Kas20a]. . . . .	107
3.4	Temperature evolution of the forward and backward heat fluxes, as functions of (a) $T_1(L_1)$ and (b) $T_2(L_2)$ . Calculations were done for $T_c = 300$ K and $\rho = 0$ mm <sup>2</sup> KW <sup>-1</sup> [Kas20a]. . . . .	108
3.5	Interface temperatures for the (a) forward [ $T_1(L_1)$ and $T_2(L_1)$ ] and (b) backward [ $T_2(L_2)$ and $T_1(L_2)$ ] configurations, as functions of the temperature $T_h$ . Calculations were done for $T_c = 300$ K and $\rho = 1$ mm <sup>2</sup> KW <sup>-1</sup> [Kas20a]. . . . .	110
3.6	Temperature profiles within the terminals of the conductive thermal diode operating in the forward and backward configurations. Arrows stand for the direction of heat flux and calculations were done for $T_c = 300$ K, $T_h = 550$ K, and two values of the interface thermal resistance $\rho$ [Kas20a]. . . . .	111
3.7	Rectification factor of the conductive thermal diode, as a function of the interface thermal resistance $\rho$ . Calculations were done using $R = [1 - \min(q_F, q_B) / \max(q_F, q_B)]$ and $T_c = 300$ K [Kas20a]. . . . .	111
3.8	Density plot of the conductive thermal diode rectification factor as a function of the temperature $T_h$ and interface thermal resistance $\rho$ . Calculations were done using $R = [1 - \min(q_F, q_B) / \max(q_F, q_B)]$ and $T_c = 300$ K [Kas20a]. . . . .	112
3.9	Rectification factor $R$ of the conductive thermal diode as a function of the temperature $T_h$ . Calculations were done by using the alternative definition $R_a = [\max(q_F, q_B) / \min(q_F, q_B)] - 1$ for three representative interface thermal resistances and $T_c = 300$ K [Kas20a]. . . . .	113
3.10	Schéma d'une diode thermique conductive à double PCM fonctionnant dans les configurations (a) avant et (b) arrière. Les coques thermiques chaudes et froides sont réglées aux températures $T_h$ et $T_c$ , respectivement [Kas20a]. . . . .	117
4.1	Scheme of a plane radiative thermal diode made up with terminals of GST and VO <sub>2</sub> operating in the (a) forward and (b) backward configurations. Hot and cold thermal baths are set at the temperatures $T_h$ and $T_c$ , respectively [Kas20b]. . . . .	124

4.2	Scheme of a spherical (or cylindrical) radiative thermal diode made up of GST and VO <sub>2</sub> operating in the forward and backward configurations. The radii $r_1$ and $r_2$ are set at the temperatures $T_h$ and $T_c$ for the forward configuration, while they are interchanged for the backward one [Kas20b]. In practice, a spherical diode could be implemented by using the classical Langmuir-Blodgett law [I L24].	125
4.3	Effective emissivities of GST and VO <sub>2</sub> as functions of temperature within their MITs. Dots and rectangles represent experimental data reported in the literature [Ord18b; Du17], while lines stand for fits of equation (1.11) [Kas20b].	126
4.4	Temperature dependence of the radiative heat flows for the (a) forward and backward configurations of a plane radiative diode operating with terminals of GST and VO <sub>2</sub> . Inset: Zoom-in of the first maximum and minimum values of $q_B$ . (b) Rectification factor as a function of $T_h$ . Calculations were done for $T_c = 300$ K [Kas20b].	134
4.5	Temperature dependence of the radiative heat flows for the (a) forward and backward configurations of a cylindrical radiative diode operating with terminals of GST and VO <sub>2</sub> along with (b) its corresponding rectification factor. The solid line stand for the thermal diode shown in Fig. 2, while the dashed one corresponds to a system with interchanged terminals. The inset in (a) shows a zoom-in of the first maximum and minimum values of $q_B$ . Calculations were done for $T_c = 300$ K and $r_1/r_2 = 0.8$ [Kas20b].	136
4.6	Temperature dependence of the radiative heat flows for the (a) forward and backward configurations of a spherical radiative diode operating with terminals of GST and VO <sub>2</sub> along with (b) its corresponding rectification factor. The solid line stand for the thermal diode shown in Fig. 2, while the dashed one corresponds to a system with interchanged terminals. The inset in (a) shows a zoom-in of the first maximum and minimum values of $q_B$ . Calculations were done for $T_c = 300$ K and $r_1/r_2 = 0.8$ [Kas20b].	138
4.7	Comparison of the rectification factors obtained for the plane, cylindrical, and spherical diodes operating with terminals of GST and VO <sub>2</sub> . Calculations were done for $T_c = 300$ K and $r_1/r_2 = 0.8$ [Kas20b].	140
4.8	Temperature dependence of the rectification factor of plane, cylindrical, and spherical diodes with terminals of (a) VO <sub>2</sub> and a black body and (b) GST and black body. Calculations were done for $T_c = 300$ K and $r_1/r_2 = 0.8$ [Kas20b].	141
4.9	Rectification factors of (a) plane (b) cylindrical and (c) spherical diodes based on one PCM and two PCMs, as functions of $T_h$ . Calculations were done for $T_c = 300$ K and $r_1/r_2 = 0.8$ [Kas20b].	142
4.10	Schéma d'une diode thermique radiative plane composée de bornes de GST et VO <sub>2</sub> fonctionnant dans les configurations (a) directe et (b) inverse. Les bains thermaux chauds et froids sont réglés aux températures $T_h$ et $T_c$ , respectivement [Kas20b].	145

- 4.11 Schéma d'une diode thermique radiative sphérique (ou cylindrique) composée de GST et VO<sub>2</sub> fonctionnant dans les configurations avant et arrière. Les rayons  $r_1$  et  $r_2$  sont fixés aux températures  $T_h$  et  $T_c$  pour la configuration vers l'avant, alors qu'ils sont interchangés pour celle vers l'arrière [Kas20b]. En pratique, une diode sphérique pourrait être implémentée en utilisant la loi classique de Langmuir-Blodgett [L24]. . . . . 146



# List of Tables

1.1	Slopes for the three phases shown in Figure 1.17 [Sep08]. . . . .	45
3.1	Properties of materials involved in equations (3.2a) and (3.2b) [Kas20a]. .	99
4.1	Properties of materials involved in equations (4.3a) and (4.3b) [Kas20b]. .	128



# List of Abbreviations

<b>PCM</b>	<b>Phase Change Material</b>
<b>Non-PCM</b>	<b>non- Phase Change Material</b>
<b>PE</b>	<b>Polyethylene</b>
<b>Ge<sub>2</sub>Sb<sub>2</sub>Te<sub>5</sub></b>	<b>Germanium Antimony Tellurium</b>
<b>MIT</b>	<b>Metal- Insulator Transition</b>
<b>VO<sub>2</sub></b>	<b>Vanadium Dioxide</b>
<b>CHT</b>	<b>Conductive Heat Transfer</b>
<b>RHT</b>	<b>Radiative Heat Transfer</b>
<b>FFRHT</b>	<b>Far- Field Radiative Heat Transfer</b>
<b>NFRHT</b>	<b>Near- Field Radiative Heat Transfer</b>
<b>FE</b>	<b>Fluctuation Electrodynamics</b>
<b>TIR</b>	<b>Total Internal Reflection</b>
<b>MOCVD</b>	<b>Metal Organic Chemical Vapor Deposition</b>
<b>OMCVD</b>	<b>Organometallic Chemical Vapor Deposition</b>
<b>CVD</b>	<b>Chemical Vapor Deposition</b>
<b>APCVD</b>	<b>Atomic Pressure Chemical Vapor Deposition</b>
<b>PLD</b>	<b>Pulsed Laser Deposition</b>
<b>PVD</b>	<b>Physical Vapor Deposition</b>
<b>FET</b>	<b>Field Effect Transistor</b>
<b>MEMS</b>	<b>Micro Electro Mechanical System</b>
<b>AMM</b>	<b>Acoustic Mismatch Model</b>
<b>ITR</b>	<b>Interface Thermal Resistance</b>
<b>He</b>	<b>Helium</b>
<b>N<sub>2</sub></b>	<b>Nitrogen</b>
<b>CO<sub>2</sub></b>	<b>Carbon Dioxide</b>
<b>VOCl<sub>3</sub></b>	<b>Vanadium Oxychloride</b>
<b>KrF</b>	<b>Krypton Fluoride</b>
<b>IR</b>	<b>Infrared</b>
<b>IV</b>	<b>Current Voltage</b>
<b>Si</b>	<b>Silica</b>
<b>CMOS</b>	<b>Complementary Metal Oxide Semiconductor</b>
<b>MOSFET</b>	<b>Metal Oxide Semiconductor Field Effect Transistor</b>



# List of Symbols

$T$	Temperature, K
$T_0$	Transition temperature, K
$T_h$	Hot temperature, K
$T_c$	Cold temperature, K
$T_0$	Transition temperature, K
$t$	Time, s
$r$	Radius, m
$A$	Area, $m^2$
$\beta$	Phase transition slope, $K^{-1}$
$E_{\lambda,b}$	Spectral emissive power of a blackbody, $W m^{-2} \mu m$
$h$	Planck's constant, J s
$c$	Speed of light, $m s^{-1}$
$\lambda_{th}$	Thermal wavelength, m
$\lambda_{max}$	Wien's wavelength, m
$\lambda$	Wavelength m
$L$	Position, m
$a$	Radius, m
$b$	Radius, m
$c$	Radius, m
$h$	Height, m
$x$	Position, m
$\rho$	interface thermal resistance, $mm^2 K W^{-1}$
$C_p$	Specific heat, $J mol^{-1} K^{-1}$
$\varepsilon$	Effective emissivities
$k_B$	Boltzmann constant, $J K^{-1}$
$q$	Heat flux, $W m^{-2}$
$\kappa$	Thermal conductivity, $W m^{-1} K^{-1}$
$\kappa_m$	Thermal conductivity of metallic phase, $W m^{-1} K^{-1}$
$\kappa_i$	Thermal conductivity of insulating phase, $W m^{-1} K^{-1}$
$R$	Interface thermal resistance, $m^2 K W^{-1}$
$\sigma$	Steffan-Boltzmann constant, $W m^{-2} K^{-4}$
$\tau$	Pulse time s
<i>max</i>	maximum
<i>min</i>	minimum



*À mes parents*  
*À mes soeurs*  
*À mon frère*  
*À ma chérie Bashirat*  
*À mon fils Anas*  
*À mes amis.*



# General Introduction

Since the first experimental observation of Starr in 1936 at the interface between copper and cuprous oxide [Sta36], thermal rectification has received significant interest due to their potential applications in heat flow management related to limited energy and global warming problems [Li04; Rob11; Shi15; Li12; Jou15b]. It consists in allowing the transportation of heat flux between two terminals along a specific direction and blocking it in the opposite one when their temperatures are reversed. After Starr, a lot of experimental and theoretical work has been demonstrated in order to understand the physics behind this tuning of heat transport. The determination of a device which undergo this type of strange behavior have paved way to the realization of thermal circuits in a way similar to their non-linear electronics counterparts [Bar03; Day63]. With the improvement in understanding how thermal rectification is realized, thermal diodes [Rob11], thermal transistor [Ord16], thermal switch [Gu15], optical switch [Rin08], thermal memristor [Ben17; Ord19a], thermal memories [Ito16], and thermal logic circuits [Lo08; Wan07] devices has been theoretically designed and optimized. A general question that often come up while studying thermal rectification is whether the heat flows between the two terminals at low temperature is different than the one at high temperature when their temperatures are interchanged. If the aforementioned scenario is the case, then the two terminals are said to exhibits thermal rectification, a thermal analogy to electrical rectification known as a thermal diodes. During the last decades, heat currents exhibiting thermal rectification have been studied. In these devices, the carriers of heat flow behave asymmetrically either by the involving materials or by guiding the heat flow carriers in a different form whether

they are moving in one direction or the opposite [Li04; Cha06; Pey06; Ter02]. More recently, very promising thermal rectification devices has been proposed based on phase-change materials (PCMs) such as vanadium oxides, nitinol, polyethylene (PE), and  $\text{Ge}_2\text{Sb}_2\text{Te}_5$  (GST). Among these PCMs, there has been a lot of interest in vanadium oxides since the first work of Morin [Mor59]. These materials exhibit metal-insulator transitions (MITs) which are accompanied by significant changes in their optical, thermal and electrical properties. Out of several types of vanadium oxides,  $\text{VO}_2$  has been most studied theoretically and experimentally, due to the fact its MIT occurs close to room temperature. Based on the hysteresis effect of  $\text{VO}_2$ , Ordonez-Miranda *et al.* [Ord18b] studied a plane geometry conductive thermal diode operating within the terminal of a  $\text{VO}_2$  and phase invariant one. The authors proposed that the main vital parameter to achieved thermal rectification is thermal conductivity contrast of the involving PCM. Following this idea, the goal of this thesis is to study different geometries and material configurations to analyze and optimize the thermal rectification of a conductive and radiative thermal diodes based on  $\text{VO}_2$ , PE, and GST.

The thesis is structured and organized in four chapters, which are detailed below:

- In the first chapter of this thesis, we described the fundamental concepts of heat transfer and different modes of heat transfer by focusing on the conductive and radiative (far- and near-field) ones. In this context, we discussed about the radiative heat transfer in a black body. These basic concepts are important to understand the rate of heat transfer between solids materials. We explain the concept of thermal rectification and its components, where we shed more light on certain thermal properties such as thermal diodes, thermal conductivity, effective emissivity and interface thermal resistance (ITR), which is the main parameter that affect the thermal property. We described very promising

materials (thermochromic and PCMs) capable of rectifying heat currents. Significant emphasis is put on  $\text{VO}_2$ , given that its MIT occur at a temperature closer to room one. Furthermore, we explain the MIT of  $\text{VO}_2$ , along with a qualitative discussion on the mechanism leading to the phase transition and the properties accompanied during the MIT. Finally, we discussed different aspect of the application of  $\text{VO}_2$  and as well as different thin film deposition techniques.

- The second chapter is devoted to the study of the geometrical effects of a conductive thermal diode based on PCM where the heat conduction follows Fourier's law. Here, we look at the previous work of Ordonez- Miranda in a geometrical perspective. We derive and analyze simple analytical expressions for the temperature profiles, heat flows and optimal rectification factor of both diode geometries supporting steady-state heat conduction. We demonstrate that the change in geometry has a strong impact on the temperature profiles and heat flows, but not so much on the diode optimal rectification factor.

- The third chapter includes the detailed study of conductive thermal diodes between two PCMs whose thermal conductivities change significantly with respect to the temperature. We consider a planar system of two PCMs exchanging heat through steady-state condition due to their temperature differences. Again, thanks to Fourier's law, explicit and simple analytical expressions are derived and numerically evaluated for the heat fluxes, temperature profiles and optimal rectification factor. We show that the optimization of the rectification factor of the conductive thermal diode requires a high temperature jumps at the interface of its terminals, for a given ITR. We report that the combined effect of two PCMs is expected to generate higher rectification factors than a thermal diode based on a single PCM. This fact indicates that two PCMs could also be applied to optimize the rectification factor of radiative thermal diodes, which is not reported in the literature yet, to the best of our knowledge, as presented in

chapter 4.

-In the fourth chapter, we describe a far-field radiative thermal diodes in the plane, cylindrical and spherical geometries based on two PCMs. We derive and analyze analytical expression for the optimal rectification factor of the three diode geometries. We demonstrate that the change of geometry has a significant impact on the optimal rectification factors. We show that the combination of two PCMs can generate higher rectification factors as reported for the conductive thermal diode in chapter 3.

Finally, the general conclusions and perspectives of the thesis are presented.

## Résumé de l'introduction générale

Depuis la première observation expérimentale de Starr en 1936 à l'interface entre le cuivre et l'oxyde cuivreux [Sta36], la rectification thermique a suscité un intérêt considérable en raison de ses applications potentielles dans la gestion des flux thermiques notamment dans le contexte d'un accès limité aux ressources en énergie et du réchauffement climatique [Li04; Rob11; Shi15; Li12; Jou15b]. La rectification thermique consiste à permettre le transport du flux thermique entre deux bornes selon une direction spécifique et à le bloquer dans l'autre lorsque leurs températures sont inversées. Après Starr, de nombreux travaux expérimentaux et théoriques ont été poursuivis afin de comprendre la physique sous-jacente à cette problématique du transport thermique. La conception et la fabrication d'un dispositif présentant ce type de comportement étrange a ouvert la voie à la réalisation de circuits thermiques de manière similaire à leurs homologues électroniques non linéaires [Bar03; Day63]. Avec l'amélioration de la compréhension de la manière dont la rectification thermique est réalisée, les diodes thermiques [Rob11], le transistor thermique [Ord16], l'interrupteur thermique [Gu15], l'interrupteur optique [Rin08], le memristor thermique [Ben17; Ord19a], les mémoires thermiques [Ito16] et les circuits de logique thermique [Lo08; Wan07] dispositifs ont été théoriquement conçus et optimisés. La question générale qui se pose pour obtenir une rectification thermique est de savoir si les flux de chaleur entre les deux bornes à basse température sont différents de ceux à haute température lorsque leurs températures sont échangées. Si c'est le cas, on dit que le dispositif présente une rectification thermique. Au cours des dernières décennies, de nombreux dispositifs présentant une rectification thermique ont été étudiés. Dans ces dispositifs, les porteurs de flux de chaleur se comportent de manière asymétrique soit par les matériaux impliqués, soit en guidant les porteurs de flux de chaleur sous une forme différente, qu'ils se déplacent dans un sens ou dans l'autre sens [Li04; Cha06; Pey06; Ter02]. Plus récemment, des dispositifs de rectification thermique très

prometteurs ont été proposés à base de matériaux à changement de phase (PCM) tels que les oxydes de vanadium, le nitinol, le polyéthylène (PE) et  $\text{Ge}_2\text{Sb}_2\text{Te}_5$  (GST). Parmi ces PCM, il y a eu un grand intérêt pour les oxydes de vanadium depuis les premiers travaux de Morin [Mor59]. Ces matériaux présentent des transitions métal-isolant (MIT) qui s'accompagnent de changements significatifs de leurs propriétés optiques, thermiques et électriques. Parmi plusieurs types d'oxydes de vanadium, le dioxyde de vanadium ( $\text{VO}_2$ ) a été le plus étudié théoriquement et expérimentalement, en raison du fait que sa MIT se produit pour des températures proches de la température ambiante. En tenant en compte l'effet d'hystérésis de la transition de phase de  $\text{VO}_2$ , Ordonez-Miranda *et al.* [Ord18b] a étudié une diode thermique conductive à géométrie plane entre une borne constituée de  $\text{VO}_2$  et d'une autre composée d'un matériau ne présentant pas de changement de phase. Les auteurs ont établi que le principal paramètre nécessaire à la réalisation de la rectification thermique est le contraste de conductivité thermique du PCM. Suivant cette idée, le but de cette thèse est d'étudier différentes géométries et configurations de matériaux pour analyser et optimiser la rectification thermique d'une diodes thermiques conductive ou radiative à base de  $\text{VO}_2$ , PE et GST.

La thèse est structurée et organisée en quatre chapitres, qui sont rapidement décrits ci-dessous:

- Dans le premier chapitre de cette thèse, nous avons décrit les mécanismes fondamentaux du transfert de chaleur, ses différents modes: conductifs et radiatifs (champ lointain et proche). Dans ce contexte, nous avons discuté du rayonnement corps noir. Ces concepts de base sont importants pour comprendre le taux de transfert de chaleur entre les matériaux solides. Nous expliquons le concept de rectification thermique et celui de composants thermiques tel que les diodes thermiques. Nous introduisons également les notions de conductivité

thermique, émissivité effective et de résistance thermique d'interface (ITR), qui sont les principaux facteurs qui influent sur les échanges thermiques. Nous avons décrit des matériaux très prometteurs (thermochromiques et PCM) que nous utiliserons dans la suite pour redresser les courants de chaleur. Un accent particulier est mis sur le  $\text{VO}_2$ , en raison du fait que sa MIT se produit à une température proche de la température ambiante. De plus, nous expliquons la MIT du  $\text{VO}_2$ , et discutons qualitativement sur le mécanisme conduisant à la transition de phase. Enfin, nous avons discuté de différentes applications possibles pour  $\text{VO}_2$  ainsi que de différentes techniques de dépôt de couches minces.

- Le deuxième chapitre est consacré à l'étude des effets géométriques d'une diode thermique conductive basée sur l'utilisation d'un PCM où les flux de chaleur obéissent à la loi de Fourier. Ici, nous analysons les travaux précédents d'Ordonez-Miranda pour les étendre à d'autres géométries. Nous obtenons et analysons des expressions analytiques simples pour les profils de température, les flux thermiques et le facteur de rectification optimal des deux géométries de diodes conductive en régime permanent. Nous démontrons que le changement de géométrie a un fort impact sur les températures et les flux de chaleur, mais pas tant sur le facteur de redressement de la diode.

- Le troisième chapitre comprend l'étude détaillée des diodes thermiques conductive entre deux PCM dont les conductivités thermiques varient significativement en fonction de la température. Nous considérons ainsi un système plan de deux PCM échangeant de la chaleur dans un état stationnaire en raison de leurs différences de température. Encore une fois, grâce à la loi de Fourier, des expressions analytiques explicites et simples sont établies et évaluées numériquement pour les flux thermiques, les profils de température et le facteur de rectification optimal. Nous montrons que l'optimisation du

facteur de redressement de la diode thermique conductive nécessite un saut de température élevé à l'interface de ses bornes, pour une ITR donné. Nous rapportons que l'effet combiné de deux PCM devrait générer des facteurs de redressement plus élevés que pour une diode thermique basée sur l'utilisation d'un seul PCM. Ce fait indique que deux PCM pourraient également être utilisés pour optimiser le facteur de rectification des diodes thermiques radiatives, ce qui n'est pas encore rapporté dans la littérature, à notre connaissance, comme présenté au chapitre 4.

- Dans le quatrième chapitre, nous décrivons une diodes thermiques radiatives en champ lointain dans les géométries plan, cylindrique et sphérique basées sur deux PCM. Nous obtenons et analysons l'expression analytique du facteur de rectification optimal des trois géométries de diodes. Nous démontrons que le changement de géométrie a un impact significatif sur les facteurs de rectification optimaux. Nous montrons que la combinaison de deux PCM peut générer des facteurs de redressement plus élevés, comme indiqué pour la diode thermique conductive au chapitre 3.

La conclusion générale présente un résumé du travail ainsi que les différentes perspectives.

Chapter 1



## Chapter 1

---

# The theory of heat transfer in solid materials

### Contents

---

<b>1.1</b>	<b>Introduction</b> . . . . .	<b>13</b>
1.1.1	Heat equation . . . . .	14
1.1.2	Conductive heat transfer . . . . .	14
1.1.3	Radiative heat transfer . . . . .	16
1.1.4	Radiative heat transfer in Blackbody . . . . .	17
1.1.5	Far and Near-field radiative heat transfer . . . . .	19
<b>1.2</b>	<b>Thermal components</b> . . . . .	<b>22</b>
1.2.1	Thermal diode and rectification factor . . . . .	22
1.2.2	Thermal conductivity . . . . .	23
1.2.3	Effective emissivity . . . . .	24
1.2.4	Interface thermal resistance . . . . .	25
<b>1.3</b>	<b>Thermochromic materials: so-called "smart" materials</b> . . . . .	<b>26</b>
1.3.1	Phase-change materials . . . . .	27
<b>1.4</b>	<b>A review of VO<sub>2</sub></b> . . . . .	<b>29</b>
1.4.1	Properties of vanadium oxides . . . . .	30
1.4.2	The MIT of VO <sub>2</sub> . . . . .	30
<b>1.5</b>	<b>The elementary mechanism of MIT</b> . . . . .	<b>33</b>
1.5.1	Percolation process during the MIT of VO <sub>2</sub> . . . . .	37
<b>1.6</b>	<b>Crystallography Structure of VO<sub>2</sub></b> . . . . .	<b>37</b>
1.6.1	Energy Band Structure of VO <sub>2</sub> . . . . .	40

1.6.2	Optical properties of VO <sub>2</sub> . . . . .	41
1.6.3	Mechanical properties of VO <sub>2</sub> . . . . .	44
1.6.4	The excitation of the MIT of VO <sub>2</sub> . . . . .	46
<b>1.7</b>	<b>Applications of VO<sub>2</sub></b> . . . . .	<b>47</b>
1.7.1	Thermal sensor MIT in VO <sub>2</sub> thin film . . . . .	48
1.7.2	Memristor devices using the MIT of VO <sub>2</sub> . . . . .	51
1.7.3	Three-terminal field effect transistor switches utilizing the MIT of VO <sub>2</sub> . . . . .	53
<b>1.8</b>	<b>The deposition techniques of VO<sub>2</sub> thin film</b> . . . . .	<b>55</b>
1.8.1	Chemical vapor deposition . . . . .	55
1.8.2	Sol-gel Technique . . . . .	57
1.8.3	Pulsed laser deposition . . . . .	58
<b>1.9</b>	<b>Conclusions</b> . . . . .	<b>60</b>
<b>1.10</b>	<b>Résumé du chapitre 1</b> . . . . .	<b>62</b>

---

## 1.1 Introduction

Heat transfer in a given system can be defined as the transfer of thermal energy between two physical systems due to a spatial difference in temperature between them [Ber11]. This process can occur in solids, liquids or gases. The transfer of energy flows from the medium with higher temperature to the medium with the lower one, hence follow the well-known laws of thermodynamics. However, the rate of heat transfer also depend on the properties of the interacting medium through which the heat is transferred. Heat transfer is commonly applied in our everyday life ranging from biological processes to industrial systems in macro, micro and nanoscale. Heat transfer can occur through three different modes: conduction, convection and radiation. The transfer of heat that occurs between a stationary medium due to temperature gradient is referred to as conduction. At a microscopic level, conduction may be seen as the transfer of energy in steps by successive shocks between neighboring heat carriers. The heat carriers which ensure exchange by conduction vary according to the type of materials. For example, atoms and molecules dominate in gases, electrons dominate in metals while phonons contributed largely to the exchange in the dielectric. For convection, the heat transfer is between a surface and a moving fluid when they are at different temperatures, but it is actually a conductive process in a fluid layer named boundary layer. On the other hand, radiation is the type of heat transfer that occurs due to the emission and absorption of electromagnetic waves between two systems, and propagating in vacuum. Given that every bodies at a finite temperature emit energy in form of photons, therefore, even without any intervening medium, heat transfer due to radiation often occurs between bodies at different temperatures. This fact indicates that thermal radiation is a ubiquitous physical phenomenon and its understanding is particularly vital for many different technologies [How10; Mod13; Zha07].

### 1.1.1 Heat equation

Heat equation is a diffusion equation that can be obtained by considering microscopic heat carriers [Ein05]. The general heat equation gives the temporal variation in the temperature of a system by considering the different fluxes exchanged within its environment and any internal thermal sources. For instance, these sources could be the joule effect or a chemical reaction in combustion. The heat equation reads mathematically as follow:

$$\rho C_p \frac{\partial T}{\partial t} = \phi + Q, \quad (1.1)$$

where  $\rho$  is the density of the system,  $C_p$  is the specific heat,  $T$  is the temperature,  $t$  is the time,  $Q$  is the quantity of heat per unit volume generated by any internal sources and  $\phi$  is all the densities of heat fluxes exchanged. Heat exchange can occur through these three transfer modes: conduction, convection and radiation. However, for the sake of this thesis, we will focus on conductive and radiative heat transfers, respectively.

### 1.1.2 Conductive heat transfer

Conductive heat transfer (CHT) is the process in which heat is being transferred by means of molecular excitation within materials excluding the bulk motion of the matter. This phenomenon occurs in gases and liquids as a result of diffusion and collisions of the molecules during their random motion. Besides, CHT takes place in solid materials due to the combination of lattice vibrations of the molecules and the energy transport by free electrons.

In order to examine the problem of CHT, we will look at its thermal and geometrical properties. Let us consider a one-dimensional plane system separated by a thickness  $L$ , exchanging heat through steady-state conduction due to their

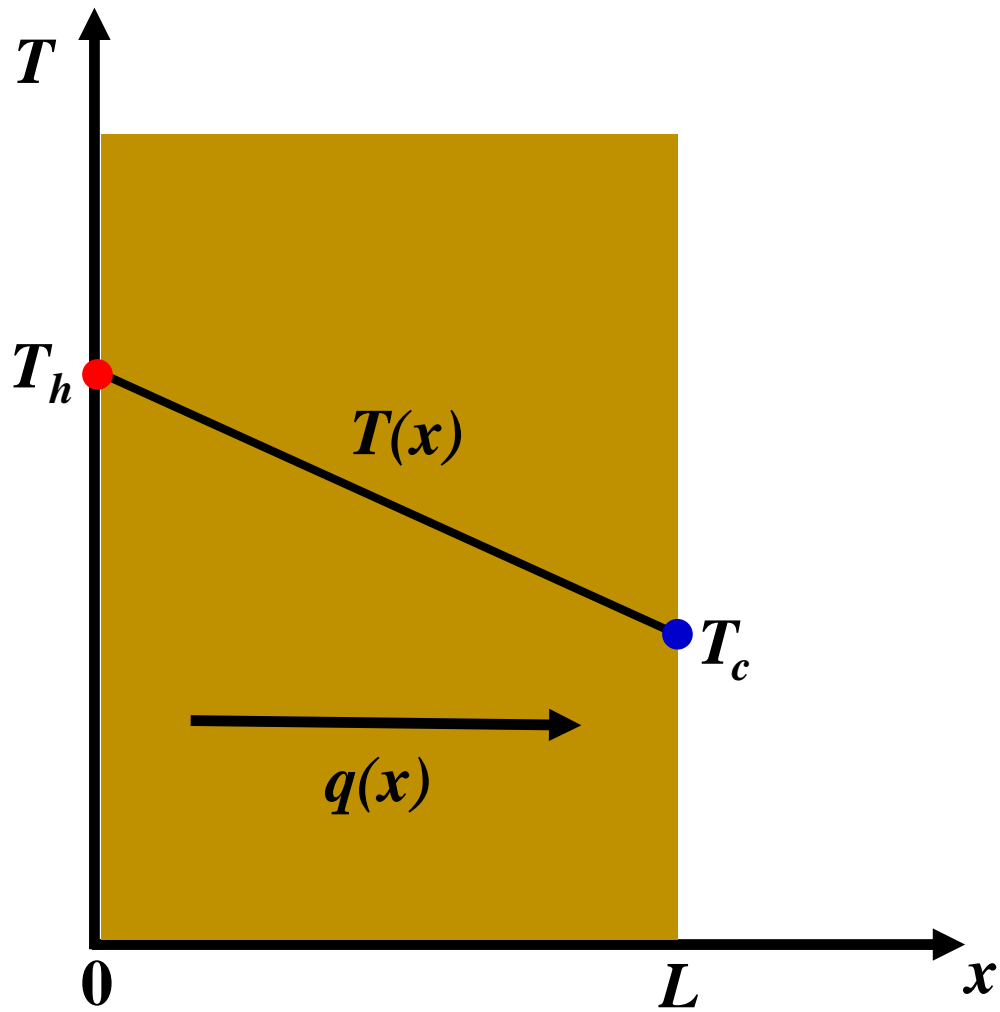


FIGURE 1.1: Scheme of a one-dimensional heat conduction situation.

temperature difference  $T_h > T_c$ , with a temperature profile  $T(x)$  inside the system as shown in Figure 1.1. According to Fourier's law, the heat flux is proportional to the temperature gradient, is given as follows:

$$q \propto -A \frac{dT}{dx}, \quad (1.2a)$$

$$q = -\kappa A \frac{dT}{dx}, \quad (1.2b)$$

where  $\kappa$  is the thermal conductivity of the medium in which the heat transfer takes place,  $A$  is the area of the conducting surface and  $dT/dx$  is the temperature gradient. The negative sign in equations (1.2a) and (1.2b) indicates that the heat

is transferred in the direction of decreasing temperature. By applying separation of variable method and integrating from  $x = 0$ , equation (1.2b) becomes

$$q = -\kappa A \frac{T(x)}{L}, \quad (1.3)$$

where  $T(x)$  is the temperature profile and  $L$  is the thickness of the plane system. By properly using the following boundary conditions:  $T(0) = T_h$  and  $T(L) = T_c$ , the heat flux in equation (1.3) is given as

$$q = \kappa A \frac{T_h - T_c}{L}. \quad (1.4)$$

Note that equation (1.4) is the heat rate by conduction in  $W$  through a plane system and is different than that of the rate of heat transfer per unit area. Note also that the latter equation can be applied in the case of the spherical and cylindrical geometries. The two latter geometries will be discussed in details in chapter 2.

### 1.1.3 Radiative heat transfer

All bodies set at a given temperature emit energy in the form of electromagnetic waves or photons. Therefore, even without an intervening medium, heat transfer will always occur via thermal radiation between bodies at different temperatures. This makes radiative heat transfer (RHT) of great interest for numbers of application in different areas of science and engineering [Pal85; Roh98; Mod13; Ber11]. In contrary to other two types of the fundamental mode of heat transfer, RHT is not proportioned to the temperature gradient but rather its temperature difference. It also depends on the wavelength of the considered radiation and on the properties of the involving materials during the heat transfer process.

### 1.1.4 Radiative heat transfer in Blackbody

A blackbody is often considered as an ideal surface or volume that absorbs all the incident radiation at any wavelength and direction. At thermal equilibrium, no surface can emit a higher quantity of energy than a blackbody at any given wavelength and temperature. The radiation emitted by a blackbody is a function of wavelength and temperature. It is independent of direction, so that the blackbody is a diffuse emitter, also called a Lambertian emitter where its specific intensity is isotropic. Given that a blackbody is a perfect absorber and emitter, it is served as a standard in which the properties of other radiating surfaces could be compared.

The traditional origin to understanding blackbody radiation is based on Planck's law [Pla14], which states that a blackbody is an object that absorbs all the radiation with respect to the distribution of the body's temperature. Over the last centuries, scientists have been trying to perfectly predict the electromagnetic spectrum of the blackbody emission. In this quest, Wien performed a few experiments alongside the law of thermodynamics to demonstrate that large part of the spectral distribution of the blackbody emissive power is accurately correct. Based on the spectral distribution of the blackbody emissive power, Lord Rayleigh and Sir Jeans assumed that the equipartition theorem is valid and derived the equation for the blackbody emissive power [Ser04; How10]. They found out that the mean energy of an oscillator of temperature  $T$  is independent of the frequency and equal to  $\kappa_B T$ , where  $\kappa_B$  is the Stefan-Boltzmann constant. They also proposed that the classical physics can be used to generate an equation which describes the intensity of blackbody radiation, as functions of frequency at constant temperature, which is known as Rayleigh-Jeans law. However, the law

did not work at high frequency since the energy diverges, this is known as the ultraviolet catastrophe or Rayleigh-Jeans catastrophe. After Rayleigh-Jeans ultraviolet catastrophe, Planck [Pla14] explained the blackbody radiation in 1900, he introduced the concept of quanta by assuming that the energy in a given frequency mode can only be proportional to integral multiples of the frequency. This correct spectral emissive spectrum power of a blackbody proposed by Planck can be defined mathematically as [Pla14; Mod13; Ber11]:

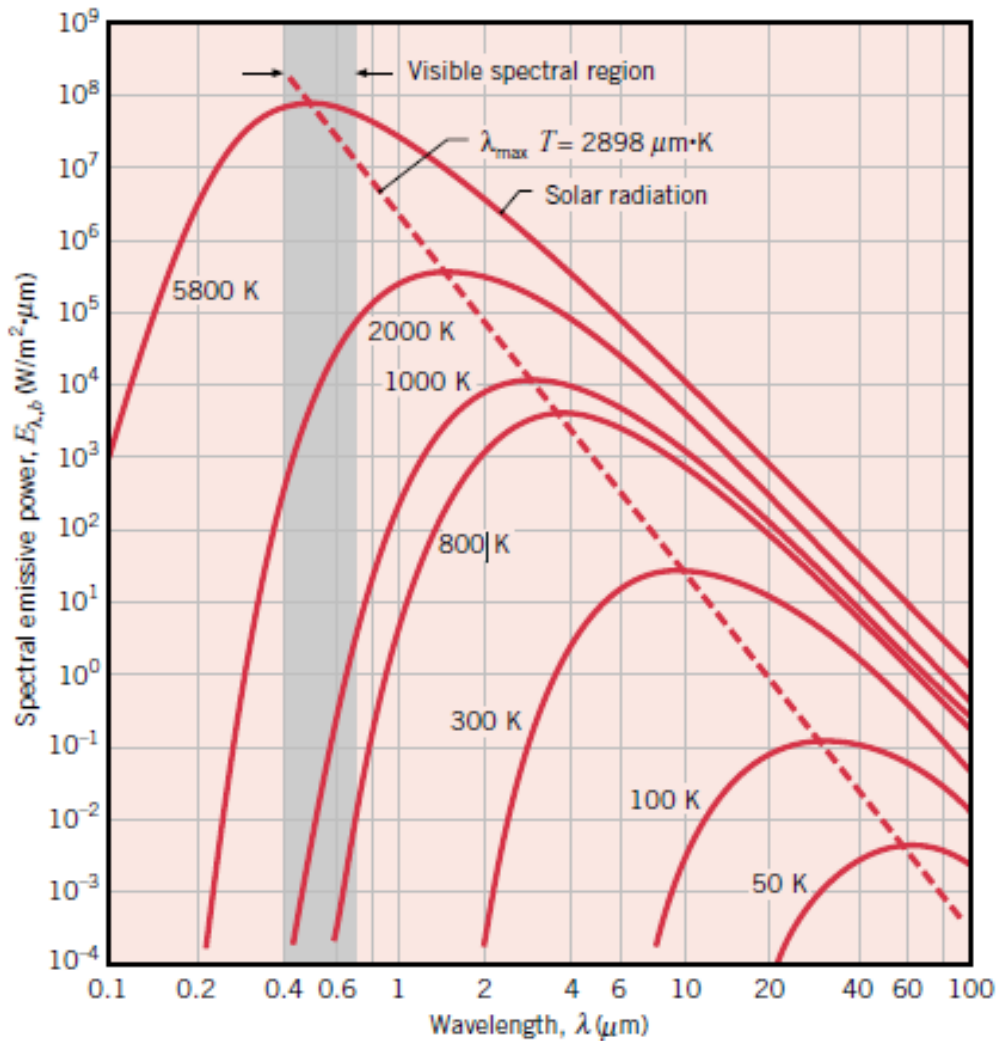


FIGURE 1.2: Spectral emissive power of a blackbody [Inc96].

$$E_{\lambda,b}(\lambda, T) = \frac{2hc^2}{\lambda^5 \left[ e^{\frac{hc}{\kappa_B \lambda T}} - 1 \right]}, \quad (1.5)$$

where  $c = 2.998 \times 10^8 \text{ m/s}$  is the speed of light,  $E_{\lambda,b}(\lambda, T)$  is the intensity of the blackbody,  $\kappa_B = 1.38 \times 10^{-23} \text{ J/K}$  is the Stefan-Boltzmann constant and  $h = 6.626069 \times 10^{-34} \text{ J.s}$  is the Planck constant. The emissive power of blackbody is described as  $e_{\lambda,b}(\lambda, T) = \pi E_{b,\lambda}(\lambda, T)$ . The integration of the aforementioned emissive power for the whole spectrum yields the well-known Stefan-Boltzmann law's law of far-field thermal radiation as  $e_b = \sigma T^4$ , with  $\sigma = 5.67 \times 10^{-8} \text{ W/(m}^2\text{K}^4)$ . The wavelength  $\lambda_{\text{max}}$  at which the emitted power of blackbody is maximum, is given by

$$\lambda_{\text{max}} = \frac{C_1}{T}, \quad (1.6)$$

where  $C_1 = 2898 \mu\text{m K}$  is the radiation constant. Equation (1.6) is called the Wien's displacement law, which relates the thermal emission wavelength and medium temperature. The combination of equations (1.5) and (1.6) yields the spectral emissive power as functions of thermal wavelength as shown in Figure 1.2. It can be seen that the power increases as Wien's displacement reduces with temperatures.

### 1.1.5 Far and Near-field radiative heat transfer

A typical RHT phenomenon is the study of thermal energy transfer between two bodies with different emissivities and temperatures, separated by a vacuum gap of distance  $d$ . RHT between two semi-infinite bodies classically depends on the materials optical properties rather than the vacuum gap between them. There are two types of RHT as shown in Figure 1.3: (i) Far-field radiative heat transfer (FFRHT) and (ii) Near-field radiative heat transfer (NFRHT). The former is when the heat transfer between the two bodies is separated by a vacuum gap of distance  $d$  that is far greater than the thermal wavelength ( $d \gg \lambda_{\text{th}}$ ), therefore the main contribution to the heat transfer is only via the propagative waves.

The evanescent waves emanated in the vacuum gap due to total internal reflection (TIR) when the angle of incidence is greater than the critical angle decay exponentially and as a result are not able to tunnel through the second bodies, therefore do not contribute to the heat transfer (no photon tunnelling). On the other hand, evanescent waves tunnelling is possible when  $d \ll \lambda_{\text{th}}$ , hence, they contribute significantly to the RHT, and as a result, the heat transfer limitation between two blackbodies in the far-field can be overcome.

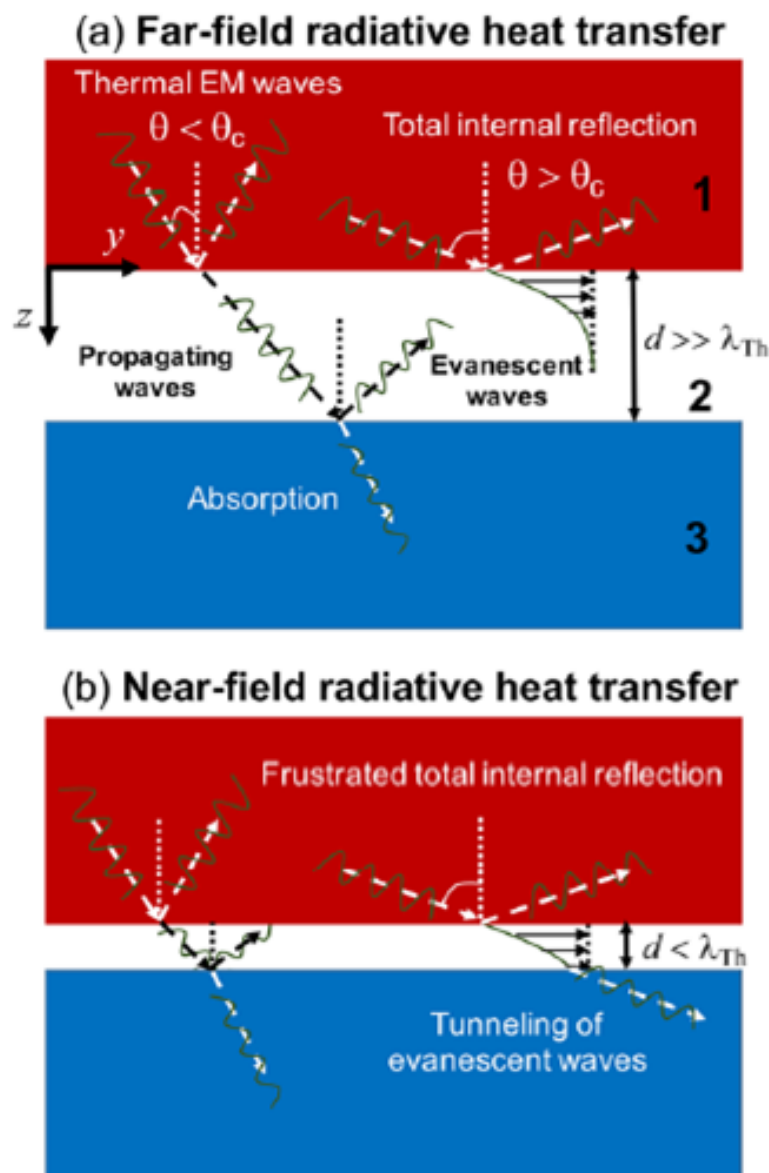


FIGURE 1.3: Scheme of (a) far-field and (b) near-field radiative heat transfer [Bie20].

For the FFRHT, classical theory can be used to calculate the heat flux, given

that  $d \gg \lambda_{\text{th}}$ . For example let us consider a system of two bodies separated by a vacuum gap of distance  $d$  with effective emissivities given as  $\varepsilon_1$  and  $\varepsilon_2$  at temperatures  $T_c$  and  $T_h$ , with  $T_h > T_c$ , respectively. According to [Inc96], when the two bodies are considered as perfect absorbers (blackbodies), the radiative heat flux becomes maximum and can be described by Stefan-Boltzmann law of thermal radiation as

$$q = \sigma(T_h^4 - T_c^4), \quad (1.7)$$

where  $\sigma = 5.67 \times 10^{-8} \text{ Wm}^{-2}\text{K}^{-4}$  is the Stefan-Boltzmann constant. On the contrary, for real opaque bodies, equations (1.7) can be described, as follows [Inc96]:

$$q = \sigma\varepsilon_{12}(T_h^4 - T_c^4), \quad (1.8)$$

where  $\varepsilon_{12}$  is effective emissivities of the two bodies. We have presented more details about FFRHT in chapter 4. For the NFRHT, on the other hand, the classical theory is not applicable, since both propagative and evanescent waves contributed to the RHT. Fluctuation electrodynamic (FE) is the theory that has been used to calculate the heat flux in the case of NFRHT. It is based on Maxwell equations and fluctuation-dissipation theorem (FDT). Basically, FDT gives the electric and magnetic fluctuating currents due to thermal fluctuation in the materials whereas Maxwell equation relates currents to the electromagnetic field and energy flux in a given geometry [Bas11; Bie18; Cha08b; Wan13; Shc00; Ben09; Bas09; Cra67; Pol71; Yan13; Van12; Gu15; Vol07; Nar08; Son15].

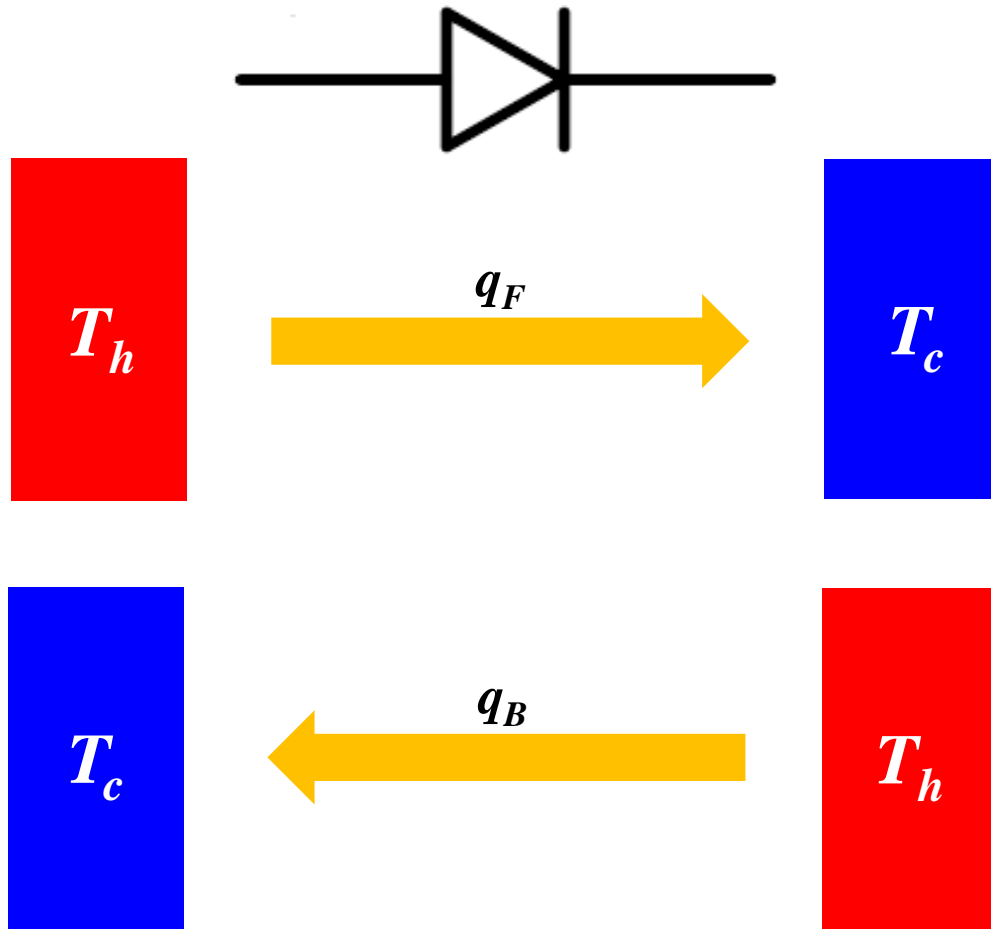


FIGURE 1.4: Scheme of a thermal diode operating in the (a) forward and (b) backward configurations.  $T_h$  and  $T_c$  denotes hot and cold temperatures respectively.

## 1.2 Thermal components

### 1.2.1 Thermal diode and rectification factor

A device that rectifies the magnitude of the heat flux is called a thermal diode, which allows larger heat flux in the forward configuration than that in the backward one at the same temperature difference as shown in Figure 1.4. In the case of electronic diode counterpart, electric rectification is such that the absolute value of the electric flux differs by reversing the potential difference applied to each terminal. The ability of this thermal diode to transport heat along a preferential direction can be quantified by a factor which relates the ratio of the heat fluxes in the forward and backward configurations, is referred to as rectification

factor. The rectification factor  $R$  of a thermal diode represents its ability to switch on and switch off heat fluxes and can be defined in this thesis, as follows [Kas19]:

$$R = \frac{|q_F - q_B|}{\max(q_F, q_B)}, \quad (1.9)$$

where  $q_F$  and  $q_B$  are the magnitudes of the heat fluxes at the initial state and when their temperatures are reversed. Equation (1.9) establishes that a nonzero rectification is achieved when the reversal of the temperature gradient induces not only the inversion of the heat fluxes direction but also a significant variation of their magnitudes. Optimal rectification ( $R = 1$ ) is reached when one of the heat fluxes is zero.

### 1.2.2 Thermal conductivity

Thermal conductivity often denoted by the symbol  $k$  is the ability of a material to conduct or transfer heat. Higher thermal conductivity generates larger thermal flux inside the material. Materials with high thermal conductivity are utilized in heat sinks while materials with low one are used as a thermal insulator. Thermal conductivity of a material is temperature-dependent and its reciprocal is thermal resistivity [Hua17]. The thermal conductivities of PCMs employed throughout this thesis can be described according to Ordonez-Miranda *et al.* [Ord18b], as follows:

$$\kappa_n(T) = \kappa_{in} + \frac{\kappa_{mn} - \kappa_{in}}{1 + e^{-\beta_n(T-T_{0n})}}, \quad (1.10)$$

where  $\kappa_{mn}$  and  $\kappa_{in}$  are the thermal conductivities in their respective high- and low-temperature phases, and  $\beta_n$  is the phase-transition slope of  $\kappa_n(T)$  at the transition temperature  $T = T_{0n}$ , for  $n = 1, 2, 3$ , depending on the number of involving materials.

### 1.2.3 Effective emissivity

The ability of a real material to emit thermal radiation is evaluated relative to that of the blackbody. The latter is pure fictitious body allowing to obtain the basic laws of thermal radiation. It describes an ideal body whose electromagnetic waves depend only on its temperature, that is, a body which re-emits all of its energy at all wavelengths. On the other hand, real bodies re-emit a quantity of radiative energy that is always less than that of a blackbody at the same temperature. The emissivity of a material or surface can be defined as the ratio between the amount of energy emitted by the surface and that of the blackbody at the same temperature. The emissivity often denoted  $\varepsilon$ , thus provides information on the ability of a material to emit radiation. The emissivity does not have a standard unit and the value is between 0 and 1 ( $0 < \varepsilon < 1$ ). Of course, for a perfect blackbody, the value of emissivity is 1. Generally, emissivity depends on the wavelength and the direction of measurement of the radiation. If it is measured for a wavelength or a narrow band of wavelengths, it is referred to as a spectral emissivity, on the other hand, when measured for a direction of emission it is called a directional emissivity. Furthermore, emissivity also depends on the nature of the materials (smooth or rough) and their temperature. The effective emissivities of PCMs used throughout this thesis can be described, as follows [Ord19b]:

$$\varepsilon_n(T) = \varepsilon_{in} + \frac{\varepsilon_{mn} - \varepsilon_{in}}{1 + e^{-\beta_n(T-T_{0n})}}, \quad (1.11)$$

where  $\varepsilon_{mn}$  and  $\varepsilon_{in}$  are the emissivities in their respective metallic (high-) and insulator (low-temperature) phases, and  $\beta_n$  is the phase-transition slope of  $\varepsilon_n(T)$  at the transition temperature  $T = T_{0n}$ , for  $n = 1, 2, 3$  etc.

### 1.2.4 Interface thermal resistance

When two materials are brought into contact, the diffusing heat that occurs at the interface is called interface thermal resistance (ITR). This phenomenon results in the discontinuity of the temperature at the interface as shown in Figure 1.5. ITR is also known as Kapitza resistance, given that it was first reported in 1941 by Kapitza [Kap41] at the interface between a wall and a superfluid helium film. A temperature drop is indeed observed at the boundary between helium and solids when the heat flows across the boundary [Swa89]. After a decade, Khalatnikov [Kha18] reported a model known as the acoustic mismatch model (AMM) to further explain that the thermal boundary resistance takes place at these interfaces. This Kapitza resistance is of first importance for heat transfer problems in many sciences and engineering applications and it can be defined as a function of the temperature difference between two sides of interface and the heat flow flowing through it. It can be mathematically described, as follows:

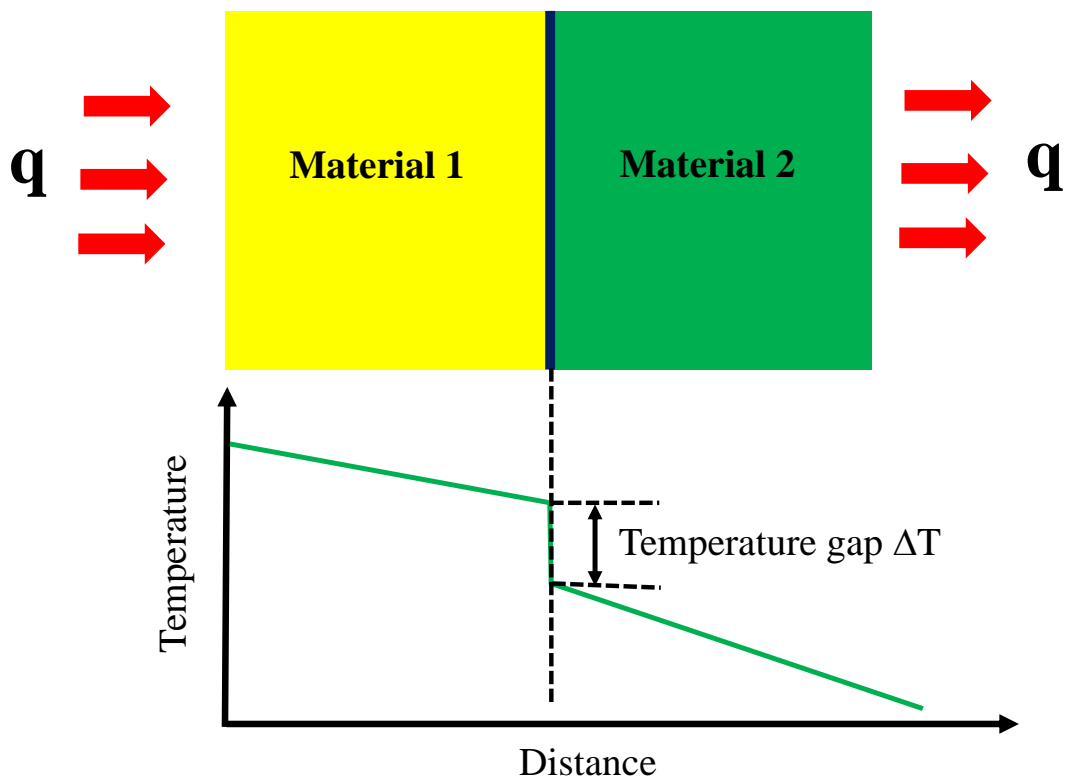


FIGURE 1.5: Scheme of a contact thermal resistance.

$$R = \frac{\Delta T}{q}, \quad (1.12)$$

where  $q$  is the density of the heat flux across the interface and  $\Delta T$  is the temperature difference between the two sides of the interface.

In order to design and optimize the heat transfer between two bodies, in this thesis, we have considered a phase transition materials, hence, it is important to discuss these very promising materials exhibiting phase change such as thermochromic materials and PCMs that has been recently proposed to designed and optimized thermal transfer devices. More recently, the study of these unique materials offers prospects of developing a novel kind of electronics with advanced functionality and advancing fundamental science and technology. The aforementioned materials have been detailed below:

### **1.3 Thermochromic materials: so-called "smart" materials**

The so-called smart materials are materials that have the capability to receive certain information from their environment and interact with this environment significantly by changing their optical, electrical and thermal properties due to exposure to external stimuli. For instant, thermochromic materials exhibit phase transition from low-temperature insulating phase to high-temperature metallic one. In this context, it implies that the materials receive thermal information from its environment and generates an optical response in the same environment. This kind of materials properties can be used to perform tunable functions similar to the ones achieved by using semiconductor or memory devices. On the other hand, unlike the latter, the desired function is being performed at the

level of the materials by a simple integration, which results in a system with increased compactness. Due to their diversification, it is complicated to achieve a precise classification of these intelligent materials. However, for the sake of this thesis, we will focus on materials with tunable conductivity. There are two main types of element that exhibit tunable components based on a change in thermal conductivity, but in this thesis, we will focus on the phase change ones.

### 1.3.1 Phase-change materials

PCMs are strongly correlated materials, that is to say, materials with strong electronic interactions. They represent a promising path for the optimizing of devices where tunability is based on variations of their conductivity. These materials contain certain atomic orbitals, especially those of type  $d$ , which generates the formation of narrower bands of energy that are filled and close to the Fermi level, generating, therefore, very strong electronic interactions. Furthermore, the free electron model, which is applied to the case of simple metals cannot be utilized, given that its assumption is based on the fact that electrons does not depend on one another. In order to shed more light on the behavior of these correlated materials, it is then vital to look into more complex theories like the Hubbard model, which proposed that electrons move from one atom of a transition metal to another without worrying about its environment (for example oxygen atoms). Under these conditions, this model considers that it is possible to determine the transport properties by only taking into account the competition between the propagation of electrons and the interaction between the lattice. Despite of this complexity, strongly-correlated materials are very interesting due to the fact that the interactions between their correlated electrons yields remarkable properties. These oxides, including vanadium family exhibit MITs, which are accompanied by a significant change in their thermal, optical and electrical properties, following the application of external stimuli such as,

temperature, electric fields and optical signals etc.

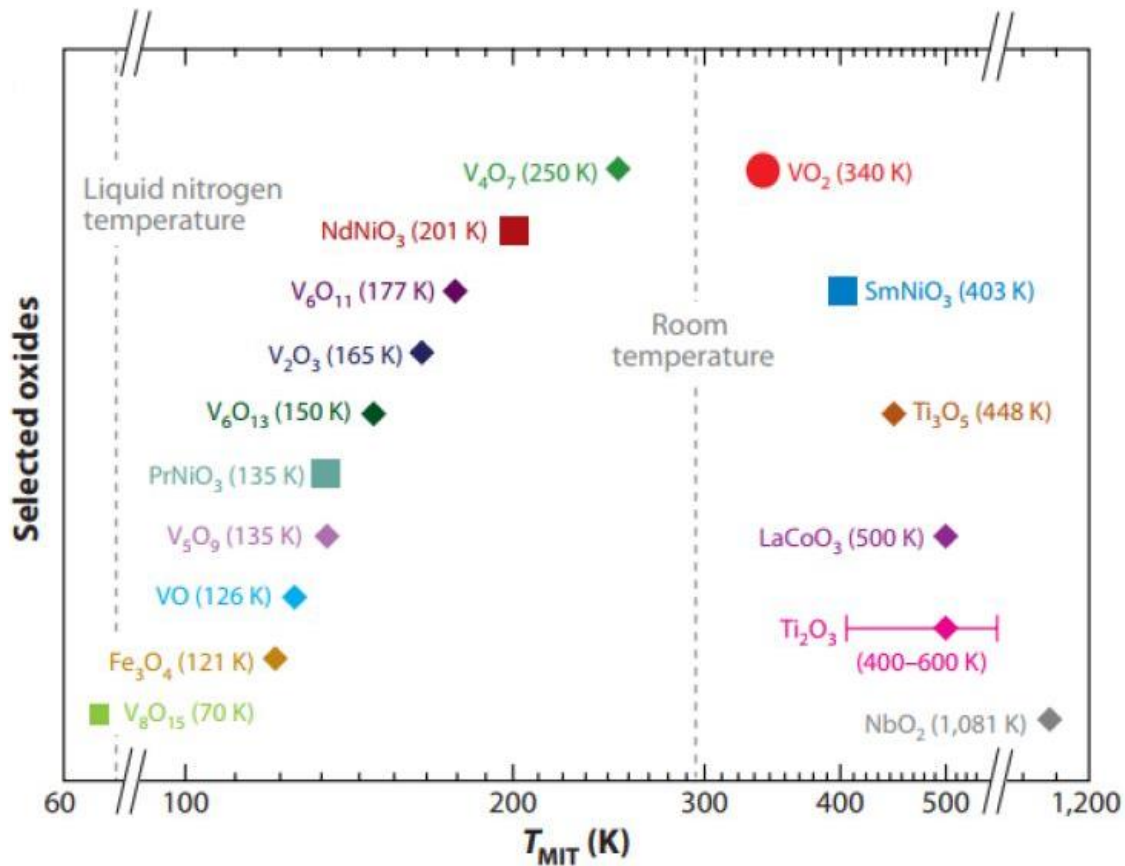


FIGURE 1.6: The MIT temperature of  $VO_2$  and some selected oxides [Yan11].

For smart materials mentioned above, the tuning ability was based on variations in a particular state, for instance, the variation in permittivity of the nematic state of liquid crystals. However, in the case of an oxide that undergoes a phase transition, one can use the conductivity variations which are observed during the MITs of the materials because they can both be rapid and huge. PCMs are characterized by their transition temperature as shown in Figure 1.6. It can be seen that there is a great diversity of metallic oxides that exhibits MITs with different values of transition temperature starting from 70 K for  $V_8O_{15}$ , to 1081 K, which is the characteristic transition temperature for  $NbO_2$ . Beside other tuning materials, tunable resistivity one can be utilized to generate several reconfigurable

systems, particularly, for the tunable filter, thermal switch, optical switch, memristors, power limiters etc. In order to discuss the phase transition and potential devices that could be realized, for the sake of this thesis, we will particularly emphasize on VO<sub>2</sub>, which undergo a sharp MIT at a temperature closer to room one.

## 1.4 A review of VO<sub>2</sub>

More recently, significant research interest has been given to the occurrence of phase transition from insulator to metallic in strongly correlated electron systems in condensed matter physics [Ima98]. The interest is strongly motivated due to the potential application of the materials exhibiting MITs in novel electronics [Lee07; Wan05; Chu02; New98]. Furthermore, particular interest has been given to understand the basic physics behind the strongly correlated electron behavior responsible for material striking characteristics such as MITs, orbital and charge ordering, high-temperature superconductivity, exotic magnetic, as well as colomagneto-resistance. Among the best known PCMs, VO<sub>2</sub>, discovered by Morin in 1959 [Mor59], is one of the most studied and applied one in both experimental and theoretical studies due to fact that its the most stable among vanadium families, and undergoes hysteretic MIT [Ord16; Jou15a; Lee17; Mor59; Zyl75] occurring in a narrow temperature interval around the critical temperature ( $T_0 \sim 342.5$  K) and extremely rapid optical switching upon the transition ( $\approx 100$ fs) [Cav04]. This solid phase transition thus results in significant changes in their electrical, optical, and thermal properties, which can be applied for a number of applications such as thermal rectifier [Ito14; Nas19; Hua13], thermal memories [Ito16], thermal memristors [Ben17; Ord19a], optical switching [Rin08], thermal switch [Gu15], radiative thermal diodes [Ben13; Nef14b; Ito14], hybrid-metamaterial [Dri08], thermal transistors [Ord16], and electrostatic devices [Qaz08b] operating in the near and far-field regions [Jou15a; Ben13; Ben14]. Its MIT around room

temperature can be modified by doping [Bro13; Lu96; Wan16; Pan16; Zha16]. The insulating monoclinic phase of VO<sub>2</sub> at low temperature change into metallic tetragonal one at high temperature [Qaz08a; Ord18a; Wan05]. The thinner film of VO<sub>2</sub> can provide much higher transmittance of visible light, but they suffer from an attenuation of the switching efficiency in the near-infrared region [Zha10]. At present time, there is no unified approach to interpret the electronic properties of the phase transition. The band and crystal field theory are the two limiting descriptions of the outer electrons in solids and the relevance of differences between metals and insulators can be understood in terms of these two models.

### 1.4.1 Properties of vanadium oxides

Vanadium oxides are among several materials that exhibit MIT. According to Chudnovskiy [Chu75], not more than 8 out of the sequences of oxides generated from vanadium oxides combine with oxygen in 2,3, 4 and 5 valent phase undergoes MIT. For instance, V<sub>2</sub>O<sub>3</sub> exhibit MIT at critical temperature  $T_c = 150\text{K}$  while that of VO<sub>2</sub> occurs at  $T_c = 300\text{K}$  with thermal conductivity changing by 4 orders of magnitude, respectively.

The phase diagram of Figures 1.7 shows that there are other stable vanadium oxide phases, for example, VO, V<sub>3</sub>O<sub>5</sub>, V<sub>4</sub>O<sub>7</sub>, V<sub>6</sub>O<sub>11</sub>, V<sub>6</sub>O<sub>13</sub>, V<sub>7</sub>O<sub>13</sub> and so on. However, the latter oxides do not have interesting phase transitions but their phase diagrams are similar to that of VO<sub>2</sub> and V<sub>2</sub>O<sub>3</sub>. On the other hand, the existence of their phases poses particular challenges to the growth of bulk and thin films of VO<sub>2</sub> [Sch04; Sch03; Ram05].

### 1.4.2 The MIT of VO<sub>2</sub>

The MIT of VO<sub>2</sub> and other vanadium oxides family especially V<sub>2</sub>O<sub>3</sub> have been known and studied for more than half a century [Mor59]. This phase transition is

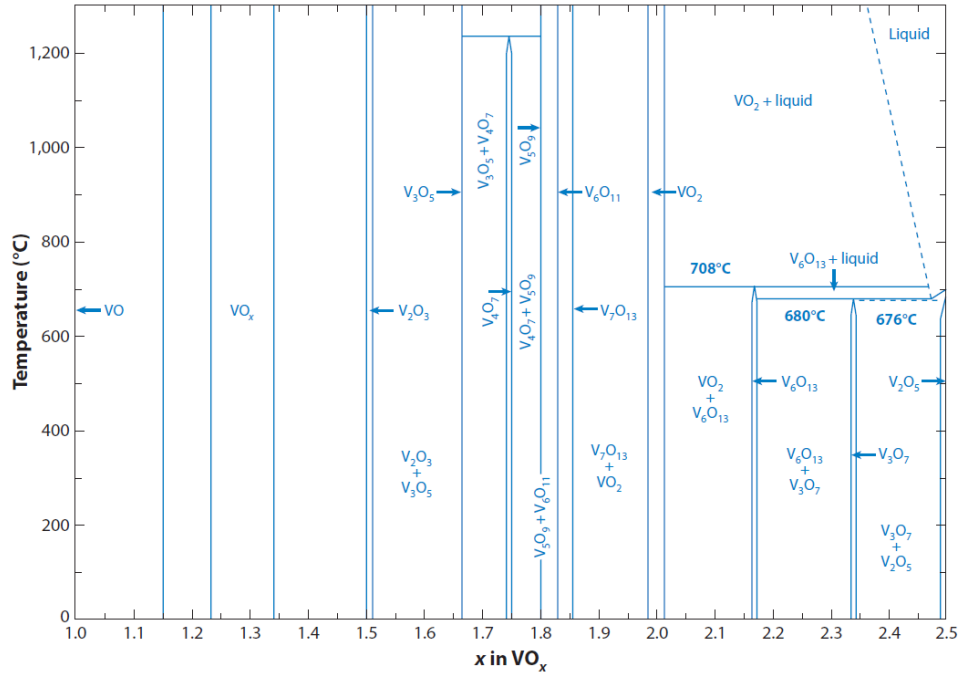


FIGURE 1.7: Phase diagram of the  $\text{VO}_x$  system [Yan11].

characterized by a subtle structural and conductivity changes that are up to several orders of magnitude occurring at a well-defined temperature. As discussed in the previous section, there are quite numbers of intermediate vanadium oxides and a few other transition metallic oxides that possess this property [Per13]. However,  $\text{VO}_2$  is the most studied one, given that its phase transition occurs around the temperature far closer to the ambient temperature, which implies that it is practically more easily accessible.  $\text{VO}_2$  phase transition can be triggered optically [Cav01; Cav04; Y03; Miy97; Fie98], thermally [Mor59; Per03], or electrically [Kim08; Kim04; Ste00; Y03; Asa97], and the efficiency of any device using such interactions is partly limited by the input energy to excite the transition, which is reduced by transitions that take place near the operating temperatures [Hor10; Whi11]. It is more convenient to operate any device at room temperature, instead of liquid nitrogen ( $\text{N}_2$ ) or Helium ( $\text{He}$ ) temperatures, which are commonly used in the laboratory but not easy to achieve in consumer products. For example, because thermochromic smart windows change their color and optical properties in response to temperature variations, commercial companies have recently used

the MIT of  $\text{VO}_2$  for the development of energy-efficient thermochromic window coatings [Bin07; Kam13; Gao12; Wu13]. Moreover, MIT of  $\text{VO}_2$  is accompanied by a significant transformation in its optical properties. As shown in Figure 1.8, the reflectivity of  $\text{VO}_2$  in the infrared (IR) region specifically increase significantly in the high-temperature tetragonal rutile phase. According to this property, coated windows allow more solar energy to pass through when the temperature is below the transition one while it reflects a larger part of the radiation when the temperature is above the transition, hence, creating a passive temperature mediation device. Given that it is preferable to work at a temperature closer to that of human body ( $< 68^\circ\text{C}$ ), dopants (typically W) are utilized to lower the transition temperature [Kam13].

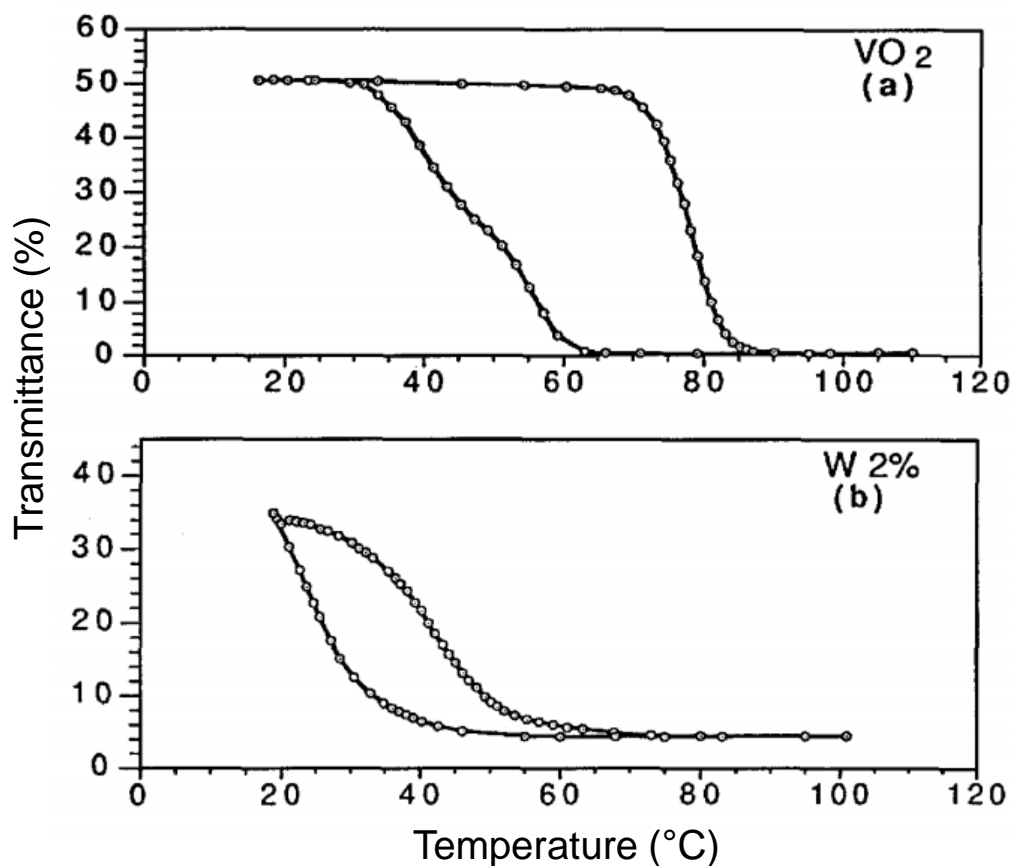


FIGURE 1.8: Temperature dependence of the infrared transmittance of (a) Undoped and (b) W-doped  $\text{VO}_2$  [Liv97].

The MIT of VO<sub>2</sub> can also be used in optical attenuators and shutters. The optical attenuators are the device used to protect sensors from saturating or damaged by intensities above the dynamic range of devices. The working principle of VO<sub>2</sub> IR attenuators is based on increasing their reflectivity as opposed to absorption at high incident intensities. The speed of this transformation is approximately 0.5ps, which makes VO<sub>2</sub> a promising material for the production of high-speed optical shutters in which a high-intensity writing beam triggers the transition and the IR beam reads the phase. Furthermore, these optical shutters are particularly vital as an element in most optical digital logic devices [Whi11; Lys06]. Even though the MIT of VO<sub>2</sub> has been known and studied for more than six decades, the exact physics behind its transition is still under debate [Per13; Whi11; Chu02]. So far, the only contested aspect in optical and electrical induced transition is whether or not the transition is field-induced as presented in gated silicon-based microelectronics or thermally induced by local heating from optical absorption and joule heating [Lys06; Whi11; Koz11]. Furthermore, possibilities of the mechanism under the understanding of the MIT in VO<sub>2</sub> are that of Mott-Hubbard and Peierls type [Nak97; Ric94; Mot04].

## 1.5 The elementary mechanism of MIT

### Mott Transition mechanism

The first theory which described the MITs is that of Mott in 1968, or more specifically Mott-Hubbard transition, which is based on purely electronic interaction [Mot68]. The phase transition occurs in certain materials called Mott insulators, once the charge carrier density is greater than the critical value. In this case, the interactions between the electrons due to the Coulomb repulsion energy ( $U$ ), becomes more vital than the interactions forming the electron-electron interaction effect, which causes delocalization of the electrons and behavior similar to that of metallic. The charge density which causes the material to have a metal-like

behavior is called the critical charge density  $n_c$  and can be mathematically described as follows [Mot68]:

$$n_c^{1/3} a_H = 0.2, \quad (1.13)$$

where  $a_H$  is the radius of the metallic atom, also known as the Bohr radius of the materials. Note that the Mott transition results in a significant change in the resistivity of the material at the macroscopic level. Mott-Hubbard-type MIT has also been demonstrated in the case of another vanadium oxides family;  $V_2O_3$ .

### **Peierls Transition mechanism**

The second theory describing the MITs is the Peierls mechanism [Pei96], which involves electron-phonon (electron lattice) interaction as shown in Figure 1.9. In this case, MIT is due to a change in the lattice structure of the material. The structural change results in a lattice deformation, which modifies the period ionic potential in the material and consequently generates a change in the band structure. At high temperature, materials responding to this mechanism are seen as structures in which the atoms are equidistant and where the thermal energy supplied allows the electrons to pass from one atom to another so that they behave like free electrons and the material has the characteristics of a metal. On the contrary, at low temperature, the crystal structure begins to change and the distance between the atoms varies. However, depending on its location, an electron needs more or less energy to move from one atom to another. The thermal energy at this stage is still enough to surpass any energy gap, while the material remains metallic. On the other hand, if the temperature decreases below a critical value, the energy becomes less strong, this generates to a localization of the electrons and the formed an insulating state, known as Peierls insulator.

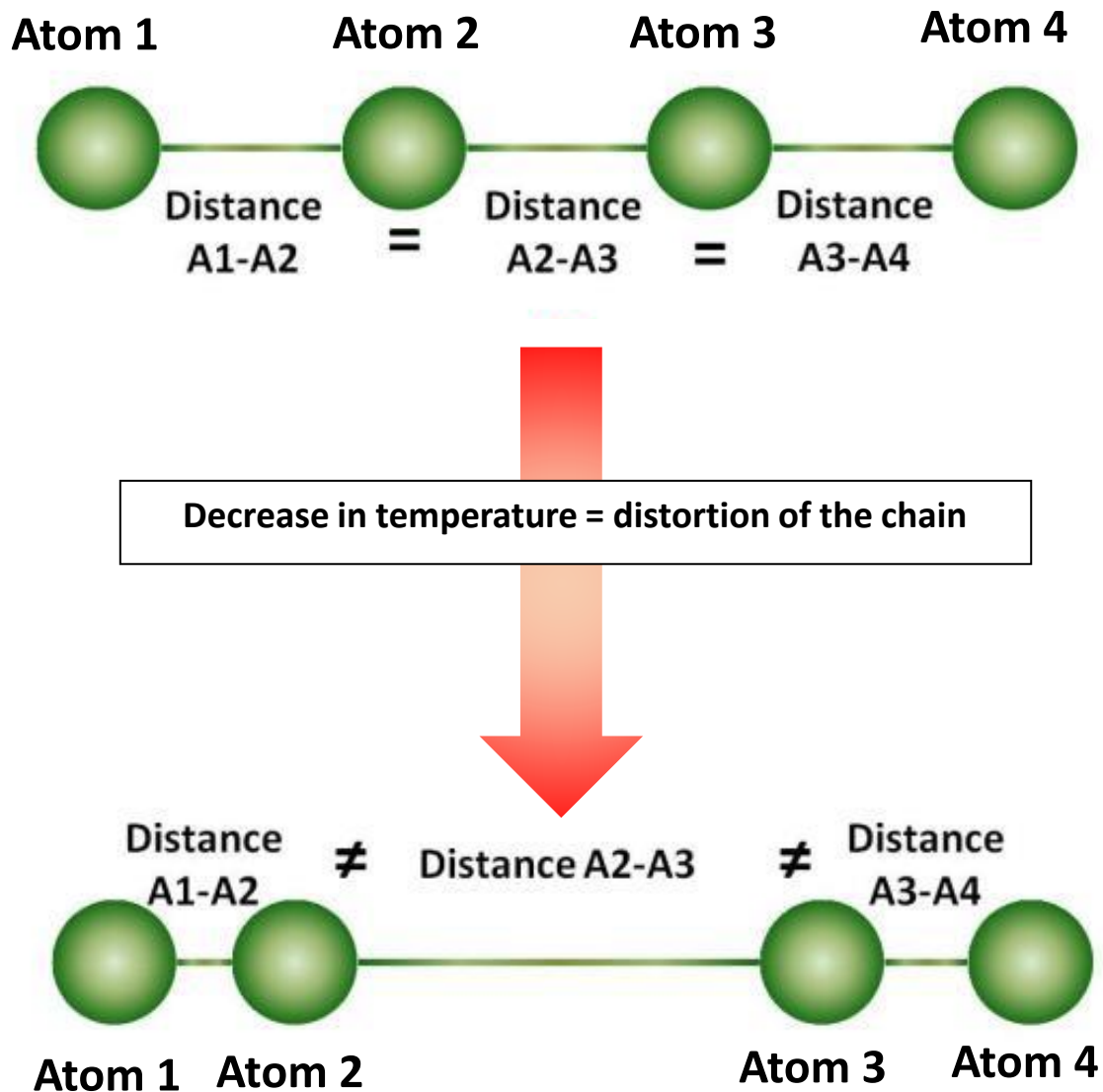


FIGURE 1.9: Scheme of a Peierls transition.

Basically, materials operating in this type of mechanism are difficult to recognise because, in addition to their MIT, they also exhibit a crystal phase transition. Among the metallic materials with these properties is the blue bronze ( $\text{K}_{0.3}\text{MoO}_3$ ) [Grü88], which exhibit a Peierls MIT at around 181K, with a change in thermal conductivity is accompanied by a structural one. Furthermore, the electron localization effect resulting from disorder can also lead to the Anderson [And58] and Bloch-Wilson insulator (also known as band insulator) mechanisms [Wil31]. The former mechanism applies to semiconductor materials that are heavily doped (eg., Si:P), hence, resulting in a significant disorder in their

structure and consequently a localization of the charge carriers. On the other hand, the latter mechanism occurs without the consideration of the electron-electron interactions. It's applicable to non-doped materials, such as, diamond and common undoped semiconductors, the metallization occurs due to a contraction of the volume which causes an overlap of the energy band gaps.

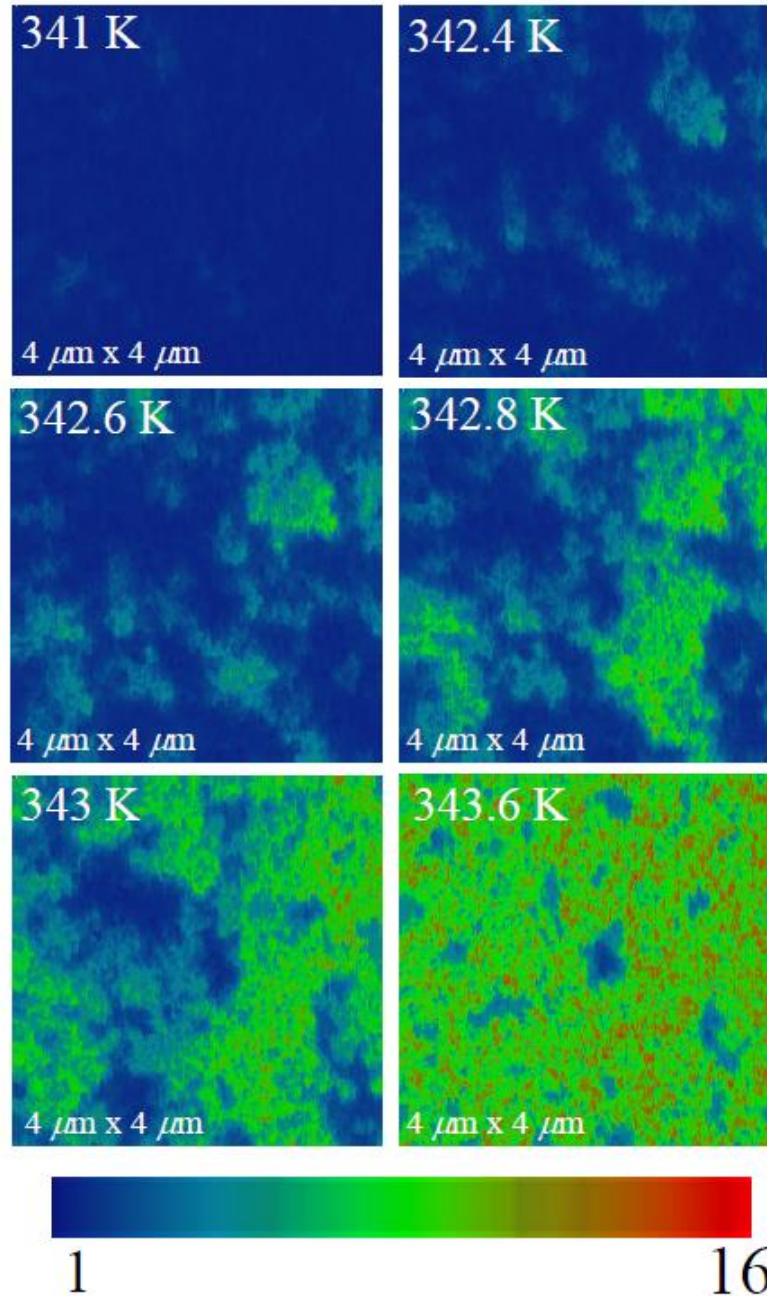


FIGURE 1.10: Images of a scanning near-field infrared microscopy of VO<sub>2</sub> film at different temperatures during its MIT process [Qaz07].

### 1.5.1 Percolation process during the MIT of VO<sub>2</sub>

Besides the origin of the mechanism discussed in the previous section, the physical evolution of the structural phases of VO<sub>2</sub> during its MIT is of particular importance. In 2007, Qazilbash *et al.* [Qaz07] proposed a very interesting study that allows one to understand the vital information regarding the evolution on the nanometric scale of VO<sub>2</sub> during the actualization in temperature of its MIT. The authors observed sample with a surface of 4 μm X 4 μm using a scanning near-field infrared microscopy, which allows them to directly image nano-scale metallic puddles that appear at the onset of the MIT as shown in Figure 1.10.

At 341K, the VO<sub>2</sub> film has a homogeneous surface (low amplitude) corresponding to an insulating phase (the blue color in Figure 1.10). As the temperature increases gradually, from 342.6K, zones of higher amplitude (green color) appear, which materialize the formation of the metallic phase in the initial insulating matrix. On the other hand, when the temperature increases, these metallic areas multiply and enlarge (green and red colors). Lastly, when the temperature approached 343.6K, the VO<sub>2</sub> film completely assumed the phase of a metal with little traces of the insulating phase. According to these results, the authors concluded that an insulating-metallic percolation mechanism appears during the MIT of the VO<sub>2</sub> film. This percolation phenomenon of the nanoscale insulating-metallic state is accompanied by a change in temperature of the resistivity of the film during its MIT and it will be able to explain some of the non-linear electrical phenomena of the current-voltage characteristics of VO<sub>2</sub> film.

## 1.6 Crystallography Structure of VO<sub>2</sub>

The thermal interaction between atomic structure, spin, charge and orbital dynamic influenced the phase transition observed in VO<sub>2</sub>. However, the interaction between the crystal structures and electronic degree of freedom pushes it into a

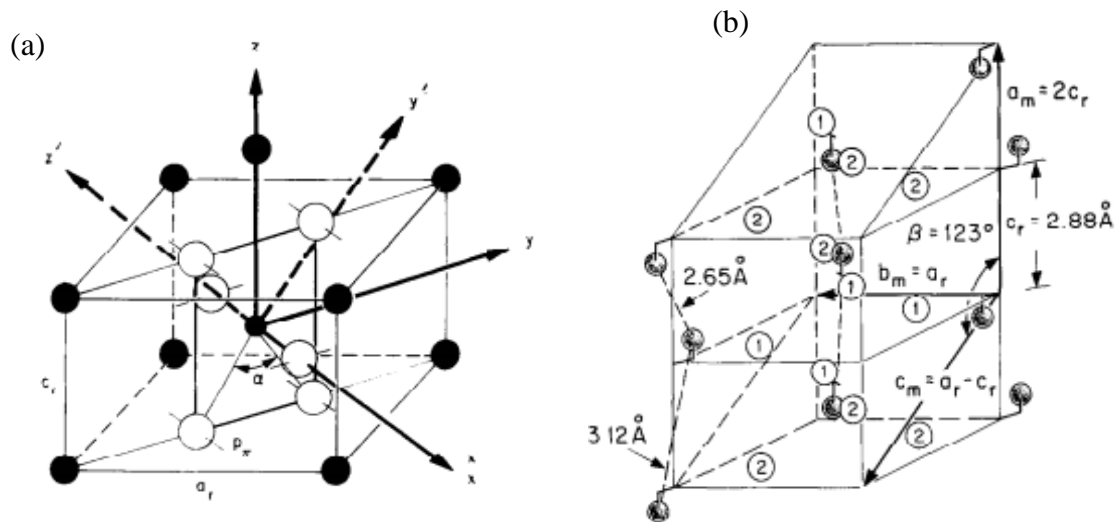


FIGURE 1.11: (a) Tetragonal  $P4_2/mnm$  high-temperature and (b) monoclinic ( $P2_1/c$ ) low-temperature structures of  $\text{VO}_2$  and its relation to the rutile structure [Goo71].

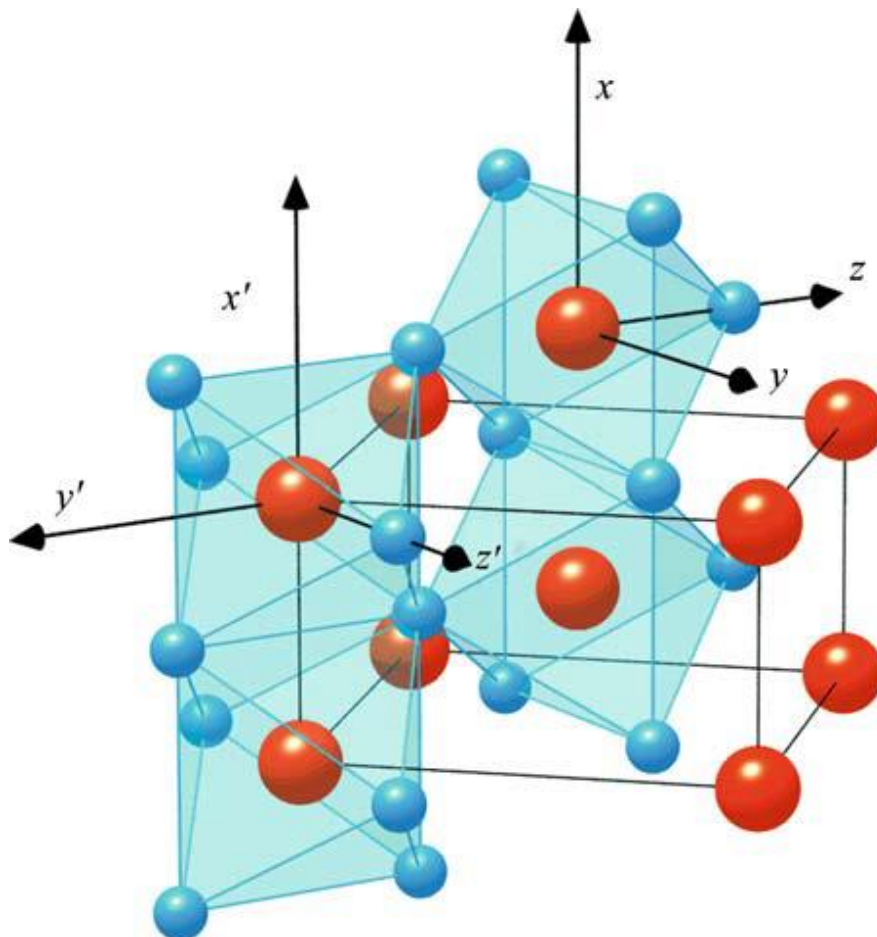


FIGURE 1.12: Tetragonal lattice structure of  $\text{VO}_2$  above the phase transition temperature. Large red spheres represent V ions while the small blue ones stand for O ions [Eye02].

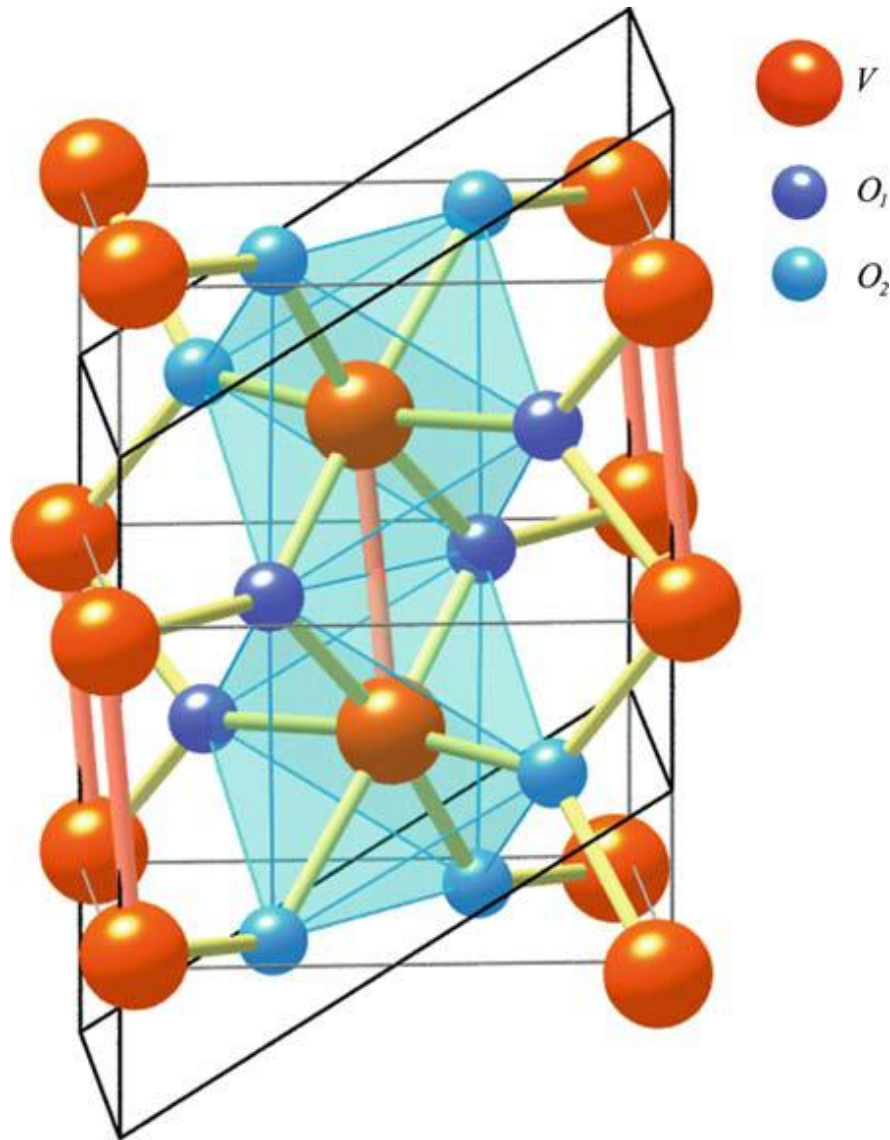


FIGURE 1.13: Low temperature monoclinic  $M_1$  lattice of VO<sub>2</sub> [Eye02].

critical phase where it exhibits a first-order transition from a low-temperature insulating phase to a high-temperature metallic one at a temperature close to room one ( $T \approx 342.5$  K). Due to this effect, there exist changes in its electronic band structure, which are related to the atomic arrangement between a more symmetric tetragonal ( $P4_2/mnm$ ) high-temperature phase to a less symmetric monoclinic ( $P2_1/c$ ) low-temperature one, as a result of dimerization of the V atoms [Goo71]. The properties of this monoclinic phase is the presence of two cation-cation along the  $a_m = 2c_r$  axis resulting to the doubling of the unit cell, which alternates the V-V separations being  $2.65 \text{ \AA}$  and  $3.12 \text{ \AA}$  instead of the consistence

2.88 Å spacing in the tetragonal phase as shown in Figure 1.11.

This is accompanied by a slight tilting with respect to the  $c_r$ -axis resulting in a short vanadium oxygen separation of  $R_{vo} = 1.76$  Å, perpendicular to the  $c_r$ -axis, the other cation-anion distances being around 2 Å. The distance between a cation and one or more anions is due to ferroelectric distortion, therefore, the driven mechanism responsible for this transition is known as anti-ferroelectric. Note that the VO<sub>2</sub> crystal structure is not the same in its insulator and metallic phases. The high-temperature metallic phase of VO<sub>2</sub> (rutile structure) is a tetragonal lattice as shown in Figure 1.12. It can be seen that the vanadium atoms are positioned at  $(0, 0, 0)$  and  $(1/2, 1/2, 1/2)$ , each of them is surrounded by an O octahedron. The oxygen atoms, on the other hand, are positioned at  $\pm(u, u, 0)$  and  $\pm(1/2 + u, 1/2 - u, 1/2)$ , where the lattice constant and other oxygen parameters are given as  $a_R = 4.5546$  Å,  $c_R = 2.8514$  Å, and  $u = 0.3001$  at 360 K [McW74; Eye02]. On the contrary, the low-temperature insulating phase of VO<sub>2</sub> is based on a monoclinic lattice (see Figure 1.13) with unit cell dimensions different than that of the tetragonal one, which is given as follows:  $a = 5.7517$  Å,  $b = 4.5378$  Å,  $c = 5.3825$  Å, and  $\beta = 122.646^\circ$  at 298 K [Lon70]. This low-temperature monoclinic lattice can be developed due to alteration of the high-temperature tetragonal one.

### 1.6.1 Energy Band Structure of VO<sub>2</sub>

In 1971, Goodenough [Goo71] has comparatively explained the electronic structure of VO<sub>2</sub>. Goodenough proposed that in the tetragonal phase (a spacing group of  $P4_2/mnm$ ), the V atoms are surrounded by O octahedra, which form an edge-sharing chain along the  $c_r$  axis. The  $d$ -levels of the V ions are split into lower-lying  $t_{2g}$  and  $e_g$  states as shown in Figure 1.14. The tetragonal crystal fields separates the  $t_{2g}$  multiple into an  $a_{1g}(d_{II})$  and  $e^\pi(\pi^*)$  double state. On the other

hand, in the monoclinic phase (a spacing group of  $P2_1/c$ ), there exist two significant effects between the dimerization and tilting of the V-V pairs. The first effect is the fact that the  $a_{1g}$  is divided into a lower-energy bonding and higher-energy anti-bonding combinations while the second effect is due to the fact that the  $V_d - O_p$  anti-bonding and the  $e^{\pi g}$  states are subjected to higher energy, as a result of the tilting of the pairs, thereby increases the overlap of these states with O states. Therefore, in this regard, the single  $d$  electron occupies the  $a_{1g}$ -binding combination, which results in a Peierls-like bandgap.

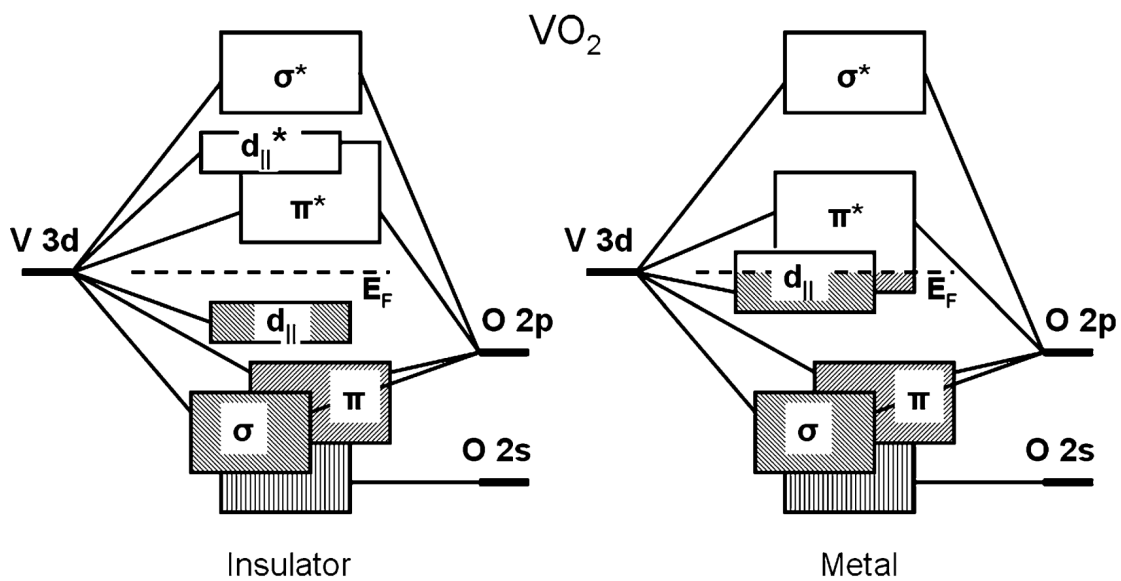


FIGURE 1.14: Band structure of VO<sub>2</sub> in its insulator and metal phases [Goo71].

### 1.6.2 Optical properties of VO<sub>2</sub>

Significant changes in the electrical properties of VO<sub>2</sub> during its MIT are accompanied by the abrupt transformation in its optical properties. Based on the sharp phase transition during the MIT of VO<sub>2</sub>, Ruzmetov and Ramanathan [Ruz10] demonstrated the evolution of a reflectance dispersion curves over its MIT and found that there is a relation between the changes in its optical properties to electrical parameters. The authors further reported that the jump of the reflectivity during its MIT can be as high as 92% at some wavelengths. The change

in resistance is more than 4 orders of magnitude when compared to the fastest phase transition proposed during the MIT of a single crystals [Lad69] and that of epitaxial thin films [Jin97], as presented in Figure 1.15.

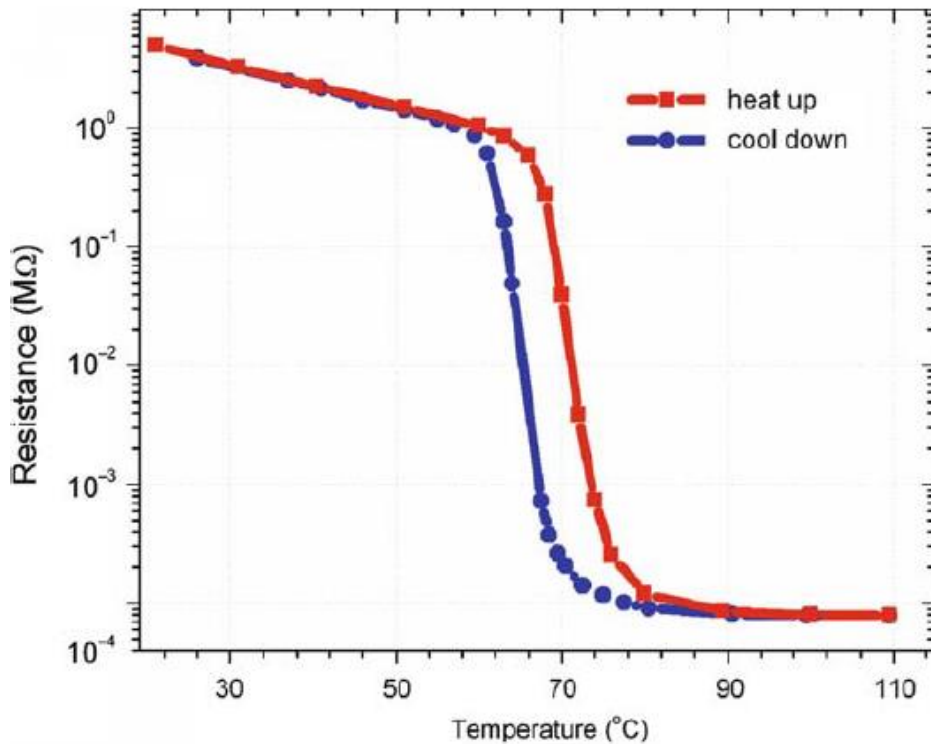


FIGURE 1.15: Electrical resistance as functions of Temperature of VO<sub>2</sub> film deposited on Al<sub>2</sub>O<sub>3</sub> [Ruz08].

Furthermore, in order to allow direct comparison between electrical and optical properties, Ruzmetov *et al.* [Ruz08] demonstrated that the optical measurement of the mid-infrared reflectance spectra of a VO<sub>2</sub> thin film prepared on c-plane Al<sub>2</sub>O<sub>3</sub> substrate as shown in Figure 1.16(a), were carried out on the film similar to the electrical transition as shown in Figure 1.15. It can be seen that there is an abrupt increase in reflectance when the film is heated above the critical temperature where VO<sub>2</sub> exhibit its MIT. It can also be seen that the phase transition happens at lower photon energies for the higher magnitude of the reflectance. For instance, in Figure 1.16(b), when the photon energy is 0.13 eV, the value of the reflectance changes from 2% to 94% during the MIT, which is more than the highest magnitudes proposed in the literature for optical reflectance

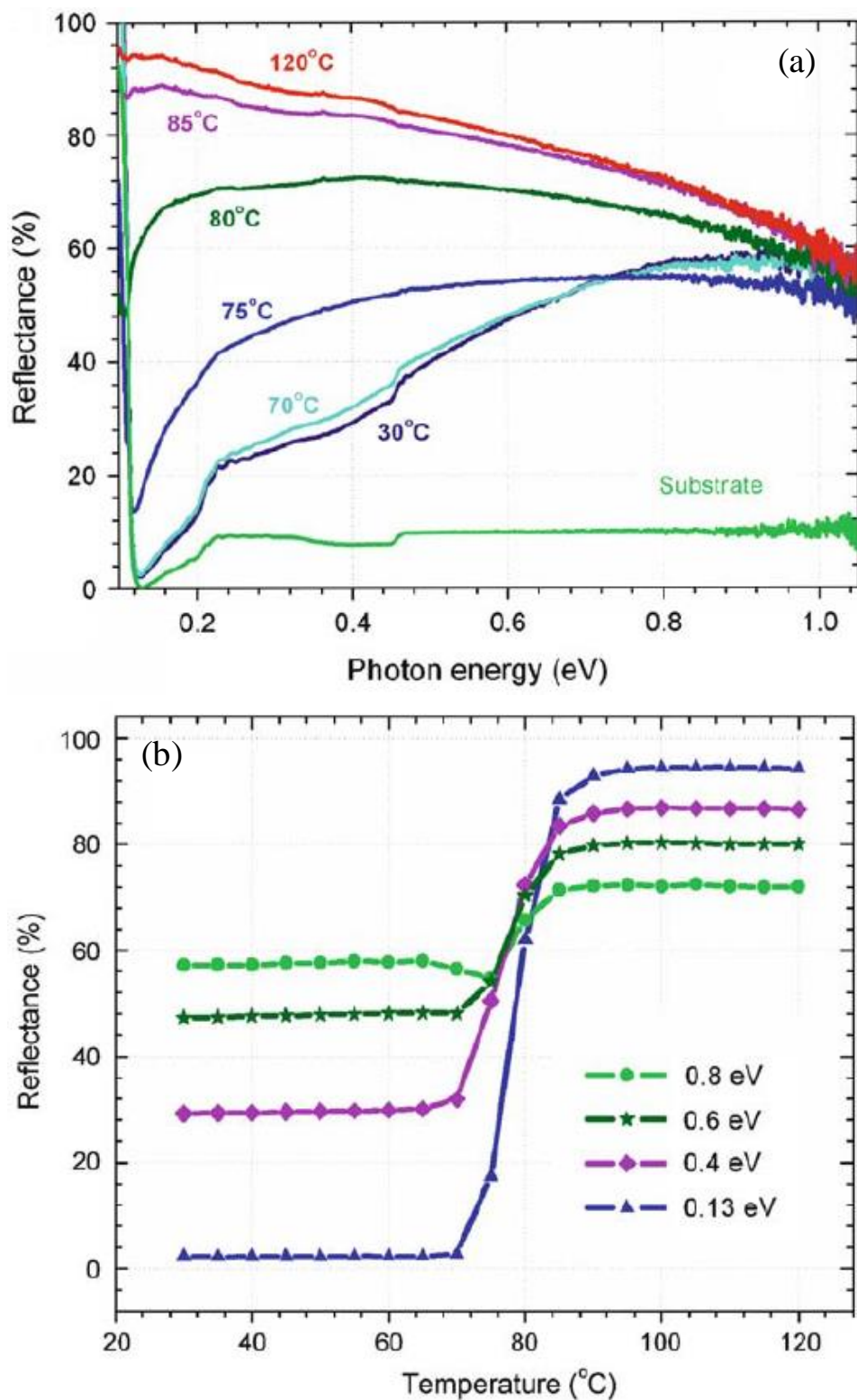


FIGURE 1.16: (a) Infrared reflectance as functions of incident photon energy for different temperatures and (b) Reflectance as a function of temperature at different photon energies [Ruz08].

and transmittance switching in VO<sub>2</sub> [Wan05; Cho96; Sol06; Oka06]. As shown in Figure 1.16(a), the spectral transformation with respect to temperature occurs mostly within the range of 15°C including the MIT.

Figure 1.16(b) shows the temperature evolution of reflectance for four different photon energies. It can be seen that the switching magnitude linearly decreases with increases in photon energy with the same transition interval as that in Figure 1.16(a). The sharp transformation during the MIT below and above transition temperature indicates the potential application in a device such as optical switches. Another interesting property in Figure 1.16(b) similar to that presented in Figure 1.16(a) is the fact that the reflectance decreases near the MIT (75°C). It is worth mentioning that the value of the energy gap in the low-temperature monoclinic phase of VO<sub>2</sub> is between 0.6 eV to 0.7 eV [Qaz06; Shi90].

### 1.6.3 Mechanical properties of VO<sub>2</sub>

According to Nelson Sepúlveda *et al.* [Sep08], there is also a change in VO<sub>2</sub> mechanical properties during its MIT apart from the significant variation in the optical, thermal and electrical ones. The authors reported the first experimental measurement of the elastic modulus of VO<sub>2</sub> thin films in temperatures ranging from 30°C to 90°C for three different lengths as shown in Figure 1.17. It can be seen that from 30°C to 62°C and from 80°C to 90°C, the Young's modulus at the lowest cantilever (100μm) decreases with respect to temperature by slopes of  $\approx -28.85\text{MPa}/^\circ\text{C}$  and  $\approx -21.79\text{MPa}/^\circ\text{C}$ , respectively. On the other hand, from the temperature ranging from 62°C to 82°C, the modulus slope increases to about  $127.75\text{MPa}/^\circ\text{C}$ . Furthermore, the other two cantilevers show similar behavior and the details are presented in Table 1.1. It can also be seen that the entire behavior observed for each cantilever was reversible and repeatable. This is expected given that they passed through heating and cooling processes. In contrast, the ratio of the modulus during the MIT significantly changes with

the linear relation between Young's modulus, as functions of the temperature of most materials, for example, the cantilevers of uncoated silicon [Ono00].

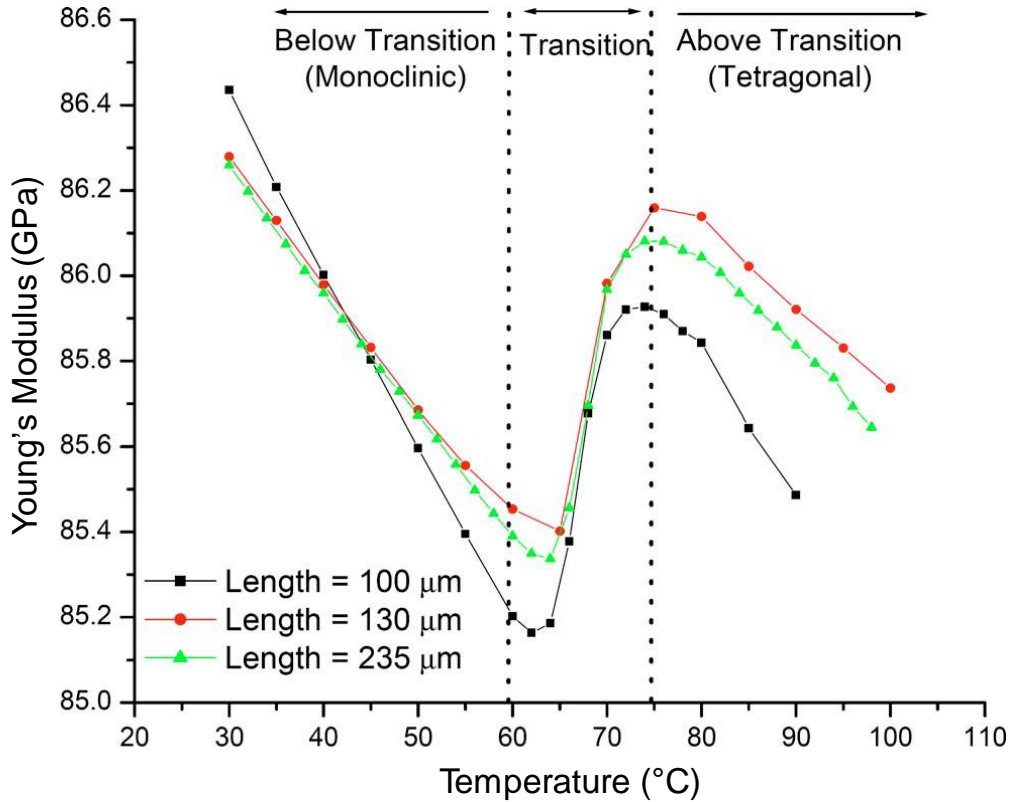


FIGURE 1.17: Young's modulus, as functions of the temperature of VO<sub>2</sub> thin films deposited on single crystal silicon for three different lengths [Sep08].

TABLE 1.1: Slopes for the three phases shown in Figure 1.17 [Sep08].

Cantilever length ( $\mu\text{m}$ )	Below transition (MPa/ $^{\circ}\text{C}$ )	During transition (MPa/ $^{\circ}\text{C}$ )	Above transition (MPa/ $^{\circ}\text{C}$ )
100	-28.85	127.75	-21.79
120	-27.98	115.93	-19.93
235	-40.91	116.08	-35.66

One can see that the value of Young's modulus increases during the heating process (in transition), this indicates that the crystal structure regarding the experiment, the material becomes stronger as the temperature increases. At high temperature closer to transition one, the materials are in its metallic phase and they become elastic at low temperature (insulating phase) for temperatures just before MIT. Taking into account this elasticity behavior, the results shed more

light to the fact that VO<sub>2</sub> thin film is a potential candidate for the development of the microelectromechanical system (MEMS).

#### 1.6.4 The excitation of the MIT of VO<sub>2</sub>

According to Figure 1.18, the advantage of the MIT of VO<sub>2</sub> thin films depends on the diversity of external stimuli utilized during its excitation. As discussed in the previous sections, besides temperature, the phase transition of VO<sub>2</sub> can be triggered electrically (voltage or current) [Kim10], optically (absorption of photons) [Rin05; Vik05] and as well as mechanically (pressure or stress) [Per08]. All these excitation processes can be used as advantages in sensor applications. However, depending on the desired application and means of availability, it may be more interesting to utilize one stimulus rather than another to excite the MIT of VO<sub>2</sub>. For instance, for the characterization of thin layers, it is better to use thermal activation which requires just a heating element (Peltier-type) and a temperature controller while for the integration of the films in the final component, it is easier to stimulate electrically (injection of carriers), which is enough to connect the channel of VO<sub>2</sub> to a power supply through control and actuation electrodes. The activation can be chosen based on the speed at which the MIT occurs.

Generally, it is not fast enough in the event of a temperature trip, however, it can be faster during an optical activation with a switching time of up to a hundred femtoseconds [Cav01]. Finally, the use of certain stimuli makes it feasible to state some particular effects of the transition, for instance, certain non-linearities which is observed in the current-voltage (IV) characteristics of VO<sub>2</sub>, during electrical activation. Note that for each of these stimuli, the conditions in which the transition is triggered depend on so many parameters, especially from the design phase of the device and integrating the material into the usage phase. For example, during the design phase, the choice of substrate and the use of metal dopants has a significant impact on the actualization of the transition temperature of the

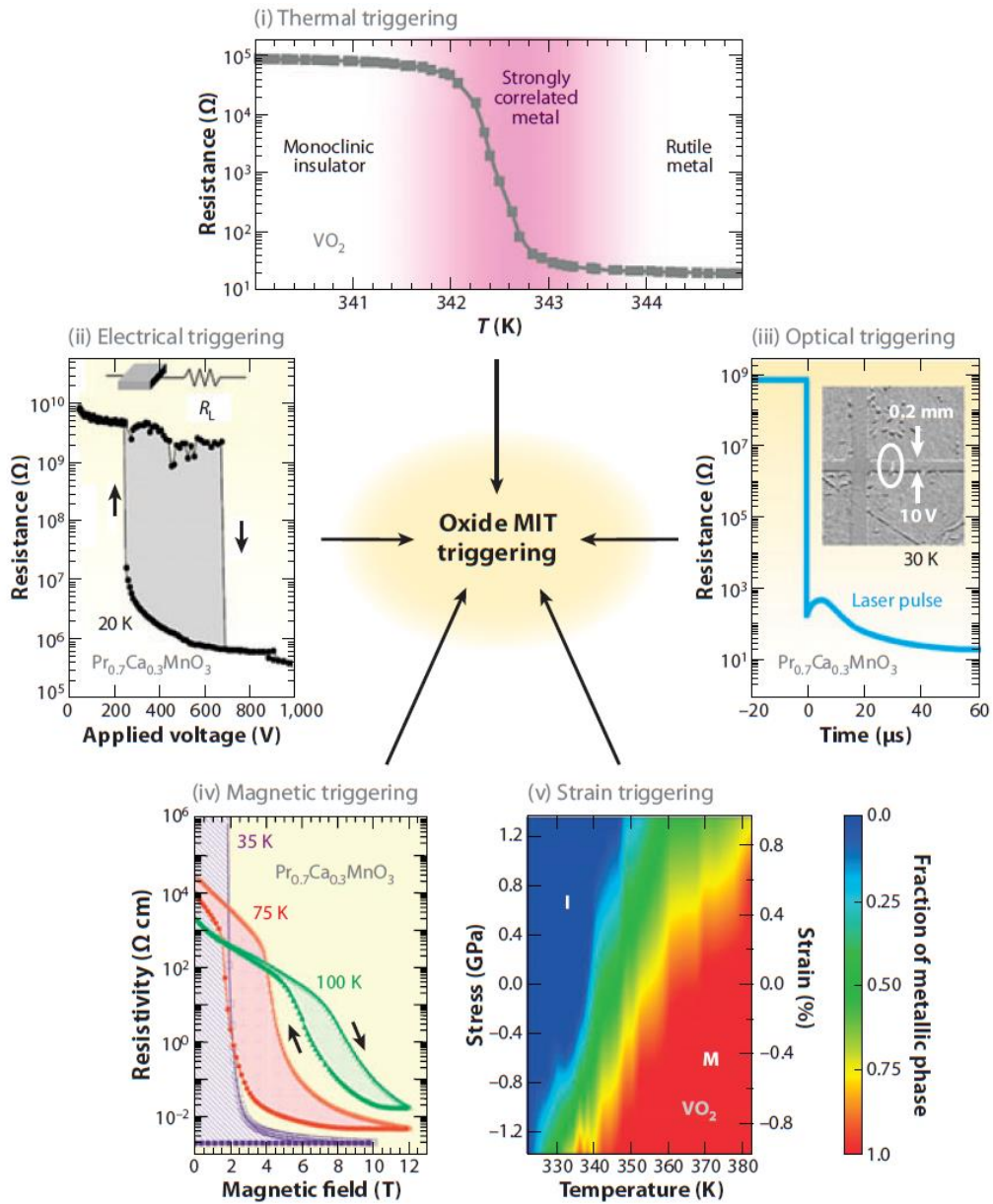


FIGURE 1.18: Different MIT-triggering in strongly-correlated oxides [Yan11].

material.

## 1.7 Applications of VO<sub>2</sub>

The significant change in the optical, electrical and thermal properties accompanied during the MIT of VO<sub>2</sub> makes it a promising material for potential applications in devices that can operate in a very wide frequency spectrum, ranging from the direct current domain to the optical wavelengths passing

through the microwave and terahertz frequency domain. The variation in the electronic spectrum on the metallic and the insulating phases of the transition makes it possible for switching application. More recently, VO<sub>2</sub> have been developed for the production of the thermal sensor, memristors, switches, diodes, rectifiers, etc

### 1.7.1 Thermal sensor MIT in VO<sub>2</sub> thin film

More recently, significant attention has been given to the use of VO<sub>2</sub> and its MIT in the field of temperature sensors. In this particular field, VO<sub>2</sub> was first utilized as a simple visual indicator for temperature which changes color according to its phase and therefore, signals if the temperature is lower or higher than a certain value. Since then, more efficient temperature sensor work has been proposed based on VO<sub>2</sub>. The new sensors developed are more sensitive to thermal variation and can be used as elements that are extremely sensitive to the electromagnetic field, which can detect the weakness of the thermal changes caused by these fields. In this regards, the sensitivity of the change in resistivity of the material during excitation as shown in Figure 1.19(a) is often for the production of microbolometers [Che00], widely used in infrared imaging systems, as shown in Figure 1.19(b).

Due to the strong thermal conductivity temperature dependance around the MIT, it can be used for several applications such as thermal switches and thermal detectors; applications have also been explored in night vision systems. For example, Yang *et al.* [Yan11] proposed a programmable critical temperature sensor. after the latter authors, Kim *et al.*[Kim07] demonstrated a thermal sensor based on VO<sub>2</sub> as presented in Figure 1.20(a). The authors used a sol-gel technique in order to deposit an approximately 100nm VO<sub>2</sub> thin film on plane

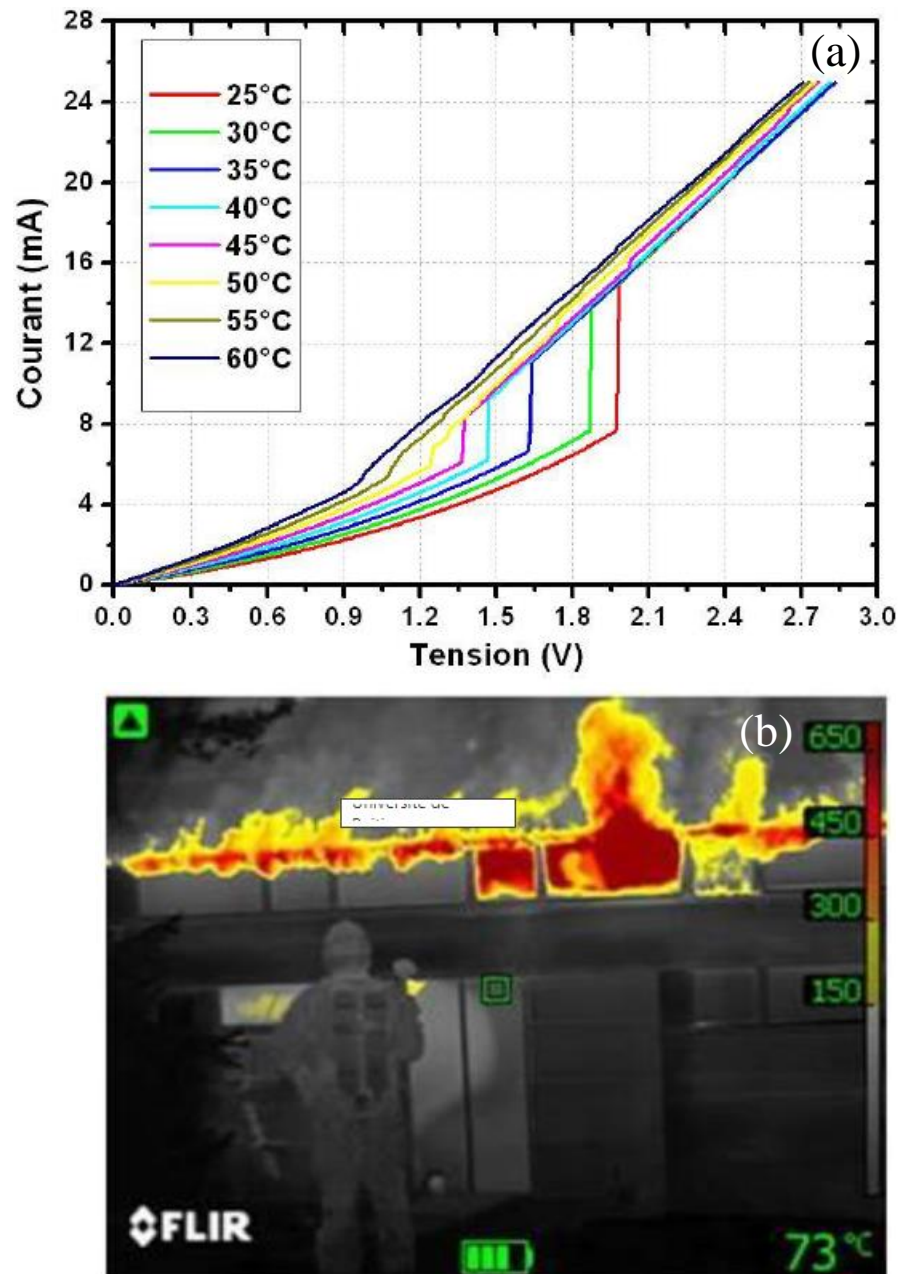


FIGURE 1.19: (a) The I-V characteristics of a  $VO_2$  based device for different temperatures and (b) Infrared image collected using a special infrared system marked by FLIR [Yan11].

silica ( $Si_2$ ) substrates. The  $VO_2$  was then used in the form of nanowires (see Figure 1.20(b)) instead of thin layers, which lead to an extremely sensitive device, and useful for the production of gas detector. Given that the pressure of the gas will be directly proportional to the number of molecules absorbed on the  $VO_2$  nanotubes, which in turn, will exhibit I-V characteristics proportional to the quantity of the absorbed molecules as presented in Figure 1.21.

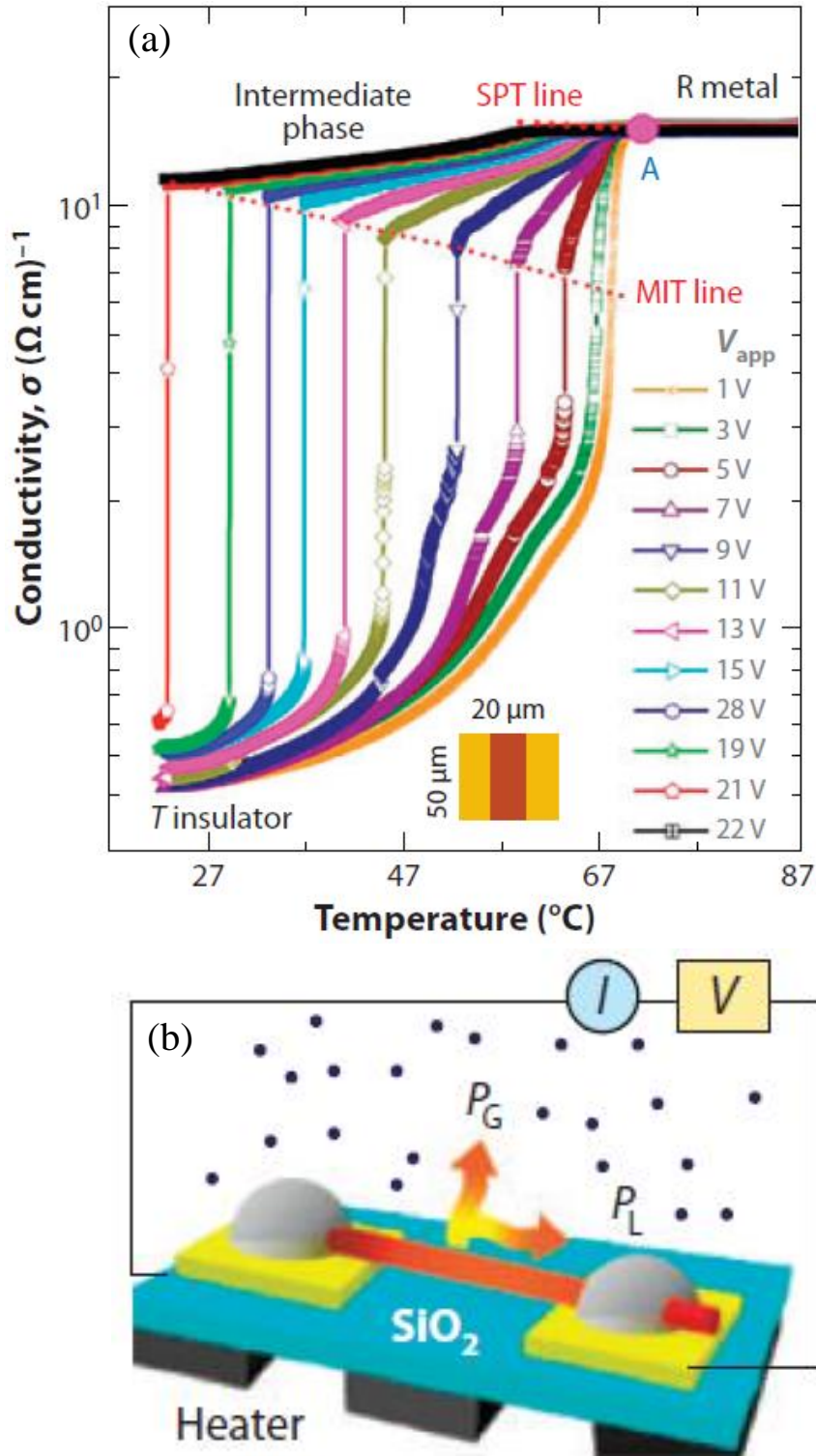


FIGURE 1.20: (a) A VO<sub>2</sub> thermal sensor device based on the temperature and voltage dependency of the conductivity and the coplanar VO<sub>2</sub> device and (b) Scheme of a nanowire gas sensor device, where  $P_G$  and  $P_L$  indicate the heat fluxes dissipating into the gas and metal contacts, respectively [Yan11].

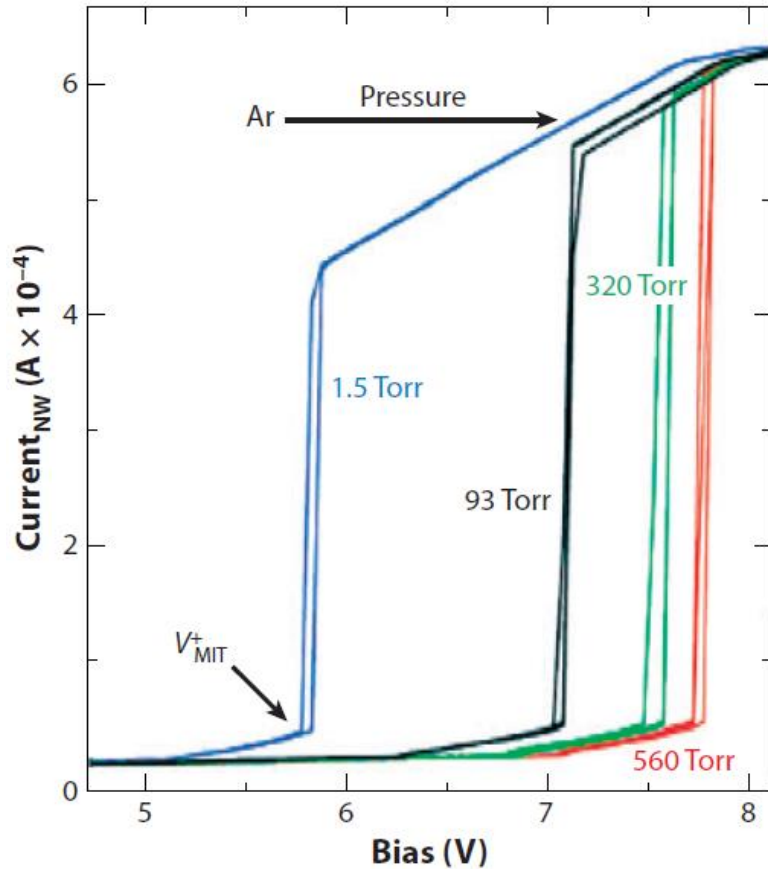


FIGURE 1.21: I-V characteristics of the VO<sub>2</sub> nanowire gas sensor device at different Ar pressure [Yan11].

### 1.7.2 Memristor devices using the MIT of VO<sub>2</sub>

A memristor, also known as memory-resistor can be defined as a two-terminal device in which the resistance can only be determined by the dynamic history of the system currents. In 1971, Chua proposed the first concept of fabricating a new memory device known as memristor as the fourth basic electronic components different from the capacitor, inductor and resistor, which broadly may lead to neuromorphic circuits [Chu71]. Forty years later, Strukov *et al.* [Str08] proposed a physical model to describe the hysteretic current-voltage behavior that characterizes an electrical memristor and found out that it can be realized and achieved using doped metallic-oxide semiconductors. Recently, researchers

have demonstrated that the presence of memory effects in VO<sub>2</sub> device, which can be used in the production of memories and neuromorphic circuits for manipulating heat flow [Ben17; Ord19a; Dri09].

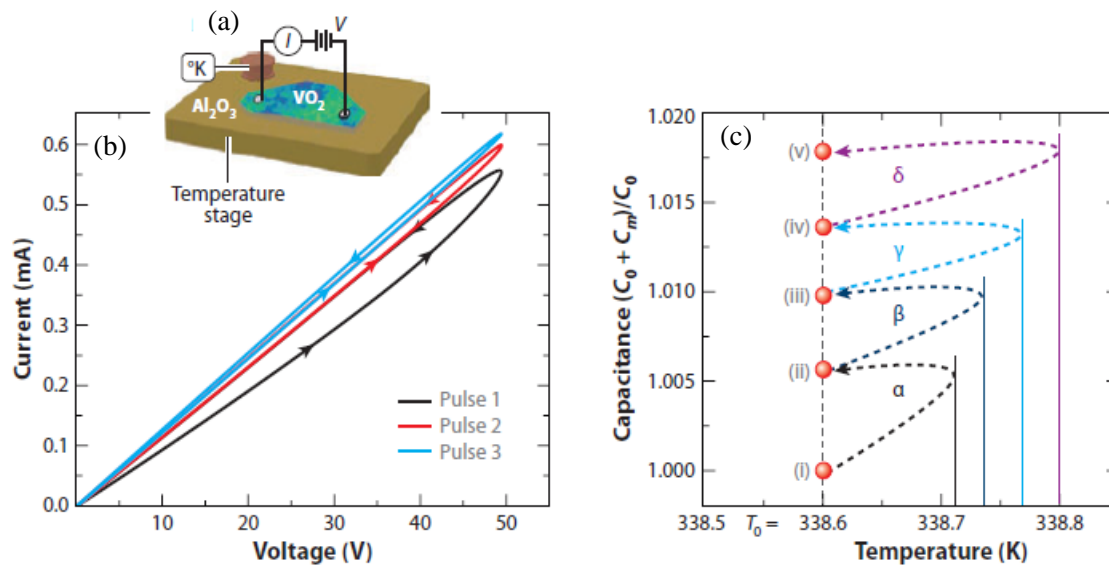


FIGURE 1.22: (a) Scheme of a VO<sub>2</sub> memristor device, (b) Three I-V curves displaying the hysteretic nonlinear memristor behavior of a VO<sub>2</sub> [Yan11] and (c) Memory capacitance of a hybrid VO<sub>2</sub> device during its heating and cooling process [Dri09].

The ability of VO<sub>2</sub> to significantly change phase at a temperature closer to room one makes it an interesting candidate for this circuit element as shown in a scheme of Figure 1.22(a). According to [Cha08a], the correlated material is grown on an Al<sub>2</sub>O<sub>3</sub> substrate using a sol-gel deposition technique, which is made up to four orders of magnitude resistivity change across its MIT. The measurement of temperature is set around room temperature closer to the onset of MIT in VO<sub>2</sub>. These effects are materialized by the value of the device's resistance to VO<sub>2</sub>, which changes according to the history of the actuation of the component. Therefore, when successive voltage pulses with similar characteristics are applied to the device, it can be seen that the values of the current measured are different as shown in Figure 1.22(b). This I-V characteristics are non-linear and are hysteretic, which is in agreement with the MIT of VO<sub>2</sub>. The hysteretic also contains the memory part of the memristor device. According to [Dri09], Figure 1.22 (c) show that a memory capacitance can also be produced by using MIT in VO<sub>2</sub>. As

it can be seen that the perturbed temperature induced the capacitance changes, lead to memory behavior, which is also related to the hysteretic behavior of MIT in VO<sub>2</sub>.

### 1.7.3 Three-terminal field effect transistor switches utilizing the MIT of VO<sub>2</sub>

The electric field introduced by an applied gate voltage in a three-terminal VO<sub>2</sub> field-effect transistor (FET) switches and modulates the resistance of a VO<sub>2</sub> channel. As a result, there is a significant change in the resistivity of this VO<sub>2</sub> channel; it may switch from high-resistivity insulating state to a low-resistivity metallic one. According to [Hor10; Zho97; New00; Ahn03], the VO<sub>2</sub> device behaves as a MottFET within its channel. On the other hand, this three-terminal switches using the MIT of VO<sub>2</sub> may be a useful device for demonstrating a functional MottFET for logic operations in a CMOS-like architecture.

In 2002, Chudnovskiy *et al.* [Chu02] proposed a simple VO<sub>2</sub> switch device as shown in Figure 1.23(a). The device contains a VO<sub>2</sub> channel, a gate dielectric layer at the top of the VO<sub>2</sub> channel, with a gate electrode above the gate dielectric layer and source/drain electrodes at both sides of the channel. The device is assumed to be operating at a temperature closer to the critical one, such that in the absence of a gate voltage, the channel is in metallic state. On the other hand, once the gate voltage is applied, the channel goes to the dielectric state. This working principle is similar to that of MOSFET operating in the depletion mode rather than the enhancement one. Figure 1.23(b) shows the possibilities of using the MIT of VO<sub>2</sub> to design a more complex circuit. One can see from the latter figure that an additional electrode enable the design of a three-terminal type device operating with the same principle as a FET. It can be seen that the VO<sub>2</sub> channel is placed between the drain and source electrode in order to vary as a function of

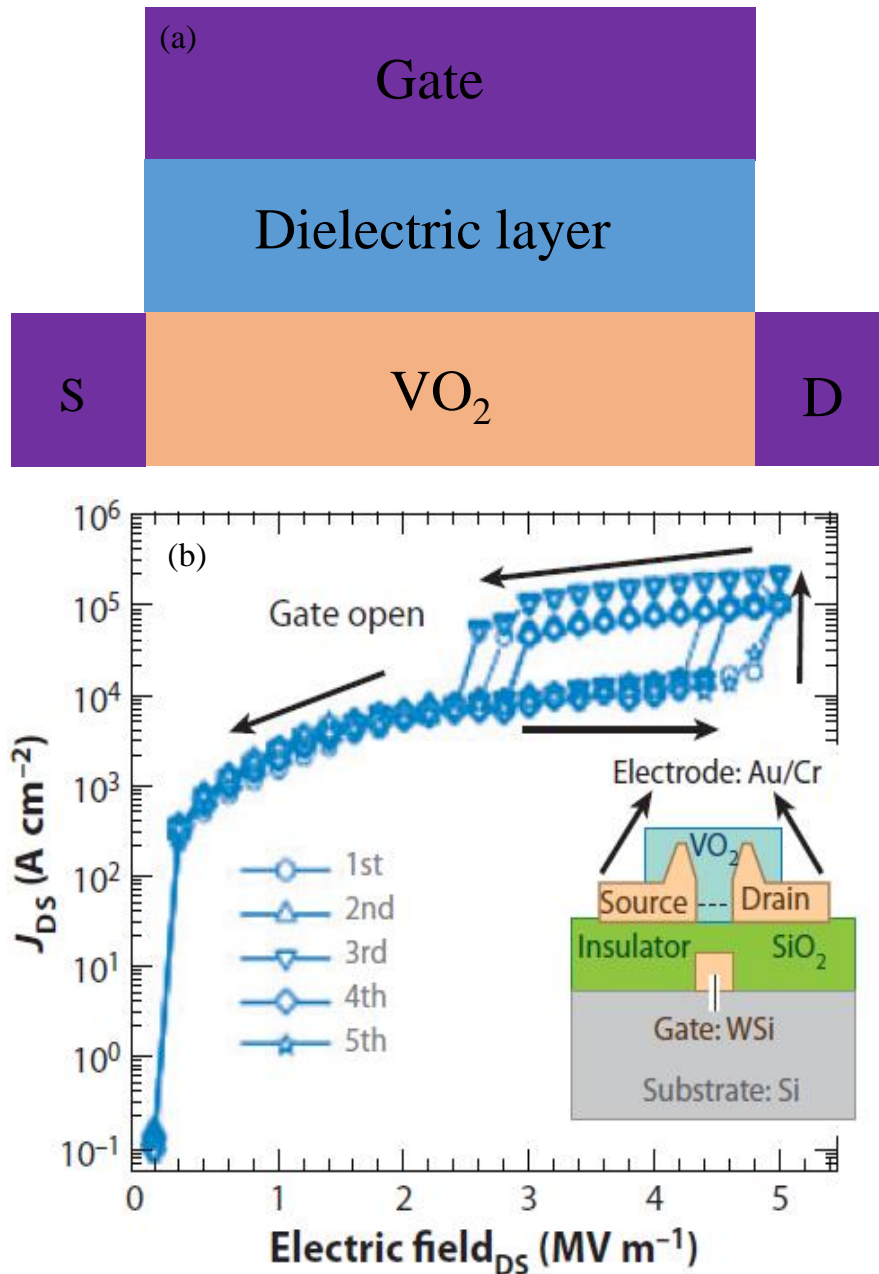


FIGURE 1.23: (a) Scheme of a three-terminal gated switch devices using MIT of  $\text{VO}_2$  and (b) Current density as functions of applied electric field on the  $\text{VO}_2$  channel with the gate open at room temperature. The inset shows the three-terminal  $\text{VO}_2$  device structure [Yan11].

the applied field, the characteristics of the transistor and, in particular, the drain-source current density [Kim04]. The inset in Figure 1.23(b) represents the device structure. It can also be seen that the  $\text{VO}_2$  thin films were deposited on a sapphire substrate using a pulsed laser deposition (PLD) technique. The  $\text{VO}_2$  thin film on the substrate shows that the MIT occurs at a temperature closer to room

one with a significant change in resistance of about four orders of magnitude across the MIT.

## 1.8 The deposition techniques of VO<sub>2</sub> thin film

A thin film of VO<sub>2</sub> can be synthesized in different forms such as nanowires [Str09], nanoparticles [Suh04], volume [Lad69], epitaxial [Sam97], polycrystalline [Ruz07a] and as well as nanostructures [Liu04; Cao09]. In all these forms, VO<sub>2</sub> undergoes MIT with more or less variable characteristics (magnitude of the variation in resistivity). Given that the potential applications of the MIT of VO<sub>2</sub> could include thin films, different techniques has thus been developed to synthesis these samples. Several deposition techniques have been used, such as chemical vapor deposition (CVD) [Sah02], pulsed laser deposition (PLD) [Dum08; Nag06], sputtering [Ruz07b; Rog91; Cha86], sol-gel deposition [Cha05], ion gun deposition [Wes08], electron gun evaporation [Man07; Ler12]. In this thesis, we will focus on the most recently used techniques for the fabrication of VO<sub>2</sub> thin film.

### 1.8.1 Chemical vapor deposition

Chemical vapor deposition (CVD) is one of the most common industrial process employed for the production of quality and high-performance thin films in semiconductors and other materials. The key routes in the CVD deposition processes are the situation whereby the substrate is exposed to one or more volatile precursors (solid or liquid), which decompose on the surface of the substrate to produce the desired film, alongside with the byproducts. These byproducts can be removed by passing the gas flow through the chamber where the reaction occurs. However, the CVD used in the case of VO<sub>2</sub> thin films production is based on organometallic precursor, therefore, it is commonly referred to as organometallic chemical vapor deposition (OMCVD) or metal-organic chemical vapor deposition (MOCVD).

In 1966, Koide and Takei were the first to propose the use of CVD for the deposition of  $\text{VO}_2$  thin films. The authors prepared bulk single crystals of  $\text{VO}_2$  using CVD technique [Tak66]. One year later, the same author deposited  $\text{VO}_2$  thin films following similar method but with vanadium oxychloride ( $\text{VOCl}_3$ ) as the precursor and nitrogen ( $\text{N}_2$ ) as the gas carrier, which then hydrolyzed on the surface of the substrates to generate epitaxial thin films of  $\text{VO}_2$  [Koi67]. A new development was proposed just after 1966 by MacChesney *et al.* [Mac68]. The authors replaced the  $\text{N}_2$  as a carrier gas by carbon dioxide ( $\text{CO}_2$ ) to transport the  $\text{VOCl}_3$  and  $\text{V}_2\text{O}_5$  was produced on single-crystal sapphire substrates. Afterwards, the  $\text{V}_2\text{O}_5$  was then reduced to  $\text{VO}_2$  by annealing between  $500^\circ\text{C}$  and  $550^\circ\text{C}$  in a well-controlled atmosphere composed of a mixture of  $\text{CO}$  and  $\text{CO}_2$ . Fifteen years later, Greenberg [Gre83] successfully carried out CVD with Vanadyl tri-isopropoxide ( $\text{VO}(\text{OC}_3\text{H}_7)_3$ ) as a single source precursor in an open atmosphere. He produced  $\text{VO}_2$  thin films with and without post-annealing on a glass substrate.

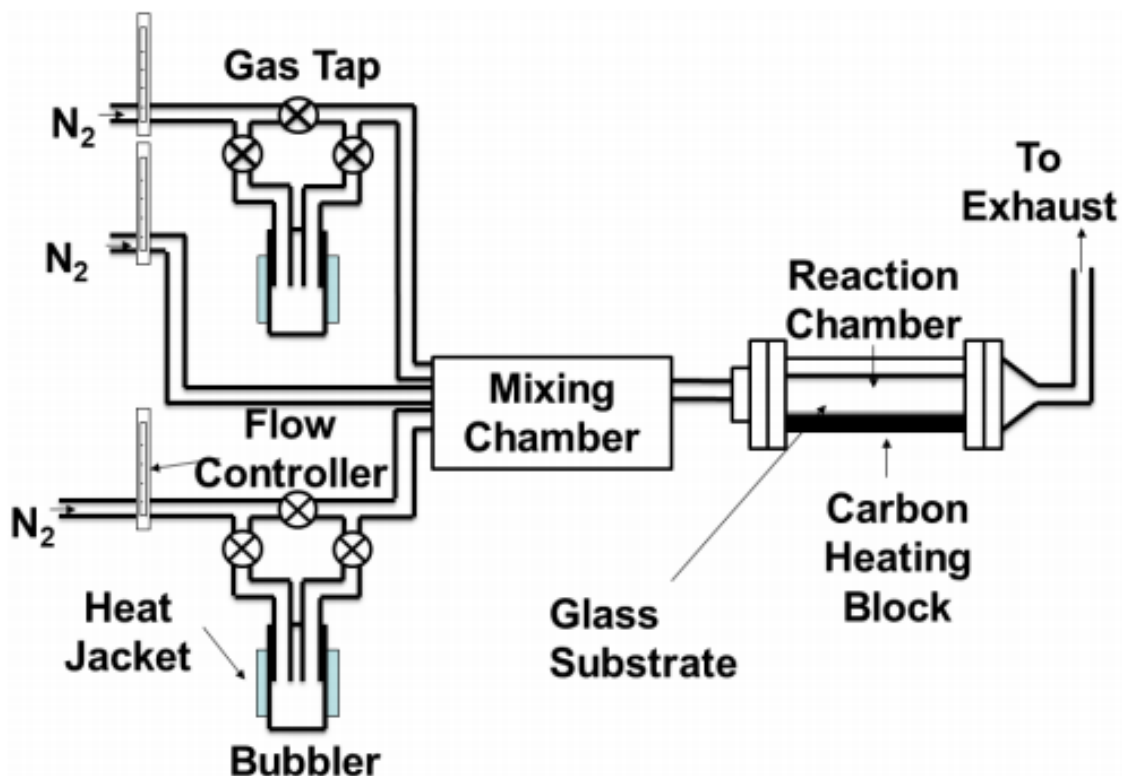


FIGURE 1.24: Scheme of a typical APCVD setup rig [War14].

Besides organometallic precursors, vanadium halide, such as VCl<sub>4</sub> or VOCl<sub>3</sub> can be utilized as precursors with water or ethanol in an appropriate atmosphere to produce VO<sub>2</sub> thin films [Man02; Fie00]. Among the types of CVD, the atomic pressure chemical vapor deposition (APCVD) (see Figure 1.24) is the most commonly used one, given that it can run as a single or multiple source processes. However, the drawback of this deposition technique is that it depends solely on the heat to enable the precursor to reach the vapor phase, as a result, the precursor becomes volatile. Extensive studies have been given to the growth of VO<sub>2</sub> thin film deposited on glass or silica substrates based on APCVD. In 1993, Maruyama and Ikuta [Mar93] were the first to propose APCVD based on annealing after deposition by using vanadium (III) acetylacetonate (V(C<sub>5</sub>H<sub>7</sub>O<sub>2</sub>)<sub>3</sub>) as a precursor and deposited polycrystalline VO<sub>2</sub> films on fused glass and sapphire single crystals substrate. Manning *et al.* [Man02] have rigorously demonstrated APCVD of VO<sub>2</sub> thin films and have proposed doping of VO<sub>2</sub> with the following materials; Ti, W, Mo and Nb.

### 1.8.2 Sol-gel Technique

The sol-gel technique is based on the sequential hydrolysis and condensation of molecular precursor steps. These molecular precursors are often metallic alkoxides. Although, metallic ions in aqueous solutions also undergo sol-gel transition [Liv88]. The sol-gel technique is commonly utilized for the synthesis of oxides such as glasses and ceramics. However, crystal structure and atomic homogeneity can be manipulated by varying the parameters during the process. Among several techniques of thin film deposition, sol-gel has been employed to prepare VO<sub>2</sub> thin film [Gre83; Dek97; Guz94; Par91] because it's not expensive, easy for metal-doping and covers a wide area of deposition.

Given that hydrothermal techniques are solution-based reactions, it is important to discuss the sol-gel techniques in order to understand different approaches

for producing VO<sub>2</sub> from solution-based procedures. A sol-gel can be defined as a colloidal solution that is composed of the precursors for the material in-situ. In 2008, Nag *et al.* [Nag08] reported that sol-gel techniques are used due to the capability to cover large areas at low cost and as well as the possibility of metal doping. The first VO<sub>2</sub> sol-gel technique was demonstrated with the use of butoxides and oxoisopropoxides. Lakeman *et al.* [Lak94] reported that the annealing conditions are more vital for the formation of the correct oxidation phase on the metallic vanadium than the first precursors. In 1988, Speck *et al.* [Spe88] proposed that the formation of VO<sub>2</sub> thin film based on sol-gel technique. The authors used the reaction of VCl<sub>4</sub> and lithium diethylamide (C<sub>4</sub>H<sub>10</sub>LiN), then added Titanium(IV)isopropoxide (C<sub>12</sub>H<sub>28</sub>O<sub>4</sub>Ti) to generate vanadium (IV) tetra-isopropoxide solution. The films were deposited by dip-coating glass slides into the prepared sol-gel solution and annealed between 400°C to 700°C under nitrogen to form polycrystalline VO<sub>2</sub>. These gel-derived VO<sub>2</sub> films undergo a reversible MIT phase transition around 67°C, exhibiting characteristic resistive and spectral switching.

### 1.8.3 Pulsed laser deposition

Pulse laser deposition (PLD) is a physical vapor deposition (PVD) technique that has been demonstrated successfully for several materials, such as thermochromic, superconducting [Kwo88a; Kwo88b; Che88; Shi91; McG17]. Given that this technique can be carried out under pressure, makes it a unique and excellent approach especially for depositing oxide thin films. In the case of VO<sub>2</sub>, good results have been generated based on R-cut sapphire substrates with post-annealing using PLD [Bor93]. PLD of VO<sub>2</sub> films has been carried out on different substrates, such as glass, sapphire, fused silica, and silicon.

As shown in Figure 1.25, PLD possessed the simplest fundamental experimental set up compared to other deposition techniques. However, the

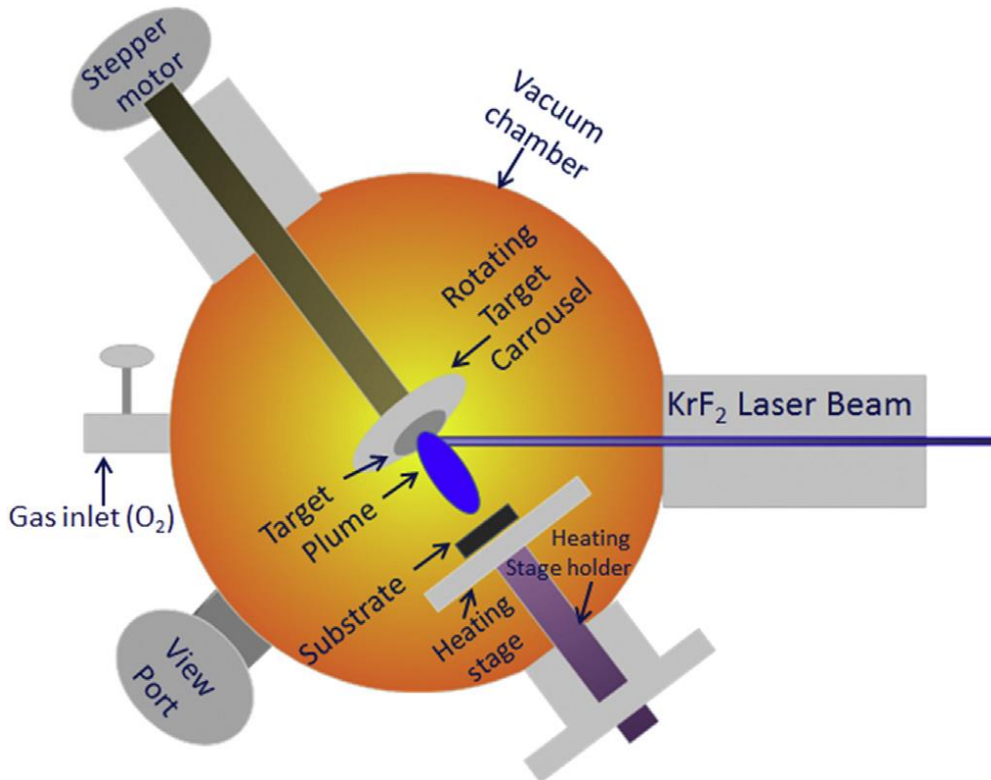


FIGURE 1.25: Scheme of a PLD process [McG17].

phenomenon of the laser-target interaction and film growth is really complicated. The working principle is such that when the pulsed laser is absorbed by the target, the energy is converted to electronic excitation and then into mechanical, thermal and chemical forms of energy, which leads to evaporation, plasma formation, and ablation. Atoms, molecules, electrons, and cluster amongst others are species ejected into the vacuum surrounding as plume [Eas07; Chr94; McG17]. The plume is directed to the substrate, which is usually heated, leading to deposition of the targeted materials. Over the years, VO<sub>2</sub> thin films have been generated by utilizing different target materials such as oxygen gas pressure, laser energies, etc. In 1993, Borek *et al.* [Bor93] carried out PLD of VO<sub>2</sub> thin films deposited on *R*-cut sapphire substrate by ablating the vanadium metal target. The authors used Krypton fluoride (KrF) laser with wavelength  $\lambda = 248 \text{ nm}$  and pulse time,  $\tau = 15 \times 10^{-9} \text{ s}$  to ablate a vanadium target under the atmospheric condition containing specified variations of oxygen and

argon, respectively. Consequently, the oxygen pressure in the chamber was found to be useful to stabilize the  $\text{VO}_2$ , given that many phases such as  $\text{V}_4\text{O}$  and  $\text{V}_2\text{O}_5$  could be present in the chamber. Suh *et al.* [Suh04] demonstrated the influence of nucleation and growth of  $\text{VO}_2$  thin films and nanoparticles on its MIT via PLD. They found out that the thickness and the shape of the hysteresis cycle can be determined by the competing effects of gain and the degree of structural order. In 2007, Pauli *et al.* [Pau07] studied the first in situ growth of  $\text{VO}_2$  nanoparticle films using a five-circle x-ray diffractometer, so as to generate structural information during the growth. The authors demonstrated that the amorphous films grown at room temperature were crystallized into  $\text{VO}_2$  phase by thermal annealing under the background of oxygen. They also showed that the crystallization is accompanied by a roughness of the film structure, given that that the crystalline state generates hemispherical islands, that does not show any preferential direction with respect to the substrate.

## 1.9 Conclusions

To conclude this state of the art chapter, we described the fundamental of heat transfer and different modes of heat transfer. We state the difference between these modes of heat transfer and also described the difference between the far and near-field radiative ones. We discussed different concepts that aimed to predict the blackbody spectrum and as well described how this spectrum was predicted correctly by Planck's theory and we defined Wien's displacement theory, which relates the wavelength of the thermal emission and medium temperature. We discussed different thermal properties responsible for heat transfer and also the parameter affecting these properties. We presented promising materials exhibiting phase change transition that have been proposed to design and optimize

---

thermal devices. Among these phase-change materials, we have particularly emphasized on the  $\text{VO}_2$ , whose phase transition occurs at a temperature closer to room one. In this regards, we reviewed different properties of this material, and we gave a brief discussion on its applications and as well as its various deposition techniques.

## 1.10 Résumé du chapitre 1

### Introduction

Ce chapitre correspond à un état de l'art, où nous avons effectué quelques rappels sur la théorie du transfert de chaleur dans les matériaux solides. Le chapitre commence par un aperçu des mécanismes physiques à l'origine du transfert de chaleur, suivi par une description des différents types de transfert. Concernant le transfert radiatif, nous rappelons la théorie classique du corps noir et ses limites dans le domaine du champ proche quand les distances mises en jeu sont plus petites que la longueur d'onde thermique. Puis, nous introduisons le concept de composants thermiques, notamment la diode thermique par analogie avec la diode électronique. Des matériaux prometteurs présentant une transition de phase qui ont été récemment proposés pour concevoir et optimiser les courants de chaleur conductifs et radiatifs sont présentés. Parmi ces matériaux, nous nous sommes davantage focalisés sur le  $\text{VO}_2$ , étant donné que sa transition de phase se produit à une température proche de la température ambiante usuelle. Les propriétés thermiques, électriques, optiques et mécaniques de ces derniers matériaux sont ensuite présentées.

Les différentes sections du chapitre sont résumées ci-dessous:

### Transfert de chaleur par conduction

La conduction thermique est un phénomène dans lequel la chaleur est transférée au moyen d'une excitation moléculaire à l'intérieur des matériaux à l'exclusion du mouvement de masse de la matière. Ce processus se produit dans les gaz et les liquides à la suite de la diffusion et des collisions des molécules lors de leur mouvement aléatoire. En outre, ce processus se déroule également dans les matériaux solides en raison de la combinaison des vibrations du réseau des molécules et du transport d'énergie par les électrons libres.

## **Transfert de chaleur radiatif**

Dans ce mode de transfert, l'énergie est transportée par le champ électromagnétique rayonné par un objet à température finie. Un exemple très important est le rayonnement infrarouge émis vers l'espace par la surface de la terre. Ainsi, même sans milieu intermédiaire, le transfert de chaleur se produira toujours par rayonnement thermique entre des corps à différentes températures. Cela rend le transfert de chaleur radiatif d'un grand intérêt pour de nombreuses applications dans différents domaines de la science et de l'ingénierie. Il dépend de la longueur d'onde du rayonnement considéré et des propriétés des matériaux impliqués pendant le processus de transfert de chaleur.

## **Transfert de chaleur radiative dans le corps noir**

Un corps noir est peut être comme une surface ou un volume idéal qui absorbe tout le rayonnement incident à n'importe quelle longueur d'onde et dans n'importe quelle direction. À l'équilibre thermique, aucune surface ne peut émettre une plus grande quantité d'énergie qu'un corps noir à une longueur d'onde et une température données. Le rayonnement émis par un corps noir est fonction de la longueur d'onde et de la température. Il est indépendant de la direction de sorte que le corps noir est un émetteur lambertien où sa luminance est isotrope. Etant donné qu'un corps noir est un absorbeur et un émetteur parfaits, il sert de norme dans laquelle les propriétés d'autres surfaces rayonnantes peuvent être comparées.

## **Matériaux à changement de phase**

Les matériaux à changement de phase (PCM) sont des matériaux fortement corrélés, c'est-à-dire des matériaux présentant de fortes interactions électroniques. Ils représentent une voie prometteuse pour l'optimisation des systèmes où l'accordabilité est basée sur les variations de leur conductivité. Ces matériaux

possèdent certaines orbitales atomiques, notamment celles de type  $d$ , qui génèrent la formation de bandes d'énergie plus étroites remplies et proches du niveau de Fermi, générant donc des interactions électroniques très fortes.

### **Le Dioxyde de Vanadium ( $\text{VO}_2$ )**

Le  $\text{VO}_2$ , découvert par Morin en 1959 est l'un des PCM les plus étudiés et appliqués dans les études expérimentales et théoriques, car il est le plus stable parmi les familles de vanadium et présente une transition métal isolant (MIT) hystérétique se produisant dans un intervalle de température étroit autour de la température critique. température ( $T_0 \sim 342.5$  K). Cette transition de phase solide entraîne ainsi des changements significatifs des propriétés électriques, optiques et thermiques, qui peuvent être appliquées pour un certain nombre d'applications telles que le redresseur thermique, les mémoires thermiques, les memristors thermiques, la commutation optique, l'interrupteur thermique, les diodes thermiques radiatives, et dispositifs électrostatiques fonctionnant dans le transfert de chaleur en champ proche et lointain.

### **Conclusions**

Ce chapitre décrit les principes fondamentaux du transfert de chaleur et les différents types de modes de transfert de chaleur. Nous énonçons la différence entre ces modes de transfert de chaleur et nous avons également décrit la différence entre les modes radiatifs de champ lointain et proche. Nous avons discuté de différents concepts qui visaient à prédire le spectre du corps noir et décrit comment ce spectre était correctement prédit par la théorie de Planck et nous avons défini la théorie du déplacement de Wien, qui relie la longueur d'onde de l'émission thermique et la température moyenne. Nous avons discuté des différentes propriétés thermiques responsables du transfert de chaleur ainsi que des

paramètres affectant ces propriétés. Nous avons présenté des matériaux prometteurs présentant une transition à changement de phase sont particulièrement indiqués pour concevoir et optimiser des dispositifs thermiques. Parmi ces matériaux à changement de phase, nous avons particulièrement mis l'accent sur le VO<sub>2</sub>, dont la transition de phase se produit à une température plus proche de celle de la pièce. A cet égard, nous avons passé en revue les différentes propriétés de ce matériau, et nous avons donné une brève discussion sur ses applications ainsi que ses différentes techniques de dépôt.

## Chapter 2

## Chapter 2

---

# Geometrical effects on conductive thermal diodes based on VO<sub>2</sub>

### Contents

---

<b>2.1</b>	<b>Introduction</b> . . . . .	<b>69</b>
<b>2.2</b>	<b>Analytical solution of spherical and cylindrical thermal diodes</b>	<b>70</b>
2.2.1	Spherical conductive thermal diode . . . . .	71
2.2.2	Cylindrical conductive thermal diode . . . . .	76
<b>2.3</b>	<b>Rectification factor</b> . . . . .	<b>80</b>
2.3.1	Spherical diode . . . . .	80
2.3.2	Cylindrical diode . . . . .	81
<b>2.4</b>	<b>Results and discussion</b> . . . . .	<b>83</b>
<b>2.5</b>	<b>Conclusions</b> . . . . .	<b>88</b>
<b>2.6</b>	<b>Résumé du chapitre 2</b> . . . . .	<b>89</b>

---



## 2.1 Introduction

Over the past years, thermal rectification has attracted significant interest due to that fact it can be accomplished through thermal diodes operating with phonons, electrons, etc. Besides, several theoretical and experimental studies have been proposed based on this tuning of heat transports [Yua15; Kan18; Wan13; Wu07; Hu09]. Given that geometry is one of the factors that affect thermal rectification [Rob11], has motivated our interest to theoretically study the performance of geometrical conductive thermal diodes based on PCM, whose thermal conductivity changes in a narrow interval of temperature. Although, thermal rectification based on conductive heat fluxes has been extensively studied in plane geometry [Pey06; Ord18b], however, less attention has been given to studies dealing with other geometries.

Thermal rectification based on materials whose thermal conductivity linearly depends on its temperature has been modeled by Sadat and Le Dez [Sad16]. The authors studied the operation of conductive thermal diodes consisted of two layers with plane, cylindrical and spherical geometries and reported that the ratio of the heat fluxes in the forward and backward scenarios does not depend on their shape and takes the value of  $\approx 1.6$ . Since this thermal rectification effect is driven by the temperature dependence of the thermal conductivity of the involved materials, thus, it is also expected to be achieved in thermal diodes based on VO<sub>2</sub>. Because the thermal conductivity of VO<sub>2</sub> significantly changes in a narrow range of temperatures ( $340 \text{ K} < T < 345 \text{ K}$ ), it will be useful as one of the diode terminals to enable achieved higher rectification effect within a relatively small temperature variation between the two diode terminals, as was proposed for a plane geometries by Ordonez-Miranda *et al.* [Ord18b]. Note that the working principle of the study presented in this chapter is different than the later authors, as the areas of cylindrical and spherical geometries were considered.

Herein, we theoretically modeled the thermal rectification effect of cylindrical and spherical conductive thermal diodes based on the temperature dependence of the VO<sub>2</sub> thermal conductivity. Firstly, we derived an analytical expression for the temperature profiles, heat flows and rectification factors for both cylindrical and spherical conductive thermal diodes supporting steady-state heat conduction. Note that the expression for the temperatures and heat flows were derived using a well known Fourier's law of heat conduction. Secondly, we solved the analytical equations of the heat flows using inbuilt Wolfram Mathematica symbol "Find Root", which returns a list of the replacement desires variables and whose accurate solution can be verified. Finally, we calculate the effectiveness of the thermal rectification from the maximum and minimum values of the heat flow in the forward and backward configurations using equation (1.9).

## 2.2 Analytical solution of spherical and cylindrical thermal diodes

As discussed in the first chapter, the thermal conductivity of the VO<sub>2</sub> used in our thermal diodes modeling was first described by Ordonez-Miranda *et al.* [Ord18b] as presented in equation (1.10). Here we consider a VO<sub>2</sub> spherical /or cylindrical thermal shell exchanging steady-state heat conduction with a non-PCM due to their temperature difference  $T_h > T_c$ , as illustrated in Figure 2.1(a) and (b), respectively. The forward configuration [Figure 2.1(a)] of this conductive thermal diode is such that the VO<sub>2</sub> inner surface ( $r = a$ ) is set at hot-temperature  $T_h$ , while the non-PCM outer surface ( $r = c$ ) is set at cold-temperature  $T_c$ , and thus the heat flow  $q_F$  flows from VO<sub>2</sub> to the non-PCM. On the other hand, the backward configuration [Figure 2.1(b)] is the opposite of the forward one, in this case, the temperatures  $T_h$  and  $T_c$  are interchanged, hence the heat flow  $q_B$  flows from non-PCM to VO<sub>2</sub>. Given that the values of the heat flows  $q_F$  and  $q_B$  are

driven by different thermal conductivities, that is to say,  $\kappa_1(T)$  of VO<sub>2</sub> and  $\kappa_2$  of the non-PCM, they are expected to be different ( $q_F \neq q_B$ ), as a result of the temperature dependence of  $\kappa_1(T)$ , for temperatures inside the MIT of VO<sub>2</sub>. For the sake of clarity, we are going to consider that the thermal conductivity  $k_2$  of the non-PCM is independent of temperature in both the forward and backward configurations. The optimization of the heat flow difference ( $q_F - q_B$ ) can therefore be achieved by setting the terminals' temperatures as follows:  $T_c < T_0 < T_h$ , with  $T_0$  being the transition temperature of VO<sub>2</sub>. According to equation (1.10), the thermal conductivity of VO<sub>2</sub> when  $n = 1$  (for single material) as shown in Figure 2.2 can be described, as follows:

$$\kappa_1(T) = \kappa_i + \frac{\kappa_m - \kappa_i}{1 + e^{-\beta(T-T_0)}}, \quad (2.1)$$

where  $\kappa_m = 6 \text{ Wm}^{-1}\text{K}^{-1}$  and  $\kappa_i = 3.6 \text{ Wm}^{-1}\text{K}^{-1}$  are thermal conductivities in their metallic and insulating phases, respectively;  $T_0 = 342.5 \text{ K}$  is the transition temperature and  $\beta = 1.7 \text{ K}^{-1}$  is the phase transition slope of  $\kappa_1(T)$  at  $T = T_0$ . The four aforementioned values were determined by fitting equation (2.1) to the experimental data shown in Figure 2.2.

## 2.2.1 Spherical conductive thermal diode

### Forward configuration

According to equation (1.3), the heat flow  $q_F$  in the forward configuration of the spherical conductive thermal diode considered in this chapter as shown in Figure 2.1(a), can be described by

$$q_F = -4\pi r^2 \kappa_1(T_1) \frac{dT_1}{dr} = -4\pi r^2 \kappa_2 \frac{dT_2}{dr}, \quad (2.2)$$

where  $T_1(r)$  and  $T_2(r)$  are the temperatures within the VO<sub>2</sub> ( $a \leq r \leq b$ ) and non-PCM ( $b \leq r \leq c$ ) regions, respectively. According to the steady-state conditions

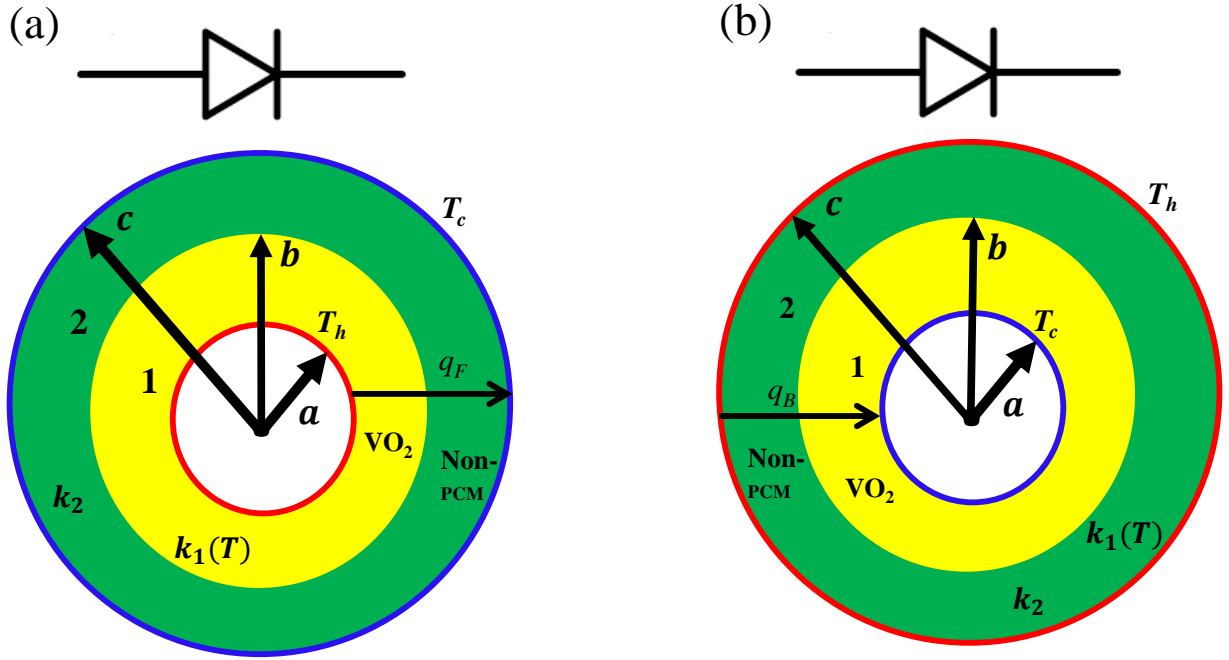


FIGURE 2.1: Scheme of a spherical (or cylindrical) conductive thermal diode consisting of a VO<sub>2</sub> and Non-PCM, and operating in the (a) forward and (b) backward configurations. The surfaces  $r = a$  and  $r = c$  are set at the temperatures  $T_h$  and  $T_c$ , for the forward configuration, while they are reversed in the backward one.

considered in this chapter,  $q_F$  is constant and can be determined by using the following three boundary conditions generated from Figure 2.1(a) and equation (1.12):  $T_1(r = a) = T_h$ ,  $T_2(r = c) = T_c$ , and  $T_1(r = b) - T_2(r = b) = R_{12}q_F/4\pi b^2$ , with  $R_{12}$  being the ITR between the VO<sub>2</sub> and non-PCM.

In the steady-state regime of heat conduction without losses of generality on the external surface of the junction, the temperature  $T_1(r)$  is determined by integrating first equality in equation (2.2) for the thermal conductivity  $\kappa_1(T_1)$  in equation (2.1), as follows:

$$-\int \frac{q_F}{4\pi r^2} dr = \int \left[ \kappa_i + \frac{\kappa_m - \kappa_i}{1 + e^{-\beta(T-T_0)}} \right] dT. \quad (2.3)$$

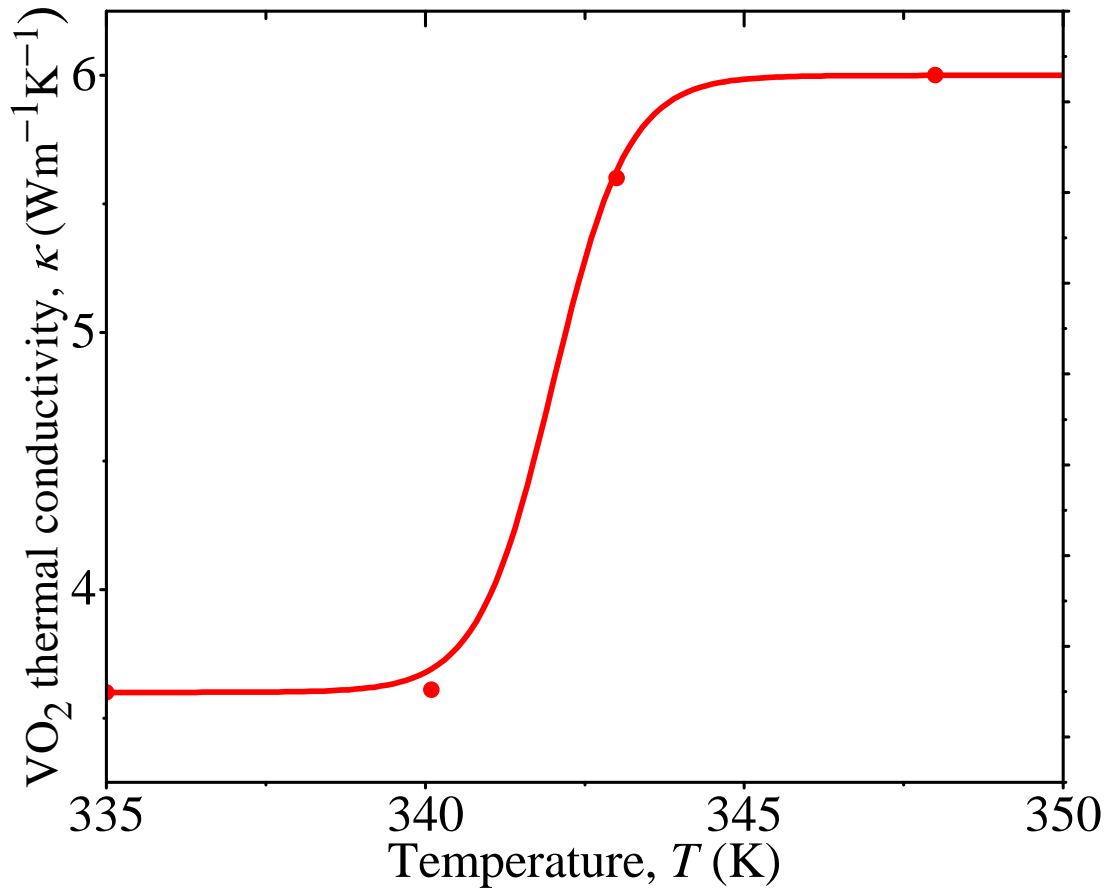


FIGURE 2.2: Thermal conductivity of  $\text{VO}_2$ , as functions of temperature within its corresponding MIT. Dots represent experimental data reported in the literature [Oh10].

The integration of equation (2.3) yields,

$$\kappa_i(T - T_0) + \frac{\kappa_m - \kappa_i}{\beta} \ln \left[ 1 + e^{\beta(T - T_0)} \right] = C + \frac{q_F}{4\pi r'}, \quad (2.4a)$$

$$\kappa_m(T - T_0) + \frac{\kappa_m - \kappa_i}{\beta} \ln \left[ 1 + e^{-\beta(T - T_0)} \right] = C + \frac{q_F}{4\pi r'}, \quad (2.4b)$$

where  $C$  is a constant of integration. The expression for the temperature  $T_1(r)$  can be written from equation (2.4b) as

$$T_1(r) - T_0 + \frac{1}{\beta\gamma} \ln[1 + \lambda(T_1(r))] = \frac{C}{\kappa_m} + \frac{q_F}{4\pi r\kappa_m}, \quad (2.5)$$

where  $\lambda(T) = e^{-\beta(T-T_0)}$ , and  $\gamma = \kappa_m / (\kappa_m - \kappa_i)$ . The evaluation of equation (2.5) at the boundary conditions stated earlier result, as follows:

$$T_h - T_0 + \frac{1}{\beta\gamma} \ln[1 + \lambda(T_h)] = \frac{C}{\kappa_m} + \frac{q_F}{4\pi a \kappa_m}, \quad (2.6a)$$

$$T_1(b) - T_0 + \frac{1}{\beta\gamma} \ln[1 + \lambda(T_1(b))] = \frac{C}{\kappa_m} + \frac{q_F}{4\pi b \kappa_m}. \quad (2.6b)$$

The expressions for  $q_F$  and  $C$  can therefore be determined by solving equations (2.6a) and (2.6b), which enables expressing the heat flow and the temperature profile as

$$q_F = \frac{1}{\beta\gamma\delta_m} \ln \left[ \frac{G(T_h)}{G(T_1(b))} \right], \quad (2.7)$$

$$G(T_1(r)) = [G(T_h)]^\alpha [G(T_1(b))]^{1-\alpha}, \quad (2.8)$$

where  $\delta_m = \rho/\kappa_m$ ,  $\rho = (b-a)/(4\pi ab)$ ,  $\alpha = a(b-r)/r(b-a)$ , and  $G(T) = [1 + \lambda(T)]/[\lambda(T)]^\gamma$ . Note that equations (2.7) and (2.8) are the heat flow and temperature profile inside VO<sub>2</sub> region, that is to say, from  $a$  to  $b$ , hence there is a need to calculate  $q_F$  flowing from  $b$  to  $c$  and  $T_2(r)$  inside the non-PCM. This has been done by integrating the second equality in equation (2.2) to enable determined the temperature  $T_1(b)$  in equations (2.7) and (2.8), respectively. By recalling the second equality in equation (2.2) and integrating both sides we have:

$$- \int \frac{q_F}{4\pi r^2} dr = \int \kappa_2 dT. \quad (2.9)$$

The integration of equation (2.9) yields,

$$\kappa_2 T = D + \frac{q_F}{4\pi r}, \quad (2.10a)$$

$$T_2(r) = \frac{D}{\kappa_2} + \frac{q_F}{4\pi r \kappa_2}, \quad (2.10b)$$

where  $D$  is a constant of integration. Again, by applying the same boundary conditions to equation (2.10b), we obtain

$$T_2(b) = \frac{D}{\kappa_2} + \frac{q_F}{4\pi b\kappa_2}, \quad (2.11a)$$

$$T_c = \frac{D}{\kappa_2} + \frac{q_F}{4\pi c\kappa_2}. \quad (2.11b)$$

The expressions for  $q_F$  and  $D$  can then be determined by solving equations (2.11a) and (2.11b), which allows to write the temperature profile  $T_2(b)$  as

$$T_2(b) = T_c + \frac{q_F}{\kappa_2}\sigma, \quad (2.12)$$

where  $\sigma = (c - b)/4\pi bc$ . The temperature  $T_1(b)$  is then determined by substituting equation (2.12) into  $T_1(r = b) - T_2(r = b) = R_{12}q_F/4\pi b^2$ , we obtain

$$T_1(b) = T_c + \delta q_F, \quad (2.13)$$

where  $\delta = [R_{12} + b(c - b)/c\kappa_2]/(4\pi b^2)$  is the effective thermal resistance. By substituting equation (2.13) into (2.7) and (2.8), we obtain

$$q_F = \frac{1}{\beta\gamma\delta_m} \ln \left[ \frac{G(T_h)}{G(T_c + \delta q_F)} \right], \quad (2.14)$$

$$G(T_1(r)) = [G(T_h)]^\alpha [G(T_c + \delta q_F)]^{1-\alpha}. \quad (2.15)$$

Equation (2.14) is strongly non-linear on  $q_F$ , whose values are driven by  $\delta$  that depends on the sizes of the spherical conductive thermal diode. It can be seen that geometry plays a significant role on the heat flow  $q_F$  and temperature profile  $T_1(r)$  of the spherical thermal diode. On the other hand, the temperature profile  $T_2(r)$  of the non-PCM is determined by solving equations (2.11a), (2.11b) and (2.10b), respectively. The final result is given as

$$T_2(r) = T_c + \frac{q_F}{\kappa_2}\sigma(1 - M), \quad (2.16)$$

where  $M = c(r - b)/r(c - b)$ .

### Backward configuration

The heat flow ( $q_B$ ) and temperature profiles [ $T_1(r)$  and  $T_2(r)$ ] for the backward configuration of the spherical conductive thermal diode [non-PCM to VO<sub>2</sub>] of Figure 2.1(b), can be determined by following a similar procedure than the one developed for the forward one and properly utilizing the following boundary conditions:  $T_1(a) = T_c$ ,  $T_2(c) = T_h$ , and  $T_2(b) - T_1(b) = R_{12}q_B/4\pi b^2$ . The final results obtained for the heat flow and temperature profiles are given, as follows:

$$q_B = \frac{1}{\beta\gamma\delta_m} \ln \left[ \frac{G(T_h - \delta q_B)}{G(T_c)} \right], \quad (2.17)$$

$$G(T_1(r)) = [G(T_c)]^\alpha [G(T_h - \delta q_B)]^{1-\alpha}, \quad (2.18)$$

$$T_2(r) = T_h - \frac{q_B}{\kappa_2} \sigma (M - 1). \quad (2.19)$$

It can be seen that the difference between the heat flow and temperature profiles in the forward and backward configurations is the sign convention. This is expected given that the temperatures  $T_h$  and  $T_c$  are interchanged. Note that the fundamental features of the analytical solutions will remain the same irrespective of the position of the two involving materials, provided all other parameters remain the same.

## 2.2.2 Cylindrical conductive thermal diode

### Forward configuration

Since the area of a cylinder is different from that of a sphere, the heat flows  $q_F$  in the forward configuration of the cylindrical conductive thermal diode is not the same as in the case of the spherical diode. The heat flows and temperature profiles for the forward and backward configurations of the cylindrical diode are determined by using the following boundary conditions:  $T_1(a) = T_h$ ,  $T_2(c) =$

$T_c$ , and  $T_1(b) - T_2(b) = R_{12}q_F/2\pi bh$ , where  $h$  is the length of the cylindrical diode shown in Figure 2.1(a). According to equation (1.3), the  $q_F$  in the forward configuration, in this case, can be written, as follows:

$$q_F = -2\pi rh\kappa_1(T_1)\frac{dT_1}{dr} = -2\pi rh\kappa_2\frac{dT_2}{dr}. \quad (2.20)$$

Applying a similar procedure developed for the spherical diode, the expression for the temperature profile  $T_1(r)$  is determined by integrating the first equality in equation (2.20) with the thermal conductivity  $\kappa_1(T_1)$  in equation (2.1), as follows:

$$-\int \frac{q_F}{2\pi rh} dr = \int \left[ \kappa_i + \frac{\kappa_m - \kappa_i}{1 + e^{-\beta(T-T_0)}} \right] dT. \quad (2.21)$$

The integration of equation (2.21) gives:

$$\kappa_m(T - T_0) + \frac{\kappa_m - \kappa_i}{\beta} \ln \left[ 1 + e^{-\beta(T-T_0)} \right] = E - \frac{q_F}{2\pi h} \ln r, \quad (2.22a)$$

$$T_1(r) - T_0 + \frac{1}{\beta\gamma} \ln[1 + \lambda(T_1(r))] = \frac{E}{\kappa_m} - \frac{q_F}{2\pi h\kappa_m} \ln r, \quad (2.22b)$$

where  $E$  is a constant of integration. By applying the aforementioned boundary conditions to equation (2.22b), we obtain the final results for the heat flow and temperature profile, as follows:

$$T_h - T_0 + \frac{1}{\beta\gamma} \ln[1 + \lambda(T_h)] = \frac{E}{\kappa_m} - \frac{q_F}{2\pi h\kappa_m} \ln a, \quad (2.23a)$$

$$T_1(b) - T_0 + \frac{1}{\beta\gamma} \ln[1 + \lambda(T_1(b))] = \frac{E}{\kappa_m} - \frac{q_F}{2\pi h\kappa_m} \ln b. \quad (2.23b)$$

The evaluation of equations (2.23a) and (2.23b) at the boundary conditions stated above for the forward configurations determines both  $q_F$  and  $E$ , which allows writing the heat flow and temperature profile as:

$$q_F = \frac{1}{\beta\gamma\mu_m} \ln \left[ \frac{G(T_h)}{G(T_1(b))} \right], \quad (2.24)$$

$$G(T_1(r)) = [G(T_h)]^J [G(T_1(b))]^{1-J}, \quad (2.25)$$

where  $\mu_m = Z/\kappa_m$ ,  $Z = \ln(b-a)/2\pi h$ , and  $J = \ln(b-r)/\ln(b-a)$ . In order to solve for  $T_1(b)$  in equations (2.24) and (2.25) using the boundary condition  $T_1(b) - T_2(b) = R_{12}q_F/2\pi bh$ , we have determined the temperature profile  $T_2(r)$  inside the non-PCM by integrating the second quality in equation (2.20), as follows:

$$- \int \frac{q_F}{2\pi r h} dr = \int \kappa_2 dT. \quad (2.26)$$

The integration of equation (2.26) yields

$$T_2(r) = \frac{F}{\kappa_2} - \frac{q_F}{2\pi\kappa_2} \ln r, \quad (2.27)$$

where  $F$  is a constant of integration. By applying the boundary conditions of the cylindrical diode to equation (2.27), we obtain

$$T_2(b) = \frac{F}{\kappa_2} - \frac{q_F}{2\pi\kappa_2} \ln b, \quad (2.28a)$$

$$T_c = \frac{F}{\kappa_2} - \frac{q_F}{2\pi\kappa_2} \ln c. \quad (2.28b)$$

The expressions for the  $q_F$  and  $F$  can be found by solving equations (2.28a) and (2.28b). The results is given as

$$T_2(b) = T_c + \frac{q_F}{\kappa_2} Q, \quad (2.29)$$

where  $Q = \ln(c-b)/2\pi h$ . By substituting equation (2.29) into  $T_1(b) - T_2(b) = R_{12}q_F/2\pi bh$ , we have

$$T_1(b) = T_c + \mu q_F, \quad (2.30)$$

where  $\mu = [R_{12} + b \ln(c - b)/\kappa_2]/2\pi bh$ . By substituting equation (2.30) into (2.24) and (2.25), we obtain

$$q_F = \frac{1}{\beta\gamma\mu_m} \ln \left[ \frac{G(T_h)}{G(T_c + \mu q_F)} \right], \quad (2.31)$$

$$G(T_1(r)) = [G(T_h)]^J [G(T_c + \mu q_F)]^{1-J}. \quad (2.32)$$

It can be seen that the effective thermal resistance  $\mu$  takes into account the geometry effect of the cylindrical diode shells on  $q_F$  and  $T_1(r)$ , as its value is different from the corresponding one for the spherical ( $\delta$ ) and plane [Ord18b] diodes. The diode geometry is therefore expected to have a key impact on the effective thermal resistance between the diode terminals and thus on the involved heat flows and temperature profiles. On the other hand, the temperature profile  $T_2(r)$  of the non-PCM is determined by solving equations (2.28a), (2.28b) and (2.27), respectively. The final result yield

$$T_2(r) = T_c + \frac{q_F}{\kappa_2} Q(1 - V), \quad (2.33)$$

where  $V = \ln(r - b)/\ln(c - b)$ .

### Backward configuration

We have derived the expressions for the heat flow  $q_B$  and temperature profiles  $T_1(r)$  and  $T_2(r)$  in the backward configuration by following a similar method employed in the forward one. Here, the boundary condition is slightly different from the forward case. They are given as:  $T_1(a) = T_c$ ,  $T_2(c) = T_h$ , and  $T_2(b) - T_1(b) = R_{12}q_B/2\pi bh$ . By properly using the later conditions, the heat flow and the temperature profiles are given as:

$$q_B = \frac{1}{\beta\gamma\mu_m} \ln \left[ \frac{G(T_h - \mu q_B)}{G(T_c)} \right], \quad (2.34)$$

$$G(T_1(r)) = [G(T_c)]^J [G(T_h - \mu q_B)]^{1-J}, \quad (2.35)$$

$$T_2(r) = T_h - \frac{q_B}{\kappa_2} Q(V - 1). \quad (2.36)$$

## 2.3 Rectification factor

### 2.3.1 Spherical diode

From the definition of the rectification factor in equation (1.9), it can be seen that, in order to maximize  $R$ , the difference between forward heat flow  $q_F$  and backward one  $q_B$  should be optimized. In this regards, we have written the thermal rectification factor defined in equation (1.9) in terms of the ratio of minimum heat flow in the backward configuration to the maximum heat flow in the forward one, as follows:

$$R_{\text{opt}} = 1 - \frac{q_{B,\text{min}}}{q_{F,\text{max}}}. \quad (2.37)$$

Equation (2.37) holds for the optimal rectification factor, can be determined by the ratio  $q_{B,\text{min}}/q_{F,\text{max}}$ . In the case of spherical diode, this ratio can be easily determined by evaluating the maximum and minimum expressions for the equations (2.14) and (2.17), respectively. In order to find the maximum values of the heat flow  $q_F$  in equation (2.14), we start by taking the exponential of both sides and substituting for  $G(T) = [1 + \lambda(T)]/[\lambda(T)]^\gamma$  and  $\lambda(T) = e^{-\beta(T-T_0)}$ , we obtain:

$$e^{(\beta\gamma\delta_m q_F)} = \left[ \frac{1 + \lambda(T_h)}{1 + \lambda(T_c + \delta q_F)} \right] \left[ \frac{\lambda(T_c + \delta q_F)}{\lambda(T_h)} \right]^\gamma, \quad (2.38a)$$

$$e^{(\beta\gamma q_F(\delta + \delta_m))} = \left[ \frac{1 + e^{-\beta(T_h - T_0)}}{1 + e^{-\beta(T_c - T_0) - \beta\delta q_F}} \right] e^{-\beta\gamma(T_h - T_c)}. \quad (2.38b)$$

The expression in equation (2.38b) can be written in terms of  $q_F$ , as follows:

$$q_F = \frac{T_h - T_c}{\delta + \delta_m} - (\beta\gamma(\delta + \delta_m))^{-1} \ln \left[ \frac{1 + e^{-\beta(T_c - T_0) - \beta\delta q_F}}{1 + e^{-\beta(T_h - T_0)}} \right]. \quad (2.39)$$

By following a similar procedure developed for the forward heat flow, the expression for the heat flow  $q_B$  can be rewritten from equation (2.17), as follows:

$$q_B = \frac{T_h - T_c}{\delta + \delta_m} + (\beta\gamma(\delta + \delta_m))^{-1} \ln \left[ \frac{1 + e^{\beta(T_h - T_0) - \beta\delta q_B}}{1 + e^{-\beta(T_c - T_0)}} \right]. \quad (2.40)$$

It can be seen that the quantities inside the logarithm in equations (2.39) and (2.40) are greater than or equal to 1, as expected. The heat flow  $q_F$  is less than or equal to  $(T_h - T_c)/(\delta + \delta_m)$  while the heat flow  $q_B$  is greater than or equal to  $(T_h - T_c)/(\delta + \delta_i)$ , with  $\delta_i = \rho/\kappa_i$ . Furthermore, if we consider the fact that  $T_c < T_0 < T_h$  and  $\beta = 1.7 \text{ K}^{-1}$ , as mentioned in previous section, the maximum of  $q_F$  is determined by the conditions  $T_h - T_c \gg \beta^{-1}$  and  $T_c - T_0 + \delta q_F \gg \beta^{-1}$ , equation (2.39) becomes

$$q_{F,\max} = \frac{T_h - T_c}{\delta + \delta_m}. \quad (2.41)$$

Further simplification of the later conditions used to derived equation (2.41), indicates that (2.41) is valid when  $T_h - T_c \gg \beta^{-1}$  and  $T_h - T_0 \gg (T_0 - T_c)\delta_m/\delta + (1 + \delta_m/\delta)\beta^{-1}$ . On the other hand, the expression for the minimum of  $q_B$  is determined when  $T_0 - T_c \gg \beta^{-1}$ ,  $T_h - T_0 - \delta q_B \gg \beta^{-1}$  and  $T_h - T_0 \gg \left[1 + \delta(\delta_m^{-1} + \delta_i^{-1})\right] \beta^{-1}$ , equation (2.40) becomes

$$q_{B,\min} = \frac{T_h - T_c - (T_0 - T_c)(1 - \kappa_i/\kappa_m)}{\delta + \delta_m}. \quad (2.42)$$

### 2.3.2 Cylindrical diode

Similar to the case of the spherical diode, according to equations (2.31) and (2.34), the expressions for the forward and backward heat flows of the cylindrical diode

can be rewritten, as follows:

$$q_F = \frac{T_h - T_c}{\mu + \mu_m} - (\beta\gamma(\mu + \mu_m))^{-1} \ln \left[ \frac{1 + e^{-\beta(T_c - T_0) - \beta\mu q_F}}{1 + e^{-\beta(T_h - T_0)}} \right], \quad (2.43a)$$

$$q_B = \frac{T_h - T_c}{\mu + \mu_m} + (\beta\gamma(\mu + \mu_m))^{-1} \ln \left[ \frac{1 + e^{\beta(T_h - T_0) - \beta\mu q_B}}{1 + e^{-\beta(T_c - T_0)}} \right]. \quad (2.43b)$$

It can be seen easily that equations (2.43a) and (2.43b) of the cylindrical diode are different from equations (2.39) and (2.40) of the spherical one by ITRs  $\mu$  and  $\mu_m$ , respectively. One can now see that their maximum and minimum values are respectively given by equations (2.41) and (2.42), provided that the ITRs  $\delta$  and  $\delta_m$  are properly replaced by  $\mu$  and  $\mu_m$ . By substituting equations (2.41) and (2.42) into (2.37), we obtain the optimal rectification factor  $R_{opt}$ , as follows:

$$R_{opt} = \left( 1 - \frac{\kappa_i}{\kappa_m} \right) \left( \frac{T_0 - T_c}{T_h - T_c} \right). \quad (2.44)$$

Note that the optimal rectification factor of the cylindrical thermal diode is the same as the rectification factor of the spherical one given by equation (2.44). This is expected since this result is in good agreement with the plane thermal diode case reported by [Ord18b]. One can see that the optimal rectification factor of plane, cylindrical and spherical thermal diodes neither depend on the size nor the shape of its terminals, as well as their ITRs. Equation (2.44) is valid for all temperatures  $T_c < T_0 < T_h$  satisfying the conditions  $T_h - T_0 \gg (T_0 - T_c)\delta_m/\delta + (1 + \delta_m/\delta)\beta^{-1}$  and  $T_h - T_0 \gg \left[ 1 + \delta(\delta_m^{-1} + \delta_i^{-1}) \right] \beta^{-1}$ , that is used to derive equations (2.41) and (2.42), which can be simultaneously satisfied for any values of the ITRs  $\delta$ ,  $\delta_m$  and  $\delta_i$ . In the limit of sharp transitions ( $\beta \rightarrow \infty$ ), these two later conditions reduced to  $T_h - T_0 \gg (T_0 - T_c)\delta_m/\delta > 0$ , which bounds the values of  $T_h$ , by setting  $T_c$  and  $T_0$  for any of the two involving materials forming the terminals of the thermal diode. Since  $T_0$  is a property of

material, equation (2.44) allows to predict the optimal rectification factor for different values of  $T_h$  and  $T_c$ . It can be seen from equation (2.44) that the optimal rectification factor of both spherical and cylindrical thermal diodes increases with the ratio of thermal conductivity  $\kappa_m/\kappa_i$  of the metallic and insulating phases of VO<sub>2</sub> and do not depend on the radii and ITR of the diode terminals. On the other hand, the temperature intervals for which equation (2.44) is valid, do not depend on ITR, as discussed in the proceeding paragraph. It is therefore clear that PCMs with higher thermal conductivity contrast  $\kappa_m/\kappa_i$  and very steep phase transition (steeper thermal conductivity slopes of  $\beta$ ) can be used to design spherical and cylindrical thermal diodes with higher rectification factors. However, in order to capitalize on this contrast, there is a need to establish a temperature difference larger enough (much greater than  $\beta^{-1}$ ) to excite the insulating and metallic phases. The larger the  $\beta^{-1}$ , the smaller the temperature gradients between the terminal to achieve optimal rectification factors.

## 2.4 Results and discussion

In this section, we numerically solved the expressions for the heat flows and temperature profiles by using the build-in tool "FindRoot" of the software Wolfram Mathematica and plotted for different parameters. We further confirmed the accuracy of the values generated from this tool by replacing each of them in equations (2.14), (2.17), (2.31) and (2.34) for the forward and backward heat flows.

In Figures 2.3(a) and 2.3(b), we have presented the heat flows  $q_F$  and  $q_B$  for the forward and backward configurations of spherical and cylindrical thermal diodes based on VO<sub>2</sub>. One can see that for a temperature lower than the transition one ( $T_0 \sim 342.5$  K), VO<sub>2</sub> do not undergo any phase transition, given that the heat flows  $q_F$  and  $q_B$  are equal. There is thus no rectification. This result

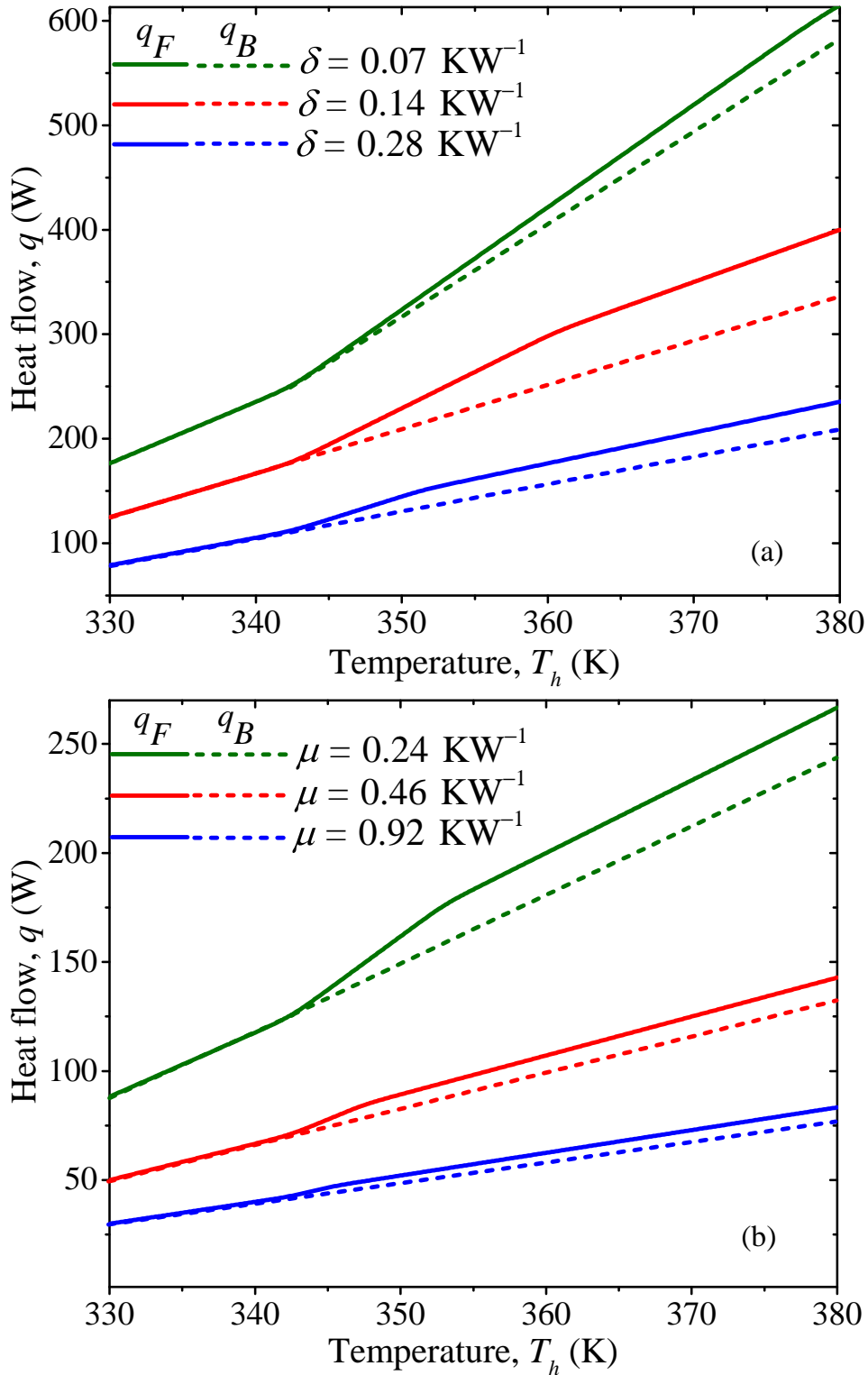


FIGURE 2.3: Temperature evolution of the forward and backward heat flows of a (a) spherical and (b) cylindrical thermal diodes operating with a terminal of VO<sub>2</sub>. Calculations were done for three representative interface thermal resistances and  $T_c = 300 \text{ K}$  [Kas19].

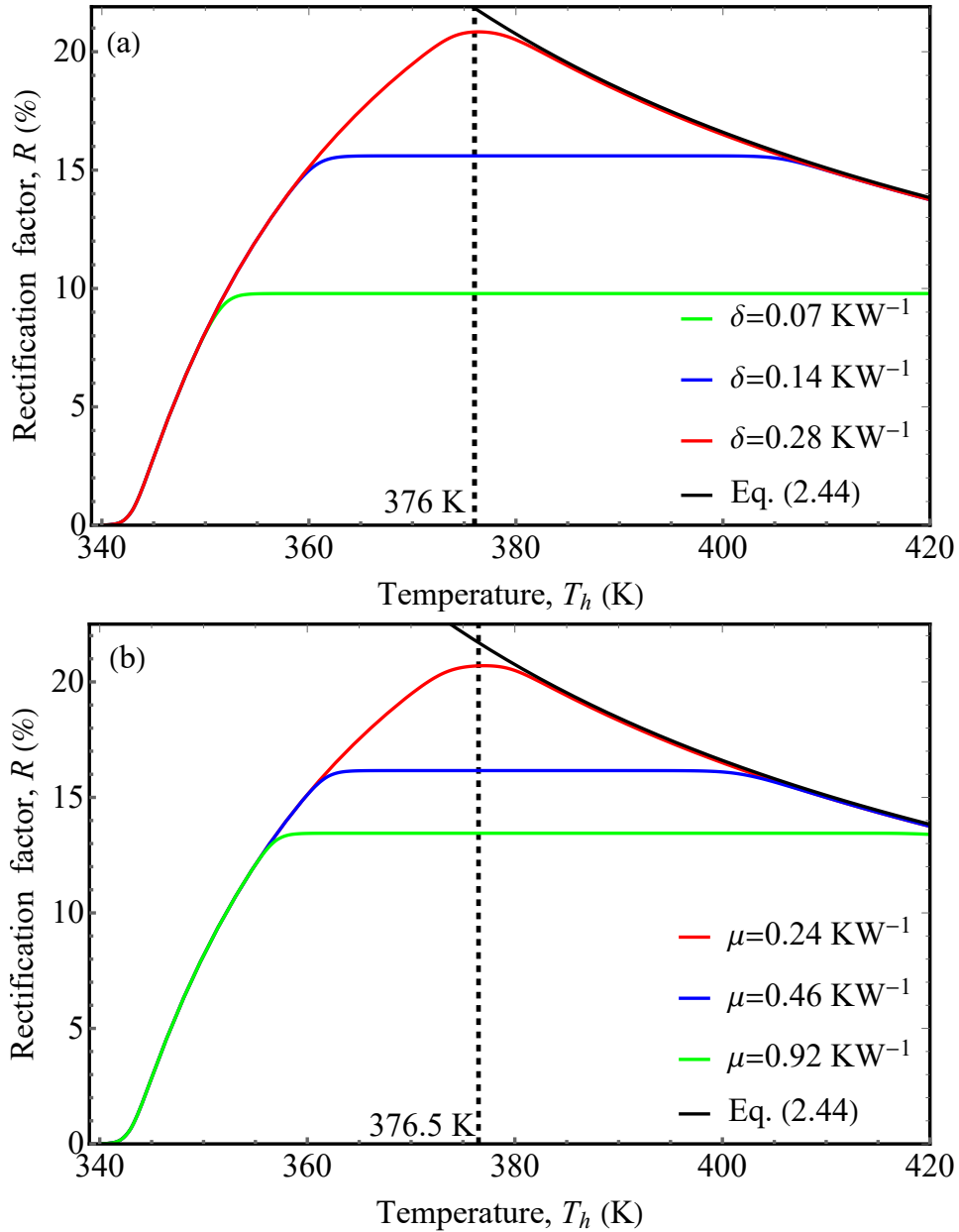


FIGURE 2.4: Rectification factor of a (a) spherical and (b) cylindrical thermal diodes, as a function of the hotter temperature  $T_h$ . Calculations were done for three representative values of the effective thermal resistances,  $T_c = 300$  K,  $a = 1$   $\mu\text{m}$  and  $b = 10$   $\mu\text{m}$  [Kas19].

is in good agreement with Figures 2.4(a) and 2.4(b) and the plane diode reported by [Ord18b]. It can be seen that the lower effective thermal resistances ( $\delta$  or/  $\mu$ ) generate higher heat flows in both configurations of the conductive thermal diodes, as expected. It can also be seen that there exists an effective thermal resistance for which the heat flow in the forward configuration is greater than the backward one  $q_F > q_B$ . In this case, the differences between the forward

and backward heat flows tend towards a constant value for  $T_h \gg T_0$ , where VO<sub>2</sub> undergo its metallic phase. The result shows that the system studied behaves like a thermal diode, reducing the heat flow in the reversed direction and as predicted by equations (2.41) and (2.42). It also shows that there exists an optimal rectification factor, which is in good agreement with the analysis established in chapter 1. Given that the thermal resistance  $\delta$  of the spherical diode is less than the corresponding one of the cylindrical diode  $\mu$ , one can see that the heat flows generated in the spherical diode are higher than cylindrical ones. It is therefore clear enough that different geometry has a significant effect on the heat flows flowing inside the thermal diodes.

It is worth pointing out the impact of geometry on the optimal rectification factor of the conductive thermal diodes. We have shown in Figures 2.4(a) and 2.4(b) the plots of rectification factor  $R$  of the spherical and cylindrical thermal diodes, as a function of the hotter temperature  $T_h$  and three values of the effective thermal resistance between the terminals of VO<sub>2</sub> and non-PCM. We have shown that the optimal rectification factors  $R_{opt} = 20.8\%$  and  $R_{opt} = 20.7\%$  of the spherical and cylindrical thermal diodes are obtained for  $\delta = 0.28 \text{ KW}^{-1}$  and  $\mu = 0.24 \text{ KW}^{-1}$ , at the temperatures  $T_h = 376 \text{ K}$  and  $T_h = 376.5 \text{ K}$ , respectively. We have also shown that higher or lower values of  $\delta$  and  $\mu$  generate higher rectification factors, as confirmed by the density plots in Figures 2.5(a) and 2.5(b), for both the spherical and cylindrical thermal diodes, respectively. One can see that the optimal rectification factors are generally independent of the diode geometry as described in equation (2.44), and as shown in the black lines in Figures 2.4(a) and 2.4(b), respectively. On the other hand, the temperature difference between the terminals of the spherical ( $376 - 300 = 76 \text{ K}$ ) and cylindrical ( $376.5 - 300 = 76.5 \text{ K}$ ) thermal diodes are larger than that ( $369.5 - 300 = 69.5 \text{ K}$ ) reported by Ordóñez-Miranda *et al.* [Ord18b] for a plane thermal diode with a comparable rectification factor. A plane thermal diode is therefore expected

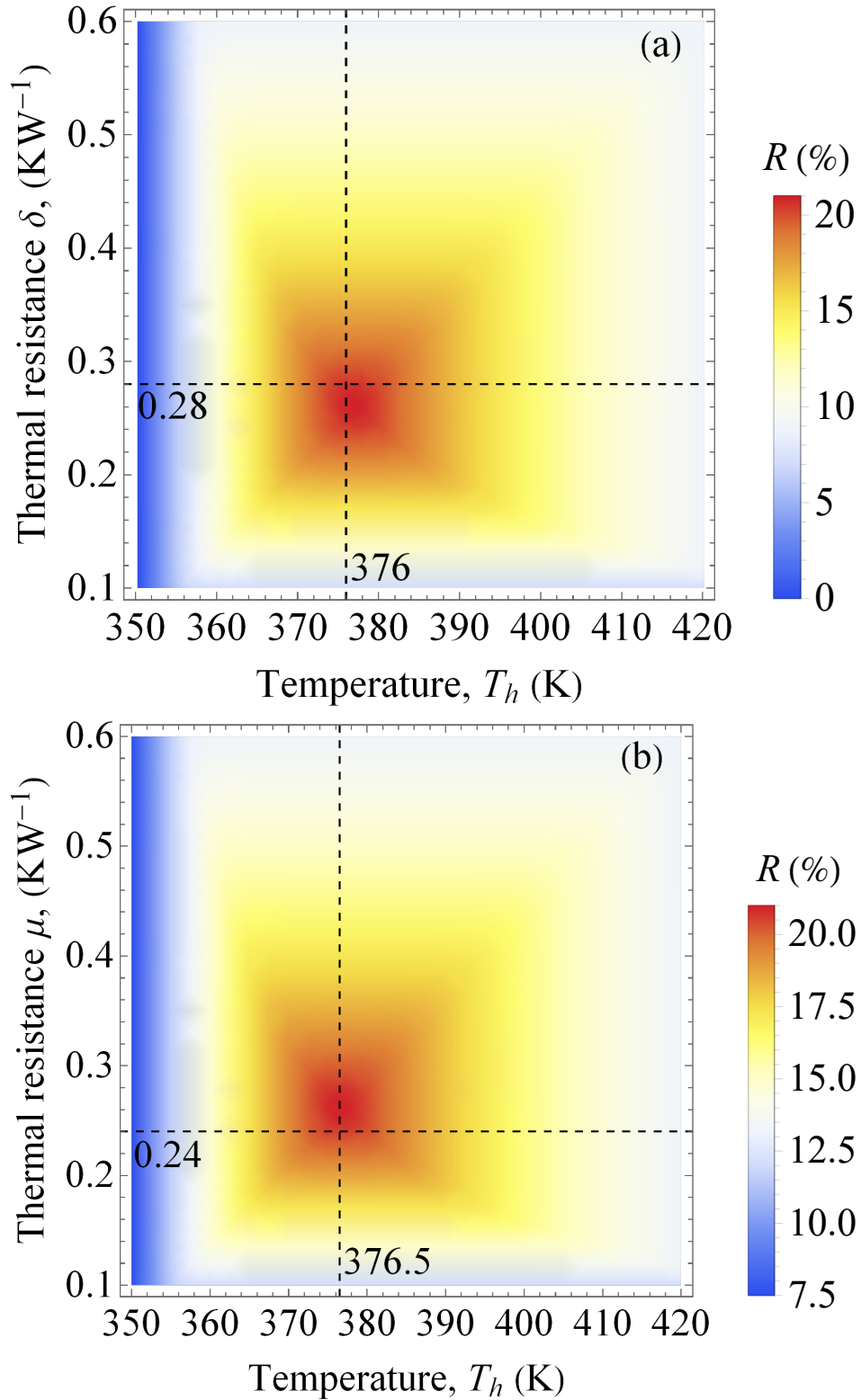


FIGURE 2.5: Rectification factor of a (a) spherical and (b) cylindrical thermal diodes, as a function of the hotter temperature  $T_h$  and effective thermal resistance  $\delta$  and  $\mu$ , respectively. Calculations were done for three representative values of the effective thermal resistances,  $T_c = 300$  K,  $a = 1$   $\mu\text{m}$  and  $b = 10$   $\mu\text{m}$  [Kas19].

to require smaller temperature gradients than spherical and cylindrical ones to reach the same optimal rectification factor.

## 2.5 Conclusions

In summary, we have theoretically analyzed and optimized the rectification factor of a spherical and cylindrical conductive thermal diodes consisted of a junction between a phase-change material, whose thermal conductivity significantly change in a narrow interval of temperature, and a non-phase-change material with a constant thermal conductivity. We have achieved this by deriving simple analytical expressions for the heat flows, temperature profiles and optical rectification factor of both spherical and cylindrical thermal diodes. It has been shown that different diode geometry has a sizeable effect in the heat flows and temperature profiles. On the other hand, it has no impact on the optical rectification factor, since its values are independent of the diode geometry. Optimal rectification factor of up to 20.8% and 20.7% have been obtained for the spherical and cylindrical thermal diodes operating with a temperature variation of 76 K and 76.5 K, respectively. The proposed model will be a useful guide for the development of phase-change materials required to optimize the rectification of conductive thermal diodes with different geometries.

## 2.6 Résumé du chapitre 2

### Introduction

Ce chapitre développe de nouvelles solutions analytiques de l'équation de la chaleur décrivant le transfert de chaleur dans des diodes thermiques conductives présentant des géométries sphériques et cylindriques. Récemment, de nombreux chercheurs ont étudié les configurations de mécanismes et de dispositifs qui pourraient conduire à des facteurs de rectification thermique importants dans les diodes thermiques à semi-conducteurs. L'un des mécanismes les plus prometteurs exploite les transitions métal-isolant. Par exemple, le changement mesuré de la conductivité thermique de  $\text{VO}_2$  à travers la transition métal-isolant fournit une non-linéarité significative qui permet la rectification thermique. Même si plusieurs modèles théoriques antérieurs ont été développés pour prédire la rectification thermique de matériaux à changement de phase dans des géométries planes, aucun modèle existant n'est disponible pour décrire les diodes thermiques conductives sphériques et cylindriques. Ici, nous avons développé des solutions analytiques pour quantifier les performances des diodes thermiques conductives sphériques et cylindriques fonctionnant avec un matériau à changement de phase, dont la conductivité thermique change de manière significative dans un intervalle étroit de températures.

Les différentes sections du chapitre peuvent se résumer comme suit:

### Modélisation théorique

Comme le montre la figure 2.6 ci-dessous, on étudie le cas d'un bain thermique sphérique/ou cylindrique  $\text{VO}_2$  échangeant par conduction thermique en

régime permanent avec un autre matériau dont l'état ne change pas avec la température. Nous considérons à la fois les configurations avant et arrière telles que le paramètre  $T_h$  est toujours supérieur à  $T_c$ . Les valeurs des flux de chaleur  $q_F$  et  $q_B$  sont pilotées par différentes conductivités thermiques, c'est-à-dire  $\kappa_1(T)$  de VO<sub>2</sub> et  $\kappa_2$  du non-PCM. Ces valeurs sont différentes ( $q_F \neq q_B$ ), en raison de la dépendance de la température de  $\kappa_1(T)$ , pour des températures prenant des valeurs de le domaine de la MIT de VO<sub>2</sub>. L'optimisation de la différence de flux thermique ( $q_F - q_B$ ) peut donc être réalisée en réglant les températures des bornes comme suit:  $T_c < T_0 < T_h$ , avec  $T_0$  étant la température de transition de VO<sub>2</sub>.

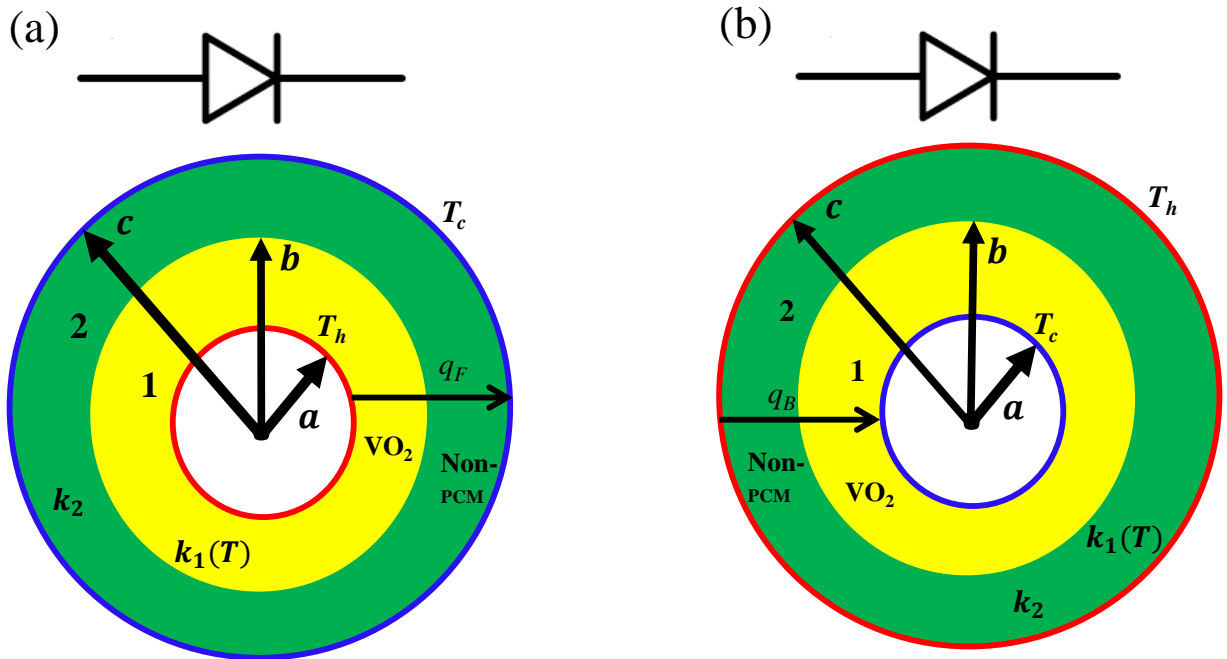


FIGURE 2.6: Schéma d'une diode thermique conductive sphérique (ou cylindrique) constituée une VO<sub>2</sub> et d'un Non-PCM, et fonctionnant dans les configurations avant et arrière. Les surfaces  $r = a$  et  $r = c$  sont fixées aux températures  $T_h$  et  $T_c$ , pour la configuration avant, alors qu'elles sont inversées dans la configuration arrière.

### Solutions analytiques décrivant le flux de chaleur dans des diodes thermiques sphériques et cylindriques

Des expressions analytiques simples sont obtenues pour les flux de chaleur

directs et inverses, notamment profil de température et les facteurs de rectification optimaux des deux diodes, comme présenté dans les sections 2.2 et 2.3, respectivement.

### **Conclusions**

Dans ce chapitre, nous avons théoriquement analysé et optimisé le facteur de redressement d'une diode thermique conductive sphériques ou cylindriques composée d'une jonction constituée d'un matériau à changement de phase, dont la conductivité thermique change de manière significative dans un intervalle de température étroit, et d'un matériau standard présentant une conductivité thermique constante. Nous avons atteint cet objectif en établissant des expressions analytiques simples pour les flux de chaleur, les profils de température et le facteur de rectification des diodes thermiques sphériques et cylindriques. Il a été montré que la géométrie différente des diodes a un effet important sur les flux thermiques et les profils de température. En revanche, il n'a pas d'impact sur le facteur de redressement optique, puisque son expression ne dépend pas de la géométrie de la diode. Un facteur de rectification optimal allant jusqu'à 20.8% et 20.7% a été obtenu pour les diodes thermiques sphériques et cylindriques fonctionnant avec une différence de température de 76 K and 76.5 K, respectivement. Le modèle proposé sera un outil utile pour le développement de matériaux à changement de phase nécessaires pour optimiser la rectification des diodes thermiques conductives de géométries différentes.

## Chapter 3

## Chapter 3

---

# Dual phase-change materials conductive thermal diode

### Contents

---

<b>3.1</b>	<b>Introduction</b> . . . . .	<b>95</b>
<b>3.2</b>	<b>Analytical solution of heat conduction model</b> . . . . .	<b>97</b>
<b>3.3</b>	<b>Heat fluxes and temperature profiles</b> . . . . .	<b>97</b>
3.3.1	Forward configuration . . . . .	97
3.3.2	Backward configuration . . . . .	102
<b>3.4</b>	<b>Rectification factor</b> . . . . .	<b>103</b>
3.4.1	Forward and backward configuration . . . . .	103
<b>3.5</b>	<b>Temperature evolution of heat fluxes and rectification factor</b> .	<b>106</b>
<b>3.6</b>	<b>Heat fluxes and interface temperatures</b> . . . . .	<b>109</b>
<b>3.7</b>	<b>Temperature dependence rectification factor</b> . . . . .	<b>112</b>
<b>3.8</b>	<b>Conclusions</b> . . . . .	<b>115</b>
<b>3.9</b>	<b>Résumé du chapitre 3</b> . . . . .	<b>116</b>

---



## 3.1 Introduction

Unlike in chapter 2 where we studied the optimization of conductive thermal diodes made up of a junction between a PCM and non-PCM for two different geometries, here, we theoretically studied and optimized the thermal rectification of a plane conductive thermal diode made up of two PCMs, whose thermal conductivities change narrowly with respect to temperatures. Given that the thermal rectification of conductive heat fluxes is established based on the temperature dependence of the thermal conductivities of the thermal diodes terminals [Li14], therefore, it can, in principle, be generated using arbitrary solid materials subjected to a large temperature gradient. According to Fourier's law of heat conduction, Yang *et al.* [Yan18] theoretically studied and optimized the thermal rectification effect of a conductive thermal diode made up of two-component materials, whose thermal conductivities depend linearly and quadratically with temperature. For the linear temperature-dependent thermal conductivities, they predicted a maximum rectification ratio of 0.5, which reached 0.86, for the quadratic temperature-dependent one. These relatively high thermal rectification ratios required a temperature variation greater than 100 K between the diode terminals, which could be practically difficult and expensive to achieve. This drawback can be subdued by using PCMs, such as VO<sub>2</sub>, Ge<sub>2</sub>Sb<sub>2</sub>Te<sub>5</sub> (GST), nitinol, and polyethylene (PE), whose thermal conductivities significantly change in a narrow interval of temperatures [Ord16; Ito14; Rin08; Ito16]. Recently, these strongly phonon-electron correlated PCMs have received significant attention in both theoretical and experimental studies, as a result of their MIT at a temperature near the room one. For example, the thermal conductivities of VO<sub>2</sub> and PE considered in this chapter, change within a narrow interval of temperatures as  $340 \text{ K} < T < 345 \text{ K}$  and  $395 \text{ K} < T < 400 \text{ K}$ , respectively [Zha15; Ord18b]. The fact that the MIT of VO<sub>2</sub> occurs at a temperature closer to room one has motivated

Ordóñez-Miranda *et al.* [Ord18b] to combine it with another non-PCM, as a terminal of a plane conductive thermal diode. However, optimal rectification factors reported was lower ( $\sim 20\%$ ) than the ones reported by Yang *et al.* [Yan18]. It is thus clear that the operation of a conductive thermal diode made up of two PCMs terminal maximizes its rectification factors and, as well reduces the temperature difference between its terminal, as reported by Cottrill *et al.* [Cot18].

Based on the alternative definition of the rectification factor  $R_a = [\max(q_F, q_B) / \min(q_F, q_B)] - 1$  [Kan18], which is different than the one we presented in equation (1.9). Hyungmook *et al.* [Kan18] recently reported a maximum rectification factor of up to 147% for a conductive thermal diode operating within the terminal of VO<sub>2</sub> and PE, whose thermal conductivities also change significantly with temperatures. Even though their rectification factor is relatively high, however, it was generated by describing the thermal conductivities of the PCMs as step functions, which is similar but not equal to their real behaviors, as the phase transitions of VO<sub>2</sub> and PE occur in a temperature variation greater than 5K. Due to this fact, we report in this chapter a more realistic description of the thermal conductivities for the rectification of conductive thermal diode made up of a junction of these two PCMs. Firstly, we consider the temperature dependence of the thermal conductivities of both PCMs within their MIT. Secondly, we derive and analyze expressions for the temperature profiles, heat fluxes and lastly, we calculate the optimal rectification factor for the steady-state heat conduction following a similar procedure than the one developed in chapter 2. Note that the conductive thermal diode described in this chapter is based on the combination of two PCMs. As a result, these elements are expected to generate rectification factors higher than the single PCM thermal diode predicted in chapter 2 for different geometries and as well as the single PCM reported by Ordóñez-Miranda *et al.* [Ord18b].

## 3.2 Analytical solution of heat conduction model

Here, we discuss the effect of thermal rectification in a system, as illustrated in Figures 3.1(a) and 3.1(b), where dual PCMs are exchanging heat through steady-state conduction due to their temperature difference  $T_h - T_c > 0$ . We examine the system in two thermal operating configurations, as follows: (i) In the forward configuration [Figure 3.1(a)], the heat flux  $q_F$  flows from VO<sub>2</sub> (PCM1) to PE (PCM2) i.e, (PCM1 is in its metallic phase while PCM2 is in its insulating one) and (ii) In the backward one [Figure 3.1(b)], the heat flux  $q_B$  flows in the opposite direction (PCM1 is in its insulating phase while PCM2 is in its metallic one), as a result of the interchange of the temperatures  $T_h$  and  $T_c$ . For the sake of this chapter, we assume that the values of  $q_F$  and  $q_B$  are driven by the thermal conductivities of  $\kappa_1(T)$  of PCM1 and  $\kappa_2(T)$  of PCM2. Therefore, they are expected not to be the same ( $q_F \neq q_B$ ), due to the temperature dependence of  $\kappa_1(T)$  and  $\kappa_2(T)$ , respectively.

## 3.3 Heat fluxes and temperature profiles

### 3.3.1 Forward configuration

The steady-state heat flux  $q_F$  in the forward configuration of the thermal diode presented in Figure 3.1(a) can be described according to the Fourier's law of heat conduction and the principle of conservation of energy, as follows:

$$q_F = -\kappa_1(T_1) \frac{dT_1}{dx} = -\kappa_2(T_2) \frac{dT_2}{dx}, \quad (3.1)$$

where  $T_1(x)$  and  $T_2(x)$  are the temperatures within the PCM1 ( $0 \leq x \leq L_1$ ) and PCM2 ( $L_1 \leq x \leq L_1 + L_2$ ), respectively. In this chapter, we consider that the thermal conductivities  $\kappa_1(T)$  and  $\kappa_2(T)$  belong to VO<sub>2</sub> and PE, respectively, and

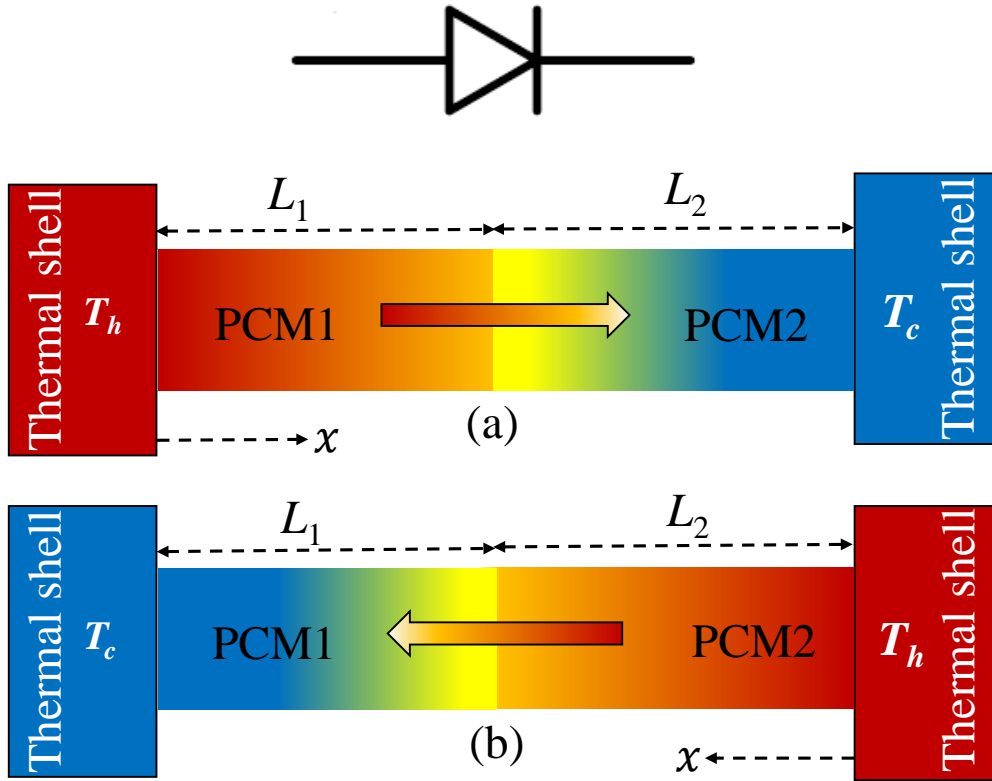


FIGURE 3.1: Scheme of a dual PCMs conductive thermal diode operating in the (a) forward and (b) backward configurations. Hot and cool thermal shells are set at the temperatures  $T_h$  and  $T_c$ , respectively [Kas20a].

their temperature differences are shown in Figure 3.2, within their corresponding MITs. It can be seen that the thermal conductivity contrast ( $25/5 = 5$ ) of PE is higher than ( $6/3.6 = 1.7$ ) of  $\text{VO}_2$ . Note that they both reach their maximum thermal conductivities for temperatures  $T < 395$  K and  $T > 345$  K, respectively. This details along with equation (3.1), shows that  $q_F$  can be maximized by properly setting the temperature of the hotter shell  $T_h$  and that of the colder one  $T_c$  to fulfill the aforementioned temperature conditions. According to equation (1.10), the thermal conductivities of  $\text{VO}_2$  and PE can be described, as follows:

$$\kappa_1(T) = \kappa_{i1} + \frac{\kappa_{m1} - \kappa_{i1}}{1 + e^{-\beta_1(T-T_{01})}}, \quad (3.2a)$$

$$\kappa_2(T) = \kappa_{i2} + \frac{\kappa_{m2} - \kappa_{i2}}{1 + e^{-\beta_2(T-T_{02})}}, \quad (3.2b)$$

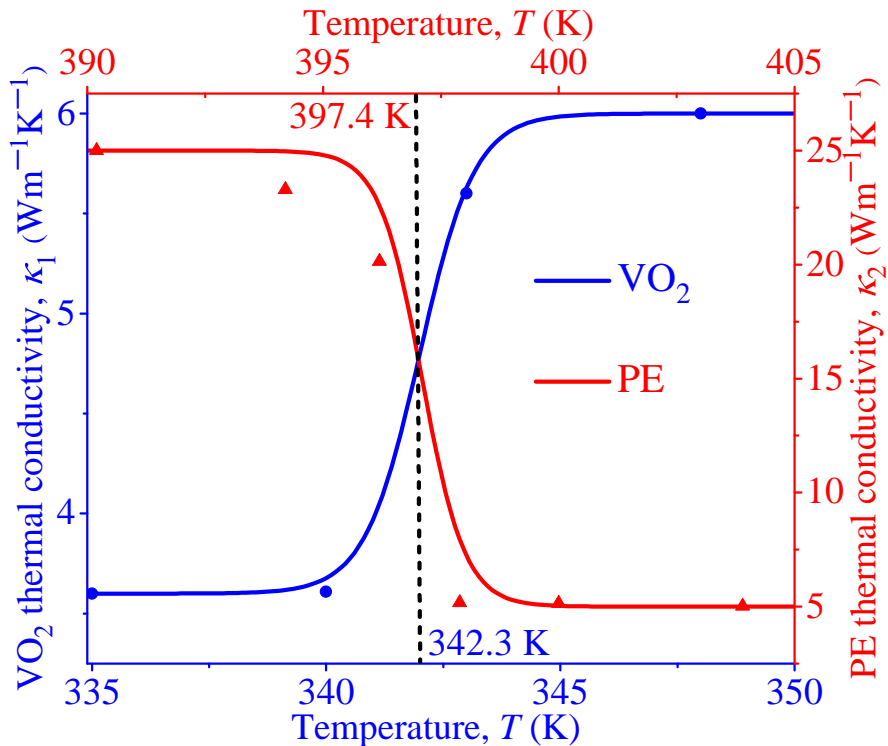


FIGURE 3.2: Thermal conductivities of VO<sub>2</sub> and PE, as functions of the temperature within their corresponding MIT. Dots and triangles stand for experimental data reported in the literature [Oh10; Zha15], while lines represent the theoretical predictions of equations (3.2a) and (3.2b), respectively [Kas20a].

where  $\kappa_{m1}$  and  $\kappa_{i1}$  are the thermal conductivities of VO<sub>2</sub> in its high- and low-temperature phases, and  $\beta_1$  is the phase-transition slope of  $\kappa_1(T)$  at the transition temperature  $T = T_{01}$ . On the other hand,  $\kappa_{m2}$  and  $\kappa_{i2}$  are the thermal conductivities of PE in its high- and low-temperature phases and  $\beta_2$  is the phase-transition slope of  $\kappa_2(T)$  at the transition temperature  $T = T_{02}$ . The values of these parameters were calculated by fitting equations (3.2a) and (3.2b) to the experimental data shown in Figure 3.2 for VO<sub>2</sub> and PE, and they are summarized in Table 3.1, respectively.

TABLE 3.1: Properties of materials involved in equations (3.2a) and (3.2b) [Kas20a].

Material	$\kappa_{in}(\text{Wm}^{-1}\text{K}^{-1})$	$\kappa_{mn}(\text{Wm}^{-1}\text{K}^{-1})$	$\beta_n(\text{K}^{-1})$	$T_{0n}(\text{K})$
VO <sub>2</sub>	3.6	6	1.7	342.3
PE	25	5	2.2	397.4

The temperature profiles  $T_1(x)$  and  $T_2(x)$  of the VO<sub>2</sub> and PE can now be determined by integrating equation (3.1) with the thermal conductivities expressions in equations (3.2a) and (3.2b) as:

$$-\int q_F dx = \int \left[ \kappa_{i1} + \frac{\kappa_{m1} - \kappa_{i1}}{1 + e^{-\beta_1(T-T_{01})}} \right] dT, \quad (3.3a)$$

$$-\int q_F dx = \int \left[ \kappa_{i2} + \frac{\kappa_{m2} - \kappa_{i2}}{1 + e^{-\beta_2(T-T_{02})}} \right] dT. \quad (3.3b)$$

The integration of equations (3.3a) and (3.3b) gives

$$\kappa_{m1}(T - T_{01}) + \frac{\kappa_{m1} - \kappa_{i1}}{\beta_1} \ln \left[ 1 + e^{-\beta_1(T-T_{01})} \right] = C_1 + q_F x, \quad (3.4a)$$

$$\kappa_{m2}(T - T_{02}) + \frac{\kappa_{m2} - \kappa_{i2}}{\beta_2} \ln \left[ 1 + e^{-\beta_2(T-T_{02})} \right] = C_2 + q_F x, \quad (3.4b)$$

where  $C_1$  and  $C_2$  are constants of integration. The expression for the temperatures  $T_1(x)$  and  $T_2(x)$  can be written from equations (3.4a) and (3.4b), as follows:

$$T_1(x) - T_{01} + \frac{1}{\beta_1 \gamma_1} \ln[1 + \lambda_1(T_1(x))] = \frac{C_1}{\kappa_{m1}} - \frac{q_F}{\kappa_{m1}} x, \quad (3.5a)$$

$$T_2(x) - T_{02} + \frac{1}{\beta_2 \gamma_2} \ln[1 + \lambda_2(T_2(x))] = \frac{C_2}{\kappa_{m2}} - \frac{q_F}{\kappa_{m2}} x, \quad (3.5b)$$

where  $\gamma_n = \kappa_{mn} / (\kappa_{mn} - \kappa_{in})$ , and  $\lambda_n(T) = \exp[-\beta_n(T - T_{0n})]$ . The evaluation of equations (3.5a) and (3.5b) with the following boundary conditions:  $T_1(0) = T_h$ ,  $T_1(L_1)$ ,  $T_2(L_1 + L_2) = T_c$ , and  $T_1(L_1) - T_2(L_1) = \rho q_F$ , where  $\rho$  is the interface

thermal resistance between the PCM1 and PCM2, respectively. The result yields:

$$T_h - T_{01} + \frac{1}{\beta_1 \gamma_1} \ln[1 + \lambda_1(T_h)] = \frac{C_1}{\kappa_{m1}}, \quad (3.6a)$$

$$T_1(L_1) - T_{01} + \frac{1}{\beta_1 \gamma_1} \ln[1 + \lambda_1(T_1(L_1))] = \frac{C_1}{\kappa_{m1}} - \frac{q_F}{\kappa_{m1}} L_1, \quad (3.6b)$$

$$T_2(L_1) - T_{02} + \frac{1}{\beta_2 \gamma_2} \ln[1 + \lambda_2(T_2(L_1))] = \frac{C_2}{\kappa_{m2}} - \frac{q_F}{\kappa_{m2}} L_1, \quad (3.6c)$$

$$T_c - T_{02} + \frac{1}{\beta_2 \gamma_2} \ln[1 + \lambda_2(T_c)] = \frac{C_2}{\kappa_{m2}} - \frac{q_F}{\kappa_{m2}} (L_1 + L_2). \quad (3.6d)$$

The expressions for the parameters  $q_F$ ,  $C_1$  and  $C_2$  are determined by solving equations (3.6a) to (3.6d), thus results in the following expressions for the heat flux and temperature profiles

$$q_F = \frac{1}{\alpha_1} \ln \left[ \frac{G_1(T_h)}{G_1(T_1(L_1))} \right], \quad (3.7a)$$

$$q_F = \frac{1}{\alpha_2} \ln \left[ \frac{G_2(T_1(L_1) - \rho q_F)}{G_2(T_c)} \right], \quad (3.7b)$$

$$G_1(T_1(x)) = [G_1(T_h)]^{1-x/L_1} [G_1(T_1(L_1))]^{x/L_1}, \quad (3.7c)$$

$$G_2(T_2(x)) = [G_2(T_1(L_1) - \rho q_F)]^{1-(x-L_1)/L_2} [G_2(T_c)]^{(x-L_1)/L_2}, \quad (3.7d)$$

where  $\alpha_n = \beta_n \gamma_n \rho_{mn}$ ,  $\rho_{mn} = L_n / \kappa_{mn}$ , and  $G_n(T) = [1 + \lambda_n(T)] / [\lambda_n(T)]^{\gamma_n}$ . By substituting equations (3.7a) into (3.7b), we obtain

$$\left( \frac{G_1(T_h)}{G_1(\theta)} \right)^{\frac{\alpha_2}{\alpha_1}} = \frac{G_2 \left( \theta - \frac{\rho}{\alpha_1} \ln \left[ \frac{G_1(T_h)}{G_1(\theta)} \right] \right)}{G_2(T_c)}, \quad (3.8)$$

where  $\theta = T_1(L_1)$ . One can see that equation (3.8) has a strongly non-linear dependence on the temperatures  $T_h$  and  $T_c$ , respectively. One can also see that equation (3.8) can not be solved analytically. Consequently, we have numerically determined the interface temperature  $\theta$  using "FindRoot" Wolfram Mathematica

inbuilt tool. The heat flux in the forward configuration and the temperature profiles can then be determined through equations (3.7a) to (3.7d), for a given values of  $T_h$  and  $T_c$ .

### 3.3.2 Backward configuration

We have determined the heat flux in the backward configuration ( $q_B$ ) and the temperature profiles [ $T_1(x)$  and  $T_2(x)$ ] by following a procedure similar to the one developed in the case of the forward configuration. The only difference here is that the boundary conditions are now in reversed form, is given as follows:  $T_2(0) = T_h$ ,  $T_1(L_1 + L_2) = T_c$ , and  $T_2(L_2) - T_1(L_2) = \rho q_B$ . The final expressions for the  $q_B$  and [ $T_1(x)$  and  $T_2(x)$ ] are

$$q_B = \frac{1}{\alpha_1} \ln \left[ \frac{G_1(T_1(L_2))}{G_1(T_c)} \right], \quad (3.9a)$$

$$q_B = \frac{1}{\alpha_2} \ln \left[ \frac{G_2(T_h)}{G_2(T_1(L_2) + \rho q_B)} \right], \quad (3.9b)$$

$$G_1(T_1(x)) = [G_1(T_1(L_2))]^{1-(x-L_2)/L_1} [G_1(T_c)]^{(x-L_2)/L_1}, \quad (3.9c)$$

$$G_2(T_2(x)) = [G_2(T_h)]^{1-x/L_2} [G_2(T_1(L_2) + \rho q_B)]^{x/L_2}. \quad (3.9d)$$

Again, by substituting equation (3.9a) into (3.9b), we obtain

$$\left( \frac{G_1(\phi)}{G_1(T_c)} \right)^{\frac{\alpha_2}{\alpha_1}} = \frac{G_2(T_h)}{G_2\left(\phi + \frac{\rho}{\alpha_1} \ln \left[ \frac{G_1(\phi)}{G_1(T_c)} \right]\right)}, \quad (3.10)$$

where  $\phi = T_1(L_2)$ . Equation (3.10) is a transcendental equation for the interface temperature  $\phi$ , which depends non-linearly on  $T_h$  and  $T_c$ . The numerical solution of  $\phi$  in equation (3.10) was then carried out by using the same tool as in the forward one, which fully describes the heat conduction in the thermal diode through equations (3.9a) to (3.9d). Given that the heat fluxes and temperature profiles in the forward configuration are not the same as the backward ones,

there exists a thermal rectification effect between the terminals of the thermal diode. This fact is in agreement with that discussed in section 3.2.

## 3.4 Rectification factor

### 3.4.1 Forward and backward configuration

In order to determine the rectification factor of a conductive thermal diode from equation (1.9), we have to maximize  $q_F$  in equations (3.7a) and (3.7b) and minimize  $q_B$  in equations (3.9a) and (3.9b). To achieve this, we have rewritten the aforementioned equations, as follows:

$$q_F = \frac{T_h - \theta}{\rho_{m1}} + \frac{(\rho_{m1})^{-1}}{\beta_1 \gamma_1} \ln \left[ \frac{1 + e^{-\beta_1(T_h - T_{01})}}{1 + e^{-\beta_1(\theta - T_{01})}} \right], \quad (3.11a)$$

$$q_F = \frac{\theta - T_c}{\rho + \rho_{m2}} + \frac{(\rho + \rho_{m2})^{-1}}{\beta_2 \gamma_2} \ln \left[ \frac{1 + e^{\beta_2(T_{02} + \rho q_F - \theta)}}{1 + e^{\beta_2(T_{02} - T_c)}} \right], \quad (3.11b)$$

$$q_B = \frac{\phi - T_c}{\rho_{m1}} - \frac{(\rho_{m1})^{-1}}{\beta_1 \gamma_1} \ln \left[ \frac{1 + e^{\beta_1(T_{01} - T_c)}}{1 + e^{\beta_1(T_{01} - \phi)}} \right], \quad (3.11c)$$

$$q_B = \frac{T_h - \phi}{\rho + \rho_{m2}} - \frac{(\rho + \rho_{m2})^{-1}}{\beta_2 \gamma_2} \ln \left[ \frac{1 + e^{-\beta_2(\phi - T_{02} + \rho q_B)}}{1 + e^{-\beta_2(T_h - T_{02})}} \right]. \quad (3.11d)$$

It can be seen in equation (3.11a) that when temperature  $T_h$  is high enough to fulfill the following conditions:  $\beta_1(T_h - T_{01}) \gg 1$  and  $\beta_1(\theta - T_{01}) \gg 1$ , the latter equation reduces to

$$q_F = \frac{T_h - \theta}{\rho_{m1}}, \quad (3.12)$$

where  $\rho_{m1} = L_1/\kappa_{m1}$ . On the other hand, in equation (3.11b) when temperature  $T_c$  is low enough to fulfil the conditions  $\beta_2(T_{02} - T_c) \gg 1$ , and  $\beta_2(\rho q_F + T_{02} - \theta) \gg 1$ , the aforementioned equation reduces to

$$q_F = \frac{\theta - T_c}{\rho + \rho_{i2}}, \quad (3.13)$$

where  $\rho_{i2} = L_2/\kappa_{i2}$ . By combining equations (3.12) and (3.13), we obtain

$$q_F = \frac{T_h - \theta}{\rho_{m1}} = \frac{\theta - T_c}{\rho + \rho_{i2}}. \quad (3.14)$$

It can clearly be seen in equation (3.14) that under the conditions used to derive them, the entire terminal 1 (PCM1) is in its high-temperature metallic phase, while the entire terminal 2 (PCM2) is in its low-temperature insulating phase. It can also be seen in Figure 3.2 that PCM1 and PCM2, respectively in their metallic and insulating phases, both exhibit their highest thermal conductivities. This configuration therefore maximizes the forward heat flux  $q_F = q_{F,\max}$  that can be obtained by solving for  $\theta$  in equation (3.14), as follows:

$$\theta = T_{1,\max}(L_1) = \frac{(\rho + \rho_{i2})T_h + \rho_{m1}T_c}{\rho_{m1} + \rho + \rho_{i2}}. \quad (3.15)$$

We recall from the forward configuration boundary condition  $T_1(L_1) - T_2(L_1) = \rho q_F$  and substitute equation (3.15), we obtain

$$T_{2,\max}(L_1) = \frac{\rho_{i2}T_h + (\rho_{m1} + \rho)T_c}{\rho_{m1} + \rho + \rho_{i2}}. \quad (3.16)$$

By substituting equations (3.15) into (3.12), we obtain the maximum  $q_F$  as

$$q_{F,\max} = \frac{T_h - T_c}{\rho_{m1} + \rho + \rho_{i2}}. \quad (3.17)$$

Note that  $T_1(L_1) = T_{1,\max}(L_1)$  and  $T_2(L_1) = T_{2,\max}(L_1)$  are the interface temperatures related to  $q_{F,\max}$ .

Similarly, one can see that in equations (3.11c) and (3.11d) the temperatures  $T_h$  and  $T_c$  are high and low enough to fulfill the conditions  $\beta_1(T_{01} - T_c) \gg 1$ ,  $\beta_1(T_{01} - \phi) \gg 1$ ,  $\beta_2(T_h - T_{02}) \gg 1$ , and  $\beta_2(\rho q_B + \phi - T_{02}) \gg 1$ . By applying the

aforementioned conditions to the latter equations, they becomes

$$q_B = \frac{\phi - T_c}{\rho_{i1}}, \quad (3.18a)$$

$$q_B = \frac{T_h - \phi}{\rho + \rho_{m2}}, \quad (3.18b)$$

where  $\rho_{i1} = L_1/\kappa_{i1}$  and  $\rho_{m2} = L_2/\kappa_{m2}$ . The combination of equations (3.18a) and (3.18b) yields

$$q_B = \frac{\phi - T_c}{\rho_{i1}} = \frac{T_h - \phi}{\rho + \rho_{m2}}. \quad (3.19)$$

Equation (3.19) explicitly indicates that under the condition used to derive them, the entire terminal 1 (PCM1) is in its low temperature insulating phase, while the whole terminal 2 (PCM2) is in its high temperature metallic one. In contrary to the forward case, one can see in Figure 3.2 that PCM1 and PCM2, respectively in their insulating and metallic phases, both exhibit their lowest thermal conductivities. This configuration therefore minimizes the backward heat flux  $q_B = q_{B,\min}$ , which can be obtained by solving for  $\phi$  in equation (3.19). The result gives

$$\phi = T_{1,\min}(L_2) = \frac{\rho_{i1}T_h + (\rho + \rho_{m2})T_c}{\rho_{i1} + \rho + \rho_{m2}}. \quad (3.20)$$

By recalling the boundary condition  $T_2(L_2) - T_1(L_2) = \rho q_B$  from the backward configuration and substitute equation (3.20), we obtain

$$T_{2,\min}(L_2) = \frac{(\rho_{i1} + \rho)T_h + \rho_{m2}T_c}{\rho_{i1} + \rho + \rho_{m2}}. \quad (3.21)$$

By substituting equations (3.20) into (3.18a), we obtain the maximum  $q_B$  as

$$q_{B,\min} = \frac{T_h - T_c}{\rho_{i1} + \rho + \rho_{m2}}. \quad (3.22)$$

Note that  $T_1(L_2) = T_{1,\min}(L_2)$  and  $T_2(L_2) = T_{2,\min}(L_2)$  are the interface temperatures related to  $q_B = q_{B,\min}$ . We determined the rectification factor by recalling equation (2.37) and substituting for equations (3.17) and (3.22). The final result yields

$$\begin{aligned}
 R_{\text{opt}} &= 1 - \frac{\rho_{m1} + \rho + \rho_{i2}}{\rho_{i1} + \rho + \rho_{m2}} \\
 &= 1 - \frac{\rho_{m1} (1 + \rho/\rho_{m1}) + (\kappa_{m1}/\kappa_{i2})r^{-1}}{\rho_{i1} (1 + \rho/\rho_{i1}) + (\kappa_{i1}/\kappa_{m2})r^{-1}} \\
 &= 1 - \frac{\kappa_{i1} (1 + \rho/\rho_{m1})r + \kappa_{m1}/\kappa_{i2}}{\kappa_{m1} (1 + \rho/\rho_{i1})r + \kappa_{i1}/\kappa_{m2}},
 \end{aligned} \tag{3.23}$$

where  $r = L_1/L_2$ . It can be seen that equation (3.23) is symmetric on the thermal resistances of both PCM1 and PCM2 and increases with the ratios of the thermal conductivities  $\kappa_{m1}/\kappa_{i1}$  and  $\kappa_{i2}/\kappa_{m2}$  between the metallic and insulating phases. It can also be seen that the optimal rectification in equation (3.23) depends on the interface thermal resistance  $\rho$  between the diode terminals. It is therefore different than the one reported in chapter 2 and than the conductive thermal diode operating with a single PCM reported by [Ord18b]. The  $R_{\text{opt}}$  presented here increases with decreasing  $\rho$ . This fact indicates that the optimization of the rectification factor of conductive thermal diodes based on two PCMs requires higher values of  $\kappa_{m1}/\kappa_{i1}$  and  $\kappa_{i2}/\kappa_{m2}$  and lower values of  $\rho$ .

### 3.5 Temperature evolution of heat fluxes and rectification factor

We show in Figure 3.3 the temperature evolution of the rectification factor and heat fluxes in the forward ( $q_F$ ) and backward ( $q_B$ ) configurations, respectively. We notice that the two heat fluxes of the conductive thermal diode increase linearly with temperature  $T_h$ , and the difference between them is positive

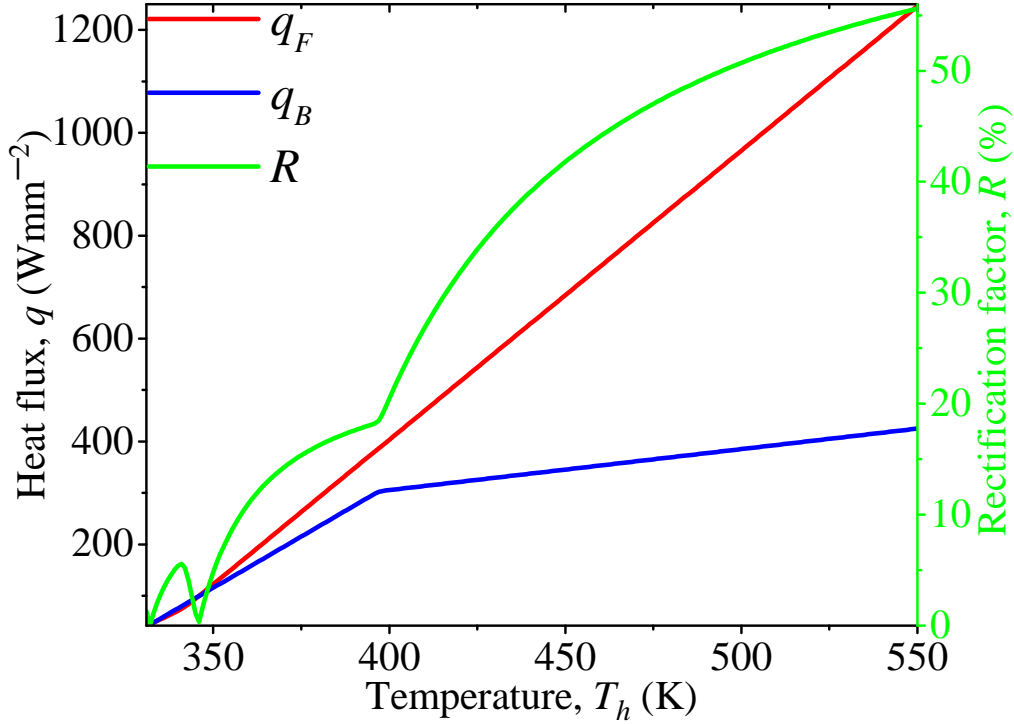


FIGURE 3.3: Rectification factor, forward and backward heat fluxes of the conductive thermal diode of VO<sub>2</sub> and PE, as functions of the temperature  $T_h$ . Calculations were done for  $T_c = 300$  K and  $\rho = 0$  mm<sup>2</sup>KW<sup>-1</sup> [Kas20a].

( $q_F > q_B$ ) for temperatures greater than the one where VO<sub>2</sub> exhibit its phase transition ( $T_{01} = 342.5$  K). The change in the slope of the forward heat flux  $q_F$  occurs, as a result of the phase transition of VO<sub>2</sub> at  $T_h = T_{01}$ . On the other hand, at temperature  $T_h \gg T_{01}$ , the difference between the two fluxes increases up to the temperature where PE is in its transition phase, before the kinks in the backward heat flux  $q_B$  at temperature  $T_h = T_{02}$ . This kink corresponds to the phase transition of PE. The local maximum and local minimum of the rectification factor occurs due to the relatively large difference and equality of the heat fluxes in the forward and backward configurations.

In Figures 3.4(a) and 3.4(b), we show the forward and backward heat fluxes of a conductive thermal diode as a function of their respective interface temperatures  $T_1(L_1)$  and  $T_2(L_2)$ . We observe that the heat fluxes  $q_F$  and  $q_B$  also increase

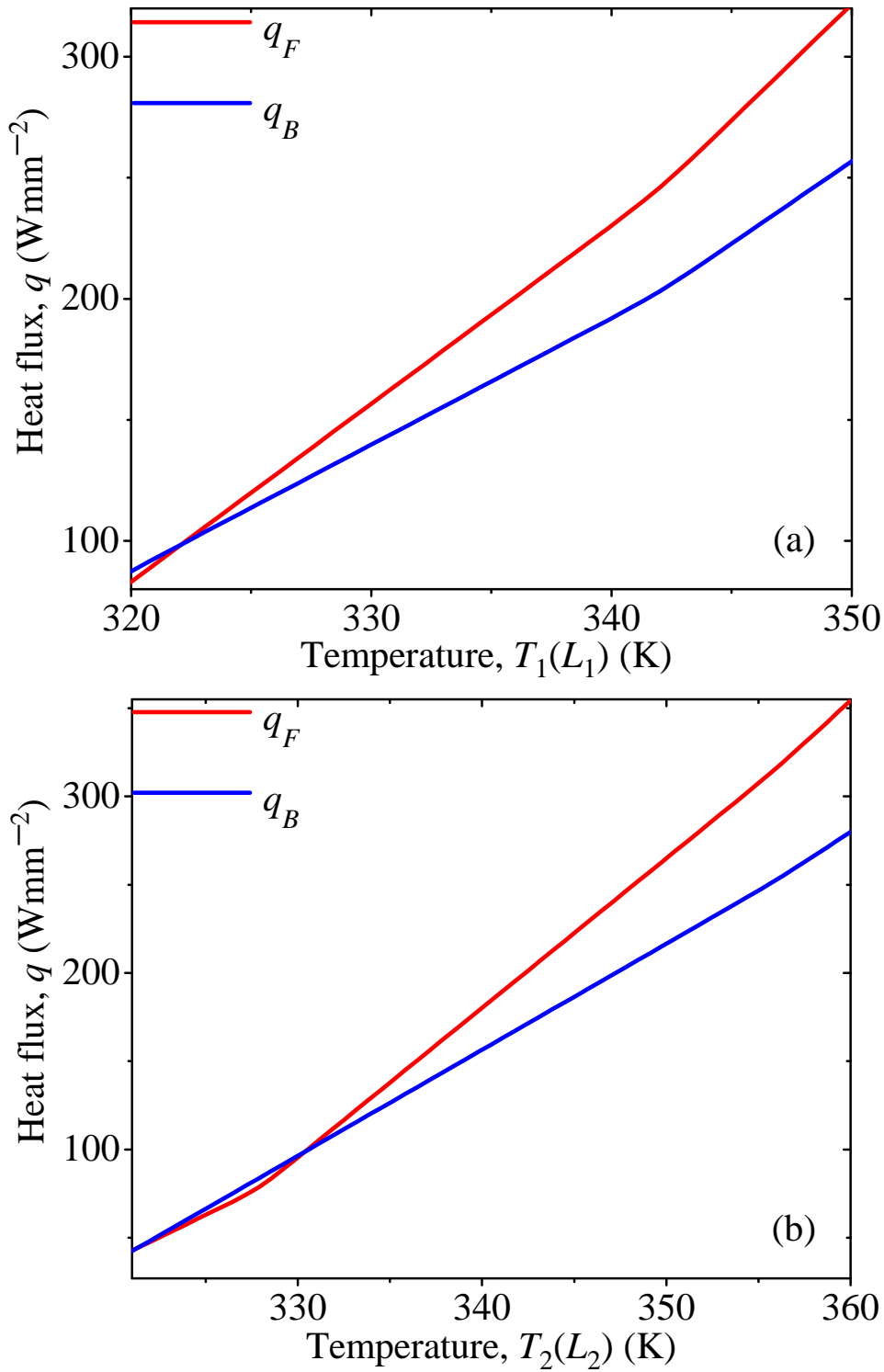


FIGURE 3.4: Temperature evolution of the forward and backward heat fluxes, as functions of (a)  $T_1(L_1)$  and (b)  $T_2(L_2)$ . Calculations were done for  $T_c = 300$  K and  $\rho = 0$   $\text{mm}^2\text{KW}^{-1}$  [Kas20a].

with  $T_1(L_1)$  and  $T_2(L_2)$  when compared to that reported in Figure 3.3, as expected. This fact is consistent with the behavior of a conductive thermal diode

presented in chapter 2. This result is also in good agreement with the theoretical studies reported by [Ord18b; Zhu18] and experimental one by [Cot18]. Furthermore, one can see that VO<sub>2</sub> in its metallic state is able to enhance the rectification factor of the reported conductive thermal diode when the temperature difference between its terminals is high enough.

### 3.6 Heat fluxes and interface temperatures

Figures 3.5(a) and 3.5(b) show the plots of the interface temperatures in the forward [ $T_1(L_1)$  and  $T_2(L_1)$ ] and backward [ $T_2(L_2)$  and  $T_1(L_2)$ ] configurations versus the hotter temperature  $T_h$ . It can be seen that the increases in these aforementioned interface temperatures with respect to  $T_h$  is driven by the combined effect of the thermal conductivities of VO<sub>2</sub> and PE, as expected. On the other hand, their differences  $T_1(L_1) - T_2(L_1) = \rho q_F$  and  $T_2(L_2) - T_1(L_2) = \rho q_B$  are determined by the forward and backward heat fluxes, as shown in Figure 3.3, respectively. We note that the temperature jumps increases as the temperature  $T_h$  increases, such that they tend towards constant values for high enough  $T_h$ . This fact is in good agreement with the temperature evolution shown in Figure 3.3 and also indicates that the maximization of the rectification factor of the conductive thermal diode would require high temperature jumps at the interface of its terminals, that is to say, for a given  $\rho > 0$ . According to the temperature profile shown in Figure 3.6, these jumps increases with a higher value of  $\rho$  and vanishes for  $\rho = 0$ . For a particular value of  $\rho = 1 \text{ mm}^2\text{KW}^{-1}$ , we obtained temperature jumps of  $T_1(L_1) - T_2(L_1) = 65 \text{ K}$  in the forward configuration while  $T_2(L_2) - T_1(L_2) = 55 \text{ K}$ , is obtained in the backward one. Given that the calculations in Figure 3.6 were carried out for maximizing the rectification factor for low-temperature  $T_c = 300\text{K}$  and high-temperature  $T_h = 500\text{K}$ , the nearly linear behavior of temperatures within the diode terminals is, therefore, as a result of

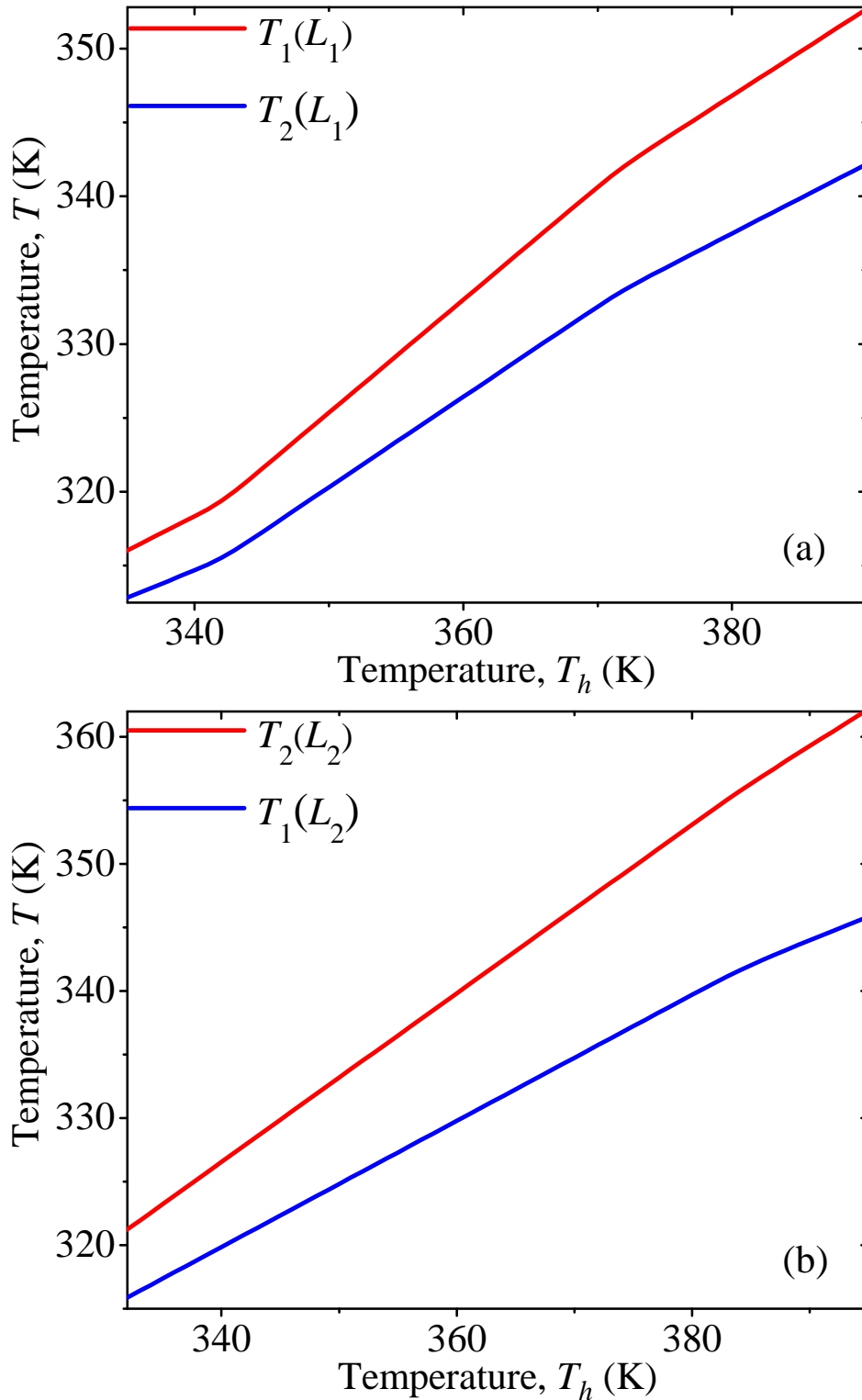


FIGURE 3.5: Interface temperatures for the (a) forward [ $T_1(L_1)$  and  $T_2(L_1)$ ] and (b) backward [ $T_2(L_2)$  and  $T_1(L_2)$ ] configurations, as functions of the temperature  $T_h$ . Calculations were done for  $T_c = 300$  K and  $\rho = 1 \text{ mm}^2\text{KW}^{-1}$  [Kas20a].

the fact that the entire terminals are either in their completely metallic or completely insulating phases. The change in the slope of the temperatures at the

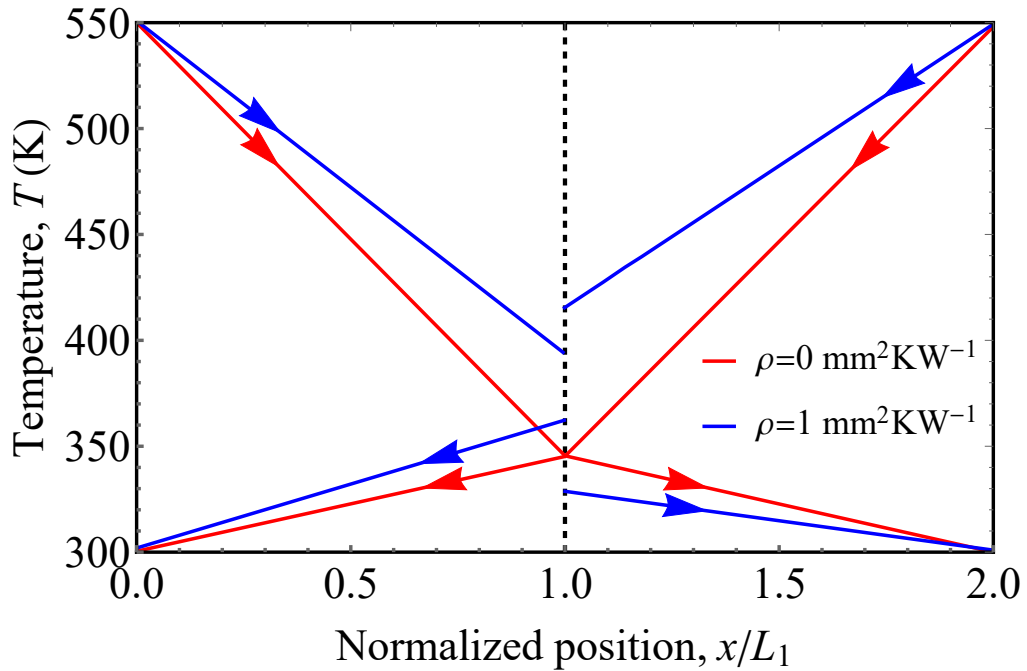


FIGURE 3.6: Temperature profiles within the terminals of the conductive thermal diode operating in the forward and backward configurations. Arrows stand for the direction of heat flux and calculations were done for  $T_c = 300$  K,  $T_h = 550$  K, and two values of the interface thermal resistance  $\rho$  [Kas20a].

interface  $x = L_1$  is, thus due to the MITs of the PCMs.

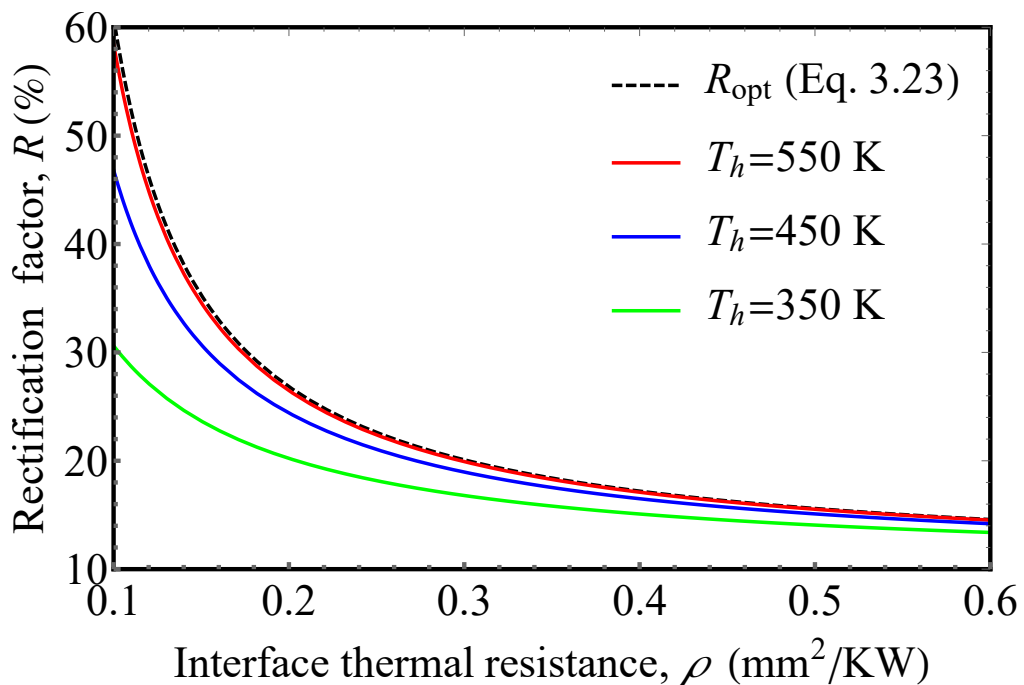


FIGURE 3.7: Rectification factor of the conductive thermal diode, as a function of the interface thermal resistance  $\rho$ . Calculations were done using  $R = [1 - \min(q_F, q_B) / \max(q_F, q_B)]$  and  $T_c = 300$  K [Kas20a].

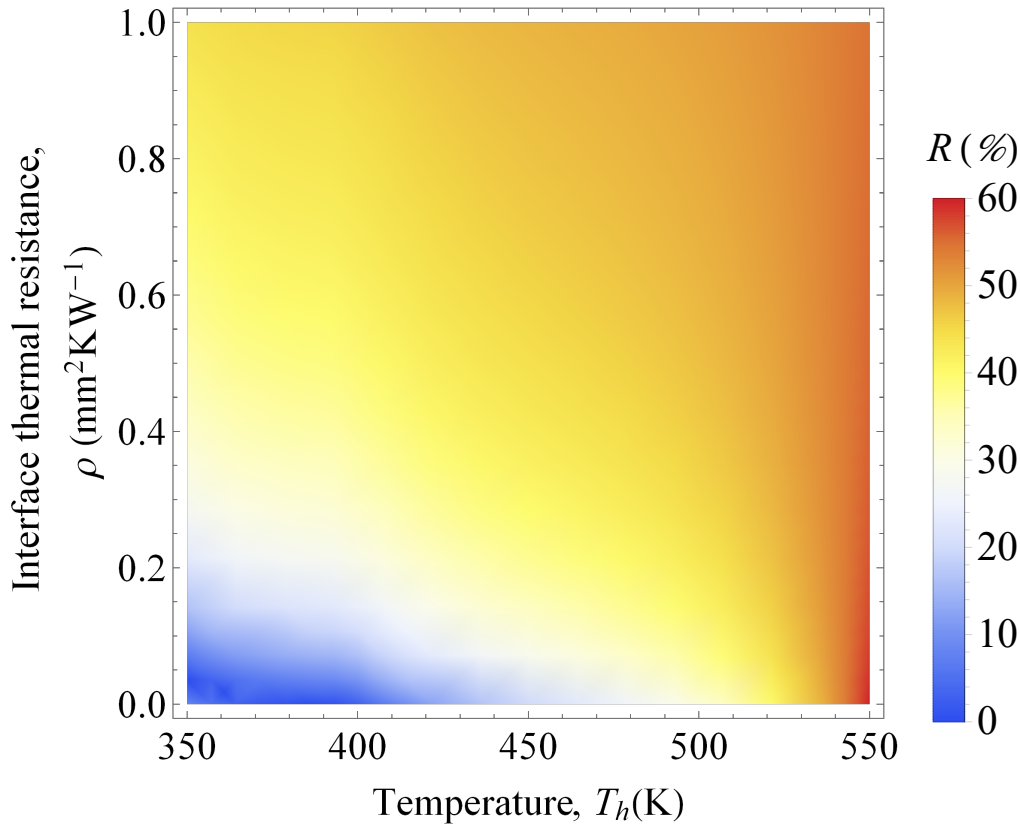


FIGURE 3.8: Density plot of the conductive thermal diode rectification factor as a function of the temperature  $T_h$  and interface thermal resistance  $\rho$ . Calculations were done using  $R = [1 - \min(q_F, q_B) / \max(q_F, q_B)]$  and  $T_c = 300$  K [Kas20a].

### 3.7 Temperature dependence rectification factor

Figure 3.7 shows the rectification factor of the conductive thermal diode, as functions of the interface thermal resistance  $\rho$ , for three different values of the hotter temperature of  $T_h$ . Note that rectification factor  $R$  increases as the values of  $\rho$  decreases for a high temperature of  $T_h = 550$ K. This fact agrees with the value of the temperature of  $T_h$ , which is well predicted by the analytical expression presented in equation (3.23). It indicates that equation (3.23) is reliable to describe the optimal rectification factor, for three different values of  $\rho$  and also shows that maximum rectification is reached for  $T_h = 550$ K. This latter fact is in good agreement with the density plot shown in Figure 3.8. Note that we did not go to zero at the interface thermal resistance axis, because there is no significant difference in the rectification factor between  $\rho = 0$  mm<sup>2</sup>KW<sup>-1</sup> and  $\rho = 0.1$  mm<sup>2</sup>KW<sup>-1</sup>,

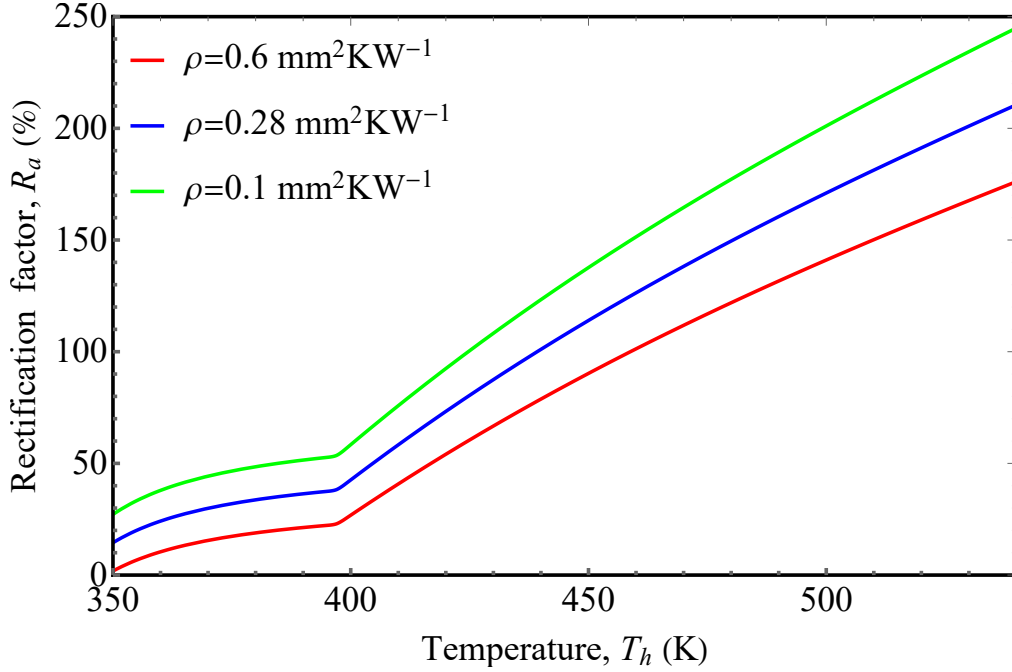


FIGURE 3.9: Rectification factor  $R$  of the conductive thermal diode as a function of the temperature  $T_h$ . Calculations were done by using the alternative definition  $R_a = [\max(q_F, q_B) / \min(q_F, q_B)] - 1$  for three representative interface thermal resistances and  $T_c = 300$  K [Kas20a].

as shown in Figure 3.8. One can see that in Figure 3.8, maximum rectification factor is obtained for lower interface thermal resistance and higher hotter temperature of  $T_h$ . The optimal rectification factor obtained in equation (3.23) by substituting the values of all the required parameters is different from the rectification factor at  $T_h = 500$ K by only 3%, therefore, reduces for higher values of  $T_h$ . We obtained optimal rectification of up to 60% for the low value of interface thermal resistance  $\rho = 0$  mm<sup>2</sup>KW<sup>-1</sup> and at a temperature variation of  $T_h - T_c = 550 - 300 = 250$  K between the diode terminals. Because  $\rho$  is the interface thermal resistance between the diode terminals, its reduction to achieve maximum rectification factor would requires to carefully adjust the PCMs properties in the heterojunction with a fine control of the deposition conditions. The results presented here are in good agreement with the similar predicted rectification factors of heterojunction between graphene-hexagonal boron nitride by

[Che16], graphene-graphene phononic crystals by [Hu17], graphene nanoribbons by [Yua15] and carbon nanotube-graphene by [Yan17], but with temperature intervals, which are relatively higher than the ones obtained here for a VO<sub>2</sub> and PE heterojunction. On the other hand, optimal rectification factor reported in this chapter is almost three times higher than the corresponding one predicted by [Ord18b] with a single PCM and as well as, the dual PCMs predicted by [Shr20]. This fact indicates the possibility to enhance the thermal effectiveness of the conductive thermal diode by properly combining the two PCMs. Furthermore, the study proposed in this chapter is correlated to that reported by [Ord18b] and any other study proposed based on heterojunction between two PCMs, given that we exploit the MITs of the PCMs to generate the rectification of heat currents. Since this diode consists of two terminals, it represents the most general configuration of a thermal diode operating with PCMs. In order to justify the fact that the definition of the rectification factor proposed here leads to higher values than the one defined by Kang *et al.* [Kan18]. We have used their alternative definition  $R_a = [\max(q_F, q_B) / \min(q_F, q_B)] - 1$ , so that we plot in Figure 3.9, the alternative rectification factor ( $R_a$ ), as a function of temperature  $T_h$  for three different interface thermal resistances. Herein, we observe that the low value of  $\rho$  generates higher rectification factor as expected. The optimal rectification factor generated between the diode terminals is around 240%, which is greater than the 147% predicted by [Kan18]. This enhancement is, thus, as a result of the difference in the thermal conductivity of tungsten-doped VO<sub>2</sub> used by Kang *et al.* [Kan18] compared to the pure VO<sub>2</sub> used in this chapter. This is reasonable because the thermal diodes with higher rectification factors require larger thermal conductivities ratios ( $\kappa_{high} / \kappa_{low}$ ) for both of its terminals as developed in equation (3.23).

## 3.8 Conclusions

The goal of this chapter was to study the optimization of the rectification of a conductive thermal diode by combining two phase-change materials in order to generate higher rectification factor. We have theoretically modeled and optimized the conductive thermal diode by deriving analytical expressions for the temperature profiles, heat fluxes and optimal rectification factor. We obtained an optimal rectification factor of up to 60% for a conductive thermal diode operating between terminals of VO<sub>2</sub> and polyethylene, which is 3% greater than the optimal one obtained analytically from equation (3.23). By taking into account the alternative definition of the rectification factor, we obtained a value of around 240%. To the best of our knowledge, this record-breaking rectification has not yet been predicted in literature. Maximum rectification factors in a narrower temperature range could be obtained with phase-change materials exhibiting higher thermal conductivity contrasts and faster phase transitions. The proposed model could therefore be useful for guiding the development of phase-change materials capable of optimizing the rectification of conductive thermal diodes, which represent a basic building block for developing thermal circuits based on heat currents.

## 3.9 Résumé du chapitre 3

### Introduction

Dans ce chapitre, le redressement thermique d'une diode thermique conductive composée de deux matériaux à changement de phase, dont les conductivités thermiques changent de manière significative dans un intervalle de température étroit, est théoriquement modélisé et optimisé. Le redressement thermique des courants de chaleur conductif est une conséquence de la dépendance à la température des conductivités thermiques aux bornes de la diode. Il peut ainsi, en principe, être réalisé avec des matériaux solides arbitraires soumis à un gradient de température suffisamment grand.

Les différentes sections du chapitre sont résumées ci dessous:

### Modélisation théorique

Contrairement au chapitre 2 où nous avons considéré les diodes thermiques conductives composées d'une jonction constituée d'un matériau à changement de phase et d'un matériau dont l'état ne change pas pour les géométries sphérique et cylindrique, nous avons ici modélisé un système de deux matériaux à changement de phase échangeant de la chaleur par conduction en régime permanent en raison de leur différence de température, voir la figure 3.10. Nous considérons à la fois les configurations directes et inverses telles que le paramètre  $T_h$  est toujours supérieur à  $T_c$ . Les valeurs de  $q_F$  et  $q_B$  sont déterminées par les conductivités thermiques de  $\kappa_1(T)$  de PCM1 et  $\kappa_2(T)$  de PCM2. Par conséquent, on s'attend à ce qu'ils ne soient pas les mêmes ( $q_F \neq q_B$ ), en raison de la dépendance à la température de  $\kappa_1(T)$  et  $\kappa_2(T)$ .

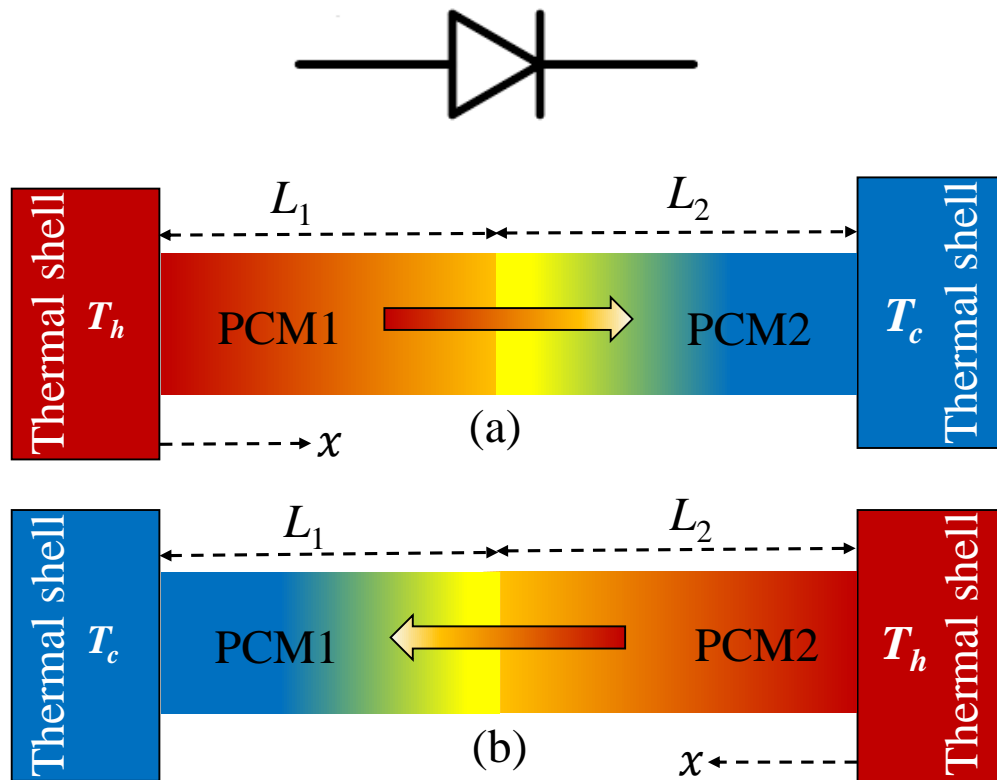


FIGURE 3.10: Schéma d'une diode thermique conductive à double PCM fonctionnant dans les configurations (a) avant et (b) arrière. Les coques thermiques chaudes et froides sont réglées aux températures  $T_h$  et  $T_c$ , respectivement [Kas20a].

### Cas d'un modèle de conduction thermique plan

Des expressions analytiques simples sont établies pour les flux de chaleur directs et inverses, le profil de température et les facteurs de rectification optimaux des deux diodes, comme présenté dans les sections 3.3 et 3.4, respectivement.

### Conclusions

Dans ce chapitre, nous avons théoriquement analysé et optimisé le facteur de redressement d'une diode thermique conductive constituée d'une jonction entre deux matériaux à changement de phase, dont les conductivités thermiques changent de manière significative dans un intervalle de températures étroit. Cela a été fait en établissant des expressions analytiques pour les profils de température, les flux thermiques et le facteur de rectification. Un facteur de redressement

jusqu'à 60% a été déterminé pour une diode thermique conductive fonctionnant avec des bornes de VO<sub>2</sub> et de polyéthylène avec une différence de température de 250 K de chaque côté des températures du MIT. Des facteurs de rectification plus élevés dans un intervalle de température plus étroit pourraient être obtenus avec des matériaux à changement de phase présentant des contrastes de conductivité thermique plus élevés et des transitions de phase plus raides en fonction de la température. Le modèle proposé pourrait ainsi être utile pour guider le développement de matériaux à changement de phase capables d'optimiser la rectification de diodes thermiques conductives, qui représentent une étape cruciale pour le développement de circuits thermiques basés sur des courants de chaleur.

## Chapter 4



## Chapter 4

---

# Radiative thermal diodes based on two phase-change materials

### Contents

---

<b>4.1</b>	<b>Introduction</b> . . . . .	<b>123</b>
<b>4.2</b>	<b>Modeling of plane, cylindrical and spherical radiative thermal diodes</b> . . . . .	<b>125</b>
4.2.1	Plane radiative thermal diode . . . . .	128
4.2.2	Cylindrical radiative thermal diode . . . . .	130
4.2.3	Spherical radiative thermal diode . . . . .	131
<b>4.3</b>	<b>Temperature dependence and rectification factor of a plane geometry</b> . . . . .	<b>133</b>
<b>4.4</b>	<b>Temperature dependence and rectification factors of cylindrical geometry</b> . . . . .	<b>135</b>
<b>4.5</b>	<b>Temperature dependence and rectification factor of a spherical geometry</b> . . . . .	<b>137</b>
<b>4.6</b>	<b>Rectification factors of plane, cylindrical and spherical geometries</b> . . . . .	<b>139</b>
<b>4.7</b>	<b>Conclusions</b> . . . . .	<b>142</b>
<b>4.8</b>	<b>Résumé du chapitre 4</b> . . . . .	<b>144</b>

---



## 4.1 Introduction

PCMs, whose optical, electrical and thermal properties change with temperature have been employed as one of the major methods utilized to rectify heat currents. These changes in their properties are due to the strongly correlated interactions of phonons and electrons and can be applied for several applications [Jou15a; Ito16; Ben17; Ord19a], including radiative thermal diodes operating in both near- and far-field regimes [Ben13; Jou15b; Nef14b; Nef14a; Ito14; Ote10; Bas11]. This wide area of applications has motivated growing attention on PCMs, such as  $\text{Ge}_2\text{Sb}_2\text{Te}_5$  (GST),  $\text{VO}_2$ , PE and nitinol, whose emissivities can be driven thermally. These four thermochromic materials have recently attracted great attention in both experimental and theoretical studies due to their metal-insulator transition (MIT) at temperatures near room temperature. According to Barker *et al.* [Bar66], the effective emissivities of GST and  $\text{VO}_2$  undergo the MIT within the temperature variations of  $420 \text{ K} < T < 430 \text{ K}$  and  $340 \text{ K} < T < 345 \text{ K}$ , respectively. Given that the MIT of  $\text{VO}_2$  occurs in a temperature range of only 5K has motivated its combination with  $\text{SiO}_2$  by Ben Abdallah *et al.* [Ben13], predicted a rectification factor of up to 90%. This relatively high rectification is more than eight times the typical ones obtained with non-PCM [Ruo09] and more than the predicted 70% and 80% rectification factors generated with heavily doped silicon, gold and superconducting materials by [Nef14b; Nef14a]. This fact indicates that there is great potential in using PCMs to rectify radiative heat currents. Since a thermal diode composed of two terminals and that two PCMs provide more degree of freedom than a single PCM to modify the heat transfer between them, thus, the thermal effectiveness of radiative thermal diodes is expected to be enhanced by combining two PCMs, as was reported by [Kas20a; Ord18b; Cot15] for conductive thermal diodes. For example, we have shown in chapter 3 that the combination of two PCMs generates an optimal rectification factor higher than the typical one obtained with a single PCM. According to this

fact, two PCMs could also be used to improve the rectification factor of radiative thermal diodes.

In this chapter, we theoretically study and optimize the thermal rectification effect of plane, cylindrical and spherical radiative thermal diodes operating within the terminals of two PCMs, whose emissivities significantly change in a narrow interval of temperatures. This work is done by considering the temperature dependence of the emissivities of the two PCMs within their phase transitions. We derive and analyze simple analytical expressions for the optimal rectification factors of the three different geometrical diodes supporting thermal radiation. Our calculations shed more light on the fact that rectification factor can be improved significantly by using two PCMs instead of a single one.

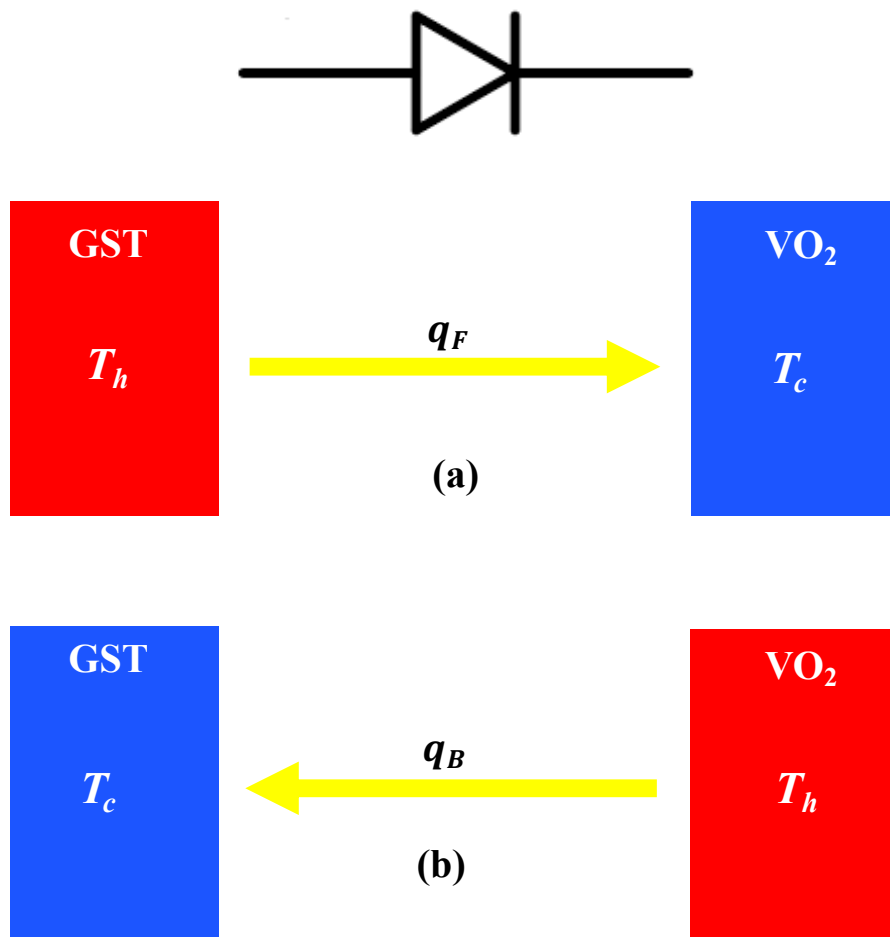


FIGURE 4.1: Scheme of a plane radiative thermal diode made up with terminals of GST and  $\text{VO}_2$  operating in the (a) forward and (b) backward configurations. Hot and cold thermal baths are set at the temperatures  $T_h$  and  $T_c$ , respectively [Kas20b].

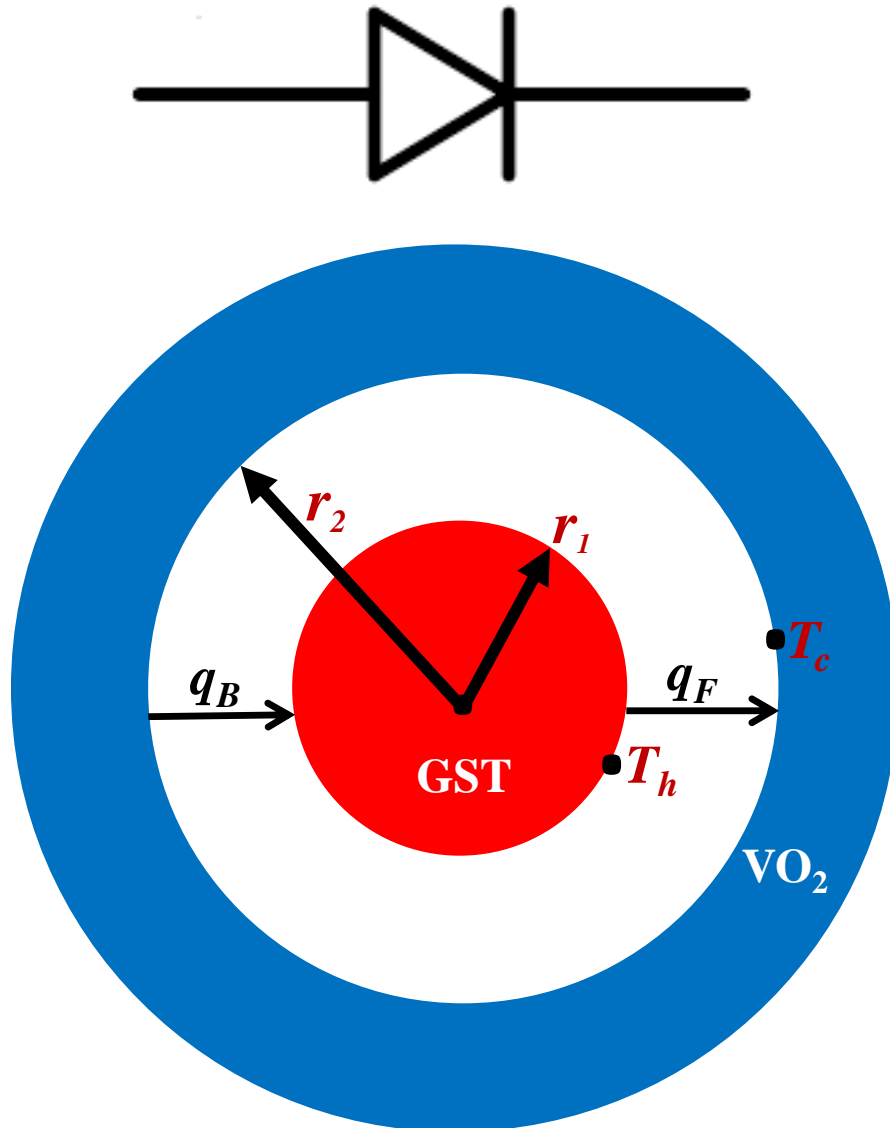


FIGURE 4.2: Scheme of a spherical (or cylindrical) radiative thermal diode made up of GST and VO<sub>2</sub> operating in the forward and backward configurations. The radii  $r_1$  and  $r_2$  are set at the temperatures  $T_h$  and  $T_c$  for the forward configuration, while they are interchanged for the backward one [Kas20b]. In practice, a spherical diode could be implemented by using the classical Langmuir-Blodgett law [L24].

## 4.2 Modeling of plane, cylindrical and spherical radiative thermal diodes

In order to model radiative thermal diodes in different geometries, we consider the thermal transport set up between two semi-infinite bodies made up of GST and VO<sub>2</sub> exchanging heat in form of radiation due to their temperature difference  $T_h > T_c$ , as depicted in Figures 4.1(a) and (b), respectively. We assume that

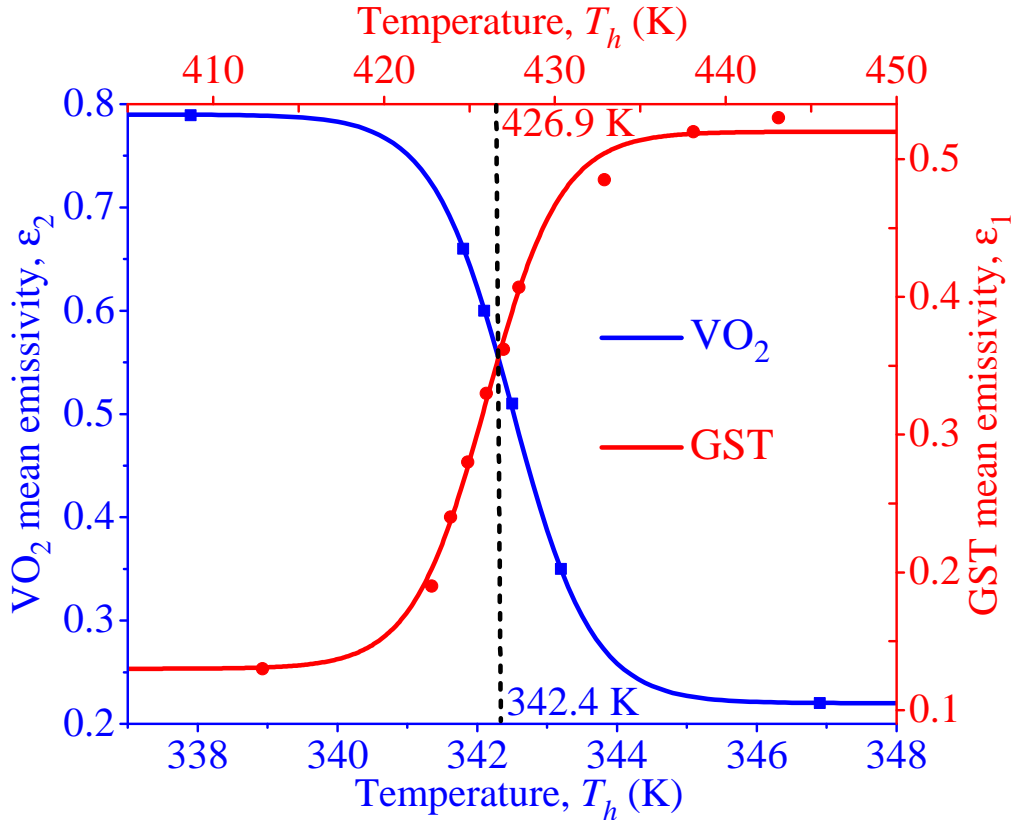


FIGURE 4.3: Effective emissivities of GST and  $\text{VO}_2$  as functions of temperature within their MITs. Dots and rectangles represent experimental data reported in the literature [Ord18b; Du17], while lines stand for fits of equation (1.11) [Kas20b].

both bodies are separated by a vacuum gap of thickness  $d$  which is much greater than their thermal wavelengths i.e. we are working in the far-field regime so that the contribution to the heat exchange is only due to the propagating wave. More specifically, we concentrate on two configurations: the first one is the forward configuration [Figure 4.1(a)], where the heat flow  $q_F$  flows from GST to  $\text{VO}_2$ , while the second is the backward one [Figure 4.1(b)], here, the heat flow  $q_B$  flows in the opposite direction due to the fact that the temperatures  $T_h$  and  $T_c$  are reversed. It is important to note that these two heat flows correspond to the two configurations are expected to be different ( $q_F \neq q_B$ ), as a result of the temperature dependence of the emissivities of GST and  $\text{VO}_2$ , within their MITs. Similar to the case of the plane diode, this behavior of the two heat flows ( $q_F$  and  $q_B$ ) is also applicable for the spherical or cylindrical radiative thermal diodes, as illustrated in Figure 4.2.

Recalling the Stefan-Boltzmann's law of thermal radiation in the far-field regime, the heat flows in the forward and backward configurations of the plane, cylindrical and spherical radiative thermal diodes proposed here, is given as follows [Inc96]:

$$q_F = A_1 \sigma \varepsilon_F (T_h^4 - T_c^4), \quad (4.1a)$$

$$q_B = A_2 \sigma \varepsilon_B (T_h^4 - T_c^4), \quad (4.1b)$$

where  $\sigma = 5.67 \times 10^{-8} \text{ Wm}^{-2}\text{K}^{-4}$  is the Stefan-Boltzmann constant,  $A_1$  and  $A_2$  are the areas of the radiating surfaces, while  $\varepsilon_F$  and  $\varepsilon_B$  are their effective emissivities in the forward and backward configurations, respectively. By combining equations (1.9) and (4.1), we obtain the following rectification factor which looks similar but different from equation (1.9), as follows:

$$R = \frac{|A_1 \varepsilon_F - A_2 \varepsilon_B|}{\max(A_1 \varepsilon_F, A_2 \varepsilon_B)}. \quad (4.2)$$

Equation (4.2) shows that the values of  $R$  are driven by the combined effect of the radiating surfaces and the effective emissivities of the diodes. It is thus clear that the rectification factors of the plane, spherical and cylindrical radiative diodes made up with terminals of GST and VO<sub>2</sub> are expected not to be equal, as a result of the differences in  $A_1$  and  $A_2$ , respectively. According to equation (1.11), the effective emissivities of GST and VO<sub>2</sub> can be described, as follows:

$$\varepsilon_1(T) = \varepsilon_{i1} + \frac{\varepsilon_{m1} - \varepsilon_{i1}}{1 + e^{-\beta_1(T-T_{01})}}, \quad (4.3a)$$

$$\varepsilon_2(T) = \varepsilon_{i2} + \frac{\varepsilon_{m2} - \varepsilon_{i2}}{1 + e^{-\beta_2(T-T_{02})}}, \quad (4.3b)$$

where  $\varepsilon_{m1}$  and  $\varepsilon_{i1}$  are the effective emissivities of GST in its high- and low-temperature phases, and  $\beta_1$  is the phase-transition slope of  $\varepsilon_1(T)$  at the transition

temperature  $T = T_{01}$ . On the other hand,  $\varepsilon_{m2}$  and  $\varepsilon_{i2}$  are the effective emissivities of VO<sub>2</sub> in its high- and low-temperature phases, and  $\beta_2$  is the phase-transition slope of  $\varepsilon_2(T)$  at the transition temperature  $T = T_{02}$ . The values of the aforementioned parameters were determined by fitting equations (4.3a) and (4.3b) to the experimental data depicted in Figure 4.3 for both GST and VO<sub>2</sub> and they are presented in Table 4.1.

TABLE 4.1: Properties of materials involved in equations (4.3a) and (4.3b) [Kas20b].

Materials	$\varepsilon_{in}$	$\varepsilon_{mn}$	$\beta_n(\text{K}^{-1})$	$T_{0n}(\text{K})$
GST	0.13	0.52	0.46	426.9
VO <sub>2</sub>	0.79	0.22	1.6	342.4

In order to evaluate the predictions of the rectification factor  $R$  described in equation (4.2), we have derived and optimized explicit expressions for the plane, cylindrical and spherical radiative thermal diodes, as follows:

### 4.2.1 Plane radiative thermal diode

In this case, we have assumed that the area of the radiating surfaces are equal, that is to say ( $A_1 = A_2 = A$ ) for the sake of clarity and simplicity, thus, according to Frank and DeWitt [Inc96], the effective emissivities in the forward and backward configurations can be written in terms of  $T_h$  and  $T_c$ , as follows:

$$\varepsilon_F = \left( \frac{1}{\varepsilon_1(T_h)} + \frac{1}{\varepsilon_2(T_c)} - 1 \right)^{-1}, \quad (4.4a)$$

$$\varepsilon_B = \left( \frac{1}{\varepsilon_1(T_c)} + \frac{1}{\varepsilon_2(T_h)} - 1 \right)^{-1}, \quad (4.4b)$$

where  $\varepsilon_n(T_h)$  and  $\varepsilon_n(T_c)$  are the effective emissivities of the two PCMs (provided  $n = 1;2$ ) in their high- and low-temperature phases, respectively. It is worthwhile to note that we have properly replaced the original  $T_1$  and  $T_2$  used by the latter authors with  $T_h$  and  $T_c$  in the forward configuration and they are

reversed in the backward one [equations (4.4a) and (4.4b)]. Given that the areas of the radiating surfaces are equal, it is more convenient to determine the optimal rectification factor  $R$  of the plane diode from equation (4.2). By recalling equation (2.37),  $R$  can be written in terms of the ratio  $\varepsilon_{B,\min}/\varepsilon_{F,\max}$  between the minimum emissivity in the backward configuration to the maximum emissivity in the forward one, as follows:

$$R_{\text{opt}} = 1 - \frac{\varepsilon_{B,\min}}{\varepsilon_{F,\max}}. \quad (4.5)$$

In order to determine  $R_{\text{opt}}$  in equation (4.5), we capitalized on the temperature variation of the two PCMs within their MITs, such that they fulfill the condition  $T_c < T_{0n} < T_h$ . According to Figure 4.3, in the forward configuration, the effective emissivity  $\varepsilon_F$  becomes maximum  $\varepsilon_F = \varepsilon_{F,\max}$  when the entire GST terminal is in its high-temperature phase i.e. ( $\varepsilon_1(T_h) = \varepsilon_{m1}$ ), while the whole VO<sub>2</sub> terminal is in its low-temperature phase ( $\varepsilon_2(T_c) = \varepsilon_{i2}$ ). On the contrary, in the backward configuration, the effective emissivity  $\varepsilon_B$  becomes minimum  $\varepsilon_B = \varepsilon_{B,\min}$  when the whole GST terminal is in its low-temperature phase ( $\varepsilon_1(T_c) = \varepsilon_{i1}$ ), and the entire VO<sub>2</sub> terminal is in its high-temperature phase ( $\varepsilon_2(T_h) = \varepsilon_{m2}$ ). By applying these conditions to equations (4.5a) and (4.5b), we obtain

$$\varepsilon_{F,\max} = \left( \frac{1}{\varepsilon_{m1}} + \frac{1}{\varepsilon_{i2}} - 1 \right)^{-1}, \quad (4.6a)$$

$$\varepsilon_{B,\min} = \left( \frac{1}{\varepsilon_{i1}} + \frac{1}{\varepsilon_{m2}} - 1 \right)^{-1}. \quad (4.6b)$$

By substituting equations (4.6a) and (4.6b) into (4.5), we have obtained the optimal rectification of a plane radiative thermal diode as

$$\begin{aligned}
R_{\text{opt}} &= 1 - \frac{(\varepsilon_{i1}\varepsilon_{m2})(\varepsilon_{i2} + \varepsilon_{m1} - \varepsilon_{i2}\varepsilon_{m1})}{(\varepsilon_{i2}\varepsilon_{m1})(\varepsilon_{i1} + \varepsilon_{m2} - \varepsilon_{i1}\varepsilon_{m2})}, \\
&= 1 - \frac{\varepsilon_{m2} (1 + \varepsilon_{i2}/\varepsilon_{m1} - \varepsilon_{i2})}{\varepsilon_{i2} (1 + \varepsilon_{m2}/\varepsilon_{i1} - \varepsilon_{m2})}.
\end{aligned} \tag{4.7}$$

Equation (4.7) shows that the optimal rectification factor is symmetric on the emissivities of both PCMs and increases with their ratios  $\varepsilon_{m1}/\varepsilon_{i1}$  and  $\varepsilon_{m2}/\varepsilon_{i2}$ , respectively. This fact is similar to the conductive thermal diode described in chapter 3, as expected. This indicates that materials with greater emissivity contrast are therefore expected to generate radiative thermal diodes with larger rectification factors.

### 4.2.2 Cylindrical radiative thermal diode

Unlike in the case of plane diode where the areas of the radiating surfaces are equal, here, the areas  $A_1$  and  $A_2$  depends on their respective radii  $r_1$  and  $r_2$ , such that  $A_1/A_2 = r_1/r_2$ . The effective emissivities in the forward and backward configurations are given, as follows [Inc96]:

$$\varepsilon_F = \left( \frac{1}{\varepsilon_1(T_h)} + \frac{1 - \varepsilon_2(T_c)}{\varepsilon_2(T_c)} \left( \frac{r_1}{r_2} \right) \right)^{-1}, \tag{4.8a}$$

$$\varepsilon_B = \left( \frac{1}{\varepsilon_1(T_c)} + \frac{1 - \varepsilon_2(T_h)}{\varepsilon_2(T_h)} \left( \frac{r_2}{r_1} \right) \right)^{-1}, \tag{4.8b}$$

where  $r_1$  and  $r_2$  are radii of the cylindrical radiating surfaces depicted in Figure 4.2. It can be seen that the effective emissivities in equations (4.8a) and (4.8b) do depend on the ratio of the radii  $r_1/r_2$ , which provide another degree of freedom to maximize the rectification factor of the cylindrical diode and thus enable expressing equation (2.37), as follows:

$$R_{\text{opt}} = 1 - \frac{r_2 \varepsilon_{B,\text{min}}}{r_1 \varepsilon_{F,\text{max}}}. \quad (4.9)$$

By following a similar procedure used to derived equations (4.6a) and (4.6b) of the plane radiative diode, we have maximized and minimized the effective emissivities  $\varepsilon_F = \varepsilon_{F,\text{max}}$  and  $\varepsilon_B = \varepsilon_{B,\text{min}}$  in the forward and backward configurations. The final result yields

$$\varepsilon_{F,\text{max}} = \left( \frac{1}{\varepsilon_{m1}} + \frac{1 - \varepsilon_{i2}}{\varepsilon_{i2}} \left( \frac{r_1}{r_2} \right) \right)^{-1}, \quad (4.10a)$$

$$\varepsilon_{B,\text{min}} = \left( \frac{1}{\varepsilon_{i1}} + \frac{1 - \varepsilon_{m2}}{\varepsilon_{m2}} \left( \frac{r_2}{r_1} \right) \right)^{-1}. \quad (4.10b)$$

By substituting equations (4.10a) and (4.10b) into (4.9), we obtain the optimal rectification factor  $R_{\text{opt}}$  of the cylindrical radiative diode, as follows:

$$\begin{aligned} R_{\text{opt}} &= 1 - \left( \frac{r_1}{r_2} \right) \frac{(r_1 \varepsilon_{i1} \varepsilon_{m2})(r_2 \varepsilon_{i2} + r_1 \varepsilon_{m1} - r_1 \varepsilon_{i2} \varepsilon_{m1})}{(r_2 \varepsilon_{i2} \varepsilon_{m1})(r_2 \varepsilon_{i1} + r_1 \varepsilon_{m2} - r_2 \varepsilon_{i1} \varepsilon_{m2})}, \\ &= 1 - \frac{\varepsilon_{m2}}{\varepsilon_{i2}} \left( \frac{r_1}{r_2} \right) \frac{(1 + r_2 \varepsilon_{i2} / r_1 \varepsilon_{m1} - \varepsilon_{i2})}{(1 + r_1 \varepsilon_{m2} / r_2 \varepsilon_{i1} - \varepsilon_{m2})}. \end{aligned} \quad (4.11)$$

By comparing equations (4.11) and (4.7), it can be seen that the values of  $R_{\text{opt}}$  of the cylindrical radiative thermal diode is higher than the corresponding ones of the plane diode, provided the ratio  $r_1/r_2$  is carefully modulated, and as well as the emissivity ratios of the PCMs.

### 4.2.3 Spherical radiative thermal diode

Similar to the case of the cylindrical radiative thermal diode, the areas of the radiating surfaces of the spherical ones are not equal, but rather depends on the square of the ratio of their radii, given as ( $A_1/A_2 = (r_1/r_2)^2$ ). The effective emissivities in the forward and backward configurations are given by [Inc96]

$$\varepsilon_F = \left( \frac{1}{\varepsilon_1(T_h)} + \frac{1 - \varepsilon_2(T_c)}{\varepsilon_2(T_c)} \left( \frac{r_1}{r_2} \right)^2 \right)^{-1}, \quad (4.12a)$$

$$\varepsilon_B = \left( \frac{1}{\varepsilon_1(T_c)} + \frac{1 - \varepsilon_2(T_h)}{\varepsilon_2(T_h)} \left( \frac{r_2}{r_1} \right)^2 \right)^{-1}. \quad (4.12b)$$

One can see that equations (4.12a) and (4.12b) of the spherical diode are similar to equations (4.8a) and (4.8b) of the cylindrical one, such that the only significant difference is that the ratio of the radii  $r_1/r_2$  is now squared. This indicates that the spherical diode will have a different impact on the optimal rectification factor when compared to the cylindrical one. By recalling equation (2.37), the optimal rectification of the spherical diode can be express in terms of the effective emissivities, as follows:

$$R_{\text{opt}} = 1 - \frac{r_2^2 \varepsilon_{B,\text{min}}}{r_1^2 \varepsilon_{F,\text{max}}}. \quad (4.13)$$

Again, by following a similar procedure applied in the plane and cylindrical diodes, the maximum and minimum of the effective emissivities  $\varepsilon_F = \varepsilon_{F,\text{max}}$  and  $\varepsilon_B = \varepsilon_{B,\text{min}}$  in the forward and backward configurations of the spherical diode are given as:

$$\varepsilon_{F,\text{max}} = \left( \frac{1}{\varepsilon_{m1}} + \frac{1 - \varepsilon_{i2}}{\varepsilon_{i2}} \left( \frac{r_1}{r_2} \right)^2 \right)^{-1}, \quad (4.14a)$$

$$\varepsilon_{B,\text{min}} = \left( \frac{1}{\varepsilon_{i1}} + \frac{1 - \varepsilon_{m2}}{\varepsilon_{m2}} \left( \frac{r_2}{r_1} \right)^2 \right)^{-1}. \quad (4.14b)$$

The optimal rectification factor of the spherical diode is then determined by substituting equations (4.14a) and (4.14b) into (4.13). The final result gives

$$\begin{aligned}
R_{\text{opt}} &= 1 - \left(\frac{r_1}{r_2}\right)^2 \frac{(r_1^2 \varepsilon_{i1} \varepsilon_{m2})(r_2^2 \varepsilon_{i2} + r_1^2 \varepsilon_{m1} - r_1^2 \varepsilon_{i2} \varepsilon_{m1})}{(r_2^2 \varepsilon_{i2} \varepsilon_{m1})(r_2^2 \varepsilon_{i1} + r_1^2 \varepsilon_{m2} - r_2^2 \varepsilon_{i1} \varepsilon_{m2})} \\
&= 1 - \frac{\varepsilon_{m2}}{\varepsilon_{i2}} \left(\frac{r_1}{r_2}\right)^2 \frac{(1 + r_2^2 \varepsilon_{i2} / r_1^2 \varepsilon_{m1} - \varepsilon_{i2})}{(1 + r_1^2 \varepsilon_{m2} / r_2^2 \varepsilon_{i1} - \varepsilon_{m2})}.
\end{aligned} \tag{4.15}$$

It can be seen that the optimal rectification factor in equation (4.15) of the spherical diode is also symmetrical on the emissivities of the two PCMs. However, it strongly depends on the square of the ratio of the radii  $(r_1/r_2)^2$  unlike the case of the cylindrical diode. This fact indicates that the higher optimal rectification factor will be generated in the spherical diode compared to the cylindrical one. More details about this fact are explained in the next section.

### 4.3 Temperature dependence and rectification factor of a plane geometry

Figure 4.4(a) shows the temperature evolution of the radiative heat flows of a plane radiative thermal diode in the forward and backward configurations operating with terminals of GST and VO<sub>2</sub>, respectively. The heat flows  $q_F$  and  $q_B$  exhibit an almost linear increase with the hotter temperature  $T_h$  and there exists a change of slope at a temperature where both PCMs undergo their phase transition ( $T_h \approx T_{0n}$  with  $n = 1, 2$ ), as expected. This fact is consistent with the heat flows presented in chapter two and three. One can see that the transition of backward heat flows  $q_B$  at  $T_h = 340.6$  K corresponds to the MIT of VO<sub>2</sub>, while that of  $q_F$  at  $T_h = 423.9$  K is driven by the MIT of GST. The result is consistent with the rectification shown in Figure 4.4(b). According to Figure 4.4(a), when the temperature  $T_h < 340.6$  K, the heat flows are equal ( $q_F = q_B$ ), hence both PCMs do not undergo any phase transition, and thus there is no rectification, as confirmed by Figure 4.4(b). On the contrary, for temperature just above the MIT

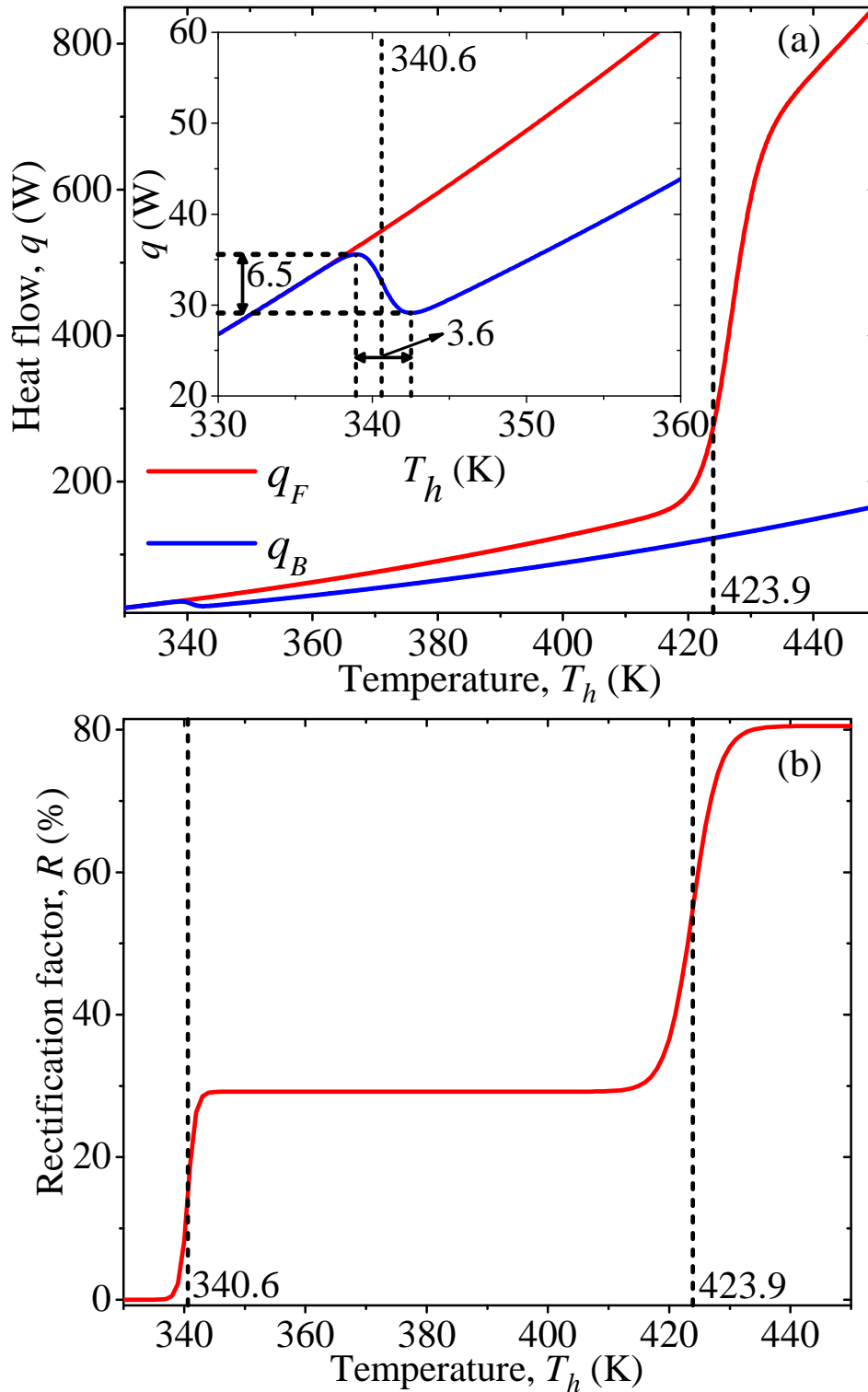


FIGURE 4.4: Temperature dependence of the radiative heat flows for the (a) forward and backward configurations of a plane radiative diode operating with terminals of GST and VO<sub>2</sub>. Inset: Zoom-in of the first maximum and minimum values of  $q_B$ . (b) Rectification factor as a function of  $T_h$ . Calculations were done for  $T_c = 300$  K [Kas20b].

of VO<sub>2</sub> ( $T_h > 340.6$  K), the rectification factor reaches its first plateau at  $R \simeq 30\%$ , as shown in Figure 4.4(b). For higher temperature ( $T_h > 423.9$  K), both PCMs undergo their MITs and the rectification factor increases to  $R \simeq 82\%$ , as confirmed by 4.4(b) and also agrees with the predictions of equation (4.7). This fact shows that the combination of the MITs of the two PCMs is able to maximize the rectification of a plane diode up to the values greater than the typical one predicted with a single PCM and superconducting materials [Ord18b; Nef14b; Ruo09].

## 4.4 Temperature dependence and rectification factors of cylindrical geometry

The temperature dependence of the radiative heat flows  $q_F$  and  $q_B$  for the forward and backward configurations of a cylindrical radiative thermal diode along with its rectification factors (thermal diode in Figure 4.2 and its reversed) are shown in Figures 4.5(a) and 4.5(b), respectively. The values of the heat flows generated here exhibits a similar behavior as the typical ones developed for the plane diode, however, these values are relatively higher than the corresponding ones of the plane diode. This is expected, given that the area of the radiating surfaces are not equal in the case of a cylindrical diode. This indicates that the diode geometry has a significant impact on the values of the heat flows, whose behavior is determined by the temperature-dependent effective emissivities of both PCMs. This agrees with the heat flows reported in chapter 2. As expected, it can be seen that both heat flow increase linearly with increase in  $T_h$ , such that their difference is positive for temperature  $T_h \leq 342.9$  K. Similar to the case of the plane diode, for temperature  $T_h < 340.6$  K the heat flows are equal, thus there is no rectification factor. On the other hand, when the temperature is above the MIT of VO<sub>2</sub> ( $T_h > 342.9$  K), the rectification factor reaches its first plateau at  $R \simeq 48\%$ , as shown in the thick line of Figure 4.5(b). For higher temperature

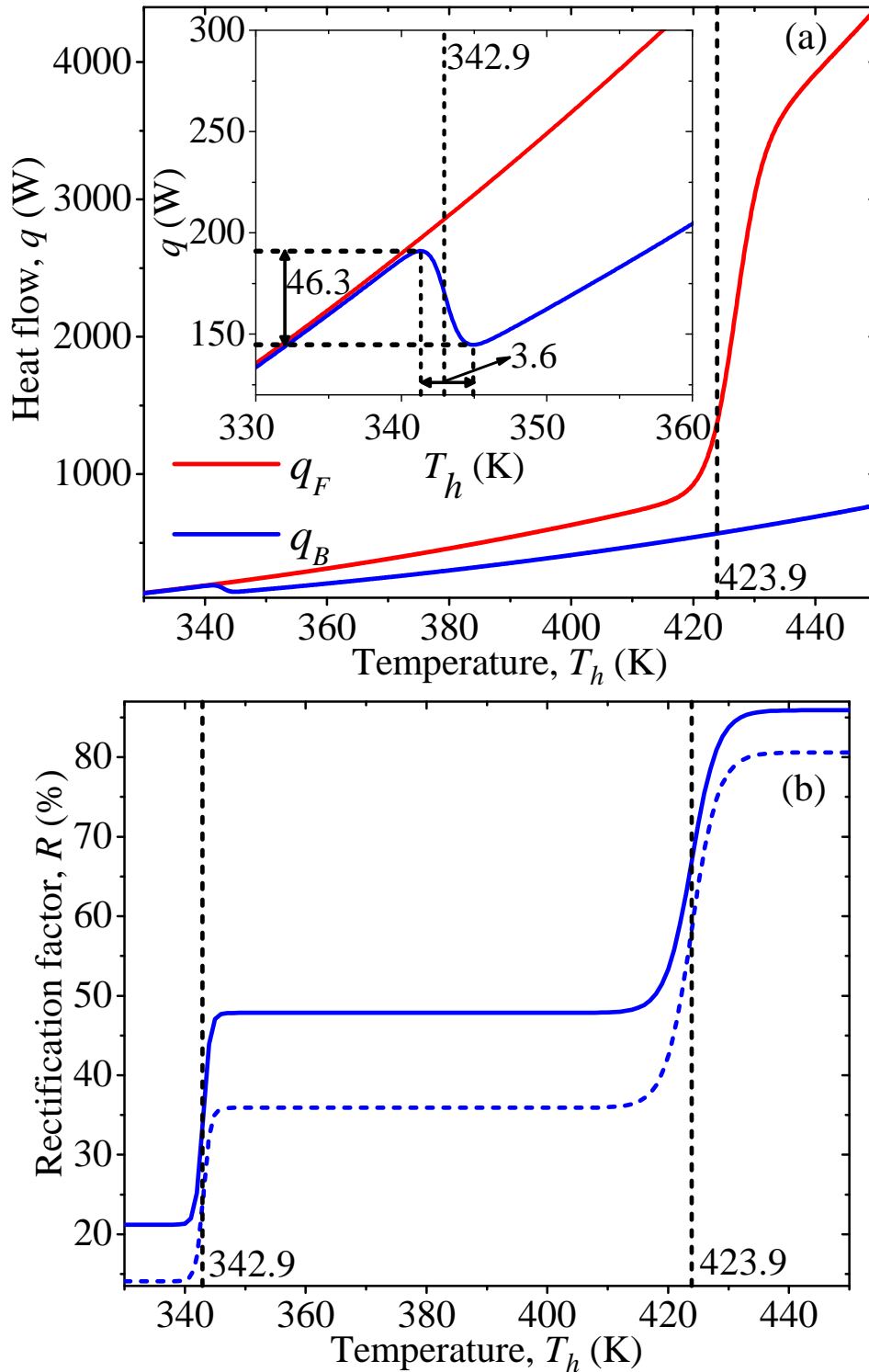


FIGURE 4.5: Temperature dependence of the radiative heat flows for the (a) forward and backward configurations of a cylindrical radiative diode operating with terminals of GST and VO<sub>2</sub> along with (b) its corresponding rectification factor. The solid line stand for the thermal diode shown in Fig. 2, while the dashed one corresponds to a system with interchanged terminals. The inset in (a) shows a zoom-in of the first maximum and minimum values of  $q_B$ . Calculations were done for  $T_c = 300$  K and  $r_1/r_2 = 0.8$  [Kas20b].

( $T_h > 423.9$  K), the two PCMs are within their MITs, therefore the rectification factor increases to  $R \simeq 86\%$ , as confirmed by the thick line in 4.5(b) and also agrees with the analytical predictions of equation (4.11). Note that the sharp increase in  $q_F$  at temperature  $T_h \geq 423.9$  K is generated by the GST emissivity. It is worth mentioning the dashed line in Figure 4.5(b), which corresponds to a system whereby the terminals of the PCMs presented in Figure 4.2 are interchanged. In this case, the rectification factor generated (dashed line) is less than the corresponding one depicted in Figure 4.2 (thick line). This is due to the fact that both GST and VO<sub>2</sub> strongly depends on the effective emissivities contrasts  $\varepsilon_{m1}/\varepsilon_{i1}$  and  $\varepsilon_{m2}/\varepsilon_{i2}$  and, as well as the areas of the radiating surfaces. This is different than the geometrical effect presented in chapter 2 with single PCM, whose value of the rectification factor will remain the same irrespective of the position of the materials.

## 4.5 Temperature dependence and rectification factor of a spherical geometry

Figure 4.6(a) reports the heat flows  $q_F$  and  $q_B$  of a spherical diode operating with terminals of GST and VO<sub>2</sub>, respectively. We observe that the linear increasing in  $q_F$  and  $q_B$  with increasing in  $T_h$  is consistent with the ones presented in the case of the plane and cylindrical radiative thermal diodes. This is expected given that thermal diodes reduce the rate of heat flow in the opposite direction. On one hand, the values of the heat flows  $q_F$  and  $q_B$  for the spherical radiative thermal diode are relatively higher than the corresponding ones of the plane and cylindrical diodes. It is important to note that the radiative thermal diodes have the same temperature variations (3.6 K in width) between the first minimum and first maximum of  $q_B$ , which confirms that the behavior of the heat flow is driven

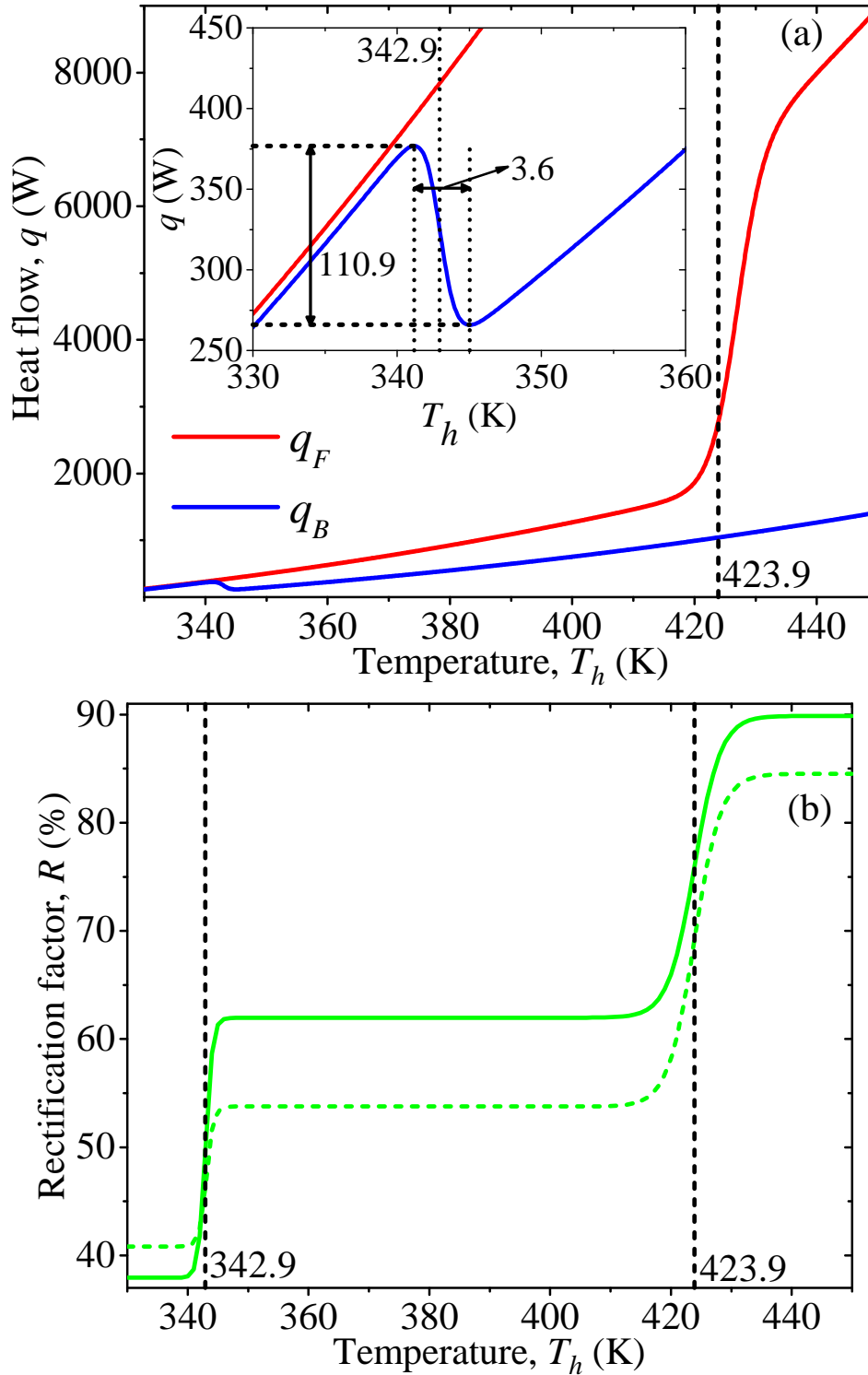


FIGURE 4.6: Temperature dependence of the radiative heat flows for the (a) forward and backward configurations of a spherical radiative diode operating with terminals of GST and VO<sub>2</sub> along with (b) its corresponding rectification factor. The solid line stand for the thermal diode shown in Fig. 2, while the dashed one corresponds to a system with interchanged terminals. The inset in (a) shows a zoom-in of the first maximum and minimum values of  $q_B$ . Calculations were done for  $T_c = 300$  K and  $r_1/r_2 = 0.8$  [Kas20b].

by the effective emissivities of both PCMs. It is interesting to note that these relatively high values of  $q_B$  occur at temperatures close to those that determine the boundaries of the MITs of VO<sub>2</sub> (see Figure 4.3). However, the local maximum of  $q_B$  is associated with the appearance of this phase change, while the local minimum of  $q_B$  is related to its disappearance at a high enough temperature  $T_h$ . In addition, we report in Figure 4.6(b) the rectification factor of the spherical radiative thermal diode as a function of  $T_h$  (thick line), together with the one in which the diodes terminal are reversed (dashed line). Again, similar to the case of the cylindrical diode, one can see that the rectification factor obtained from the scheme depicted in Figure 4.2 (thick line) is higher than the typical one obtained when the scheme is reversed (dashed line). In contrast, this is not applicable to the case of plane radiative thermal diode even though the rectification factor depends on the ratios of the effective emissivities, given that the areas of the radiating surfaces are equal. The first and second plateaux of the rectification factor occurs at  $R \simeq 63\%$  and  $R \simeq 90.5\%$ , respectively. These latter values are higher than the corresponding ones of the plane and cylindrical radiative thermal diodes, which shows that the spherical geometry is better than the other two diode geometries to optimize the rectification of radiative heat transfer. This latter fact is confirmed by the plot of the rectification for the three diode geometries in Figure 4.7.

## 4.6 Rectification factors of plane, cylindrical and spherical geometries

In order to confirm that the combination of two PCMs could generate higher rectification factors than a single PCM in the three geometries presented here, we have replaced the GST terminal by a blackbody, whose emissivity is equal

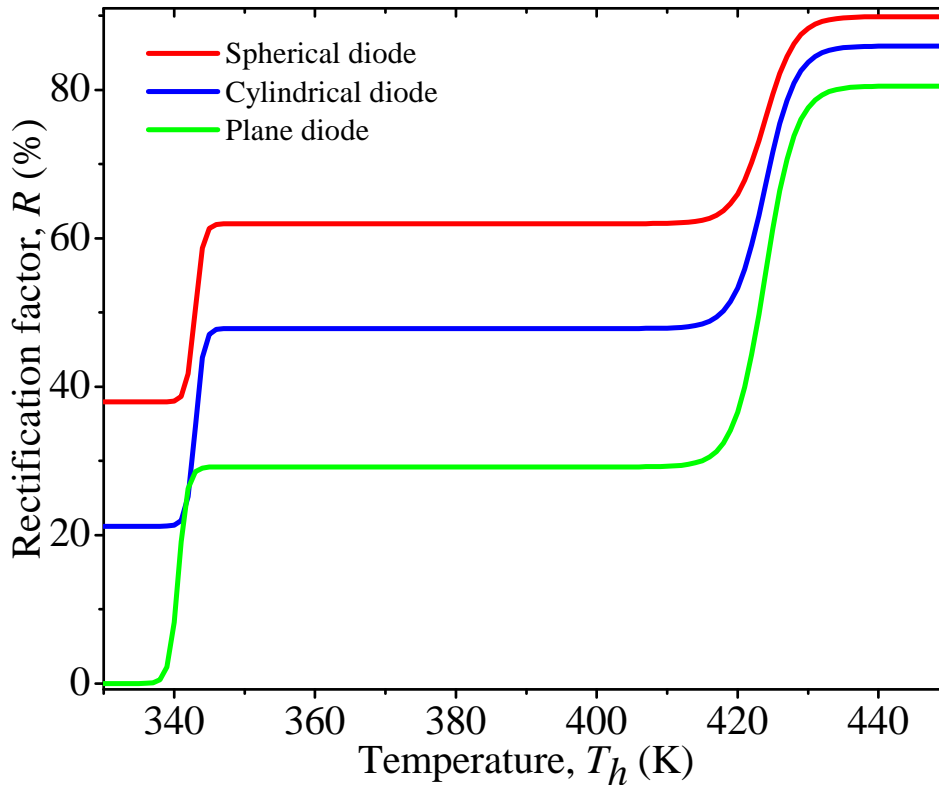


FIGURE 4.7: Comparison of the rectification factors obtained for the plane, cylindrical, and spherical diodes operating with terminals of GST and VO<sub>2</sub>. Calculations were done for  $T_c = 300$  K and  $r_1/r_2 = 0.8$  [Kas20b].

to unity and reported the temperature dependence of the rectification factor between the new terminals [blackbody and VO<sub>2</sub>], as shown in Figure 4.8(a). One can see that the rectification factor exhibits a single phase transition, which is generated due to MIT of VO<sub>2</sub>, such that it reaches its maximum for temperatures that correspond to that of VO<sub>2</sub> transition one. On the other hand, we replaced the VO<sub>2</sub> terminal by a blackbody, similar behavior of rectification is observed, as shown in Figure 4.8(b). This is expected given that the emissivity of the blackbody is constant. It is important to note that in any of the two latter cases, the optimal rectification factors obtained are lower than the typical ones generated with two PCMs, as confirmed in Figures 4.9(a) to 4.9(c) for the three radiative thermal diodes, respectively. The differences between the increase in the optimal rectification factors generated by two PCMs and a single PCM are  $82 - 75 = 7\%$ ,  $86 - 80 = 6\%$ , and  $90.5 - 84 = 6.5\%$  for the plane, cylindrical and spherical

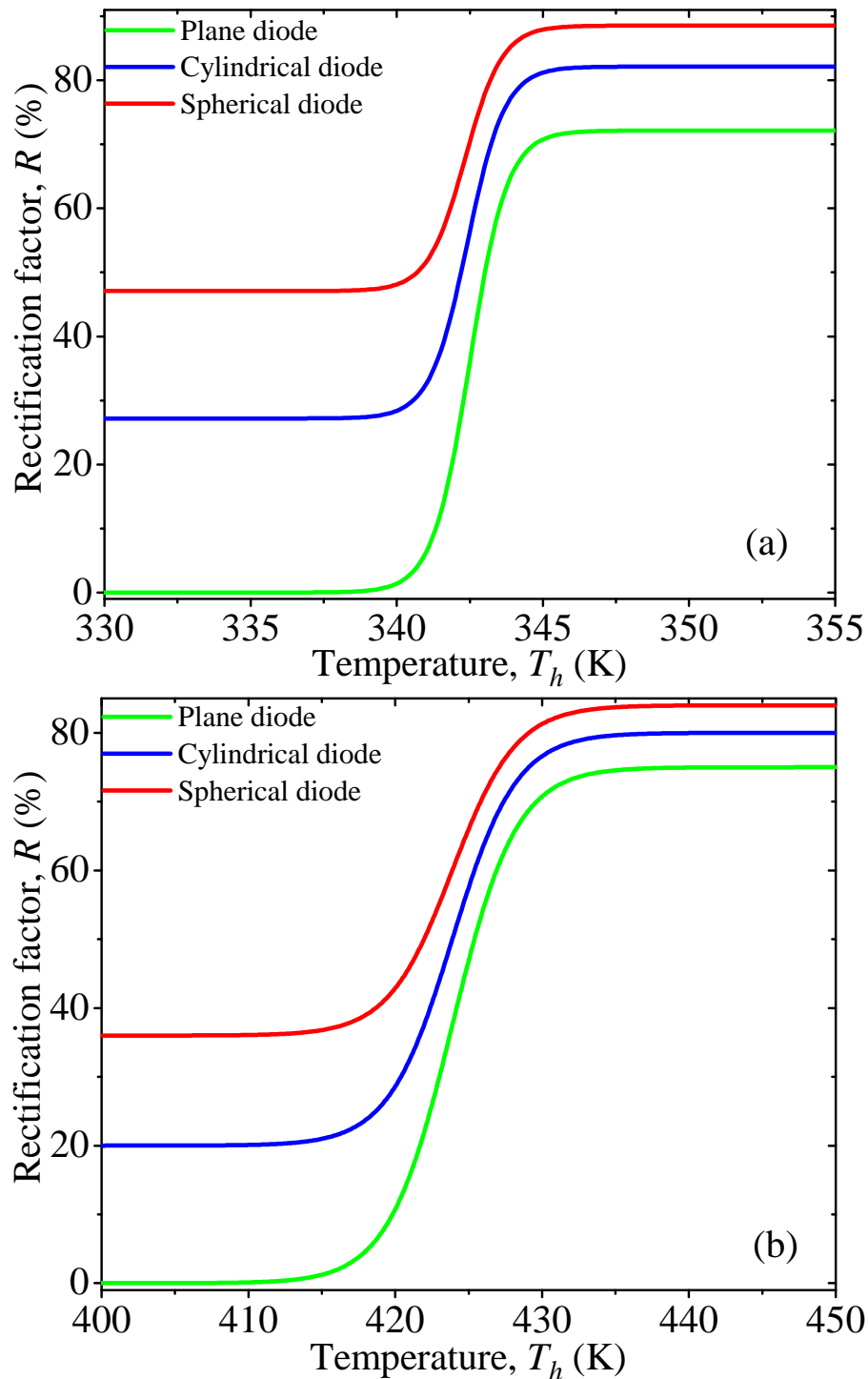


FIGURE 4.8: Temperature dependence of the rectification factor of plane, cylindrical, and spherical diodes with terminals of (a)  $\text{VO}_2$  and a black body and (b) GST and black body. Calculations were done for  $T_c = 300$  K and  $r_1/r_2 = 0.8$ [Kas20b].

diodes, respectively. It is therefore clear that for a given geometry, the enhancement of the rectification factor is mainly due to the combined effect of the phase transition of both PCMs. The rectification factors predicted here for two PCMs

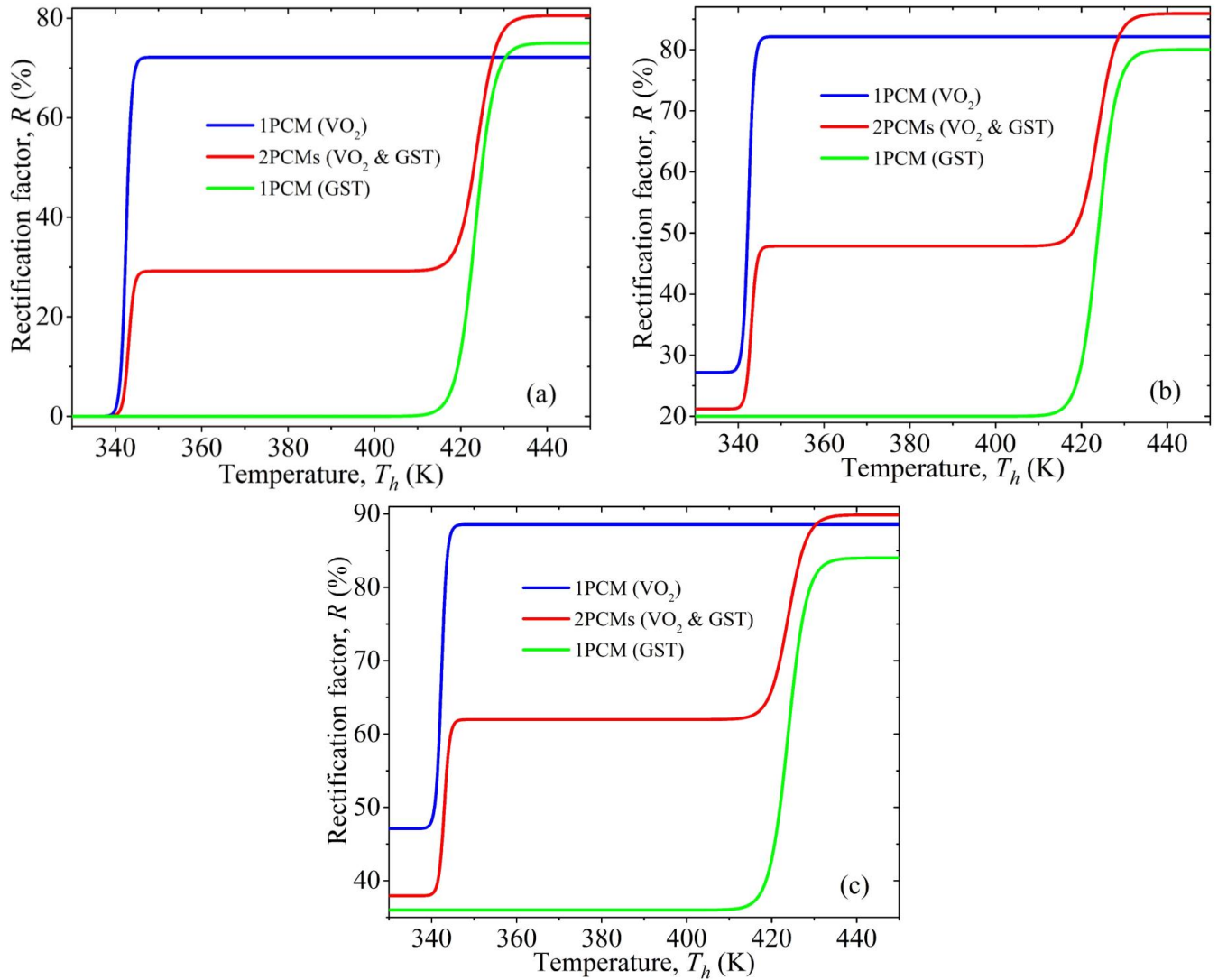


FIGURE 4.9: Rectification factors of (a) plane (b) cylindrical and (c) spherical diodes based on one PCM and two PCMs, as functions of  $T_h$ . Calculations were done for  $T_c = 300$  K and  $r_1/r_2 = 0.8$  [Kas20b].

are higher than the typical single ones reported by [Ote10; Iiz12; Nef14b; Ben13]. The results, therefore, provides a theoretical model to analyze and optimize the thermal effectiveness of radiative thermal diodes operating with two PCMs in different geometries.

## 4.7 Conclusions

An approach based on the consideration the temperature dependence of the effective emissivities of two phase-change materials within their metal-insulator

transition has been done by deriving analytical expressions for the optimal rectification factors of three radiative thermal diodes in different geometries. We have typically shown that the combination of two phase-change materials generates higher rectification factors compared to the case of a single phase-change material. We have also shown that change in geometry has a significant impact on the optimization of the rectification factor. We obtain optimal rectification factors of up to 82%, 86% and 90.5% for the plane, cylindrical, and spherical radiative thermal diodes operating within the terminals of  $\text{Ge}_2\text{Sb}_2\text{Te}_5$  and  $\text{VO}_2$  with a temperature variation of 150 K. It has been shown that the highest rectification factor is obtained for the spherical radiative thermal diode while the lowest is obtained for the plane one. It has also been shown that based on the effective emissivities contrast of the involving phase-change materials, these relatively high optimal rectification factors predicated here can be even higher. The results presented here can therefore be a useful guide for the development of similar phase-change materials that are capable of maximizing the rectification factors of radiative thermal diodes in different geometries.

## 4.8 Résumé du chapitre 4

### Introduction

Des diodes thermiques transportant la chaleur dans une direction préférentielle et le bloquer dans la direction opposée ont récemment attiré de l'attention en raison de leurs applications prometteuses sur le contrôle de la chaleur et la modulation thermique à l'échelle nanométrique. Le comportement inhabituel des diodes thermiques a ouvert la voie au contrôle du taux de chaleur de manière analogue à leurs homologues utilisant le courant électrique dans les appareils électroniques modernes.

Dans ce chapitre, nous avons théoriquement étudié et optimisé les performances de rectification thermique des diodes thermiques radiatifs en champ lointain, constituées de deux matériaux à changement de phase séparés par un vide. Trois conceptions géométriques, à savoir les structures planes, cylindriques et sphériques, ont été considérées. Les résultats ont montré que l'utilisation de deux matériaux à changement de phase améliorerait les performances de la rectification thermique par rapport à l'utilisation d'un seul matériau à changement de phase dans le système. En outre, les résultats ont indiqué que les diodes thermiques sphériques présentaient la meilleure rectification thermique parmi les trois structures géométriques étudiées.

Les différentes sections du chapitre sont résumées ci-dessous:

### Modélisation théorique

Dans ce chapitre, nous considérons deux plaques semi-infinies constituées de GST et VO<sub>2</sub> échangeant de la chaleur par rayonnement en raison de leur différence de température  $T_h - T_c > 0$ , comme illustré respectivement sur

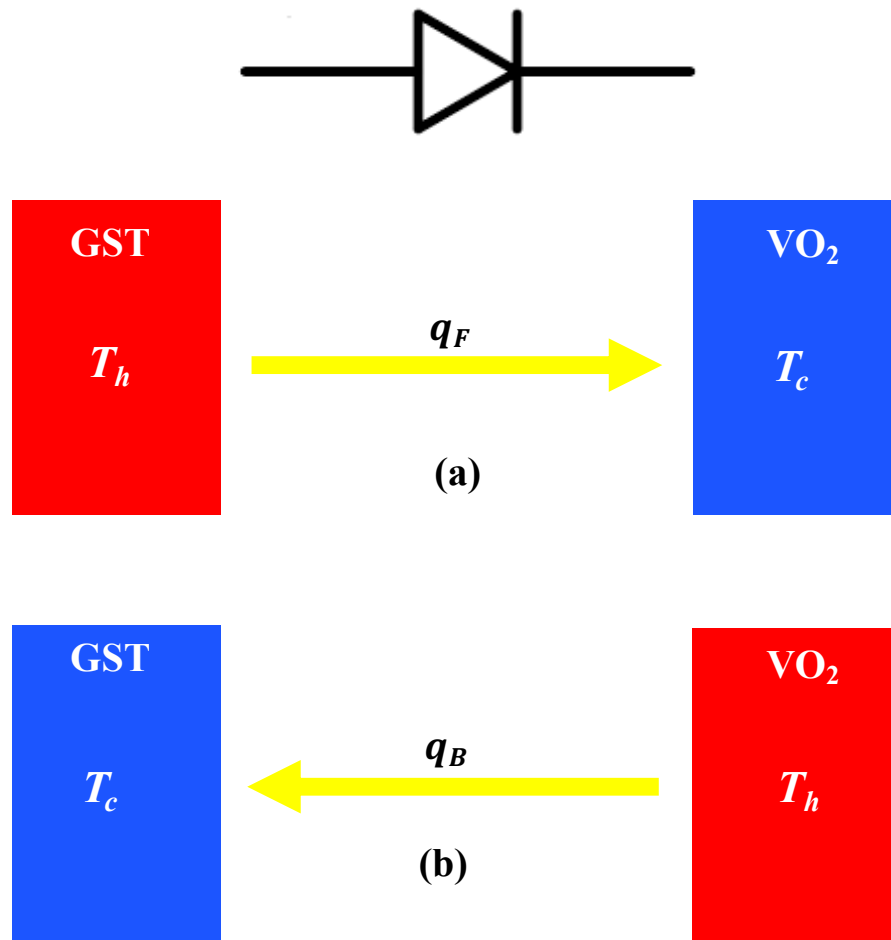


FIGURE 4.10: Schéma d'une diode thermique radiative plane composée de bornes de GST et VO<sub>2</sub> fonctionnant dans les configurations (a) directe et (b) inverse. Les bains thermiques chauds et froids sont réglés aux températures  $T_h$  et  $T_c$ , respectivement [Kas20b].

les figures 4.10 et 4.11. Les deux plaques sont séparées par un espace vide d'épaisseur  $d$  beaucoup plus longue que les longueurs d'onde thermiques impliquées de manière à ce que nous nous placions dans le régime en champ lointain de transport de chaleur. Nous considérons à la fois les configurations directes et inverses telles que le paramètre  $T_h$  est toujours supérieur à  $T_c$  dans les deux figures. Notez que les deux flux de chaleur correspondant aux deux configurations devraient être différents ( $q_F \neq q_B$ ), en raison de la dépendance en température des émissivités de GST et VO<sub>2</sub>, au sein de leurs MIT.

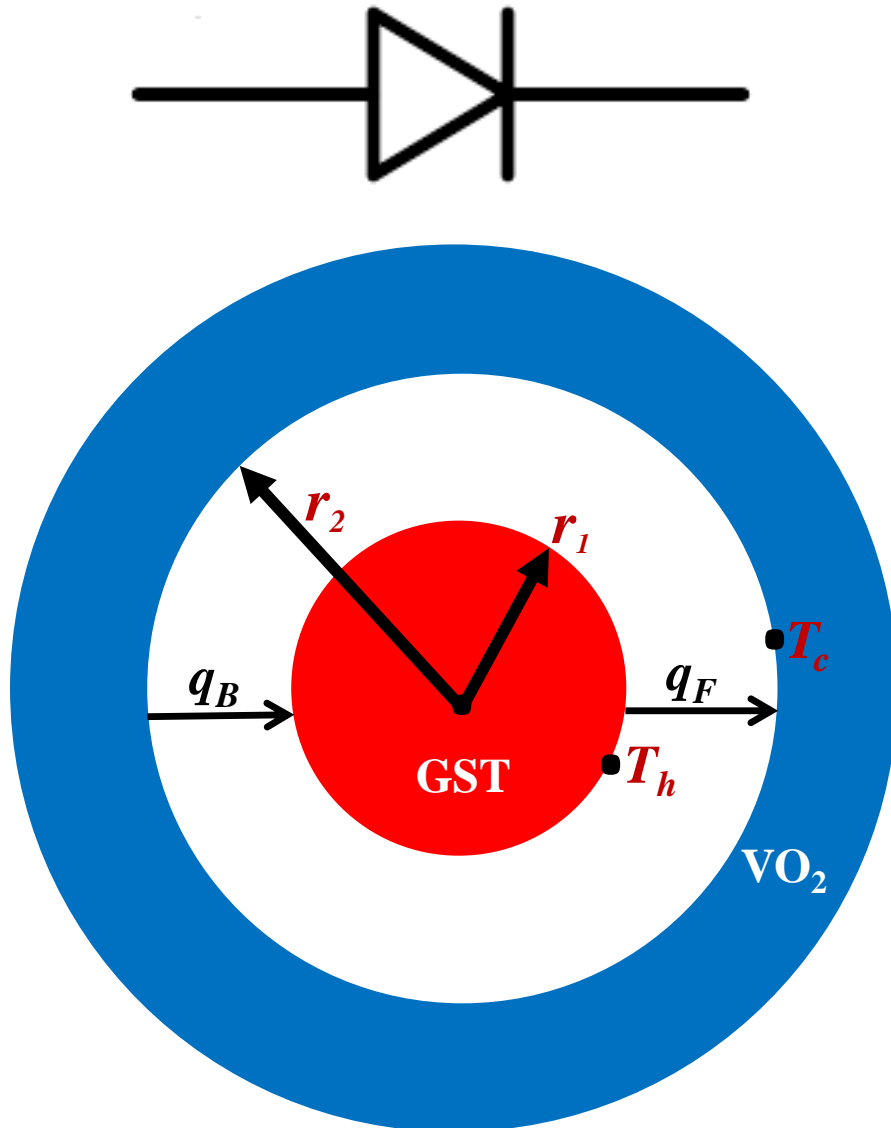


FIGURE 4.11: Schéma d'une diode thermique radiative sphérique (ou cylindrique) composée de GST et VO<sub>2</sub> fonctionnant dans les configurations avant et arrière. Les rayons  $r_1$  et  $r_2$  sont fixés aux températures  $T_h$  et  $T_c$  pour la configuration vers l'avant, alors qu'ils sont interchangeés pour celle vers l'arrière [Kas20b]. En pratique, une diode sphérique pourrait être implémentée en utilisant la loi classique de Langmuir-Blodgett [L24].

### La solution du modèle de conduction thermique plan

Dans ce chapitre, afin d'obtenir les expressions analytiques des facteurs de rectification optimaux de ces trois diodes, nous avons considéré deux matériaux à changement de phase présentant une transition métal-isolant, de telle sorte qu'ils remplissent la condition  $T_c < T_{0n} < T_h$ , voir la figure 4.3. Nous avons présenté

les expressions analytiques dans les sections 4.2.

### **Conclusions**

Ici, nous avons théoriquement analysé et optimisé les facteurs de rectification de diodes thermiques radiatifs planes, cylindriques et sphériques avec des jonctions constituées de deux matériaux à changement de phase. Cela a été fait en démontrant des expressions analytiques pour les facteurs de rectification optimaux de ces trois diodes. Il a été montré que l'effet combiné de deux matériaux à changement de phase avec la géométrie de la diode thermique a un impact significatif sur son facteur de redressement. Des facteurs de rectification optimaux de 82%, 86% et 90.5% ont été déterminés pour les diodes planes, cylindriques et sphériques constituées de  $\text{Ge}_2\text{Sb}_2\text{Te}_5$  et  $\text{VO}_2$  avec une différence de température allant jusqu'à 150 K. Les facteurs de rectification obtenus indiquent que la combinaison de deux matériaux à changement de phase est plutôt élevée par rapport aux précédents concepts de diodes thermiques radiatifs basées sur un matériau à changement de phase unique. Le redressement le plus élevé des flux de chaleur radiatifs est ainsi obtenu pour la diode sphérique et le plus bas pour la diode plane. Ces facteurs de rectification élevés pourraient devenir encore plus élevés dans un intervalle de températures plus étroit en utilisant des matériaux à changement de phase avec des variations d'émissivité plus importantes et des transitions de phase plus rapides que ceux correspondants de  $\text{Ge}_2\text{Sb}_2\text{Te}_5$  et  $\text{VO}_2$ . Les résultats obtenus peuvent ainsi aider le développement de matériaux à changement de phase capables d'optimiser les facteurs de rectification de diodes thermiques radiatifs de géométries différentes.



## General conclusions and Perspectives

This thesis has been dedicated to theoretically study the rectification of conductive and radiative heat currents through thermal diodes operating with phase-change materials. A nonlinear thermal exchange can occur naturally in materials whose thermal conductivities and/or emissivities significantly changes within a narrow interval of temperature, although this is extremely scarce. However, if a fundamental concept could be proposed to generate a nonlinear heat transfer, it would pave a way for promising applications on heat control and thermal modulation. Phase-change materials, whose thermal conductivities and/or emissivities change with temperature, provide a potential opportunity to achieve nonlinear thermal transport. This thesis has aimed to theoretically model and optimize the thermal rectification effect of conductive and radiative thermal diodes with different geometries and it is divided into three parts. The first part is the case of the conductive thermal diodes (chapter 2), where we looked at the work of later authors from the cylindrical and spherical geometries point of view, given that that geometry is one of the factors that influence thermal rectification. Here we comparatively analyzed and optimized the thermal rectification effect of spherical and cylindrical diodes made up with a terminal of phase-change material in thermal contact with a non-phase-change material. By using Fourier's law of steady-state heat conduction, we have derived the analytical expressions for the temperature profiles, heat flows and optimal rectification factor of both diode geometries. Thanks to the built-in tool "FindRoot" of the Wolfram Mathematical software, we have numerically solved these aforementioned parameters, which

allowed us to describe thermal rectification effect in two different geometries, respectively. We have shown that the change of geometry has a significant effect on the temperatures and heat flows, but not on the optimal rectification factors, whose values are in principle independent of the diode geometry as confirmed by [Equation 2.44]. We have reported maximum theoretical rectification factors of approximately 20.8% and 20.7% for the spherical and cylindrical diodes operating with a thermal bias of  $376 - 300 = 76$  K and  $376.5 - 300 = 76.5$  K, respectively.

In the second part, we focused on the combined effect of the two phase-change materials to enhance the optimal rectification factor of a conductive thermal diode (chapter 3). The ideas here are to use the combination of two phase-change materials, whose thermal conductivities change significantly within a narrow interval of temperatures to generate a rectification factor higher than the single PCM reported in chapter 2. We have determined the analytical expressions for the heat fluxes, temperature profiles and optimal rectification factor by considering the Fourier's law of steady-state heat conduction and the principle of conservation of energy. We generated a maximum rectification factor of 60%, which is greater than that the one obtained for the single phase-change materials in literature. This indicates the advantage of using two phase-change materials to optimize conductive thermal diode. Taking into account the alternative definition of rectification factor [ $R_a = [\max(q_F, q_B) / \min(q_F, q_B)] - 1$ ] by Kang *et al.* [Kan18], which predicted a maximum rectification of 147%, we obtained a maximum rectification of up to 240%. Our relative high rectification is due to the fact we used the real behavior of the involving phase-change materials. In the third part, on the other hand, we look at far-field radiative thermal diodes based on the combined effect of two phase-change materials with different geometries. In contrast to chapter 2 and 3, we employed here the Stefan-Boltzmann's law of far-field radiation between two bodies. We have derived the analytical expressions for the heat flows for the optimal rectification factor of plane, cylindrical and

spherical radiative thermal diodes. We have done this by taking into account that the metal-insulator transition of the two phase-change materials illustrated in Figure 4.3 fulfils the temperature condition  $T_c < T_{0n} < T_h$ . We have shown that for radiative thermal diodes, the combination of two phase-change materials also generates higher rectification factor than that of a single one. We have also shown that different geometry has a significant impact on the optimal rectification factor. We believe that the obtained results will be useful for guiding the establishment of phase-change materials required to maximize the rectification factor of both conductive and radiative thermal diodes operating with different geometries.

In order to continue this work in the future, we have envisaged the following prospects:

- It will be interesting to look at the combined effect of two phase-change materials presented in chapter 3, in cylindrical and spherical geometries, as we already did for the radiative thermal diodes in chapter 4. This will be useful for guiding the development of conductive thermal diodes in three different geometries.

- To determine the optimal rectification factor of the radiative thermal diodes reported in chapter 4 in the near-field, where the transition temperature will be taking into account. This will shed more light on the fact that the contribution of propagative and evanescent waves could generate higher optimal rectification factor.

- Given that steady-state heat transfer depends solely on the thermal conductivity of the involving materials but not on the specific heat or latent heat of a phase transition, it will be interesting to analyze and optimize the conductive thermal diodes based on phase-change materials in modulated state.

- To study the near-field thermal memristor with Lissajous (heat flux to temperature difference) curves based on the thermal hysteresis of a phase-change material exchanging heat through radiation with a non-phase-change material.

Even though a far-field radiative thermal memristor has been recently proposed by Ordonez-Miranda *et al.* [Ord19a] and Yang *et al.* [Yan19], it will be interesting to realize a thermal memristor in the near-field regime, which has not been achieved in literature yet.

## Résumé de la conclusion générale et perspective

Cette thèse a été consacrée à l'étude théorique de la rectification des courants thermiques conducteurs et radiatifs à travers des diodes thermiques fonctionnant avec des matériaux à changement de phase. Un échange thermique non linéaire peut se produire naturellement dans les matériaux dont les conductivités thermiques et/ou les émissivités changent de manière significative dans un intervalle de température étroit, bien que cela soit extrêmement rare. Cependant, si un concept fondamental pouvait être proposé pour générer un transfert de chaleur non linéaire, il ouvrirait la voie à des applications prometteuses sur le contrôle de la chaleur et la modulation thermique. Les matériaux à changement de phase, dont les conductivités thermiques et/ou les émissivités changent avec la température, sont de bons candidats pour ce type d'application. Cette thèse a pour objectif de modéliser et d'optimiser théoriquement l'effet de rectification thermique de diodes thermiques conductives et radiatives de géométries différentes et est divisée en trois parties. La première partie étudie le cas des diodes thermiques conductives (chapitre 2), où nous avons étendu des résultats de travaux précédents au cas des géométries cylindrique et sphérique, étant donné que cette géométrie est l'un des facteurs qui influencent la rectification thermique. Ici, nous avons comparé et optimisé l'effet de rectification thermique de diodes sphériques et cylindriques constituées d'une borne en matériau à changement de phase en contact thermique avec un matériau ordinaire ne présentant pas de transition de phase. En utilisant la loi de Fourier de la conduction thermique en régime permanent, nous avons obtenu les expressions analytiques des profils de température, des flux thermiques et du facteur de rectification optimal des deux géométries de diodes. Grâce à l'outil intégré "FindRoot" du logiciel Wolfram Mathematical, nous avons résolu numériquement ces paramètres susmentionnés, ce qui nous a permis de décrire respectivement l'effet de rectification thermique dans deux géométries

différentes. Nous avons montré que le changement de géométrie a un effet significatif sur les températures et les flux thermiques, mais pas sur les facteurs de redressement optimaux, dont les valeurs sont en principe indépendantes de la géométrie de la diode comme le confirme [Equation 2.44]. Nous avons rapporté des facteurs de rectification théoriques maximaux d'environ 20.8% et 20.7% pour les diodes sphériques et cylindriques fonctionnant avec une différence de température aux bornes de  $376 - 300 = 76$  K et  $376.5 - 300 = 76.5$  K, respectivement.

Dans la deuxième partie, nous nous sommes concentrés sur l'effet combiné des deux matériaux à changement de phase pour améliorer le facteur de rectification optimal d'une diode thermique conductive (chapitre 3). L'idée ici est d'utiliser la combinaison de deux matériaux à changement de phase, dont les conductivités thermiques changent de manière significative dans un intervalle étroit de températures pour générer un facteur de rectification supérieur au cas de l'utilisation d'un seul PCM rapporté dans le chapitre 2. Nous avons déterminé les expressions analytiques du flux de chaleur, des profils de température et du facteur de rectification optimal en considérant la loi de Fourier de la conduction thermique en régime permanent et le principe de conservation de l'énergie. Nous avons généré un facteur de rectification maximum de 60%, ce qui est supérieur à celui obtenu pour les matériaux à changement de phase unique dans la littérature. Cela indique l'avantage d'utiliser deux matériaux à changement de phase pour optimiser la diode thermique conductive. Prenant en compte la définition alternative du facteur de rectification [ $R_a = [\max(q_F, q_B) / \min(q_F, q_B)] - 1$ ] par Kang *et al.* [Kan18], qui prévoyait une rectification maximale de 147%, nous avons obtenu une rectification maximale de 240%. Notre rectification relativement élevée est due au fait que nous avons utilisé le comportement réel des matériaux à changement de phase. Dans

la troisième partie, par contre, nous examinons des diodes thermiques radiatives à champ lointain basées sur l'effet combiné de deux matériaux à changement de phase de géométries différentes. Contrairement aux chapitres 2 et 3, nous avons utilisé ici la loi de Stefan-Boltzmann du rayonnement valable dans le cas du calcul des échanges radiatifs en champ lointain entre deux corps. Nous avons dérivé les expressions analytiques des flux thermiques pour le facteur de rectification optimal des diodes thermiques radiatives planes, cylindriques et sphériques. Nous avons fait cela en tenant compte du fait que la transition métal-isolant des deux matériaux à changement de phase illustrés sur la figure 4.3 remplit la condition de température  $T_c < T_{0n} < T_h$ . Nous avons montré que pour les diodes thermiques radiatives, la combinaison de deux matériaux à changement de phase génère également un facteur de rectification plus élevé que dans le cas où un seul PCM est utilisé. Nous avons également montré qu'une géométrie différente a un impact significatif sur le facteur de rectification optimal. Nous pensons que les résultats obtenus seront utiles pour guider l'établissement des matériaux à changement de phase nécessaires pour maximiser le facteur de rectification des diodes thermiques conductives et radiatives fonctionnant avec différentes géométries.

Afin de poursuivre ce travail à l'avenir, nous avons envisagé les perspectives suivantes:

- Il sera intéressant de regarder l'effet combiné de deux matériaux à changement de phase présentés au chapitre 3, en géométries cylindrique et sphérique, comme nous l'avons déjà fait pour les diodes thermiques radiatives au chapitre 4. Cela sera utile pour orienter le développement de diodes thermiques conductives dans les trois géométries différentes.

- Déterminer le facteur de rectification optimal des diodes thermiques radiatives reportées au chapitre 4 en champ proche, où la température de transition sera prise en compte. Cela permettra de mieux comprendre comment les contributions respectives des ondes propagatives et évanescentes pourrait permettre

d'obtenir un facteur de rectification optimal plus élevé.

- Etant donné que le transfert de chaleur en régime permanent dépend uniquement de la conductivité thermique des matériaux impliqués mais pas de la chaleur spécifique ou latente d'une transition de phase, il sera intéressant d'analyser et d'optimiser les diodes thermiques conductives à base de matériaux à changement de phase lorsque ceux-ci sont modulés en température..

- Étudier le memristor thermique en champ proche avec des courbes de Lisajous (flux thermique/différence de température) basé sur l'hystérésis thermique d'un matériau à changement de phase échangeant de la chaleur par rayonnement avec un matériau sans changement de phase. Même si un memristor thermique radiatif en champ lointain a été récemment proposé par Ordonez-Miranda *et al.* [Ord19a] et Yang *et al.* [Yan19], il sera intéressant de réaliser un memristor thermique en régime de champ proche, ce qui n'a pas encore été étudié dans la littérature.

# Bibliography

- [Ahn03] CH Ahn, J-M Triscone, and Jochen Mannhart, “Electric field effect in correlated oxide systems”, *Nature* 424.6952 (2003), pp. 1015–1018.
- [And58] Philip W Anderson, “Absence of diffusion in certain random lattices”, *Phys. Rev.* 109.5 (1958), p. 1492.
- [Asa97] A Asamitsu, Y Tomioka, H Kuwahara, and Y Tokura, “Current switching of resistive states in magnetoresistive manganites”, *Nature* 388.6637 (1997), pp. 50–52.
- [Bar03] MG Baron and M Elie, “Temperature sensing using reversible thermochromic polymeric films”, *Sens. Actuator B-Chem.* 90.1-3 (2003), pp. 271–275.
- [Bar66] AS Barker Jr, HW Verleur, and HJ Guggenheim, “Infrared optical properties of vanadium dioxide above and below the transition temperature”, *Phys. Rev. Lett.* 17 (1966), p. 1286.
- [Bas09] S Basu, ZM Zhang, and CJ Fu, “Review of near-field thermal radiation and its application to energy conversion”, *Int. J. Energy Res.* 33.13 (2009), pp. 1203–1232.
- [Bas11] Soumyadipta Basu and Mathieu Francoeur, “Near-field radiative transfer based thermal rectification using doped silicon”, *Appl. Phys. Lett.* 98 (2011), p. 113106.
- [Ben09] Philippe Ben-Abdallah, Karl Joulain, Jérémie Drevillon, and Gilberto Domingues, “Near-field heat transfer mediated by surface wave hybridization between two films”, *J. Appl. Phys.* 106.4 (2009), p. 044306.

- [Ben13] Philippe Ben-Abdallah and Svend-Age Biehs, "Phase-change radiative thermal diode", *Appl. Phys. Lett.* 103 (2013), p. 191907.
- [Ben14] Philippe Ben-Abdallah and Svend-Age Biehs, "Near-field thermal transistor", *Phys. Rev. Lett.* 112 (2014), p. 044301.
- [Ben17] Philippe Ben-Abdallah, "Thermal memristor and neuromorphic networks for manipulating heat flow", *AIP Adv.* 7 (2017), p. 065002.
- [Ber11] Theodore L Bergman, Frank P Incropera, David P DeWitt, and Adrienne S Lavine, *Fundamentals of heat and mass transfer*. John Wiley & Sons, 2011.
- [Bie18] S-A Biehs and Philippe Ben-Abdallah, "Fluctuations of radiative heat exchange between two bodies", *Phys. Rev. B* 97.20 (2018), p. 201406.
- [Bie20] Svend-Age Biehs, Riccardo Messina, Prashanth S Venkataram, Alejandro W Rodriguez, Juan Carlos Cuevas, and Philippe Ben-Abdallah, "Near-field Radiative Heat Transfer in Many-Body Systems", *arXiv preprint arXiv:2007.05604* (2020).
- [Bin07] Russell Binions, Geoffrey Hyett, Clara Piccirillo, and Ivan Paul Parkin, "Doped and un-doped vanadium dioxide thin films prepared by atmospheric pressure chemical vapour deposition from vanadyl acetylacetonate and tungsten hexachloride: the effects of thickness and crystallographic orientation on thermochromic properties", *J. Mater. Chem.* 17.44 (2007), pp. 4652–4660.
- [Bor93] Mark Borek, F Qian, V Nagabushnam, and RK Singh, "Pulsed laser deposition of oriented VO<sub>2</sub> thin films on R-cut sapphire substrates", *Appl. Phys. Lett.* 63.24 (1993), pp. 3288–3290.

- [Bro13] BL Brown et al., “Electrical and optical characterization of the metal-insulator transition temperature in Cr-doped VO<sub>2</sub> thin films”, *J. Appl. Phys.* 113.17 (2013), p. 173704.
- [Cao09] J Cao et al., “Strain engineering and one-dimensional organization of metal-insulator domains in single-crystal vanadium dioxide beams”, *Nature Nanotech.* 4.11 (2009), pp. 732–737.
- [Cav01] Andrea Cavalleri, Cs Tóth, Craig W Siders, JA Squier, F Ráksi, P Forget, and JC Kieffer, “Femtosecond structural dynamics in VO<sub>2</sub> during an ultrafast solid-solid phase transition”, *Phys. Rev. Lett.* 87.23 (2001), p. 237401.
- [Cav04] Andrea Cavalleri, Th Dekorsy, Henry HW Chong, Jean-Claude Kieffer, and Robert W Schoenlein, “Evidence for a structurally-driven insulator-to-metal transition in VO<sub>2</sub>: A view from the ultrafast timescale”, *Phys. Rev. B* 70.16 (2004), p. 161102.
- [Cha05] Byung-Gyu Chae, Hyun-Tak Kim, Sun-Jin Yun, Bong-Jun Kim, Yong-Wook Lee, Doo-Hyeb Youn, and Kwang-Yong Kang, “Highly oriented VO<sub>2</sub> thin films prepared by sol-gel deposition”, *Electrochem. Solid State Lett.* 9.1 (2005), p. C12.
- [Cha06] CW Chang, D Okawa, A Majumdar, and A Zettl, “Solid-state thermal rectifier”, *Science* 314 (2006), p. 1121.
- [Cha08a] Byung Gyu Chae, Hyun Tak Kim, and Sun Jin Yun, “Characteristics of W- and Ti-doped VO<sub>2</sub> thin films prepared by sol-gel method”, *Electrochem. Solid State Lett.* 11.6 (2008), p. D53.
- [Cha08b] Pierre-Olivier Chapuis, Sebastian Volz, Carsten Henkel, Karl Joulain, and Jean-Jacques Greffet, “Effects of spatial dispersion in near-field radiative heat transfer between two parallel metallic surfaces”, *Phys. Rev. B* 77.3 (2008), p. 035431.

- [Cha86] EE Chain, "The influence of deposition temperature on the structure and optical properties of vanadium oxide films", *J. Vac. Sci. Technol.* 4.3 (1986), pp. 432–435.
- [Che00] Changhong Chen, Xinjian Yi, Xingrong Zhao, and Bifeng Xiong, "Preparation and properties of vanadium dioxide thin films for uncooled microbolometer", *25th International Conference on Infrared and Millimeter Waves (Cat. No. 00EX442)*. IEEE. 2000, pp. 145–146.
- [Che16] Xue-Kun Chen, Zhong-Xiang Xie, Wu-Xing Zhou, Li-Ming Tang, and Ke-Qiu Chen, "Thermal rectification and negative differential thermal resistance behaviors in graphene/hexagonal boron nitride heterojunction", *Carbon* 100 (2016), pp. 492–500.
- [Che88] Jeffrey T Cheung and Haluk Sankur, "Growth of thin films by laser-induced evaporation", *Crit. Rev. Solid State Mater. Sci.* 15.1 (1988), pp. 63–109.
- [Cho96] HS Choi, JS Ahn, JH Jung, TW Noh, and DH Kim, "Mid-infrared properties of a VO<sub>2</sub> film near the metal-insulator transition", *Phys. Rev. B* 54.7 (1996), p. 4621.
- [Chr94] DB Chrisey and GK Hubler, "Pulsed Laser Deposition of Thin Films, John Wiley & Sons", *New York* (1994).
- [Chu02] Feliks Chudnovskiy, Serge Luryi, and Boris Spivak, "Switching device based on first-order metal-insulator transition induced by external electric field", *Future trends in microelectronics: the nano millennium* (2002), pp. 148–155.
- [Chu71] Leon Chua, "Memristor-the missing circuit element", *IEEE Trans. Circuit Theory* 18.5 (1971), pp. 507–519.

- [Chu75] FA Chudnovskii, "Metal-semiconductor phase transition in vanadium oxides and technical applications", *ZhTFi* 45 (1975), pp. 1561–1583.
- [Cot15] Anton L Cottrill and Michael S Strano, "Analysis of thermal diodes enabled by junctions of phase change materials", *Adv. Energy Mater.* 5.23 (2015), p. 1500921.
- [Cot18] Anton L Cottrill, Song Wang, Albert Tianxiang Liu, Wen-Jun Wang, and Michael S Strano, "Dual phase change thermal diodes for enhanced rectification ratios: theory and experiment", *Adv. Energy Mater.* 8.11 (2018), p. 1702692.
- [Cra67] Ernest G Cravalho, Chang L Tien, and RP Caren, "Effect of small spacings on radiative transfer between two dielectrics", (1967).
- [Day63] Jesse H Day, "Thermochromism.", *Chem. Rev.* 63.1 (1963), pp. 65–80.
- [Dek97] S Deki, Y Aoi, and A Kajinami, "A novel wet process for the preparation of vanadium dioxide thin film", *J. Mat. Sci.* 32.16 (1997), pp. 4269–4273.
- [Dri08] Tom Driscoll et al., "Dynamic tuning of an infrared hybrid-metamaterial resonance using vanadium dioxide", *Appl. Phys. Lett.* 93 (2008), p. 024101.
- [Dri09] Tom Driscoll et al., "Memory metamaterials", *Science* 325.5947 (2009), pp. 1518–1521.
- [Du17] Kai-Kai Du, Qiang Li, Yan-Biao Lyu, Ji-Chao Ding, Yue Lu, Zhi-Yuan Cheng, and Min Qiu, "Control over emissivity of zero-static-power thermal emitters based on phase-changing material GST", *Light Sci. Appl.* 6 (2017), e16194.

- [Dum08] Frédéric Dumas-Bouchiat, Corinne Champeaux, Alain Catherinot, Julien Givernaud, Aurelian Crunteanu, and Pierre Blondy, "RF microwave switches based on reversible metal-semiconductor transition properties of VO<sub>2</sub> thin films: an attractive way to realise simple RF microelectronic devices", *Symposium V-Materials and Devices for Smart Systems III*. Vol. 1129. 2008.
- [Eas07] Robert Eason, *Pulsed laser deposition of thin films: applications-led growth of functional materials*. John Wiley & Sons, 2007.
- [Ein05] Albert Einstein, "Über die von der molekularkinetischen Theorie der Wärme geforderte Bewegung von in ruhenden Flüssigkeiten suspendierten Teilchen", *Ann. Phys.* 4 (1905).
- [Eye02] Volker Eyert, "The metal-insulator transitions of VO<sub>2</sub>: A band theoretical approach", *Ann. Phys.* 11.9 (2002), pp. 650–704.
- [Fie00] MN Field and IP Parkin, "Atmospheric pressure chemical vapour deposition of vanadium (V) oxide films on glass substrates from reactions of VOCl<sub>3</sub> and VCl<sub>4</sub> with water", *J. Mater. Chem.* 10.8 (2000), pp. 1863–1866.
- [Fie98] Manfred Fiebig, Kenjiro Miyano, Yasuhide Tomioka, and Yoshinori Tokura, "Visualization of the local insulator-metal transition in Pr<sub>0.7</sub>Ca<sub>0.3</sub>MnO<sub>3</sub>", *Science* 280.5371 (1998), pp. 1925–1928.
- [Gao12] Yanfeng Gao et al., "Nanoceramic VO<sub>2</sub> thermochromic smart glass: A review on progress in solution processing", *Nano Energy* 1.2 (2012), pp. 221–246.
- [Goo71] John B Goodenough, "The two components of the crystallographic transition in VO<sub>2</sub>", *J. Solid State Chem.* 3.4 (1971), pp. 490–500.
- [Gre83] Charles B Greenberg, "Undoped and doped VO<sub>2</sub> films grown from VO (OC<sub>3</sub>H<sub>7</sub>)<sub>3</sub>", *Thin solid films* 110.1 (1983), pp. 73–82.

- [Grü88] George Grüner, "The dynamics of charge-density waves", *Rev. Mod. Phys.* 60.4 (1988), p. 1129.
- [Gu15] Wei Gu, Gui-Hua Tang, and Wen-Quan Tao, "Thermal switch and thermal rectification enabled by near-field radiative heat transfer between three slabs", *Int. J. Heat Mass Trans.* 82 (2015), pp. 429–434.
- [Guz94] Guillermo Guzman, Roger Morineau, and Jacques Livage, "Synthesis of vanadium dioxide thin films from vanadium alkoxides", *Mat. Res. Bull.* 29.5 (1994), pp. 509–515.
- [Hor10] S Hormoz and S Ramanathan, "Limits on vanadium oxide Mott metal–insulator transition field-effect transistors", *Solid-State Electron.* 54.6 (2010), pp. 654–659.
- [How10] John R Howell, M Pinar Menguc, and Robert Siegel, *Thermal radiation heat transfer*. CRC press, 2010.
- [Hu09] Jiuning Hu, Xiulin Ruan, and Yong P Chen, "Thermal conductivity and thermal rectification in graphene nanoribbons: a molecular dynamics study", *Nano lett.* 9 (2009), p. 2730.
- [Hu17] Shiqian Hu, Meng An, Nuo Yang, and Baowen Li, "A series circuit of thermal rectifiers: an effective way to enhance rectification ratio", *Small* 13.6 (2017), p. 1602726.
- [Hua13] Jinguo Huang, Qiang Li, Zhiheng Zheng, and Yimin Xuan, "Thermal rectification based on thermochromic materials", *Int. J. Heat Mass Trans.* 67 (2013), pp. 575–580.
- [Hua17] Y Huang, "Electrical and thermal properties of activated carbon fibers", *Activated carbon fiber and textiles*. Elsevier, 2017, pp. 181–192.
- [I L24] K. B. Blodgett I. Langmuir, "Currents limited by space charge between concentric spheres", *Phys. Rev.* 24 (1924), pp. 49–59.

- [Iiz12] Hideo Iizuka and Shanhui Fan, "Rectification of evanescent heat transfer between dielectric-coated and uncoated silicon carbide plates", *J. Appl. Phys.* 112 (2012), p. 024304.
- [Ima98] Masatoshi Imada, Atsushi Fujimori, and Yoshinori Tokura, "Metal-insulator transitions", *Rev. Mod. Phys.* 70.4 (1998), p. 1039.
- [Inc96] Frank P. Incropera and David P DeWitt, *Fundamentals of heat and mass transfer*. Vol. 4. Wiley New York, 1996.
- [Ito14] Kota Ito, Kazutaka Nishikawa, Hideo Iizuka, and Hiroshi Toshiyoshi, "Experimental investigation of radiative thermal rectifier using vanadium dioxide", *Appl. Phys. Lett.* 105 (2014), p. 253503.
- [Ito16] Kota Ito, Kazutaka Nishikawa, and Hideo Iizuka, "Multilevel radiative thermal memory realized by the hysteretic metal-insulator transition of vanadium dioxide", *Appl. Phys. Lett.* 108 (2016), p. 053507.
- [Jin97] P Jin, K Yoshimura, and S Tanemura, "Dependence of microstructure and thermochromism on substrate temperature for sputter-deposited VO<sub>2</sub> epitaxial films", *J. Vac. Sci. Technol.* 15.3 (1997), pp. 1113–1117.
- [Jou15a] Karl Joulain, Younès Ezzahri, Jérémie Drevillon, and Philippe Ben-Abdallah, "Modulation and amplification of radiative far field heat transfer: Towards a simple radiative thermal transistor", *Appl. Phys. Lett.* 106.13 (2015), p. 133505.
- [Jou15b] Karl Joulain, Younes Ezzahri, Jérémie Drevillon, Benoit Rousseau, and Domingos De Sousa Meneses, "Radiative thermal rectification between SiC and SiO<sub>2</sub>", *Opt. Express* 23.24 (2015), A1388–A1397.
- [Kam13] M Kamalisarvestani, R Saidur, S Mekhilef, and FS Javadi, "Performance, materials and coating technologies of thermochromic thin

- films on smart windows”, *Renew. Sust. Energ. Rev.* 26 (2013), pp. 353–364.
- [Kan18] Hyungmook Kang, Fan Yang, and Jeffrey J Urban, “Thermal rectification via heterojunctions of solid-state phase-change materials”, *Phys. Rev. Appl.* 10.2 (2018), p. 024034.
- [Kap41] PL Kapitza, “The study of heat transfer in helium II”, *J. Phys.(Moscow)* 4 (1941), p. 181.
- [Kas19] Suraju Olawale Kasali, Jose Ordonez-Miranda, and Karl Joulain, “Spherical and cylindrical conductive thermal diodes based on VO<sub>2</sub>”, *Eur. Phys. J. Plus* 134.7 (2019), p. 340.
- [Kas20a] Suraju Olawale Kasali, Jose Ordonez-Miranda, and Karl Joulain, “Conductive thermal diode based on two phase-change materials”, *Int. J. Therm. Sci.* 153 (2020), p. 106393.
- [Kas20b] Suraju Olawale Kasali, Jose Ordonez-Miranda, and Karl Joulain, “Optimization of the rectification factor of radiative thermal diodes based on two phase-change materials”, *Int. J. Heat Mass Trans.* 154 (2020), p. 119739.
- [Kha18] Isaac M Khalatnikov, *An introduction to the theory of superfluidity*. CRC Press, 2018.
- [Kim04] Hyun-Tak Kim, Byung-Gyu Chae, Doo-Hyeb Youn, Sung-Lyul Maeng, Gyungock Kim, Kwang-Yong Kang, and Yong-Sik Lim, “Mechanism and observation of Mott transition in VO<sub>2</sub>-based two- and three-terminal devices”, *New J. Phys.* 6.1 (2004), p. 52.

- [Kim07] Bong-Jun Kim, Yong Wook Lee, Byung-Gyu Chae, Sun Jin Yun, Soo-Young Oh, Hyun-Tak Kim, and Yong-Sik Lim, "Temperature dependence of the first-order metal-insulator transition in VO<sub>2</sub> and programmable critical temperature sensor", *Appl. Phys. Lett.* 90.2 (2007), p. 023515.
- [Kim08] Hyun-Tak Kim, Bong-Jun Kim, Yong Wook Lee, Byung-Gyu Chae, and Sun Jin Yun, "Switching of the Mott transition based on hole-driven MIT theory", *Physica B Condens. Matter* 403.5-9 (2008), pp. 1434-1436.
- [Kim10] Hyun-Tak Kim et al., "Electrical oscillations induced by the metal-insulator transition in VO<sub>2</sub>", *J. Appl. Phys.* 107.2 (2010), p. 023702.
- [Koi67] Shigenao Koide and Humihiko Takei, "Epitaxial growth of VO<sub>2</sub> single crystals and their anisotropic properties in electrical resistivities", *J. Phys. Soc. Jpn.* 22.3 (1967), pp. 946-947.
- [Koz11] Jakub A Koza, Zhen He, Andrew S Miller, and Jay A Switzer, "Resistance switching in electrodeposited VO<sub>2</sub> thin films", *Chem. Mater.* 23.18 (2011), pp. 4105-4108.
- [Kwo88a] Hoi Sing Kwok, JP Zheng, Sarath Witanachchi, Lei Shi, and DT Shaw, "Growth of CdS x Se<sub>1-x</sub> thin films by laser evaporation deposition", *Appl. Phys. Lett.* 52.21 (1988), pp. 1815-1816.
- [Kwo88b] HS Kwok, "J. P. Zheng, S. Witanachchi, P. Mattocks, L. Shi, QY Ying, XW Wang, and D. T. Shaw", *Appl. Phys. Lett* 52 (1988), p. 1095.
- [Lad69] Larry A Ladd and William Paul, "Optical and transport properties of high quality crystals of V<sub>2</sub>O<sub>4</sub> near the metallic transition temperature", *Solid State Commun.* 7.4 (1969), pp. 425-428.

- [Lak94] Charles DE Lakeman and David A Payne, "Sol-gel processing of electrical and magnetic ceramics", *Mater. Chem. Phys.* 38.4 (1994), pp. 305–324.
- [Lee07] M-J Lee et al., "Two series oxide resistors applicable to high speed and high density nonvolatile memory", *Adv. Mater* 19.22 (2007), pp. 3919–3923.
- [Lee17] Sangwook Lee et al., "Anomalously low electronic thermal conductivity in metallic vanadium dioxide", *Science* 355 (2017), p. 371.
- [Ler12] Jonathan Leroy, Annie Bessaudou, Françoise Cosset, and Aurelian Crunteanu, "Structural, electrical and optical properties of thermochromic VO<sub>2</sub> thin films obtained by reactive electron beam evaporation", *Thin Solid Films* 520.14 (2012), pp. 4823–4825.
- [Li04] Baowen Li, Lei Wang, and Giulio Casati, "Thermal diode: Rectification of heat flux", *Phys. Rev. Lett.* 93 (2004), p. 184301.
- [Li12] Nianbei Li, Jie Ren, Lei Wang, Gang Zhang, Peter Hänggi, and Baowen Li, "Colloquium: Phononics: Manipulating heat flow with electronic analogs and beyond", *Rev. Mod. Phys.* 84 (2012), p. 1045.
- [Li14] Nianbei Li and Jie Ren, "Non-reciprocal geometric wave diode by engineering asymmetric shapes of nonlinear materials", *Sci. Rep.* 4.1 (2014), pp. 1–6.
- [Liu04] Junfeng Liu, Qiuhong Li, Taihong Wang, Dapeng Yu, and Yadong Li, "Metastable vanadium dioxide nanobelts: hydrothermal synthesis, electrical transport, and magnetic properties", *Angew. Chem. Int. Ed.* 43.38 (2004), pp. 5048–5052.
- [Liv88] Jacques Livage, Marc Henry, and Clément Sanchez, "Sol-gel chemistry of transition metal oxides", *Prog. Solid State Chem.* 18.4 (1988), pp. 259–341.

- [Liv97] J Livage, G Guzman, F Beteille, and P Davidson, "Optical properties of sol-gel derived vanadium oxide films", *J. Sol-Gel Sci. Technol.* 8.1-3 (1997), pp. 857–865.
- [Lo08] Wei Chung Lo, Lei Wang, and Baowen Li, "Thermal transistor: heat flux switching and modulating", *J. Phys. Soc. Japan* 77.5 (2008), pp. 054402–054402.
- [Lon70] John M Longo, Peder Kierkegaard, CJ Ballhausen, U Ragnarsson, SE Rasmussen, E Sunde, and NA Sørensen, "A refinement of the structure of VO<sub>2</sub>", *Acta Chem. Scand.* 24.2 (1970), pp. 420–426.
- [Lu96] Songwei Lu, Lisong Hou, and Fuxi Gan, "Synthesis and phase transition of Cu<sup>2+</sup> ion doped VO<sub>2</sub> thin films", *J. Mater. Sci. Lett.* 15.10 (1996), pp. 856–857.
- [Lys06] S Lysenko, AJ Rua, V Vikhnin, J Jimenez, F Fernandez, and H Liu, "Light-induced ultrafast phase transitions in VO<sub>2</sub> thin film", *Appl. Surf. Sci.* 252.15 (2006), pp. 5512–5515.
- [Mac68] JB MacChesney, JF Potter, and HJ Guggenheim, "Preparation and properties of vanadium dioxide films", *J. Phys. Chem. Solids* 115.1 (1968), p. 52.
- [Man02] Troy D Manning, Ivan P Parkin, Robin JH Clark, David Sheel, Martyn E Pemble, and Dimitra Vernadou, "Intelligent window coatings: atmospheric pressure chemical vapour deposition of vanadium oxides", *J. Mater. Chem.* 12.10 (2002), pp. 2936–2939.
- [Man07] RG Mani and S Ramanathan, "Observation of a uniform temperature dependence in the electrical resistance across the structural phase transition in thin film vanadium oxide (VO<sub>2</sub>)", *Appl. Phys. Lett.* 91.6 (2007), p. 062104.

- [Mar93] T Maruyama and Y Ikuta, "Vanadium dioxide thin films prepared by chemical vapour deposition from vanadium (III) acetylacetonate", *J. Mater. Sci.* 28.18 (1993), pp. 5073–5078.
- [McG17] Ryan McGee, Ankur Goswami, Behnam Khorshidi, Kristi McGuire, Calvin Schofield, and Thomas Thundat, "Effect of process parameters on phase stability and metal-insulator transition of vanadium dioxide (VO<sub>2</sub>) thin films by pulsed laser deposition", *Acta Mater.* 137 (2017), pp. 12–21.
- [McW74] DB McWhan, M Marezio, JP Remeika, and PD Dernier, "X-ray diffraction study of metallic V O 2", *Phys. Rev. B* 10.2 (1974), p. 490.
- [Miy97] K Miyano, T Tanaka, Y Tomioka, and Y Tokura, "Photoinduced insulator-to-metal transition in a perovskite manganite", *Phys. Rev. Lett.* 78.22 (1997), p. 4257.
- [Mod13] Michael F Modest, *Radiative heat transfer*. Academic press, 2013.
- [Mor59] FJ Morin, "Oxides which show a metal-to-insulator transition at the Neel temperature", *Phys. Rev. Lett.* 3.1 (1959), p. 34.
- [Mot04] Nevill Mott, *Metal-insulator transitions*. CRC Press, 2004.
- [Mot68] NF Mott, "Metal-insulator transition", *Rev. Mod. Phys.* 40.4 (1968), p. 677.
- [Nag06] Kazuki Nagashima, Takeshi Yanagida, Hidekazu Tanaka, and Tomoji Kawai, "Stress relaxation effect on transport properties of strained vanadium dioxide epitaxial thin films", *Phys. Rev. B* 74.17 (2006), p. 172106.
- [Nag08] Joyeeta Nag and RF Haglund Jr, "Synthesis of vanadium dioxide thin films and nanoparticles", *J. Phys. Condens. Matter* 20.26 (2008), p. 264016.

- [Nak97] Hiroshi Nakatsugawa and E Iguchi, "Electronic structures in VO 2 using the periodic polarizable point-ion shell model and DV-X $\alpha$  method", *Phys. Rev. B* 55.4 (1997), p. 2157.
- [Nar08] Arvind Narayanaswamy, Sheng Shen, and Gang Chen, "Near-field radiative heat transfer between a sphere and a substrate", *Phys. Rev. B* 78.11 (2008), p. 115303.
- [Nas19] MG Naso, E Vuk, and F Zullo, "On the optimization of heat rectification in graded materials", *Int. J. Heat Mass Trans.* 143 (2019), p. 118520.
- [Nef14a] Elyes Nefzaoui, Jérémie Drevillon, Younès Ezzahri, and Karl Joulain, "Simple far-field radiative thermal rectifier using Fabry–Perot cavities based infrared selective emitters", *Appl. Opt.* 53 (2014), p. 3479.
- [Nef14b] Elyes Nefzaoui, Karl Joulain, Jérémie Drevillon, and Younès Ezzahri, "Radiative thermal rectification using superconducting materials", *Appl. Phys. Lett.* 104 (2014), p. 103905.
- [New00] DM Newns et al., "The Mott transition field effect transistor: A nanodevice?", *J. Electroceramics* 4.2-3 (2000), pp. 339–344.
- [New98] DM Newns, JA Misewich, CC Tsuei, A Gupta, BA Scott, and A Schrott, "Mott transition field effect transistor", *Appl. Phys. Lett.* 73.6 (1998), pp. 780–782.
- [Oh10] Dong-Wook Oh, Changhyun Ko, Shriram Ramanathan, and David G Cahill, "Thermal conductivity and dynamic heat capacity across the metal-insulator transition in thin film VO 2", *Appl. Phys. Lett.* 96.15 (2010), p. 151906.
- [Oka06] K Okazaki, S Sugai, Yuji Muraoka, and Z Hiroi, "Role of electron-electron and electron-phonon interaction effects in the optical conductivity of VO 2", *Phys. Rev. B* 73.16 (2006), p. 165116.

- [Ono00] Naoki Ono, Kounosuke Kitamura, Ken Nakajima, and Yasushi Shi-manuki, "Measurement of Young's modulus of silicon single crystal at high temperature and its dependency on boron concentration using the flexural vibration method", *Jpn. J. Appl. Phys.* 39.2R (2000), p. 368.
- [Ord16] Jose Ordonez-Miranda, Younès Ezzahri, Jérémie Drevillon, and Karl Joulain, "Transistorlike Device for Heating and Cooling Based on the Thermal Hysteresis of VO<sub>2</sub>", *Phys. Rev. Appl.* 6 (2016), p. 054003.
- [Ord18a] Jose Ordonez-Miranda, Younès Ezzahri, Karl Joulain, Jérémie Drevillon, and JJ Alvarado-Gil, "Modeling of the electrical conductivity, thermal conductivity, and specific heat capacity of VO<sub>2</sub>", *Phys. Rev. B* 98 (2018), p. 075144.
- [Ord18b] Jose Ordonez-Miranda, James M Hill, Karl Joulain, Younès Ezzahri, and Jérémie Drevillon, "Conductive thermal diode based on the thermal hysteresis of VO<sub>2</sub> and nitinol", *J. Appl. Phys.* 123 (2018), p. 085102.
- [Ord19a] Jose Ordonez-Miranda, Younès Ezzahri, Jose A Tiburcio-Moreno, Karl Joulain, and Jérémie Drevillon, "Radiative thermal memristor", *Phys. Rev. Lett.* 123.2 (2019), p. 025901.
- [Ord19b] Jose Ordonez-Miranda, Karl Joulain, Younès Ezzahri, Jérémie Drevillon, and JJ Alvarado-Gil, "Periodic amplification of radiative heat transfer", *J. Appl. Phys.* 125 (2019), p. 064302.
- [Ote10] Clayton R Otey, Wah Tung Lau, Shanhui Fan, et al., "Thermal rectification through vacuum", *Phys. Rev. Lett.* 104 (2010), p. 154301.
- [Pal85] ED Palik, "Handbook of Optical Constants of solids Vol. 1 p. 760-761 Academic Press Inc", *London Ltd.* (1985).

- [Pan16] M Panagopoulou, E Gagaoudakis, N Boukos, E Aperathitis, G Kiridakidis, D Tsoukalas, and YS Raptis, "Thermochromic performance of Mg-doped VO<sub>2</sub> thin films on functional substrates for glazing applications", *Sol. Energy Mater. Sol. Cells* 157 (2016), pp. 1004–1010.
- [Par91] DP Partlow, SR Gurkovich, KC Radford, and LJ Denes, "Switchable vanadium oxide films by a sol-gel process", *J. Appl. Phys.* 70.1 (1991), pp. 443–452.
- [Pau07] SA Pauli, R Herger, PR Willmott, EU Donev, JY Suh, and RF Haglund Jr, "X-ray diffraction studies of the growth of vanadium dioxide nanoparticles", *J. Appl. Phys.* 102.7 (2007), p. 073527.
- [Pei96] Rudolf Ernst Peierls, *Quantum theory of solids*. Clarendon Press, 1996.
- [Per03] Alexander Pergament, "Metal–insulator transition: the Mott criterion and coherence length", *J. Phys: Condens. Matter* 15.19 (2003), p. 3217.
- [Per08] A Perucchi, L Baldassarre, E Arcangeletti, D Di Castro, P Postorino, and S Lupi, "Infrared study of pressure-induced insulator to metal transitions in vanadium oxide compounds at the SISSI@ Elettra beamline", *Infrared Phys. Technol.* 51.5 (2008), pp. 440–442.
- [Per13] AL Pergament, GB Stefanovich, NA Kuldin, and AA Velichko, "On the problem of metal-insulator transitions in vanadium oxides", *Int. Sch. Res. Notices* 2013 (2013).
- [Pey06] Michel Peyrard, "The design of a thermal rectifier", *Europhys. Lett.* 76 (2006), p. 49.
- [Pla14] Max Planck, "The Theory of Heat Radiation", *M. Masius, P. Blakiston's Son & Co, Philadelphia* (1914).
- [Pol71] DVHM Polder and M Van Hove, "Theory of radiative heat transfer between closely spaced bodies", *Phys. Rev. B* 4.10 (1971), p. 3303.

- [Qaz06] MM Qazilbash, KS Burch, D Whisler, D Shrekenhamer, BG Chae, HT Kim, and DN Basov, "Correlated metallic state of vanadium dioxide", *Phys. Rev. B* 74.20 (2006), p. 205118.
- [Qaz07] Mumtaz M Qazilbash et al., "Mott transition in VO<sub>2</sub> revealed by infrared spectroscopy and nano-imaging", *Science* 318.5857 (2007), pp. 1750–1753.
- [Qaz08a] Mumtaz M Qazilbash et al., "Electrodynamics of the vanadium oxides V O<sub>2</sub> and V<sub>2</sub> O<sub>3</sub>", *Phys. Rev. B* 77 (2008), p. 115121.
- [Qaz08b] Mumtaz M Qazilbash et al., "Electrostatic modification of infrared response in gated structures based on VO<sub>2</sub>", *Appl. Phys. Lett.* 92 (2008), p. 241906.
- [Ram05] Chintalapalle Venkata Ramana, RJ Smith, OM Hussain, Charles C Chusuei, and CM Julien, "Correlation between growth conditions, microstructure, and optical properties in pulsed-laser-deposited V<sub>2</sub>O<sub>5</sub> thin films", *Chem. Mater.* 17.5 (2005), pp. 1213–1219.
- [Ric94] TM Rice, H Launois, and JP Pouget, "Comment on" V O<sub>2</sub>: Peierls or Mott-Hubbard? A View from Band Theory"", *Phys. Rev. Lett* 73.22 (1994), p. 3042.
- [Rin05] Matteo Rini et al., "Photoinduced phase transition in VO<sub>2</sub> nanocrystals: ultrafast control of surface-plasmon resonance", *Opt. Lett.* 30.5 (2005), pp. 558–560.
- [Rin08] Matteo Rini et al., "Optical switching in VO<sub>2</sub> films by below-gap excitation", *Appl. Phys. Lett.* 92 (2008), p. 181904.
- [Rob11] Nick A Roberts and DG Walker, "A review of thermal rectification observations and models in solid materials", *Int. J. Therm. Sci.* 50 (2011), p. 648.

- [Rog91] KD Rogers, JA Coath, and MC Lovell, "Characterization of epitaxially grown films of vanadium oxides", *J. Appl. Phys.* 70.3 (1991), pp. 1412–1415.
- [Roh98] Warren M Rohsenow, James P Hartnett, Young I Cho, et al., *Handbook of heat transfer*. Vol. 3. McGraw-Hill New York, 1998.
- [Ruo09] Tomi Ruokola, Teemu Ojanen, and Antti-Pekka Jauho, "Thermal rectification in nonlinear quantum circuits", *Phys. Rev. B* 79.14 (2009), p. 144306.
- [Ruz07a] Dmitry Ruzmetov, Kevin T Zawilski, Venkatesh Narayanamurti, and Shriram Ramanathan, "Structure-functional property relationships in rf-sputtered vanadium dioxide thin films", *J. Appl. Phys.* 102.11 (2007), p. 113715.
- [Ruz07b] Dmitry Ruzmetov, Kevin T Zawilski, Venkatesh Narayanamurti, and Shriram Ramanathan, "Structure-functional property relationships in rf-sputtered vanadium dioxide thin films", *J. Appl. Phys.* 102.11 (2007), p. 113715.
- [Ruz08] Dmitry Ruzmetov, Kevin T Zawilski, Sanjaya D Senanayake, Venkatesh Narayanamurti, and Shriram Ramanathan, "Infrared reflectance and photoemission spectroscopy studies across the phase transition boundary in thin film vanadium dioxide", *J. Phys. Condens. Mat.* 20.46 (2008), p. 465204.
- [Ruz10] Dmitry Ruzmetov and Shriram Ramanathan, "Metal-insulator transition in thin film vanadium dioxide", *Thin Film Metal-Oxides*. Springer, 2010, pp. 51–94.
- [Sad16] Hamou Sadat and Vital Le Dez, "On the thermal rectification factor in steady heat conduction", *Mech. Res. Commun.* 76 (2016), p. 48.

- [Sah02] MB Sahana, GN Subbanna, and SA Shivashankar, "Phase transformation and semiconductor-metal transition in thin films of VO<sub>2</sub> deposited by low-pressure metalorganic chemical vapor deposition", *J. Appl. phys.* 92.11 (2002), pp. 6495–6504.
- [Sam97] M Sambti, G Sangiovanni, G Granozzi, and Fulvio Parmigiani, "Growth and the structure of epitaxial VO<sub>2</sub> at the TiO<sub>2</sub> (110) surface", *Phys. Rev. B* 55.12 (1997), p. 7850.
- [Sch03] Udo Schwingenschlögl, Volker Eyert, and Ulrich Eckern, "From VO<sub>2</sub> to V<sub>2</sub>O<sub>3</sub>: The metal-insulator transition of the Magnéli phase V<sub>6</sub>O<sub>11</sub>", *EPL-Europhys. Lett.* 61.3 (2003), p. 361.
- [Sch04] Udo Schwingenschlögl and Volker Eyert, "The vanadium Magnéli phases V<sub>n</sub>O<sub>2n-1</sub>", *Ann. Phys.* 13.9 (2004), pp. 475–510.
- [Sep08] Nelson Sepúlveda, Armando Rúa, Rafmag Cabrera, and Félix Fernández, "Young's modulus of VO<sub>2</sub> thin films as a function of temperature including insulator-to-metal transition regime", *Appl. Phys. Lett.* 92.19 (2008), p. 191913.
- [Ser04] Raymond A Serway, Clement J Moses, and Curt A Moyer, *Modern physics*. Cengage Learning, 2004.
- [Shc00] Andrei V Shchegrov, Karl Joulain, Rémi Carminati, and Jean-Jacques Greffet, "Near-field spectral effects due to electromagnetic surface excitations", *Phys. Rev. Lett.* 85.7 (2000), p. 1548.
- [Shi15] Tien-Mo Shih, Zhaojing Gao, Ziquan Guo, Holger Merlitz, Patrick J Pagni, and Zhong Chen, "Maximal rectification ratios for idealized bi-segment thermal rectifiers", *Sci. Rep.* 5 (2015), p. 12677.
- [Shi90] Shik Shin et al., "Vacuum-ultraviolet reflectance and photoemission study of the metal-insulator phase transitions in VO<sub>2</sub>, V<sub>6</sub>O<sub>13</sub>, and V<sub>2</sub>O<sub>3</sub>", *Phys. Rev. B* 41.8 (1990), p. 4993.

- [Shi91] Lei Shi, Yuichi Hashishin, SY Dong, JP Zheng, and Hoi Sing Kwok, "Laser deposition of CdS/Y-Ba-Cu-O heterostructures", *Appl. Phys. Lett* 59.11 (1991), pp. 1377–1379.
- [Shr20] Ramesh Shrestha et al., "Dual-mode solid-state thermal rectification", *Nat. Commun.* 11.1 (2020), pp. 1–7.
- [Sol06] M Soltani, M Chaker, E Haddad, and R Kruzelesky, "1 × 2 optical switch devices based on semiconductor-to-metallic phase transition characteristics of VO<sub>2</sub> smart coatings", *Meas. Sci. Technol.* 17.5 (2006), p. 1052.
- [Son15] Bai Song et al., "Enhancement of near-field radiative heat transfer using polar dielectric thin films", *Nature Nanotech.* 10.3 (2015), pp. 253–258.
- [Spe88] KR Speck, HS-W Hu, ME Sherwin, and RS Potember, "Vanadium dioxide films grown from vanadium tetra-isopropoxide by the sol-gel process", *Thin Solid Films* 165.1 (1988), pp. 317–322.
- [Sta36] Chauncey Starr, "The copper oxide rectifier", *Phys.* 7.1 (1936), pp. 15–19.
- [Ste00] G Stefanovich, A Pergament, and D Stefanovich, "Electrical switching and Mott transition in VO<sub>2</sub>", *J. Phys. Condens. Matter* 12.41 (2000), p. 8837.
- [Str08] Dmitri B Strukov, Gregory S Snider, Duncan R Stewart, and R Stanley Williams, "The missing memristor found", *Nature* 453.7191 (2008), pp. 80–83.
- [Str09] Evgheni Strelcov, Yigal Lilach, and Andrei Kolmakov, "Gas sensor based on metal-insulator transition in VO<sub>2</sub> nanowire thermistor", *Nano Lett.* 9.6 (2009), pp. 2322–2326.

- [Suh04] Jae Yong Suh, Rene Lopez, Leonard C Feldman, and RF Haglund Jr, "Semiconductor to metal phase transition in the nucleation and growth of VO<sub>2</sub> nanoparticles and thin films", *J. Appl. Phys.* 96.2 (2004), pp. 1209–1213.
- [Swa89] Eric T Swartz and Robert O Pohl, "Thermal boundary resistance", *Rev. Mod. Phys.* 61.3 (1989), p. 605.
- [Tak66] Humihiko Takei and Shigenao Koide, "Growth and electrical properties of vanadium-oxide single crystals by oxychloride decomposition method", *J. Phys. Soc. Jpn.* 21.5 (1966), pp. 1010–1010.
- [Ter02] M Terraneo, M Peyrard, and G Casati, "Controlling the energy flow in nonlinear lattices: a model for a thermal rectifier", *Phys. Rev. Lett.* 88.9 (2002), p. 094302.
- [Van12] PJ Van Zwol, Laurent Ranno, and Joël Chevrier, "Tuning near field radiative heat flux through surface excitations with a metal insulator transition", *Phys. Rev. Lett.* 108 (2012), p. 234301.
- [Vik05] VS Vikhnin, S Lysenko, A Rua, F Fernandez, and H Liu, "The model of ultrafast light-induced insulator-metal phase transition in vanadium oxide", *J. Phys.: Conf. Ser.* Vol. 21. 2005, pp. 44–49.
- [Vol07] AI Volokitin and Bo NJ Persson, "Near-field radiative heat transfer and noncontact friction", *Rev. Mod. Phys.* 79.4 (2007), p. 1291.
- [Wan05] Hongchen Wang, Xinjian Yi, Sihai Chen, and Xiaochao Fu, "Fabrication of vanadium oxide micro-optical switches", *Sens. Actuator A-Phys.* 122 (2005), p. 108.
- [Wan07] Lei Wang and Baowen Li, "Thermal logic gates: computation with phonons", *Phys. Rev. Lett.* 99.17 (2007), p. 177208.

- [Wan13] LP Wang and ZM Zhang, "Thermal rectification enabled by near-field radiative heat transfer between intrinsic silicon and a dissimilar material", *Nanosc. Microsc. Therm.* 17 (2013), p. 337.
- [Wan16] Jinyu Wan, Qinghua Ren, Ningning Wu, and Yanfeng Gao, "Density functional theory study of M-doped (M= B, C, N, Mg, Al) VO<sub>2</sub> nanoparticles for thermochromic energy-saving foils", *J. Alloy Compd.* 662 (2016), pp. 621–627.
- [War14] Michael EA Warwick and Russell Binions, "Chemical vapour deposition of thermochromic vanadium dioxide thin films for energy efficient glazing", *J. Mater. Sci.* 214 (2014), pp. 53–66.
- [Wes08] Kevin G West et al., "Growth and characterization of vanadium dioxide thin films prepared by reactive-biased target ion beam deposition", *J. Vac. Sci. Technol. A* 26.1 (2008), pp. 133–139.
- [Whi11] Luisa Whittaker, Christopher J Patridge, and Sarbajit Banerjee, "Microscopic and nanoscale perspective of the metal- insulator phase transitions of VO<sub>2</sub>: some new twists to an old tale", *J. Phys. Chem. Lett.* 2.7 (2011), pp. 745–758.
- [Wil31] Alan Herries Wilson, "The theory of electronic semi-conductors.-ii", *P. Roy. Soc. A-Math. Phy.* 134.823 (1931), pp. 277–287.
- [Wu07] Gang Wu and Baowen Li, "Thermal rectification in carbon nanotube intramolecular junctions: Molecular dynamics calculations", *Phys. Rev. B* 76.8 (2007), p. 085424.
- [Wu13] Jing Wu, Wanxia Huang, Qiwu Shi, Jinghan Cai, Dong Zhao, Yubo Zhang, and Jiazhen Yan, "Effect of annealing temperature on thermochromic properties of vanadium dioxide thin films deposited by organic sol-gel method", *Appl. Surf. Sci.* 268 (2013), pp. 556–560.

- [Y03] Tokura Y., “Correlated-electron physics in transition-metal oxides”, *Phys. Today* 56 (2003), pp. 50–55.
- [Yan11] Zheng Yang, Changhyun Ko, and Shriram Ramanathan, “Oxide electronics utilizing ultrafast metal-insulator transitions”, *Annu. Rev. Mater. Sci.* 41 (2011), pp. 337–367.
- [Yan13] Yue Yang, Soumyadipta Basu, and Liping Wang, “Radiation-based near-field thermal rectification with phase transition materials”, *Appl. Phys. Lett.* 103 (2013), p. 163101.
- [Yan17] Xueming Yang, Dapeng Yu, Bingyang Cao, and Albert C To, “Ultrahigh Thermal Rectification in Pillared Graphene Structure with Carbon Nanotube–Graphene Intramolecular Junctions”, *ACS Appl. Mater. Interfaces* 9.1 (2017), pp. 29–35.
- [Yan18] Yu Yang, Hongyuan Chen, Huan Wang, Nianbei Li, and Lifa Zhang, “Optimal thermal rectification of heterojunctions under Fourier law”, *Phys. Rev. E* 98.4 (2018), p. 042131.
- [Yan19] Fan Yang, Madeleine P Gordon, and Jeffrey J Urban, “Theoretical framework of the thermal memristor via a solid-state phase change material”, *J. Appl. Phys.* 125.2 (2019), p. 025109.
- [Yua15] Kunpeng Yuan, Mingman Sun, Zhaoliang Wang, and Dawei Tang, “Tunable thermal rectification in silicon-functionalized graphene nanoribbons by molecular dynamics simulation”, *Int. J. Therm. Sci.* 98 (2015), pp. 24–31.
- [Zha07] Zhuomin M Zhang, *Nano/microscale heat transfer*. Springer, 2007.
- [Zha10] Zongtao Zhang, Yanfeng Gao, Zhang Chen, Jing Du, Chuanxiang Cao, Litao Kang, and Hongjie Luo, “Thermochromic VO<sub>2</sub> thin films: solution-based processing, improved optical properties, and

- lowered phase transformation temperature", *Langmuir* 26.13 (2010), pp. 10738–10744.
- [Zha15] Teng Zhang and Tengfei Luo, "Giant thermal rectification from polyethylene nanofiber thermal diodes", *Small* 11.36 (2015), pp. 4657–4665.
- [Zha16] Ruibo Zhang, Hai-Bo Jin, Deyu Guo, Jiasong Zhang, Zhengjing Zhao, Yongjie Zhao, and Jing-Bo Li, "The role of Fe dopants in phase stability and electric switching properties of Fe-doped VO<sub>2</sub>", *Ceram. Int.* 42.16 (2016), pp. 18764–18770.
- [Zho97] C Zhou, DM News, JA Misewich, and PC Pattnaik, "A field effect transistor based on the Mott transition in a molecular layer", *Appl. phys. Lett.* 70.5 (1997), pp. 598–600.
- [Zhu18] Weiwei Zhu, Gaomin Wu, Hong Chen, and Jie Ren, "Nonlinear heat radiation induces thermal rectifier in asymmetric holey composites", *Front. Energy Res.* 6 (2018), p. 9.
- [Zyl75] AMNF Zylbersztein and Nevill Francis Mott, "Metal-insulator transition in vanadium dioxide", *Phys. Rev. B* 11.11 (1975), p. 4383.

# List of publications and conferences

## I Publications

### Articles in peer-reviewed journals

1. Suraju Olawale Kasali, Jose Ordonez-Miranda, and Karl Joulain, *Spherical and cylindrical conductive thermal diodes based on VO<sub>2</sub>*, Eur. Phys. J. Plus 134, 340 (2019).  
[URL: <https://doi.org/10.1140/epjp/i2019-12782-y>]. (Chapter 2)
2. Suraju Olawale Kasali, Jose Ordonez-Miranda, and Karl Joulain, *Conductive thermal diode based on two phase-change materials*, Int. J. Therm. Sci. 153, 106393 (2020).  
[URL: <https://doi.org/10.1016/j.ijthermalsci.2020.106393>]. (Chapter 3)
3. Suraju Olawale Kasali, Jose Ordonez-Miranda, and Karl Joulain, *Optimization of the rectification factor of radiative thermal diodes based on two phase-change materials*, Int. J. Heat Mass Trans. 154, 119739 (2020).  
[URL:<https://doi.org/10.1016/j.ijheatmasstransfer.2020.119739>]. (Chapter 4)

## II Conferences

### Oral presentations

1. **Suraju Olawale Kasali**, Jose Ordonez-Miranda, and Karl Joulain, *Spherical and cylindrical conductive thermal diodes based on VO<sub>2</sub>*, **European Materials Research Society (EMRS) Spring Meeting**, 27-31 May 2019, Nice, France.
2. **Suraju Olawale Kasali**, Jose Ordonez-Miranda, and Karl Joulain, *Conductive thermal diode based on two phase-change materials*, **XXVIII International Materials Research Congress (IMRS)**, 19-21 August 2019, Cancun, Mexico.

### Poster presentation

1. **Suraju Olawale Kasali**, Jose Ordonez-Miranda, and Karl Joulain, *Spherical and cylindrical conductive thermal diodes based on VO<sub>2</sub>*, **Journées des Doctorants**, Institute Pprime, March 2019, Poitiers, France.